

UNIVERSITAT POLITÈCNICA DE VALÈNCIA
Departamento de Química

Ozone and peroxymonosulfate as oxidants in water
treatments for disinfection by-products control or
pollutant degradation.

DOCTORAL THESIS

Submitted by
Francisco Bernat Quesada

Supervisors
Dr. Sergio Navalón Oltra
Dr. Hermenegildo García Baldoví

Valencia, July 2021



UNIVERSITAT
POLITÈCNICA
DE VALÈNCIA



ESCUELA TÉCNICA
SUPERIOR INGENIEROS
INDUSTRIALES VALENCIA



UNIVERSITAT
POLITÈCNICA
DE VALÈNCIA



ESCUELA TÉCNICA
SUPERIOR INGENIEROS
INDUSTRIALES VALENCIA

D. SERGIO NAVALÓN OLTRA, Profesor Titular de la Universitat Politècnica de València y D. HERMENEGILDO GARCÍA BALDOVÍ, investigador asociado doctor en Química Sostenible CERTIFICAN, que la presente tesis doctoral, titulada: "Ozone and peroxymonosulfate as oxidants in water treatments for disinfection by-products control or pollutant degradation", ha sido desarrollada por FRANCISCO BERNAT QUESADA, en el marco del Programa de Doctorado de Química, bajo su dirección, en el Departamento de Química de la Universitat Politècnica de València.

Dr. Sergio Navalón Oltra

Dr. Hermenegildo García Baldoví

To my family

ACKNOWLEDGEMENTS

Esta tesis doctoral, representa la culminación de un trabajo de muchos años que no hubiera sido posible sin la inestimable ayuda y el apoyo de muchas personas, algunas de las cuales quiero mencionar aquí, ya que mencionarlas a todas sería realmente difícil.

En primer lugar, a mi amigo y director de esta tesis, D. Sergio Navalón, cuya dedicación tanto profesional como anímica, ha sido imprescindible para que este trabajo haya visto la luz. Sin él, este trabajo no hubiera sido posible. También quiero agradecer al apoyo y el trabajo de personas tan importantes para el desarrollo de esta tesis como Mercedes Álvaro, Hermenegildo García Gómez y Hermenegildo García Baldoví, por el tiempo que le han dedicado a este trabajo.

Quiero dar un agradecimiento realmente especial a D. Lorenzo Monforte Monleón, que fue la persona que, con gran dedicación, me ayudó a dar mis primeros pasos en un laboratorio y me hizo amar el mundo de la química del agua. Siempre le estaré agradecido por aquellas charlas recién salido de la carrera, que me hicieron amar mi trabajo. Realmente aquellos primeros años junto a él y las demás personas con las que trabajé en el laboratorio de Aguas de Valencia, fueron los mejores años y el germen para la realización de este trabajo.

Por otra parte, agradecer a los distintos compañeros con los que he coincidido en estos años en el departamento de Química. Muchos de ellos acabaron sus tesis doctorales o sus TFGs y se fueron, mientras que otros todavía siguen por aquí rematando sus propias tesis. Gracias a Juan Carlos, Andrea, Sandra, Álvaro, Cristina, María, Arianna, Antón, y demás, por hacerme agradable esos ratos que llegaba corriendo del trabajo al laboratorio a recoger o llevar muestras.

Como es normal, no me puedo olvidar de todos y cada uno de los chicos que trabajan en el laboratorio de La Presa de EMIVASA. La verdad es que paso más tiempo con ellos que con mi propia familia. A ellos tengo que agradecerles todo el esfuerzo que realizan cada día y que hace posible que mi trabajo sea más fácil, ya que siempre están dispuestos a ayudar en cualquier cosa que les pueda pedir. Gracias a Patri, Sonia, Elena, Salva, Jose Castelló, Palo, y todos los demás que han estado más o menos tiempo trabajando con nosotros.

A todos mis amigos, con los he pasado tantos buenos momentos en paellas, viajes, comidas, o simplemente quedando a tomar algo y que me han ayudado a seguir adelante. A todos aquellos que tantas veces te preguntan "¿Cómo va eso de la tesis?" y "¿Cuándo la acabas?". Gracias a Carlos, Tico, Arturo-Sonia, Llombart, Sergio, Samuel, y un largo etcétera. Gracias por hacerme la vida agradable.

Mi familia, merece un lugar muy importante en estos agradecimientos, ya que siempre están a mi lado tanto en los buenos como en los no tan buenos momentos. Gracias a mis padres y a mis hermanos, Adolfo y Jose. Y sin olvidar a mi tía Babel, que ha sido una madre más desde que tengo uso de razón, a mi cuñada Laura, mi sobrino Adolfo y a mi queridísima Yoko. Gracias a todos ellos por su fortaleza, su apoyo y sus consejos.

Y finalmente pero no menos importante, gracias a mi mujer, porque ha sido uno de los motores de esta tesis, Gracias Ladda, por confiar en mí desde el principio y seguir haciéndolo sin rendirte nunca. Te quiero mucho (ผมรักคุณ).

Muchas gracias a todos

Abbreviations and Acronyms

AC	Commercial activated carbon
ACN	Commercial activated carbon functionalized by nitric acid
ACT	Commercial activated carbon functionalized by thermal treatment
ATR-FTIR	Attenuated total reflection-Infrared spectroscopy Fourier transform
AOP	Advanced oxidation process
BET	Brunauer-Emmett-Teller
BOD	Biological oxygen demand
BJH	Barret-Joyner-Halenda
Co/AC, Co/CAN or Co/ACT	AC, ACN or ACT materials with deposition of Co nanoparticles
Co_{ox}/AC, Co_{ox}/ACN or Co_{ox}/ACT	AC, ACN or ACT materials with deposition of oxidized Co nanoparticles
D	Diamond nanoparticles
D-OH	Hydroxylated diamond nanoparticles
DOC	Dissolved organic carbon
DBP	Disinfection by-products
DWTP	Drinking Water Treatment Plant
EDX	Energy dispersive X-Ray
EPA	Environmental protection agency
FID	Flame ionization detector
FT-IR	Infrared spectroscopy Fourier transform
G	Commercial graphite
GC	Gas chromatography
GC-MS	Gas chromatography coupled to mass spectrometry
GO	Graphene oxide

HAA	Haloacetic acid
HK	Haloketone
HAM	Haloacetamide
HAN	Halonitrile
HPLC	High performance liquid chromatography
HSAG	High-surface area graphite
HSAG-HNO₃	HSAG functionalized with oxygen-functional groups in both edges and basal plane
HSAG-OH	HSAG functionalized with hydroxyl groups in the edges
HSAG-OH-COOH	HSAG functionalized with OH and COOH groups in the edges
ICP-OES	Inductively coupling plasma-optical emission spectrometry
IR	Infrared spectroscopy
MWCNTs	Multiwall carbon nanotubes
NHE	Normal hydrogen electrode
NOM	Natural organic matter
PD	Pyrolyzed diamond nanoparticles
PMS	Potassium monopersulfate or potassium peroxymonosulfate
PXRD	Powder X-ray diffractograms
rGO	Reduced graphene oxide
rGO-T	Thermally reduced graphene oxide
ROS	Reactive oxygen species
TCNM	Trichloronitrometane or Chloropicrin
TGA	Thermogravimetric analysis
THM	Trihalomethane
TOC	Total organic carbon
TOF	Turnover frequency
TON	Turnover number

TPD-MS	Temperature programmed desorption coupled to a mass-spectrometer
UWWTP	Urban wastewater treatment plant
XPS	X-ray photoelectron spectroscopy
XRD	X-ray diffraction

Index

Chapter 1. Introduction	1
1.1 Historical overview of drinking water treatments	2
1.2 Historical over view of wastewater treatments	4
1.3 Disinfection by-products in waters	6
1.3.1 Occurrence, human health and environmental implications of DBPs in water	6
1.3.2 Precursors of DBPs	9
1.3.3 Formation mechanism of DBPs	13
1.4 Occurrence and origin of water pollutants	18
1.5 Water quality regulations	19
1.6 Control of DBPs and pollutants during water treatment	20
1.7 Advanced oxidation processes	25
1.7.1 Generalities	25
1.7.2 Catalytic AOPs	28
1.8 AOPs based on heterogeneous transition metal catalysts	32
1.9 AOPs based on carbocatalysts	35
1.10 Activated carbons as carbocatalysts for AOPs	36
1.11 Graphite- and graphene-based materials as carbocatalysts for AOPs	38
1.12 Nanodiamonds as AOPs carbocatalysts	41
1.13 References	45
Chapter 2. Objectives	52

Chapter 3. Impact of chlorination and pre-ozonation on disinfection by-products formation from aqueous suspensions of cyanobacteria: *Microcystis aeruginosa*, *Anabaena aequalis* and *Oscillatoria tenuis* 55

3.1 Introduction	55
3.2 Materials and methods	59
3.2.1 Reagents	59
3.2.2 Experimental procedures and analysis	60
3.2.3 Cyanobacteria characterization	61
3.3 Results and discussion	61
3.3.1 Influence of the presence of cyanobacteria on chlorine demand during chlorination	63
3.3.2 Influence of cyanobacteria chlorination and pre-ozonation on DBP formation	65
3.4 Conclusions	77
3.5 References	78
3.6 Supplementary material	83

Chapter 4. Engineering of activated carbon surface to enhance the catalytic activity of supported cobalt oxide nanoparticles in peroxydisulfate activation 91

4.1 Introduction	91
4.2 Experimental section	94
4.2.1 Materials	94
4.2.2 Methods	94
4.2.3 Catalyst and activated carbon characterization	96
4.2.4 Catalytic activity and reaction analysis	97
4.3 Results and discussion	99
4.3.1 Support preparation and characterization	99
4.3.2 Metal supported on ACs	104

4.3.3	Catalytic activity	109
4.3.4	Reaction mechanism	121
4.4	Conclusions	123
4.5	References	124
4.6	Supplementary information	131

Chapter 5. Catalytic Ozonation Using Edge-Hydroxylated Graphite-Based Materials 149

5.1	Introduction	149
5.2	Experimental section	151
5.2.1	Materials	151
5.2.2	Characterization	153
5.2.3	Catalytic reactions	154
5.3	Results and discussion	156
5.3.1	Catalyst characterization	156
5.3.2	Catalytic activity	159
5.3.3	Role of dispersibility	169
5.4	Conclusions	171
5.5	References	172
5.6	Supplementary information	179

Chapter 6. Hybrid sp^2/sp^3 nanodiamonds as heterogeneous metal-free ozonation catalysts 189

6.1	Introduction	189
6.2	Experimental section	191
6.2.1	Materials and methods	191
6.2.2	Characterization	192
6.2.3	Catalytic activity	192
6.3	Results and discussion	193
6.3.1	Catalyst preparation	193
6.3.2	Catalytic activity	199

6.3.3	Catalyst heterogeneity and stability	204
6.3.4	ROS during the carbocatalytic ozonation	210
6.4	Conclusions	211
6.5	References	213
6.6	Supplementary material	219
Chapter 7. Conclusions		235
Chapter 8. Abstract of the Thesis		239
Chapter 9. Publications & Conferences		243

Chapter 1

Introduction

Access to drinking water and adequate wastewater disposal are now the two main requisites for the development of advanced societies. The term employed to refer to all the activities necessary to ensure a sustainable drinking water supply, sanitation processes and wastewater treatments is called *the integral water cycle*.^{1,2} Important technological advances have recently been achieved in both drinking water and wastewater treatments to minimize risks to human health and the environment. As the information on water quality increases stricter water regulations aimed at protecting the public and the environment are published. These regulations limit the maximum concentration of undesirable microorganisms and organic or inorganic substances present in water. However, there are still some important factors related to drinking water and urban wastewaters that deserve more research. In the area of water treatment, especially in drinking water, there is still a compromise to ensure water disinfection while minimizing the

formation of regulated or unregulated disinfection by-products (DBPs). In the cases of DWTPs and urban wastewater treatment plants (UWWTP) it is well-known that conventional treatments cannot efficiently remove certain recalcitrant organic pollutants with low biodegradability and/or toxicity.³⁻⁶ Implementation of the so-called advanced oxidation process (AOPs) in conventional water treatments is one of the most feasible solutions for pollutant degradation. In this context, the following sections will summarize the state of the art of both drinking water and urban wastewaters with emphasis on pollutant degradation and the occurrence, formation and control of DBPs in water. Special attention will be paid to the use of ozone and peroxymonosulfate as oxidants in water treatment, as they have been used as the basis for the present Thesis.

1.1. Historical overview of drinking water treatments

Water is an essential life resource and since ancient times humans have settled close to rivers^{7,8}, when access to clear and transparent water was associated with safe and healthy drinking water. Water filtration was for centuries the main drinking water treatment.^{8,9} The increasing population in the cities was the driving force for the development of more advanced drinking water treatments. At the beginning of the 20th century slow sand filters were employed as an efficient method of providing clean water. The development of bacteriology at the end of this century demonstrated that slow sand filters not only remove turbidity but also pathogenic microorganisms responsible for common diseases such as cholera, dysentery and typhoid fever. At this time, the increase urban population together with an increasing demand for drinking water caused the replacement of slow sand filters by rapid sand filters. The combination of rapid sand filters with coagulation-flocculation chemical treatments provided increasing amounts of drinking water of certain quality for human consumption.

At the beginning of the 20th century chemical disinfection was introduced in drinking water treatment plants (DWTP).¹⁰ The first full-scale DWTP using chlorination as disinfectant was in 1908 in Jersey City, New York (EEUU).¹¹ In 1914 the US established the first federal drinking water standard including bacteriological

quality. Since then, chlorine disinfection has been commonly employed for deactivating pathogens and preventing waterborne diseases such as dysentery, cholera and typhoid, among others. The introduction of chlorine to disinfect water resources destined for human consumption is now recognized as one of the major advances in public health in the 20th century.^{8,9}

Figure 1 shows a generalized flow diagram of a conventional DWTP. Initially, raw water goes through some grids and then chlorine is added as primary disinfectant. A coagulation-flocculation treatment follows to remove colloidal particles, with a subsequent pass through a sand filter. Finally, chlorine is added as secondary disinfectant. Current DWTPs have modifications aimed to obtain a water quality that complies with water regulations.¹⁰ For example, some have replaced sand filters by activated carbon filters to remove natural colloidal and particulate organic matter (NOM) as well as some organic pollutants from the water. In other cases, primary disinfectants such as O₃ or ClO₂ can be used to improve water disinfection and reduce the chemical risk associated with the formation of the so-called DBPs. It is now well-established that chlorine added as disinfectant is not effective in controlling some protozoa present in raw water, such as *Cryptosporidium* or *Giardia*. Also, part of the chlorine added as disinfectant reacts with the NOM present in water and produces undesirable DBPs, some of which are limited by the regulations to a maximum concentration due to their risk for human health.

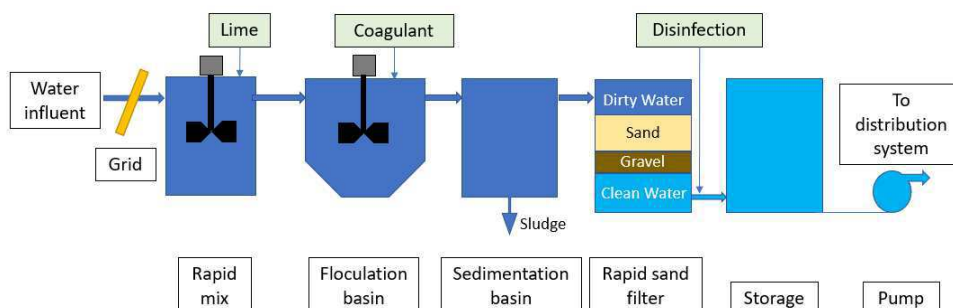


Figure 1. Simplified block diagram of a drinking water treatment plant.

1.2. Historical overview of wastewater treatments

One of the first urban wastewater management practices to protect human health and the environment was a land application treatment.¹² In contrast to the recognized importance of having good quality drinking water, the need for proper urban wastewater management or sanitation for the protection of human health was not recognized up to the beginning of the 19th century.¹³ The situation became more important with the development and growth of cities. Urban wastewater disposal close to the population caused negative health impacts as revealed by the occurrence of numerous epidemics in Europe until the 19th century.¹³

Some of the first developments in the area of urban wastewater management included the construction of collections sewers from the streets to the rivers¹³, which rapidly became polluted. The widespread construction of UWWTPs started at the beginning of the 20th century. In 1912 the British government through its Royal Commission on Sewage Disposal proposed some limitations to wastewater discharges into aquatic resources. For the first time the maximum value of the biological oxygen demand (BOD) of an urban wastewater before discharge was regulated. Since then, wastewater regulations have expanded all

over the world and new technologies for wastewater treatments have been developed.

Figure 2 shows a generalized flow diagram of a conventional UWWTP.¹³ The coarse solids or materials present in the urban wastewater are removed in the preliminary treatment, after which the settleable organic and inorganic solids are removed by sedimentation. The secondary treatment uses microorganisms for the mineralization of organic matter in the wastewater. One of the most popular secondary treatments employed is the so-called activated sludges, which combines aeration and biological floc of bacteria and protozoa for the removal of organic matter. Several water treatments can be implemented as a function of the requested wastewater effluent. In order to avoid eutrophication and algae blooms in the receiving waters, nitrogen and phosphorous can be removed. In some cases, membrane treatments or membrane bioreactors can be applied to produce high quality wastewater effluents. Urban wastewater disinfection is a common practice implemented as tertiary treatment designed to reduce the spread of diseases. One of the main problems associated with the use of chemical disinfectants such as chlorine, ozone, chlorine dioxide or chloramines is the formation of the so-called DBPs.

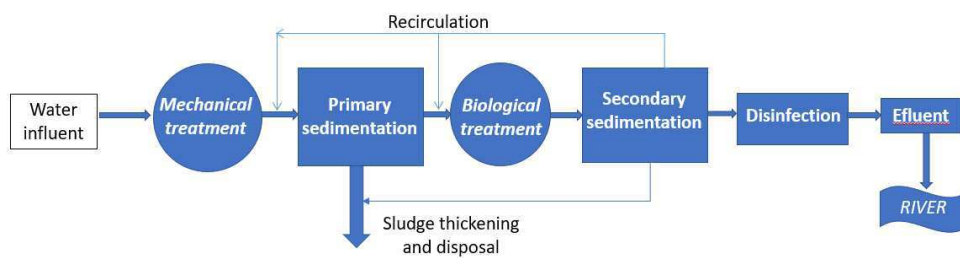


Figure 2. Simplified block diagram of a modern general urban waste water treatment.

1.3. Disinfection by-products in waters

1.3.1. Occurrence, human health and environmental implications of DBPs in water

One of the major drawbacks associated with the use of disinfectants (i.e. chlorine, ozone or chlorine dioxide) during water treatments is the formation of undesirable DBPs^{14,15}, which are generated due to the reaction of the disinfectant with the organic or inorganic compounds present in water.¹⁰ In 1974 Rook¹⁶ and Bellar¹⁷ first reported the presence of trihalomethanes (THMs) in drinking water disinfected with chlorine. Table 1 shows the chemical structures of the THMs commonly found in chlorinated drinking water. The presence of bromide atoms is due to the reaction of chlorine added to water with natural occurring bromides, causing the production of bromine aqueous species.

Table 1. Chemical formulae and names of THMs commonly found in chlorinated drinking waters.			
CHCl ₃ Chloroform	CHBr ₃ Bromoform	CHBrCl ₂ Dichlorobromo methane	CHClBr ₂ Dibromochloro methane

More than 800 DBPs have been reported due to the interaction of disinfectants such as chlorine, ozone, chlorine dioxide or chloramines among others with the NOM present in water.^{14,15,18} The total amount of halogenated DBPs is mainly constituted by organic compounds with chlorine and bromine atoms. It should be noted that iodinated-DBPs have also been found in waters that contain certain levels of iodide ions. Organic DBPs are frequently classified as C-DBPs or N-DBPs when referring to carbon or nitrogen containing DBPs, respectively.¹⁹ In addition to THMs, common halogenated C-DBPs include haloacetic acids

(HAAs), namely monochloroacetic acid (MCA), dichloroacetic acid (DCA), trichloroacetic acids (TCA), monobromoacetic acid (MBA) dibromoacetic acid (DBA), tribromoacetic acid (TBA), bromochloroacetic acid (BCA) and dibromochloroacetic acid (DBCA) and dichlorobromoacetic acid (BDCA) (Table 2). The maximum concentration of THMs and HAAs present in drinking water are frequently regulated in developed countries (Section 4.3).¹⁹ Other halogenated C-DBPs found in drinking water disinfected with chlorine are haloketones, with concentrations between 1.23-8.6 µg/L. The most commonly found haloketones are 1,1,1-trichloropropanone and 1,1-dichloropropanone. Trichloroacetaldehyde or chloral hydrate and dichloroacetaldehyde are the common DBP aldehydes. Other miscellaneous non-halogenated DBPs including ketones, and carboxylic acids have been also reported in the literature.

Table 2. Chemical formulae and names of HAAs frequently found in chlorinated drinking water.		
CH ₂ ClCOOH Monochloroacetic acid	CHCl ₂ COOH Dichloroacetic acid	Cl ₃ CCOOH Trichloroacetic acid
CH ₂ BrCOOH Bromoacetic acid	CHBr ₂ COOH Dibromoacetic acid	Br ₃ CCOOH Tribromoacetic acid
CHClBrCOOH Bromochloroacetic acid	BrCl ₂ CCOOH Dichlorobromoacetic acid	ClBr ₂ CCOOH Dibromochloroacetic acid

The common N-DBPs include cyanides, halonitromethanes, haloacetoneitriles, haloacetamides and N-nitrosamines (i.e. N-nitrosodimethylamine) (Table 3).^{14,15,20} Cyanogen chloride is the only cyanide compounds found in finished drinking water, typically at concentrations below 10 µg/L. Up to now nine halonitromethanes have been reported in chlorinated drinking water, while trichloronitromethane or chloropicrin is the most common at concentrations below 1.50 µg/L. Haloacetoneitriles are frequently found in drinking water at concentrations from 0.6 to 24 µg/L, with dichloroacetoneitrile being the most commonly re-

ported. The common haloacetamides found in drinking water include dibromoacetamide, dichloroacetamide and trichloroacetamide, and the total HAMs concentration frequently found in drinking water ranges between 1.50 to 7 µg/L. The most commonly found N-nitrosamine is N-nitrosodimethylamine, at concentrations below 0.1 ng/L.

Table 3. Chemical formulae and names of some N-DBPs.		
CNCl Cyanogen chloride	X ₃ CCN Halonitriles (X=Halogens)	Cl ₃ CNO ₂ Chloropicrin
Cl ₃ CCONH ₂ Trichloroacetamide	(CH ₃) ₂ NNO N-nitrosodimethylamine	

5

Regardless of the large number of identified DBPs in common fresh water treated by a conventional treatment using chlorine as disinfectant, the total amount of unknown halogenated DBPs can still be as high as 62.6 %.²¹ Typically, THMs represent the major fraction of known halogenated DBPs (20.1 %), followed by HAAs (CAA, DCAA, TCAA, MBAA and DBAA; 10 %), BCAA (2.81 %), haloacetonitriles (2 %), trichloroacetaldehyde (1.5 %) and cyanogen chloride (1 %). bromates and chlorite/chlorate are common inorganic DBPs found in water treated with ozone or chlorine dioxide as disinfectants and/or oxidants, respectively.

Since the detection of THMs in chlorinated waters, extensive research has been carried out to determine the potential risk of DPB ingestion on human health.²²⁻²⁴ To a lesser extent, some studies have reported that medium-long term exposure to DBPs such as THMs by skin contact and inhalation can have adverse effects on human health.²⁵⁻³⁰ Epidemiologic studies have found relationships between the continuous ingestion of chlorinated water containing DBPs

and an increased risk of cancer, especially bladder or colorectal cancer. Other studies have reported the possible negative effects of ingesting water containing chlorinated DBPs on reproduction, such as congenital anomalies and fetal development.³¹ In general, brominated-DBPs, especially iodinated-DBPs, have more adverse effects on human health than chlorinated-DBPs.³²⁻³⁴ Similarly, some N-DBPs such as haloacetonitriles have been reported to be more than one order of magnitude more cyto- or genotoxic than regulated C-DBPs such as THMs and HAAs.^{35,36}

The formation of DBPs in disinfected wastewater also has important implications for human health as well as for the environment.^{14,19,22} Wastewater effluents are sometimes directly discharged into rivers that serve as raw water for a downstream DWTP. Some studies have reported that chlorinated wastewater effluents are toxic and may harm the biota present in the receiving water resources³⁷, so that minimizing DBP formation in WWTPs will have important benefits for both human health and natural aquatic resources.²²

As already commented, the use of ozone or chlorine dioxide for water treatments also generates undesirable inorganic DBPs, e.g., the ozonation of raw water containing bromides generates undesirable bromates that are classified as human carcinogens. The use of chlorine dioxide in drinking water treatment results in the formation of chlorite, and chlorite anions can have negative effects on human health including nervous system toxicity, anemia, thyroid issues or reduced hemoglobin production, among others.

1.3.2. Precursors of DBPs

With regard to DBP formation the characterization of organic matter present in water that reacts with the disinfectants/oxidants added to water has been an important research area.^{38,39} In particular, intensive research has been conducted on the characterization of NOM present in aquatic resources.^{39,40} NOM refers to the complex mixture of organic compounds present in water derived from living plant and animal materials.³⁹⁻⁴¹ In general, NOM is not harmful to human health, although it can act as adsorbent of toxic organic compounds or a

binder of toxic metals. The most common parameters employed to measure the NOM concentration are total organic carbon (TOC) or dissolved organic carbon (DOC). DOC is defined as the fraction of organic carbon not retained by a 0.45 μm filter, while the retained fraction consists of particulate organic carbon (POC). TOC values found in natural fresh water can range between 1-6 mg/l, although higher concentrations can also be found. Fresh water typically contains a DOC fraction of more than 90 % and for this reason their constituents have been largely studied as precursors to DBPs. Some studies have focused on the characterization of the POC present in water. Figure 3 summarizes some physical properties of the main POC and DOC constituents present in natural aquatic resources.

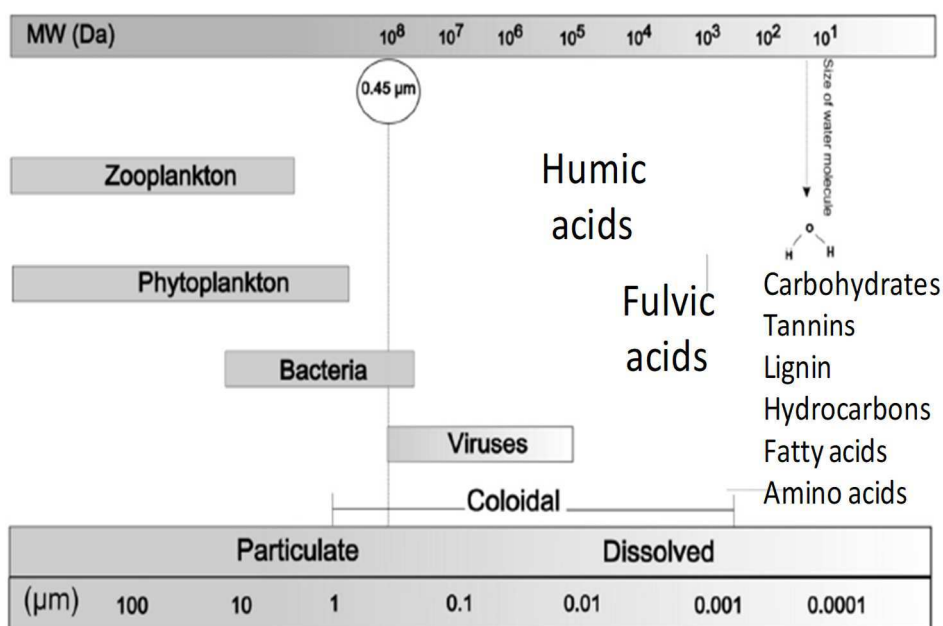


Figure 3. Organic matter size and mass distribution of some organisms and chemical molecules in aquatic systems. Adapted with permission from ref ⁴² (Bolto, B. A. Soluble polymers in water purification. Progress in Polymer Science. 1995, 20, 987-1041).

A common classification of the NOM present in water distinguishes between those organic compounds with distinct chemical formulae forming discrete compounds (non-humic substances) from organic compounds with a partially unknown chemical structure (humic substances).³⁸⁻⁴⁰ Non-humic organic compounds present in fresh water include carbohydrates, lignin and tannins as major components together with lipids, proteins and peptides as well as other small molecules such as amino acids, aromatic acids and phenols, and carboxylic acids, among others.³⁹ Humic substances are generally defined as supramolecular aggregates with a yellow to brown color and are commonly classified as a function of their solubility in water and molecular weight.³⁸ Fulvic acids are the fraction of humic substances soluble in water at any pH with molecular weights between 1,000 and 10,000 Da. Figure 4 shows a general model structure of fulvic acids characterized by aromatic subunits together with carbohydrate and diketonic moieties. Humic acids are insoluble in water at acid pH, with a molecular weight ranging from 10,000 to 100,000 Da. Humins are insoluble in water and have molecular weights ranging from 100,000 to 10,000,000 Da. It has been generally accepted for years that humic substances can represent a large fraction (40 to 80 %) of dissolved organic matter. In contrast, few studies have reported low contents of humic substances in natural surface waters. In 2008, Navalon et al. reported that the fraction of humic substances in the Turia river (Valencia, Spain) represents less than 4 % of the organic matter.⁴³ Carbohydrates of relatively low molecular weight (< 2,000 Da) were found to be the main components in this river, accompanied by other compounds such as lipids and oligopeptides.

Chapter 1. Introduction

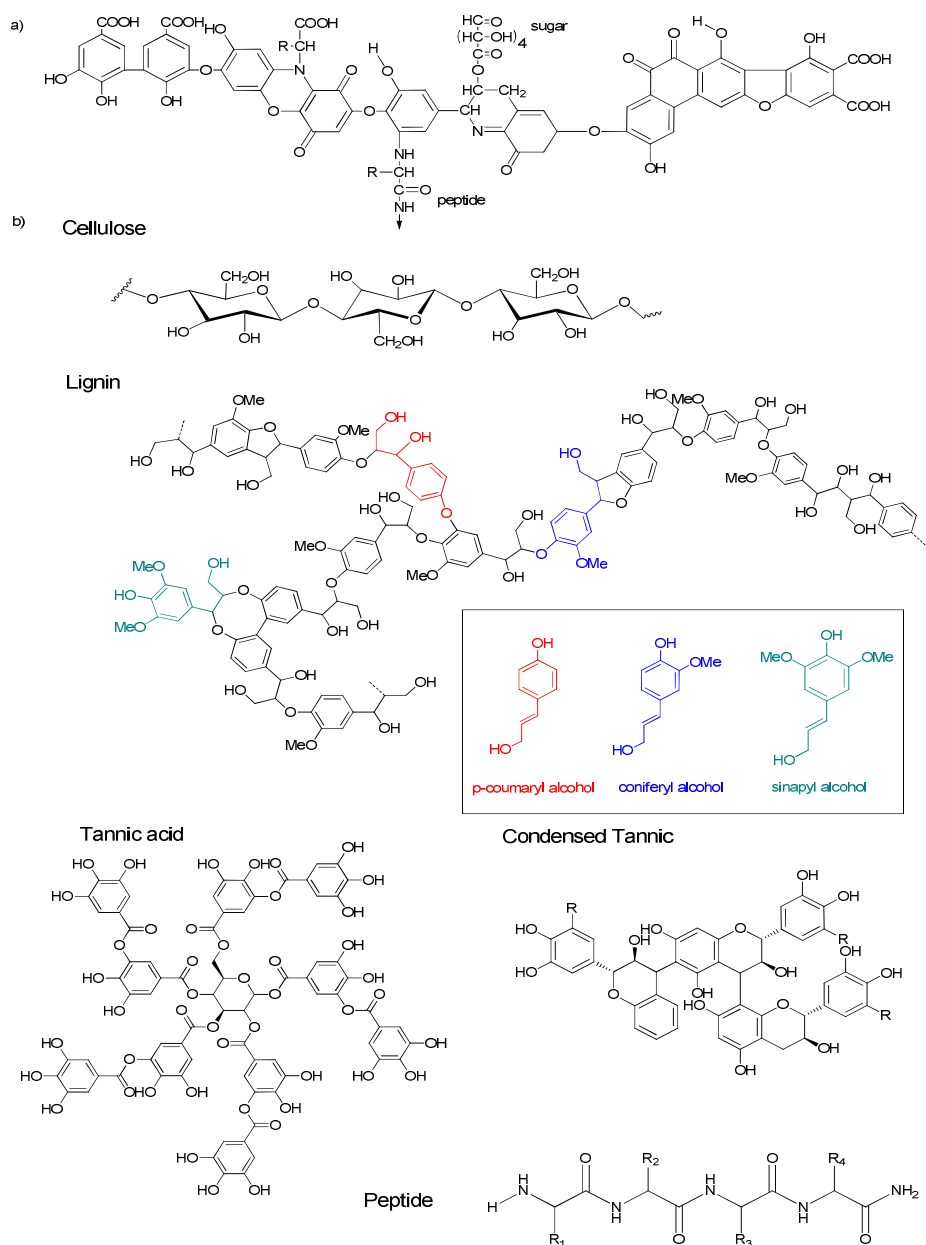


Figure 4. Chemical structures of humic substances (a) and proposed model of fulvic acids (b). Adapted with permission from ref. ⁴³ (Navalon, S.; Alvaro, M.; Garcia, H. Carbohydrates as trihalomethanes precursors. Influence of pH and the

presence of Cl(-) and Br(-) on trihalomethane formation potential. *Water Research*. 2008, 42, 3990-4000).

Other related studies have focused on the characterization of organic matter present in UWWTP effluents.⁴⁴⁻⁴⁶ As previously commented, these effluents are often discharged into natural aquatic resources that can later be used as raw water for human consumption. The composition of these effluents is a complex mixture of hydrophobic compounds used in domestic detergents or soaps as well as steroids together with a hydrophilic fraction including saccharides, hydroxyacids, carboxylic aromatic compounds and nitrogenous compounds such as amino acids, peptides or proteins.⁴⁶ UWWTP effluents also contain a large variety of emerging pollutants, including pharmaceuticals and personal care compounds among others. For example, in 2011 Navalón et al reported the presence of paracetamol and ketoprofen in the effluent of an urban WWTP at Ribarroja (Valencia, Spain).⁴⁶

1.3.3. Formation mechanisms of DBPs

Since the detection of THMs in chlorinated drinking water, intensive research has been conducted to understand the reaction mechanisms of chlorine and other disinfectants with the NOM present in water.⁴⁷ Due to the complexity of NOM, a series of works have isolated different organic matter fractions using chemical or physical fractionation.⁴⁸ The influence of the different fractions on DBP formation has also been studied. One of the common methods employed for fractionating organic matter as a function of their hydrophobic or hydrophilic properties is based on the adsorption of the organic compounds present in water on XAD resins under acid, basic or neutral conditions.⁴⁸ It has frequently been reported that the hydrophobic fraction present in water constituted by humic substances accounts for 40-60 % of the DOC and is responsible to a large extent for DBP formation.⁴⁸ Typically, aromatic organic compounds have been identified as the main precursors of DBPs, such as THMs. In this line, a series of studies

using simple organic compounds have demonstrated that phenols and related compounds are important precursors of THMs, yielding about 0.1 – 1.1 moles of CHCl_3 per mole of substrate upon chlorination.⁴⁹⁻⁵¹ In particular, 1,3-dihydroxyaromatic compounds were found to be one of the most important precursors of THMs (0.67 – 0.95 mol Cl_2). Figure 5 shows one of the classical reaction pathways for the formation of chloroform from the chlorination of substituted 2,3-dihydroxyaromatics.⁵² The reaction is initiated by several electrophilic substitutions, followed by oxidative ring opening of the activated carbon in position 2, after which chloroform formation occurs via the haloform reaction.

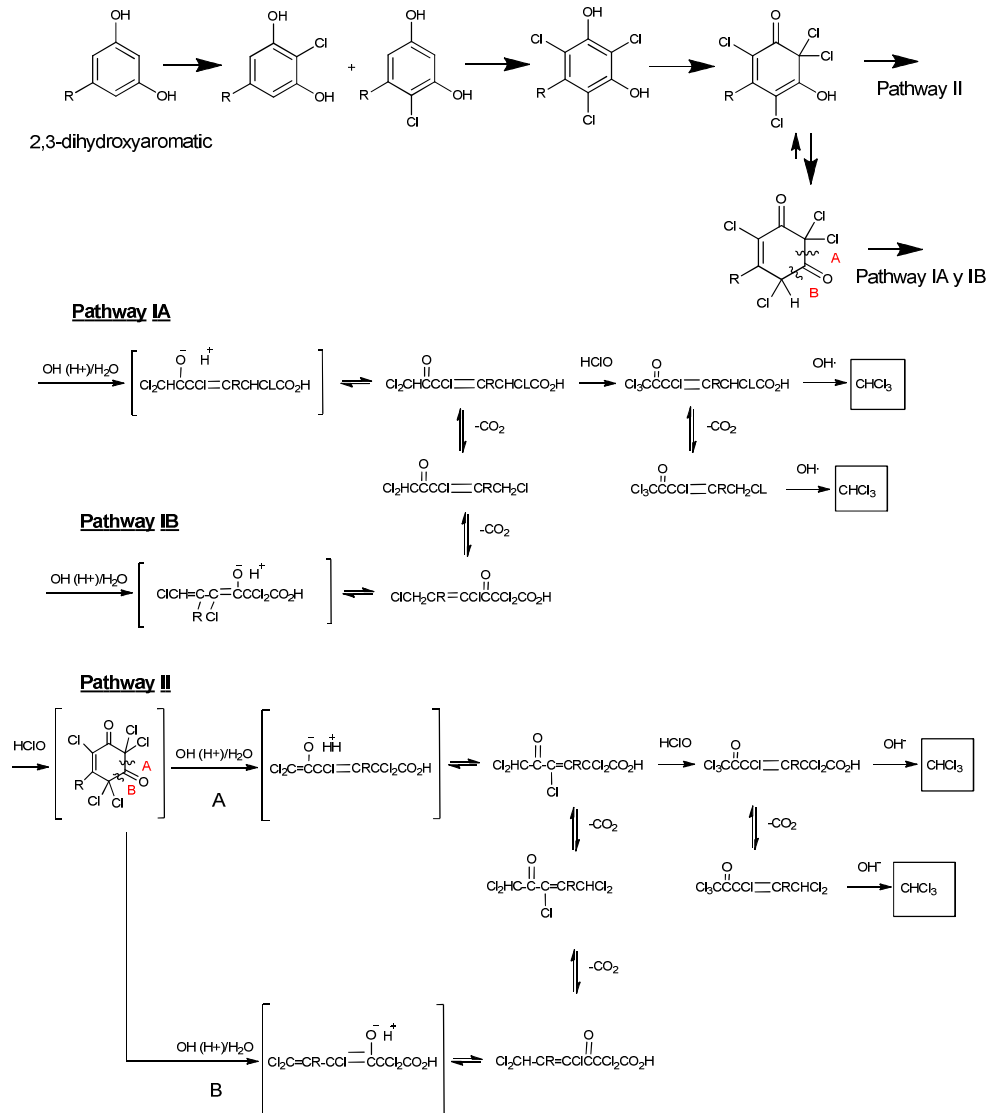


Figure 5. Reaction pathway during the chlorination of 2,3-dihydroxyaromatic substrates to chloroform. Adapted with permission from ref ⁵² (Boyce, S. D.; Hornig, F. J. Reaction pathways of trihalomethane formation from the halogena-

tion of dihydroxyaromatic model compounds for humic acid. *Environmental Science & Technology* 1983, 17 202-211). Copyright (2021) American Chemical Society.

To a lesser extent, other studies have reported that the main THM precursors present in natural fresh water characterized by small fractions of humic acids are the hydrophilic fractions.⁵³ In this context, several studies have revealed that β -dicarbonyl compounds such as 3-oxopentanedioic acid are also important precursors of THMs, yielding about 0.67 – 0.91 moles of CHCl_3 per mole of substrate upon chlorination.^{49-51,54} In a related study, Navalón et al reported that carbohydrates are significant precursors of THMs (~ 0.03 moles of CHCl_3 per mole of substrate) when these compounds represent an important fraction of the DOC.⁴³

Similarly, other studies have shown that N-containing organic compounds such as amino acids, peptides and proteins are important precursors of DBPs.^{20,55} For example, tryptophan has been reported as the amino acid with the highest chloroform formation ($147 \mu\text{g mg}^{-1} \text{C}$), followed by tyrosine ($47 \mu\text{g mg}^{-1} \text{C}$), while chloroform formation with the other amino acids is much lower.⁵⁶ In addition to THMs, the chlorination of amino acids results in the formation of HANs and HAAs. As an example, Figure 6 shows the chlorination pathway of aspartic acid leading to the formation of chlorinated aldehydes, acetonitriles and acetic acids. The aromatic amino acids together with aspartic acid have been found to be the most important precursors of HAAs. It has recently been reported that HANs can be hydrolyzed into haloacetamides as a new class of DBPs.

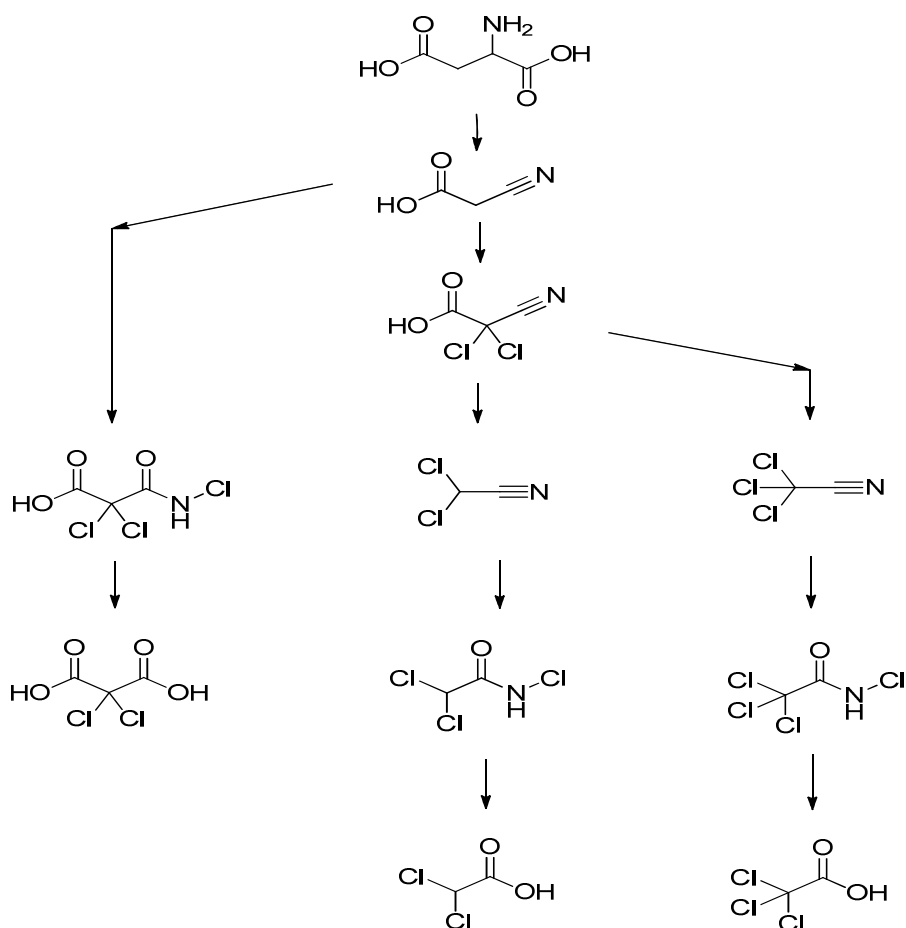


Figure 6. Chlorination pathway of aspartic acid. Adapted with permission from ref. ⁵⁶ (Hong, H. C.; Wong, M. H.; Liang, Y. Amino acids as precursors of trihalomethane and haloacetic acid formation during chlorination. *Archives environmental contamination and toxicology* 2009, 56, 638-645).

Some studies have also reported the formation of DBPs from POC present in natural waters. The cyanobacteria^{57,58} are the most frequently studied POC as DBP precursors. Thus, the chlorination of waters containing cyanobacteria such as *Microcystis Aurea* at high concentrations (1,000,000 cells/mL) have resulted in the formation of large amounts of C-DBPs, such as THMs and HAAS as well as of

N-DBPs such as HANs. However, most of these studies have reported DPB formation at pH 7 in the absence of bromide ions, conditions that are far removed from those of real fresh water.^{59,60}

1.4. Occurrence and origin of water pollutants

The presence of natural or anthropogenic contaminants in water has a negative impact on water quality.⁶¹ For example, the presence of naturally occurring geosmin and isoborneol produced by cyanobacteria in water destined for human consumption causes undesirable tastes and odors in water, even at concentrations of a few ng/L.⁶² However, most of the contaminants present in water are due to anthropogenic domestic, industry or agricultural activities.⁶¹ It is now well-known that agriculture has a negative impact on aquatic natural resources due to the use of pesticides and chemical fertilizers. Industrial effluents from different industrial processes are also an important source of a large variety of contaminants in water. Landfill leachates are also considered a common source of organic and inorganic water pollution. Domestic sewage effluents discharged into aquatic resources are another important source of organic contaminants, including the so-called emerging contaminants, such as pharmaceuticals or personal care products, among others. It should be mentioned that conventional DWTPs or UWWTPs are not designed to remove some toxic, non-biodegradable and recalcitrant organic compounds and so they are discharged with the wastewater effluent into natural aquatic resources. For all these reasons, new treatments are required in conventional water processes to ensure good water quality and comply with health regulations.

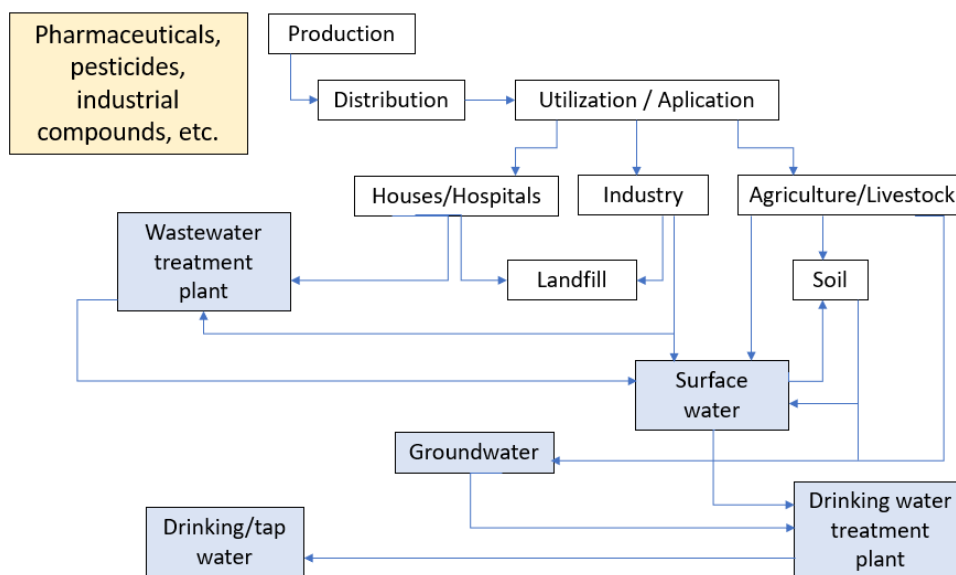


Figure 7. Representative sources and routes of pollutants in the aquatic environments. Adapted with permission from ref ⁶¹ (Barbosa, A. O.; Moreira, N. F. F.; Ribeiro, A. R.; Pereira, M. F. R.; Silva, A. M. T. Occurrence and removal of organic micropollutants: An overview of the watch list of EU Decision 2015/495. *Water Research*. 2016, *94*, 257-279).

1.5. Water quality regulations

In the context of DBPs, several regulations have restricted their maximum concentration since the detection of THMs in drinking water disinfected with chlorine and their recognized potential risk for human health. THMs were first regulated by the Environmental Protection Agency in the US in 1979, limiting their maximum concentration in drinking water to 100 µg/L. Since 1998 the same agency limited the maximum concentration of THMs and HAAs (sum of bromoacetic acid, dibromoacetic acid, chloroacetic acid, dichloroacetic acid, trichloroacetic acid) to 80 and 60 µg/L, respectively.

In Europe DBPs were first regulated by the Council Directive 98/83/EC of 3 November 1998 on the quality of water intended for human consumption. This directive was transposed to the different members of the EU and limited the maximum concentration of THMs to 100 µg/L. Directive EU 2020/2184 of the Council of 16 December 2020 on the quality of water intended for human consumption limited the concentration of HAAs (bromoacetic acid, dibromoacetic acid, chloroacetic acid, dichloroacetic acid, trichloroacetic acid) to 60 µg/L. In Spain the criteria for the quality of water intended for human consumption was laid down by Royal Decree 140/2003 of 7 February and its modifications, which limits the maximum concentration of bromates present in drinking water to 10 µg/L. Other organic compounds including pesticides or phenol derivatives are also regulated.

The USEPA, EU and WHO have also regulated other organic DBPs such as trichloroacetaldehyde, dichloroacetonitrile, dibromoacetonitrile, trichloroacetonitrile, cyanogen chloride, formaldehyde and 2,4,6-trichlorophenol. There is also an increasing interest in prioritizing unregulated DBPs in drinking water to minimize the risk to human health⁶³ by a method based on the concentration level found in finished drinking water, frequency and toxicity, among other possible factors. In particular, dichloroacetonitrile and trichloroacetaldehyde followed by trichloronitromethane have been identified as DBPs of critical and medium priority, respectively.

1.6. Control of DBPs and pollutants during water treatment

Although chlorine is one of the most generally used disinfectants in water treatment, it is not effective for disinfecting some resistant microorganisms frequently found in fresh water or urban wastewater.^{64,65} In addition, the chlorine added to water for disinfection reacts with the organic matter and generates undesirable DBPs, besides being unable to degrade many organic pollutants. Using ozone as disinfectant and oxidizing agent is one of the most cost-effective alternatives to chlorine in water treatment. In fact, ozone is a molecule with a

higher reduction potential ($E^0 = 2.07$ V vs NHE) than chlorine ($E^0 = 1.36$ V NHE) or hypochlorous acid ($E^0 = 1.49$ V NHE).⁶⁴ Ozone has greater disinfecting power than chlorine towards some resistant bacteria such as *Legionella Pneumophila* or protozoa such as *Giardia Lamblia* and *Cryptosporidium Parvum*, commonly found in fresh and urban wastewater.

Pre-oxidizing the organic matter present in water with ozone before chlorination is another general strategy for water treatment to minimize the formation of halogenated DBPs such as THMs or HAAs.^{64,65} In a DWTT this oxidation treatment is frequently applied to natural raw water while in UWWTTs oxidation is often a tertiary treatment. In order to understand the reasons for DBP control with ozone as oxidant, some studies have used simple and representative NOM probe molecules. Phenols are one of the preferred probe molecules in humic substances. The reaction of phenol with ozone forms oxidized products including hydroxylated aromatic compounds such as catechol or hydroquinone, which can be further oxidized to non-aromatic carboxylic derivatives. Ozone can directly oxidize phenol via electrophilic attack on the aromatic ring or with alkene intermediates via ozonolysis, which is the reaction mechanism by 1,3-dipolar addition of ozone, for example with an alkene, giving rise to the formation of an ozonide that usually decomposes in carbonyl compounds. This mechanism is favored at neutral and acidic pH values. At the same time, ozone can decompose in water into several reactive oxygen species (ROS) such as hydroxyl radicals in basic medium, favoring a free radical mechanism for the oxidation of phenol and its intermediates. If the ozonation is performed in such a way that the phenol is mostly oxidized into non-aromatic compounds, a subsequent chlorination will reduce the formation of THMs and HAAs. In contrast, the use of low molar ratios of ozone with respect to phenol will result in the formation of hydroxylated aromatic compounds as the main reaction products, which after chlorination will result in the formation of higher concentrations of THMs than only using chlorine. A large number of studies have reported the benefits of ozone to minimize DBP formation during water treatment under real conditions.

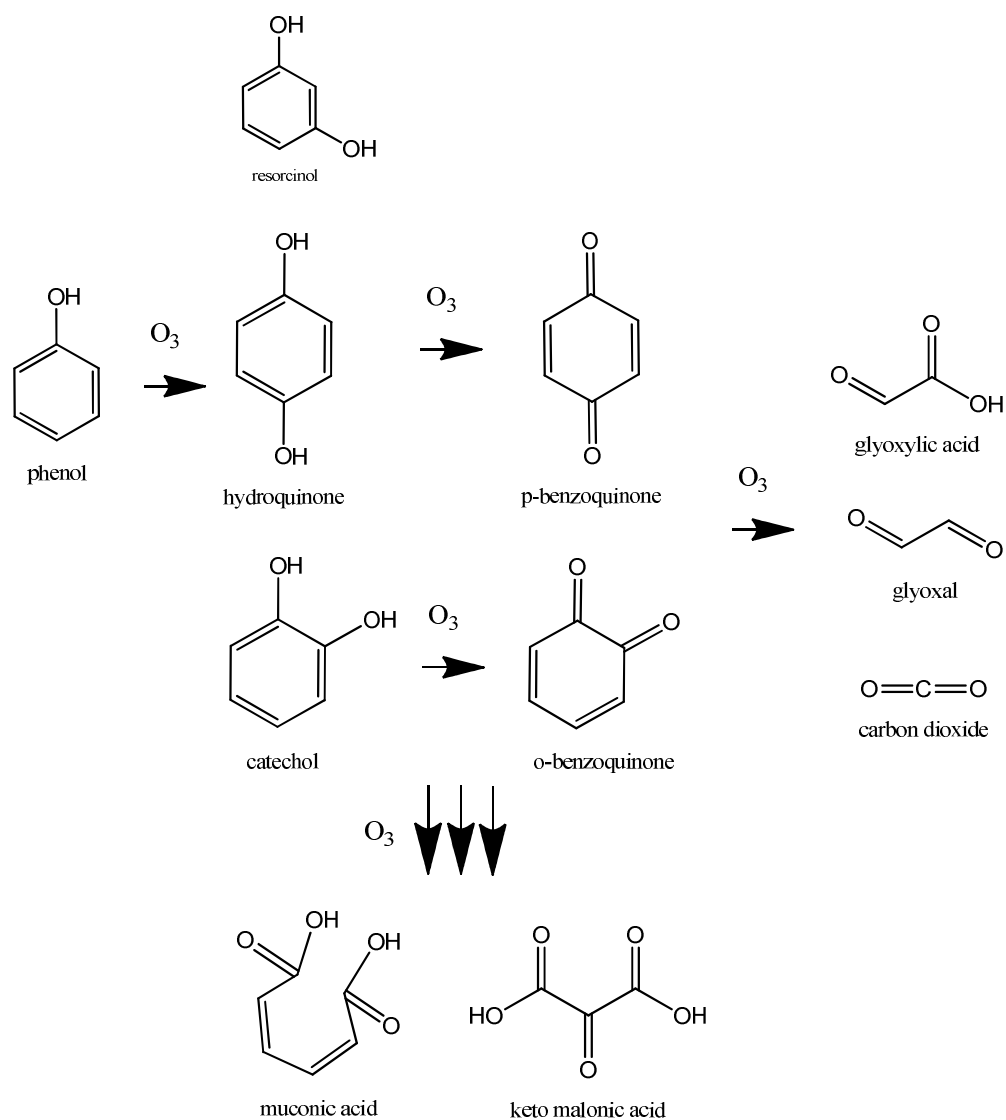


Figure 8. Phenol oxidation pathway using ozone as oxidant.

In contrast, some studies that have reported that a pre-oxidation of the organic matter present in water with ozone can increase the formation of some halogenated DBPs.⁵⁹ For example, a series of studies have reported that the pre-

ozonation of water containing large amounts of nitrogen precursors such as amino acids, proteins or even cyanobacteria can cause an adverse effect on the occurrence of halogenated DBPs. For example, a series of studies using water containing a high concentration of cyanobacteria such as *Microcystis Aurea* (>1,000,000 cells/mL) have demonstrated that the use of ozone as pre-oxidation results in an increase of THM formation.⁵⁸ Most of these studies have selected *Microcystis Aurea* as the DBP precursor due to its high ubiquity during alga blooms. The reasons, however, for this increased THM formation still remains unclear. Other related studies have reported that fresh water pre-ozonation can result in the formation of new halogenated DPBs. In particular, the ozonation of water containing organic amines followed by chlorination forms halonitroalkanes such as chloropicrin. Figure 9 shows the proposed reaction pathway to explain the formation of chloropicrin from the model compound N-methylethanolamine.⁶⁶ It is therefore necessary to further study the interaction of common disinfectants/oxidants added during water treatments and their possible impact on DBP formation.

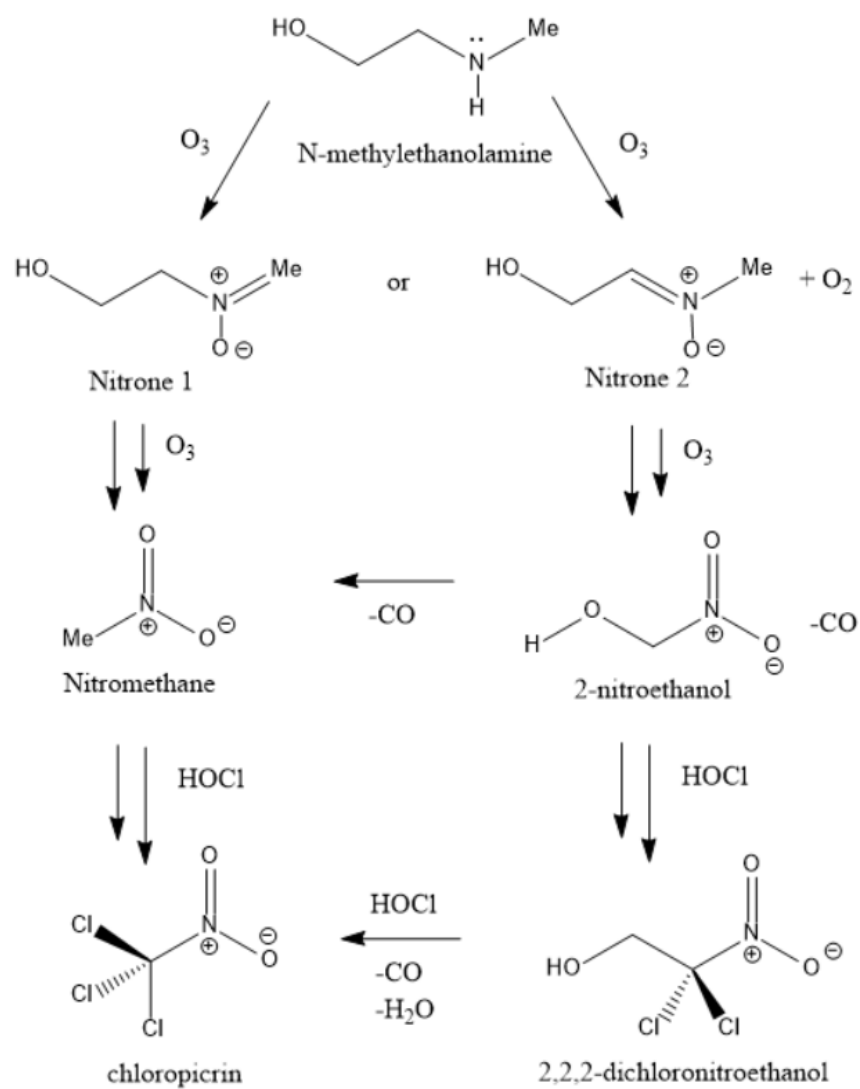


Figure 9. Reaction pathway of N-methylethanolamine with ozone and the formation of chlorinated nitro compounds. Reprinted (adapted) with permission from ref ⁶⁶ (McCurry, D. L.; Quay, A. N.; Mitch, W. A. Ozone promotes chloropicrin formation by oxidizing amines to nitro compounds. *Environmental Science & Technology* 2016, *50*, 1209–1217). Copyright (2021) American Chemical Society".

Oxidants such as ozone have also been used in water treatment for the degradation of organic pollutants.⁶⁷ For example, it has been reported that ozone is able to degrade a large number of organic compounds in water that contain functional groups rich in electrons, such as double bonds, activated aromatic rings or non-protonated organic amines. However, the presence of deactivating functional groups in the structure of the organic pollutant reduced the degradation and/or mineralization efficiency of the process. The degradation efficiency thus depends to a large extent on the pollutant structure and this oxidation process therefore cannot be regarded as a general water treatment.

With the above precedents, one of the most promising alternatives to overcome many of the drawbacks described above for conventional water treatments even though implemented with the use of ozone are the so-called advanced oxidation processes (AOPs).^{1,67,68}

1.7. Advanced oxidation processes

1.7.1. Generalities

AOPs comprise a series of technologies that consist of generating highly oxidizing ROS such as hydroxyl radicals ($\text{HO}\cdot$), hydroperoxide radicals ($\text{HOO}\cdot$), $^1\text{O}_2$ or sulphate radicals ($\text{SO}_4^{\cdot-}$) from oxidizing agents such as H_2O_2 , O_3 , potassium monopersulfate (PMS) or even from molecular O_2 .⁶⁹⁻⁷¹ AOPs are the most appropriate method of degrading or mineralizing contaminants from air, water or soil.⁷¹⁻⁷⁶ The mineralization process consists of transforming organic into inorganic compounds. The mineralization of an organic compound composed of carbon, hydrogen, nitrogen and sulfur atoms will form CO_2 , H_2O , NO_3^- or SO_4^{2-} , respectively. The oxidizing strength of these ROS is directly proportional to their reduction potential; the higher the reduction potential of the radical species the higher its oxidation capacity. Table 1 lists the reduction potential of some oxidants and radical species involved in many AOPs. Hydroxyl radicals and sulphate

radicals are among the most effective oxidizing agents. As one of the main operating costs associated with AOPs is the amount of oxidant (i.e. H₂O₂, O₃, MPS) required during the process, its concentration should be the minimum.

<i>Table 1. Relative reactivity of some oxidants species.^{77,78}</i>	
<i>Oxidant</i>	<i>Reduction Potential (E^o, V)</i>
SO ₄ ^{•-} /SO ₄ ²⁻	2.5-3.1
HO [•] , H ⁺ /H ₂ O	2.31
O ₃ ^{•-} , 2H ⁺ /H ₂ O, O ₂	1.80
O ₃ , 2H ⁺ /O ₂ , H ₂ O	2.08
H ₂ O ₂ , 2H ⁺ /2H ₂ O	1.77
HO ₂ [•] , H ⁺ /H ₂ O ₂	1.06
O ₂ ^{•-} , 2H ⁺ /H ₂ O ₂	0.94

In general, AOPs combine different oxidizing agents and/or catalysts and/or external energy, such as light, electricity or plasma.^{1,70,76} Figure 10 shows a simplified hierarchy of AOPs classified into two major homogeneous and heterogeneous groups that can be further sub-divided into several groups as a function of whether or not they use external energy, the presence or absence of a catalyst, etc.

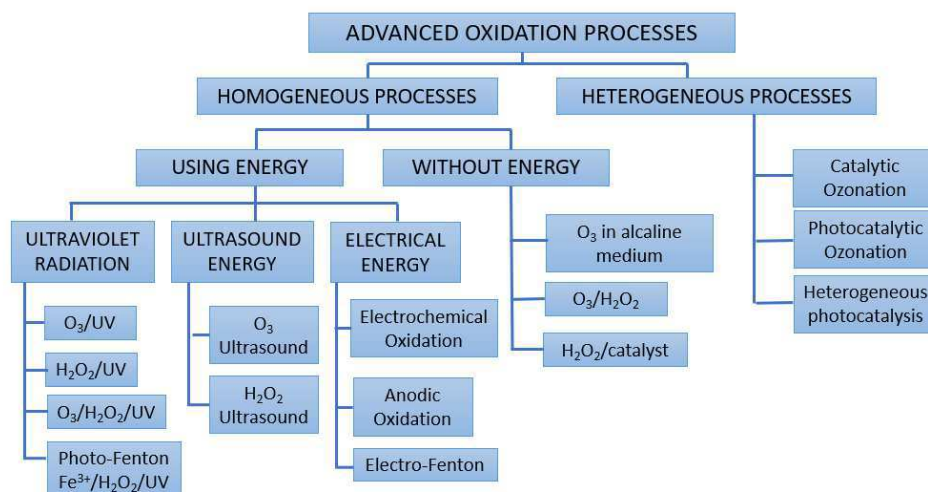


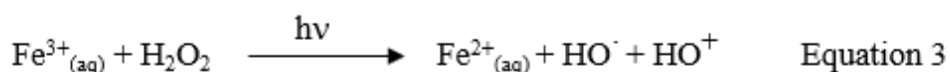
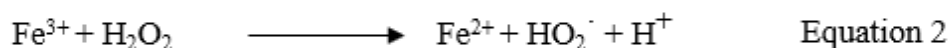
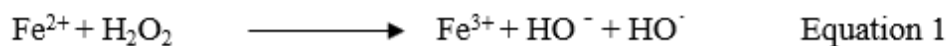
Figure 10. Classification of AOPs. Adapted with permission from ref.⁷⁹ (Mokhbi, Y.; Korichi, M.; Akchiche, Z. Combined photocatalytic and Fenton oxidation for oily wastewater treatment. *Applied Water Science*. 2019, 9, 35).

AOPs have found a large number of applications in water treatment. In the area of UWWTP they are frequently used as tertiary treatment for the degradation of recalcitrant, non-biodegradable and/or toxic organic pollutants such as aromatic compounds, among many others.⁴ They have also found wide application for the treatment of industrial wastewaters, either as a single wastewater treatment, for example during the removal of color from textile water before discharge into the public sewer or to natural aquatic resources. They are also used as a pre-oxidation treatment of industrial wastewater before a biological process. It is important to note that AOPs are more expensive than biological treatments and their optimization in terms of reagent consumption and external energy supply should thus be optimized. In the case of industrial wastewater with non-biodegradable and/or toxic organic matter, they are often used to increase the water biodegradability ($BOD_5/COD > 0.4$; BOD, biological oxygen demand; COD, chemical oxygen demand) and/or reduce its toxicity before a biological

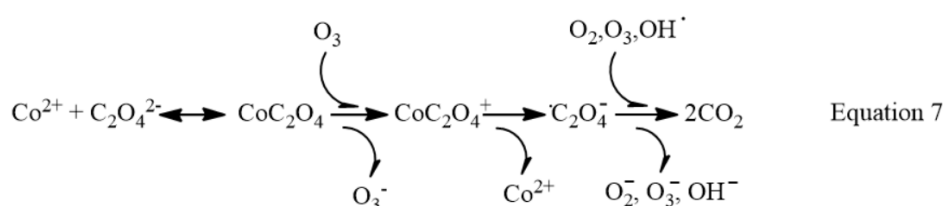
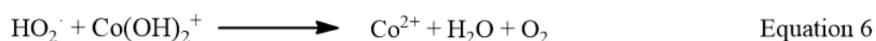
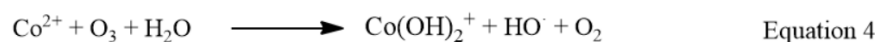
treatment.^{1,4} In all cases, the degree of oxidation required depends on the water quality required for other uses or discharge to the public sewer or natural aquatic resources. In the field of drinking water processes AOPs are commonly used as pre-oxidation treatments of raw fresh waters for disinfection of resistant pathogens, oxidation of NOM to minimize DBP or for pollutant degradation.

1.7.2. Catalytic AOPs

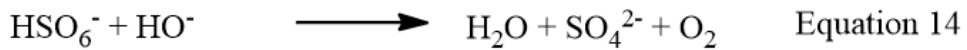
Some of the most cost-efficient catalytic AOPs are based on the use of transition metal salts (Fe^{2+} , Co^{2+} , Cu^{2+} etc.) as homogeneous catalysts for the activation of H_2O_2 , O_3 or PMS.^{71,76,80} In this context, the homogeneous Fenton reaction has been for decades one of most widely used AOP for wastewater treatments, even on a medium-large scale. This process consists of the reaction of Fe(II) salts with H_2O_2 at acidic pH (pH \sim 3) values leading to the formation of highly reactive hydroxyl radicals ($k = 70 \text{ M}^{-1} \text{ s}^{-1}$).⁸¹ The rate limiting step of the catalytic cycle is the regeneration of Fe(II) from Fe(III) and H_2O_2 (Equation 1-2), $k = 0.001 - 0.01 \text{ M}^{-1} \text{ s}^{-1}$.⁸¹ Interestingly, the use of UV-Vis irradiation during the Fenton process accelerates the regeneration of Fe(II) and thus the efficiency of the process (Equation 3), known as the photo-Fenton reaction. One of the major limitations of these processes that hamper their wider industrial application is the need to work at acidic pH values to avoid iron precipitation. In the case of the photo-Fenton process, acidic pH values are required to favor the speciation of iron in the form of active $\text{Fe}(\text{OH})^{2+}$ under UV-Vis irradiation.



O_3 can be used as an oxidant together with Co(II) salts as catalysts to overcome the limitation of pH operation during the (photo)Fenton processes.⁸⁰ This AOP can operate effectively in a range of pH values between 5 and 9 without cobalt precipitation.^{75,82} The development of AOPs based on O_3 as oxidant are of particular importance due to their easy large-scale implementation. In fact, ozone is widely employed in DWTP as well as in some WWTPs. As commented above, O_3 can react through ozonolysis or free radical pathways.⁸³ However, the degradation of electron-poor contaminants is not efficient using ozone as oxidant under real water conditions, basically room temperature and atmospheric pressure. Alternatively, the use of O_3 under strong basic conditions would favor the formation of hydroxyl radicals able to oxidize or mineralize any organic compound. However, as the required pH values above 12 again limit the application of the treatment, the decomposition of O_3 into ROS such as hydroxyl or hydroperoxyl radicals at neutral pH in the presence of catalysts based on transition metals such as Co(II) ions emerged as a good alternative to the use of molecular O_3 as oxidant (Eqs. 4-7). Oxalic acid is one of the preferred probe molecules to study catalytic ozonations for several reasons. On one hand oxalic acid together with some small organic acids such as acetic acid or formic acid are considered as recalcitrant compounds for some AOPs, while the reactivity of aqueous solutions of oxalic acid with ozone is negligible under the usual conditions of water treatment. The degradation of oxalic acid in an aqueous solution is thus an indirect test of the occurrence of a catalytic ozonation mechanism.



The generation of sulfate radicals from PMS as oxidant and Co(II) salts as homogeneous catalysts has recently emerged as a promising AOP.⁸⁰ One of the main advantage of this process is the selective formation of highly reactive radicals in a broad range of pH (Eqs. 8-11).^{78,82} PMS is an inorganic compound with a pK value of 9.4 in water, which favors its speciation at neutral pH in the form of HSO_5^- . PMS can therefore accept one electron leading to the selective formation of sulfate and/or hydroxyl radicals under these conditions (Eq. 12). Similar to H_2O_2 , basic pH values (> 10) favor the decomposition of PMS into molecular O_2 through an inefficient non-radical reaction mechanism for the degradation of pollutants (Eqs. 13-14).



Despite the good efficiencies obtained with the above-mentioned AOPs, the need to remove the transition metals used as homogeneous catalysts from the treated effluent to comply with water regulations hampers their application on an industrial scale. Numerous studies have described the negative impacts of the presence of transition metals on the environment and on human health.^{78,80} In general, the maximum permitted concentration of heavy metals in natural aquatic resources is of the order of $\mu\text{g/L}$. For example, the maximum concentration of iron in drinking water is $200 \mu\text{g/L}$.⁸⁴ As indicated above, AOPs are often used as a pre-treatment of industrial wastewater prior to biological treatment, so that even low concentrations of some transition metals can be toxic for the bacteria present in the biological reactor. Removal of these metals at the trace or micrograms-per-liter level can make the treatment process economically inviable. Among the different options to remove metals from water, chemical precipitation of metals in the form of oxides/hydroxides is a cost-effective and economically viable water treatment. However, the removal of transition metal ions by this technique may not achieve efficiencies high enough to comply with water regulations, and the formation of large amounts of metallic sludges that require

appropriate management may also limit the application of this process, especially on a large industrial scale.

1.8. AOPs based on heterogeneous transition metal catalysts.

As previously mentioned, heterogeneous catalysis is one of the most viable alternatives to overcome some of the drawbacks derived from homogeneous catalysis. In the literature there are a vast number of studies dealing with the development of heterogeneous catalysts based on transition metals for AOPs.^{76,85-87} Initially, the heterogeneous AOPs were developed using bulk metal oxides as catalyst. Later, the use of metal or metal oxide nanoparticles deposited on a high surface area resulted in highly active heterogeneous catalysts. The list of heterogeneous supports includes metal oxides, clays, zeolites, silicas or carbonaceous materials, among others.

From an industrial point of view, the use of cost-efficient carbon-based materials has been one of the preferred options for water treatment.⁸⁶ In general, carbon-based materials can combine several properties including low or negligible toxicity, good chemical resistance to acids and bases, large surface area and porosity that favors the adsorption of organic substances among others. In this context, activated carbons have for decades been the most suitable solids in water treatment as adsorbents and to a lesser extent as catalyst support. Currently millions of tons of activated carbon are used every year worldwide as adsorbents in large-scale water treatment processes. Activated carbons can be obtained from vegetable by-products such as wood, coconut and almond shells, hemp or any material with a high carbon content. The process of converting these materials to activated carbon is carried out through a double stage in which the first step consists of carbonizing the organic matter and subsequently subjecting it to a process of physical or chemical activation under controlled temperature and atmospheric conditions. The crushing, sieving and agglomeration of the carbonaceous material gives rise to activated carbon of different shapes and adsorption properties: powdered activated carbon ($\varnothing \leq 0.25$ mm) and granular activated carbon ($\varnothing \geq 0.25$ mm). This product has a large surface

area per unit volume due to its porosity and can be divided into micropores ($\varnothing \leq 2$ nm), mesopores ($\varnothing \geq 2$ nm ≥ 5 nm) and macropores ($\varnothing \geq 5$ nm). This porosity is responsible for retaining pollutants through adsorption thanks to Van der Waals forces. Generally, the greater the surface area of an activated carbon, the greater its ability to retain contaminants. It is estimated that the surface area of activated carbons can vary between 500 and 3000 m²/g. In the field of heterogeneous catalysis using activated carbons, the development of an appropriate carbon surface to stabilize catalytic sites has for years been an area of intense research. In general, the presence of oxygen-functional groups on the carbon surface is a requisite to stabilize active metal or metal oxide nanoparticles.

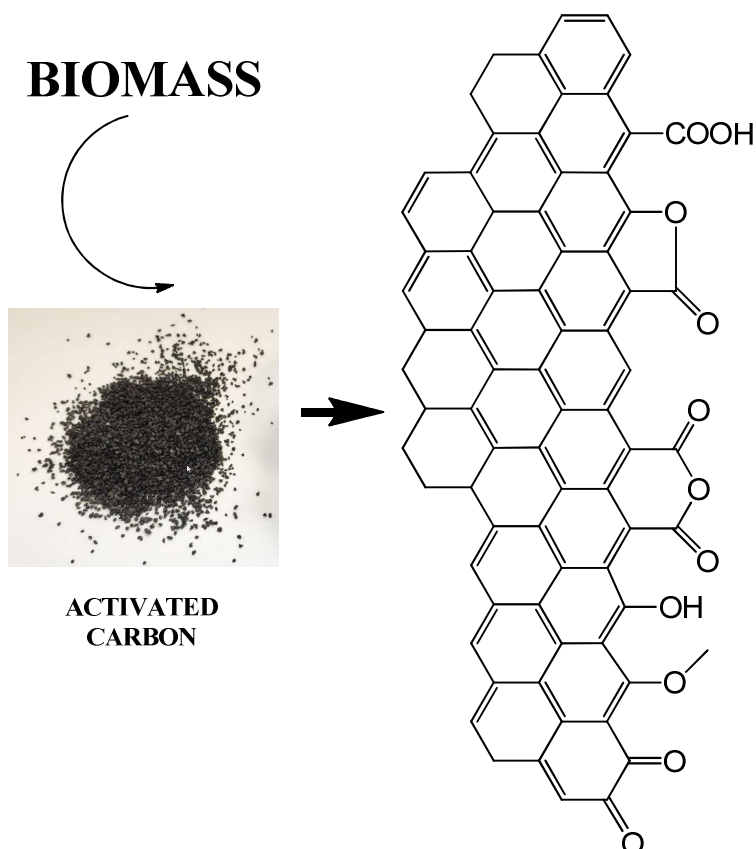


Figure 11. Simplified illustration of the possible functional groups present in an activated carbon^{88,89} (Yan, Q.-L.; Gozin, M.; Zhao, F.-Q.; Cohen, A.; Pang, S.-P. Highly energetic compositions based on functionalized carbon nanomaterials. *Nanoscale*. 2016, 8, 4799-4851) (Dreyer, D. R.; Jia, H.-P.; Bielawski, C. W. Graphene oxide: a convenient carbocatalyst for facilitating oxidation and hydration reactions. *Angewandte Chemie International Edition*. 2010, 6813-6816).

As in the case of homogeneous catalysis, some of the most active heterogeneous catalysts for the activation of O_3 ^{78,90} and PMS^{69,77,78} are based on cobalt oxides. The occurrence of cobalt leaching from the solid catalyst to the liquid phase limits the application of these processes on an industrial scale. Attempts to use other heterogeneous catalysts based on less toxic iron or copper species as reaction active sites resulted in less active materials while metal leaching still occurs.^{78,82} As one representative example, activated carbon supported cobalt oxide NPs prepared by the impregnation method have been reported as the heterogeneous catalyst for PMS activation. In this case however cobalt leaching from the solid catalyst to the liquid phase occurs. One of the possible reasons for the occurrence of cobalt leaching is the weak interaction of the cobalt sites with the support. With these precedents, further efforts towards increasing the interaction between the cobalt active sites and the carbon support are needed to increase the catalyst's stability.

1.9. AOPs based on carbocatalysts

As commented in previous sections, some of the most effective catalytic AOPs are based on the use of transition metals as active sites for the activation of oxidants such as H_2O_2 , O_3 or PMS.^{71,75,76} AOPs based on heterogeneous catalysis are preferred for homogeneous ones, especially for large-scale applications. AOPs based on heterogeneous catalysis facilitate the development of continuous flow processes with relatively easy recovery and reuse of the solid catalyst. One of the main limitations of the AOPs based on transition metal-based heterogeneous catalysts is the occurrence of metal leaching from the solid catalyst to the solution. This situation hampers its application in large scale water treatments and would result in the continuous contamination of aquatic resources with a negative impact for both the environment and human health.

For the sake of sustainability AOPs based on sustainable metal-free catalysts should be developed.^{89,91-94} In this context, carbon-based materials are among the most promising candidates for this purpose. The area of catalysis which deals with the use of carbon materials as catalysts is called carbocatalysis. Activated

carbons were among the first carbocatalysts reported. Years later, with the discovery of new carbon allotropes and carbon-based materials the number of carbocatalysis examples further increased (Figure 1a). The following sections summarize some of the representative examples of carbocatalysis with special emphasis on their use in AOPs.

1.10. Activated carbons as carbocatalysts for AOPs

The use of activated carbon-based materials obtained from biomass as carbocatalysts is one of the clearest examples of sustainable circular economy processes.^{91,95} These materials were among the first reported as carbocatalysts. In 1925 the use of charcoal as carbocatalyst was reported for the mineralization of oxalic acid using oxygen.⁹⁶ It was proposed to start the reaction by the oxidation of charcoal with oxygen, leading to the formation of peroxide intermediates that further oxidize oxalic acid to CO_2 and H_2O .

Years later, activated carbons were employed as metal-free catalysts to promote activation of oxidants such as H_2O_2 or O_3 , among others. For example, a series of studies have proposed the use of activated carbons as metal-free catalysts for H_2O_2 activation to hydroxyl radicals. In this process, one electron transfer process from reduced AC to H_2O_2 results in the formation of hydroxyl radicals.⁸⁶ Then, the catalytic cycle is restored by another H_2O_2 that acts as reductant, leading to the formation of hydroperoxyl radicals (Eqs 15-16). However, the complex composition of activated carbons makes it difficult to clearly identify the active sites of the process. In this context, attention should be paid to the possible role of metallic impurities present in the activated carbons as active sites of the catalytic process. In fact, several studies have reported that the observed catalytic activity for H_2O_2 decomposition is partially due to the presence of metal impurities such as iron, among others.



Activated carbons have been reported as metal-free ozonation catalysts. Several studies have shown a synergy between O_3 and activated carbons for pollutant degradation. In one of these studies the use of carbonaceous materials such as granular activated carbon have been employed as carbocatalyst to evaluate the efficiency of the catalytic ozonation process applied to a urban wastewater effluent.⁸³ The parameters evaluated include the reduction of TOC, COD and the degradation of some emerging pollutants in water such as paracetamol, diclofenac, sulfamethoxazoles, ketorolac and metoprolol. Interestingly, it was concluded that carbocatalytic ozonation is a more suitable technology than other water purification treatments (adsorption with activated carbon, oxidation with ozone, $\text{O}_3/\text{H}_2\text{O}_2$, UV-C photolysis, UV-C TiO_2 photocatalysis, TiO_2 solar photocatalysis) in terms of the TOC and COD reduction and elimination of emerging water pollutants. Importantly, the study concluded that carbocatalytic ozonation is the best technology in terms of energy consumption. Similar to the case of H_2O_2 , there is still some controversy regarding the active sites of the process. Some studies have proposed the presence of surface oxygen-functional groups such as hydroxyl and ketonic on the carbon surface can favor O_3 decomposition to ROS.⁹⁷

In addition to the use of activated carbons as metal-free catalysts for AOPs, these carbon-based materials also found application in the area of petrochemistry. In a series of studies, activated carbons with several functionalities have been reported as metal-free catalysts for the oxidative dehydrogenation of ethylbenzene to styrene. Based on the observed catalytic activity and the characterization data of the activated carbons it was proposed that the carbonyl/quinone functional groups present in the solid are the active sites of the process.(Pereira) More recently, our group has reported that activated carbons having

hydroquinone/quinone-like functional groups can be employed as active carbocatalysts to promote hydrazine activation (N_2H_4) and olefin reduction.⁹⁸

1.11. Graphite- and graphene-based materials as carbocatalysts for AOPs

In contrast to the use of activated carbons as carbocatalysts, the number of studies reporting the use of graphite-based materials as carbocatalysts is much lower.^{86,99} Graphite is a carbon allotrope constituted by stacking graphene layers. Each graphene layer is composed of sp^2 carbon hexagons arranged in a hexagonal lattice. The high crystallinity and relatively low surface area ($< 50 \text{ m}^2/\text{g}$) of graphite and therefore the absence of oxygen functional groups or defects such as dangling bonds have meant that this material has been rarely reported as metal-free catalyst.⁹⁹ In one of the few reported examples, graphite was employed as metal-free catalyst for H_2O_2 decomposition and 4-chlorophenol degradation. Regardless of its lower activity than activated carbon, it was proposed that H_2O_2 decomposition occurs in a similar way to the Fenton reaction.¹⁰⁰

The field of carbocatalysis greatly expanded after the discovery of graphene in 2004.¹⁰¹ As in the case of graphite, the absence of defects in graphene is one of the main reasons for its low efficiency as metal-free catalyst.^{94,102} However, the use of graphene-based materials with large amounts of oxygen functional groups, dangling bonds or heteroatoms make these materials promising candidates as carbocatalysts. In particular, graphene oxide and reduced graphene oxide have been the preferred solids in the area of carbocatalysis. One of the most widely used methods for the production of GO and rGO are based on the Hummers and Offeman method, followed by exfoliation and reduction (Figure 12). This method consists of the chemical oxidation of graphite by KMnO_4 in a strong acidic medium, followed by H_2O_2 . This oxidation process results in the formation of graphite oxide with a higher interlayer distance that facilitates the

exfoliation of the layers, for example by means of ultrasounds. In order to tune the amount and type of functional groups present in the GO a thermal ($T > 100$ °C) or chemical (N_2H_4 , $NaBH_4$) reduction process leading to the formation of reduced GO (rGO) can be carried out.

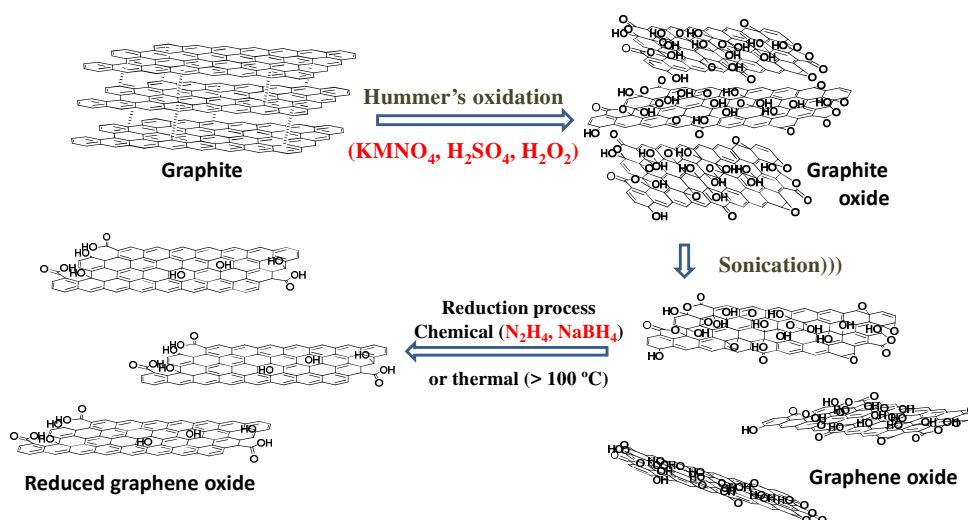


Figure 12. Illustration of GO and rGO preparation from graphite based on the Hummers and Offeman method followed by sonication and reduction. Adapted with permission from ref⁹⁴ (Navalon, S.; Dhakshinamoorthy, A.; Alvaro, M.; Garcia, H. Carbocatalysis by graphene-based materials. *Chemical reviews* 2014, *114*, 6179-6212). Copyright (2021) American Chemical Society.

The GO and rGO solids obtained have been employed as carbocatalysts for a large variety of reactions.⁹⁴ In particular, in 2010 Bielawski et al published a seminal work on the use of graphene oxide as metal-free catalyst for the oxidation of alcohols by O_2 (Figure 13).⁸⁹ It is important to note that this process had been described years earlier using noble metal-based catalysts such as

Au/CeO₂.¹⁰³ Since then, much progress has been made in the area of carbocatalysis using graphene-based materials.^{94,104} In the field of AOPs, rGO have been employed as metal-free catalyst for the activation of several oxidants. For example, our group reported the use of rGO as carbocatalyst for the Fenton reaction. Theoretical and experimental data were employed to propose that the presence of hydroquinone/quinone-based moieties in the rGO catalyst are the active site of the process (Figure 13).

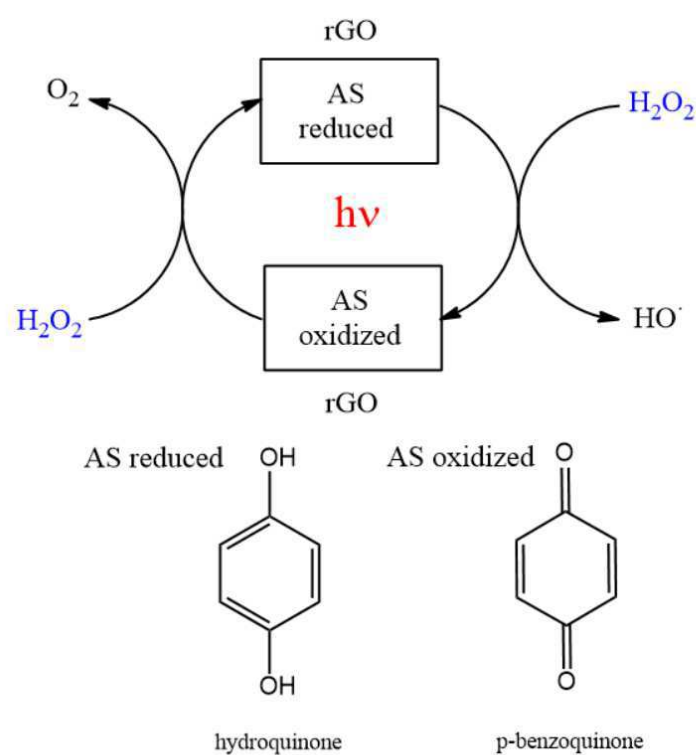


Figure 13. Mechanistic proposal for the generation of hydroxyl radicals using hydroquinone/p-benzoquinone model molecules for the active sites (AS) in rGO. Adapted with permission from ref ¹⁰⁵ (Espinosa, J. C.; Navalón, S.; Álvaro, M.; Garcia, H. Reduced graphene oxide as a metal-free catalyst for the light-assisted Fenton-like reaction. *ChemCatChem* 2016, 8, 2642 – 2648).

In a related study, rGO has been reported as metal-free ozonation catalyst for the degradation of p-hydroxybenzoic acid as water pollutant.¹⁰⁶ The presence of carbonyl groups present in the rGO were proposed to favor catalytic O₃ decomposition into ¹O₂ and O₂^{•-} radicals. The catalyst, however, rapidly deactivates upon reuse due to its partial oxidation, while reactivation can be carried out by submitting the catalyst to a pyrolysis at 300 °C.

1.12. Nanodiamonds as AOPs carbocatalysts

The use of nanodiamonds as heterogeneous catalysts has continuously grown since they become commercially available.¹⁰⁷ One of the preferred methods for the large scale production of nanodiamonds is the detonation method, which consists of the detonation of trinitrotoluene and cyclonite under defective oxygen conditions, leading to the formation of a diamond blend that contains about 75 % of nanodiamonds (< 10 nm) embedded in a carbon shoot matter (Figure 14). More specifically, the nanodiamonds are composed of a core of sp³ carbon network doped with nitrogen atoms (~2.5 wt%) and an outer shell of amorphous sp² carbon containing oxygen-functional groups. Purification of these NDs can be performed by chemical or thermal methods. Typically, the chemical method consists of oxidation of the carbon shoot matter with mineral acids such as H₂SO₄ or HNO₃, possibly combined with transition metals under harsh reaction conditions. The thermal methods consists of the controlled combustion of the diamond blend at temperatures higher than 400 °C to decompose the shoot matter while preserving the diamond core structure. In general, these NDs are frequently characterized by a BET surface area of about 260 m²/g, a total pore volume of 0.92 cm³/g and a negligible microporous volume.

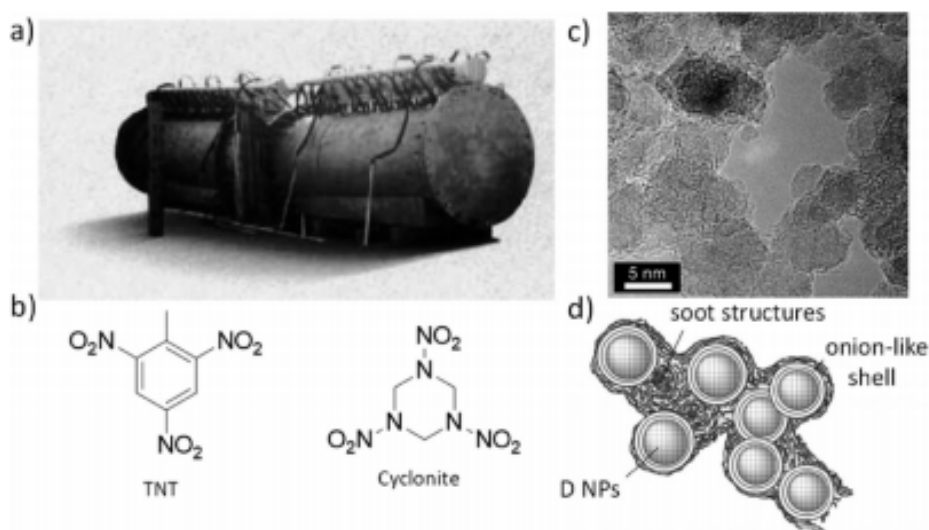


Figure 14. (a) Photograph of a reactor used for explosive detonation leading to the formation of D NPs. (b) Chemical structure of 1,3,5- trinitrotoluene (TNT) or cyclonite. (c) TEM image of D NPs and (d) illustration of D NPs embedded in carbon soot matter. Reprinted with permission from ref ¹⁰⁷ (Navalón, S.; Dhakshinamoorthy, A.; Álvaro, M.; García, H. Diamond nanoparticles in heterogeneous catalysis. *Chemistry of materials* 2020, 32, 4116-4143). Copyright (2021) American Chemical Society.

Purified NDs have been functionalized with several functionalities for the development of heterogeneous catalysis.¹⁰⁷ One of the common strategies for the development of heterogeneous catalysts based on NDs is their functionalization with oxygen functional groups. These oxygen functionalities have been used to deposit catalytic sites based on metal or metal oxide NPs, as well as covalently anchored organic molecules or metal complexes. In other approaches, the pyrolysis of commercial NDs at increased temperatures results in the decomposition and reconstitution of the amorphous outer ND shell, leading to the formation a crystalline sp^2 shell with some oxygen-functional groups.¹⁰⁸ Heating at temperatures above 1700 °C leads to the full transformation of NDs into onion-

like carbons constituted exclusively by sp^2 carbons. Interestingly, graphitized NDs have found several applications in some petrochemical reactions, fine chemicals and environmental applications. For example, a series of studies have shown that graphitized NDs can be used as carbocatalysts for the activation of oxidants commonly used in AOPs, such as peroxydisulfate or PMS as oxidants towards the formation of sulfate or hydroxyl radicals.¹⁰⁹ Based on theoretical and experimental calculations, it was proposed that the external graphitic sp^2 layers functionalized with oxygen functional groups such as ketonic can be the active sites of the process facilitating electron transfer towards the oxidant. Regardless of these observations, further studies are required to get a better insight into the use of graphitized NDs as metal-free AOP catalysts.

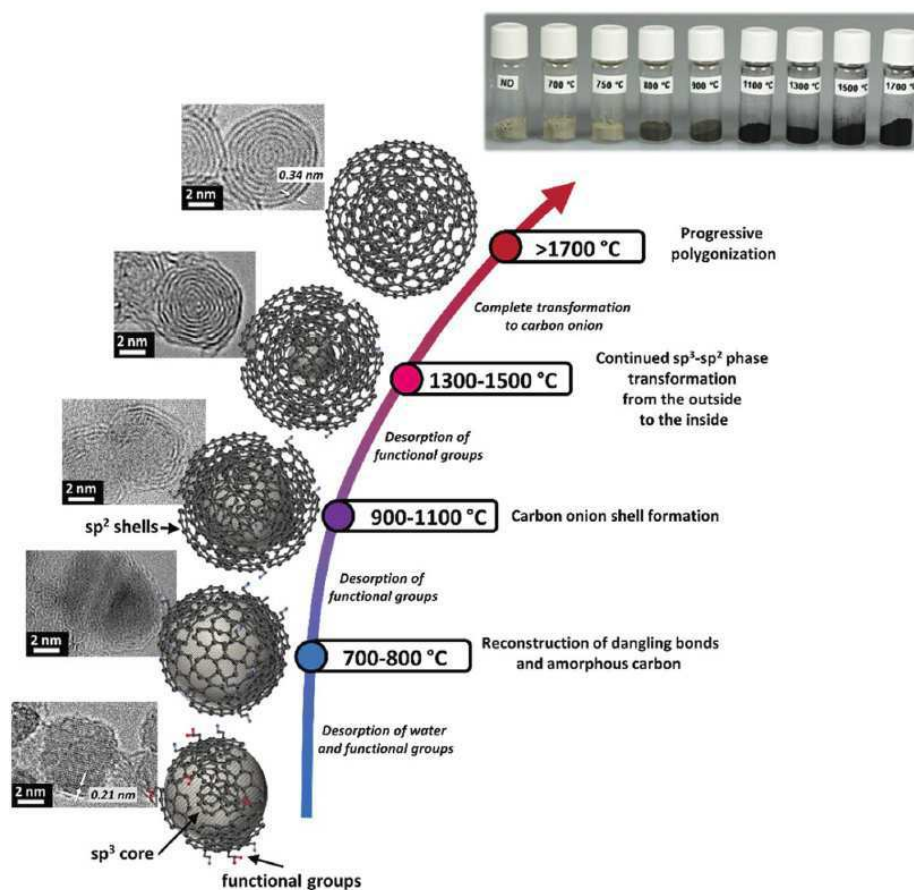


Figure 15. Formation of carbon onions by annealing of D NPs followed by TEM and optical microscopy. Reproduced from Ref. ¹⁰⁸ (Zeiger, M.; Jäckel, N.; Mochalin, V. N.; Presser, V. *Review: carbon onions for electrochemical energy storage. Journal of Materials Chemistry A* 2016, 4, 3172–3196) permission from the Royal Society of Chemistry.

1.13. References

- (1) Esplugas, S.; Ollis, D. F. *J. Adv. Ox.* **1997**, *2*, 197-204.
- (2) Mantzavinos, D.; Psillakis, E. *J. Chem. Technol. Biot.* **2004**, *79*, 431-454.
- (3) Luo, Y.; Guo, W.; Ngo, H. H.; Nghiem, L. D., IbneyHai, F.I.; Zhang, J.; Liang, S.; Wang, X. C. *Sci. Tot. Environ.* **2014**, *473-474*, 619-641.
- (4) Oller, I.; Malato, S.; Sánchez-Pérez, J. A. *Sci. Total Environ.* **2011**, *409*, 4141-4166.
- (5) Petrović, M.; Gonzalez, S.; Barceló, D. *Trends Anal. Chem.* **2003**, 685-669.
- (6) Snyder, S. A.; Westerhoff, P.; Yoon, Y.; Sedlak, D. L. *Env. Eng. Sci.* **2003**, *20*, 449-469.
- (7) Hall, E. L.; Dietrich, A. M. *Opflow* **2000**, *26*, 46-49.
- (8) Jadhav, A. S. *Int. J. Sci. Environ. Technol.* **2014**, *3*, 1415-1418.
- (9) McGuire, M. J. *J. Am. Water. Works. Ass.* **2006**, *98*, 123-149.
- (10) Collivignarelli, M. C.; Abbà, A.; Benigna, I.; Sorlini, S.; Torretta, V. *Sustainability* **2018**, *10*, 86.
- (11) Brezonik, P. L.; Arnold, W. A. *Environ. Sci. Technol* **2012**, *46*, 5650-5657.
- (12) Tzanakakis, V. E.; Paranychianaki, N. V.; Angelakis, A. N. *Water Supply* **2007**, *1*, 67-75.
- (13) Lofrano, G.; J., B. *Sci. Total Environ.* **2010**, *408*, 5254-5264.
- (14) Chaukura, N.; Marais, S. S.; Moyo, W.; Mbali, N.; Thakalekoala, L. C.; Ingwania, T.; Mamba, B. B.; Jarvis, P.; Nkambule, T. T. I. *J. Environ. Chem. Env.* **2020**, *8*, 103659.

- (15) Gilca, A. F.; Teodosiu, C.; Fiore, S.; Musteret, C. P. *Chemosphere* **2020**, *259*, 27476.
- (16) Rook, J. J. *Water Treat. Examin.* **1974**, *23* 234-43.
- (17) Bellar, T. A.; Lichtenberg, J. J.; Kroner, R. C. *J. Am. Water Works Assoc.* **1974**, *66* 703-706.
- (18) Hebert, A.; Forestier, D.; Lenes, D.; Benanou, D.; Jacob, S.; Arfi, C.; Lambalez, L.; Levi, Y. *Ocean Coast. Manag.* **2010**, *44*, 3147-3165.
- (19) Alexandrou, L.; Meehan, B. J.; Jones, O. A. H. *Sci. Total Environ.* **2018**, *637-638*, 1607-1616.
- (20) Ding, S.; Chu, W. *Trends Environ. Anal. Chem.* **2017**, *14*, 19-27.
- (21) Weinberg, H. *Anal. Chem.* **1999**, *71* 801-808.
- (22) Hrudey, S. E. *Water Res.* **2009**, *43*, 2057-2092.
- (23) Medeiros, L. d. C.; de Alencar, F. L. S.; Navoni, J. A.; de Araujo, A. L. C.; Viviane Souza do Amaral. *Environ Sci Pollut Res.* **2019**, *26*, 5316-5332.
- (24) Stalter, D.; O'Malley, E.; von Guntenbc, U.; Escher, B. I. *Environ. Sci Wat. Res.* **2020**, *6*, 2341-2351.
- (25) Aggazzotti, G.; Fantuzzi, G.; Righi, E.; Predieri, G. *Sci. Total Environ.* **1998**, *217* 155-163.
- (26) Benoit, F.; Nicolidakis, H.; Cardinall, K.; Alleyne, C.; Mori, B. *Proc. Am. Soc. Mass Spectrom.* **1997**, 212-18.
- (27) Levesque, B.; Ayotte, P.; Tardif, R.; Charest-Tardif, G.; Dewailly, E.; Prud'Homme, D.; Gingras, G.; Allaire, S.; Lavoie, R. *J. Toxicol. Environ. Health* **2000**, *61*, 225-243.
- (28) Villanueva, C. M.; Cantor, K. P.; Grimalt, J. O.; Castaño-Vinyals, G.; Malats, N.; Silverman, D.; Tardon, A.; Garcia-Closas, R.; Serra, C.; Carrato, A. *Occup. Environ. Med.* **2006**, *63* 273-77.
- (29) Villanueva, C. M.; Cantor, K. P.; Grimalt, J. O.; Malats, N.; Silverman, D.; Tardon, A.; Garcia-Closas, R.; Serra, C.; Carrato, A.; Castano-Vinyals, G.; Marcos,

R.; Rothman, N.; Real, F. X.; Dosemeci, M.; Kogevina, M. *Am. J. Epidemiol.* **2007**, *165* 148-156.

(30) Yang, L.; Chen, X.; She, Q.; Cao, G.; Liu, Y.; W.-C. Chang, V. W.-C.; Tang, C. Y. *Environ. Int.* **2018**, *121* 1039-1057.

(31) Nieuwenhuijsen, M. J.; Toledano, M. B.; Eaton, N. E.; Fawell, J.; Elliott, P. *Occup. Environ. Med.* **2000**, *57*, 73-85.

(32) Hunter, E. S. I.; Tugman, J. A. *Teratology* **1995**, *52* 317-323.

(33) Plewa, M. J.; Wagner, E. D.; Kim, A. C.; Nelson, R.; Richardson, S. D. *Environ. Mol. Mutagen* **2003**, *51*, 871-878.

(34) Singer, P. C. *J. Am. Water Works Assess* **2006**, *98*, 73-79.

(35) Kimura, S. Y.; Komaki, Y.; Plewa, M. J.; Marineas, B. J. *Environ. Sci. Technol.* **2013**, *47*, 12382-12390.

(36) Zhang, Y.; Chu, W.; Yao, D.; Yin, D. *J. Environ. Sci.* **2017**, *58*, 322-330.

(37) Watson, K.; Shaw, G.; Leusch, F. D. L.; Knight, N. L. *Water Res.* **2012**, *46* 6069.

(38) Adusei-Gyamfi, J.; Ouddane, B.; Rietveld, L.; Cornard, J.-P.; Criquet, J. *Water Res.* **2019**, *160*, 130-147.

(39) Artifon, V.; Zanardi-Lamardo, E.; Fillmann, G. *Sci. Total Environ.* **2019**, *649*, 1620-1635.

(40) Pan, Y.; Li, H.; Zhang, X.; Li, A. *Trends Environ. Anal. Chem.* **2016**, *12*, 23-30.

(41) Stevenson, F. J. *Humus Chemistry: Genesis, Composition, Reactions.* Wiley, New York **1994**.

(42) Bolto, B. A. *Prog. Pol. Sci.* **1995**, *20*, 987-1041.

(43) Navalon, S.; Alvaro, M.; Garcia, H. *Water Res.* **2008**, *42*, 3990-4000.

(44) Alves Filho, E. G.; Alexandre E Silva, L. M.; Ferreira, A. G. *Magn. Reson. Chem.* **2015**, *53*, 648-657.

(45) McPhedran, K. N.; Seth, R. *Water Environ. Res.* **2016**, *88*, 308-317.

- (46) Navalon, S.; Alvaro, M.; Garcia, H. *Environ. Technol.* **2011**, *32*, 295-306.
- (47) Kimura, S. Y.; Ortega-Hernandez, A. *Curr. Opin. Environ. Sci. Health* **2019**, *7*, 61-68.
- (48) Chow, A. T.; Gao, S.; Dahlgren, R. A. *J. Water. Supply Res. T.* **2005**, *54*, 475-507.
- (49) Dickenson, E.; Summers, R. S.; Croué, J.-P.; Gallard, H. *Environ. Sci. Technol.* **2008**, *42*, 3226-3233.
- (50) Gallard, H.; Gunten, U. *Environ. Sci. Technol.* **2002**, *36*, 884-890.
- (51) Jolley, R. L.; Brungs, W. A.; Cumming, R. B.; Jacobs, V. A. *Water chlorination: environmental impact and health effects, vol. 3. Ann Arbor Science Publishers, Michigan. (1980).*
- (52) Boyce, S. D.; Hornig, F. J. *Environ. Sci. Technol.* **1983**, *17* 202-211.
- (53) Hwang, C. J.; Sclimenti, M. J.; Krasner, S. W. *ACS Symposium Series* **2000**, 761.
- (54) Reckhow, D. A.; Singer, P. C.; Malcolm, R. L. *Environ. Sci. Technol.* **1990**, *24*, 1655-1664.
- (55) Hureiki, L.; Crou, J. P.; Legube, B. *Water Res.* **1994**, *28*, 2521-2531.
- (56) Hong, H. C.; Wong, M. H.; Liang, Y. *Arch. Environ. Contam. Toxicol.* **2009**, *56*, 638-645.
- (57) Daly, R.; Ho, L.; Brookes, J. D. *Environ. Sci. Technol.* **2007**, *41*, 4447-4453.
- (58) Fang, J.; Ma, J.; Yang, X.; Shang, C. *Water Res.* **2010**, *44*, 1934-1940.
- (59) Plummer, J. D.; Edzwald, J. *Environ. Sci. Technol.* **2001**, *35*, 3661-3668.
- (60) Shi, X.; Bi, R.; Yuana, B.; Liao, X.; Zhou, Z.; Li, F.; Sun, W. *Sci. Tot. Environ.* **2019**, *656*, 1063-1070.

- (61) Barbosa, A. O.; Moreira, N. F. F.; Ribeiro, A. R.; Pereira, M. F. R.; Silva, A. M. T. *Water Res.* **2016**, *94*, 257-279.
- (62) Young, W. F.; Horth, H.; Crane, R.; Ogden, T.; Arnott, M. *Water Res.* **1996**, *30*, 331-340.
- (63) Mian, H. R.; Hu, G.; Hewage, K.; Rodriguez, M. J.; Sadiq, R. *Water Res.* **2018**, *15*, 112-131.
- (64) Deborde, M.; von Gunten, U. *Water Res.* **2008**, *42*, 13-51.
- (65) von Gunten, U. *Water Res.* **2003**, *37*, 1469-1487.
- (66) McCurry, D. L.; Quay, A. N.; Mitch, W. A. *Environ. Sci. Technol.* **2016**, *50*, 1209-1217.
- (67) Esplugas, S.; Bila, D. M.; Krause, L. G. T.; Dezotti, M. *J. Hazard. Mater.* **2007**, *149*, 631-642.
- (68) Matilainen, A.; Sillanpää, M. *Chemosphere* **2010**, *80*, 351-365.
- (69) Ghanbari, F.; Moradi, M. *Chem. Eng. J.* **2017**, *310*, 41-62.
- (70) Malato, S.; Fernández-Ibáñez, P.; Maldonado, M. I.; Blanco, J.; Gernjak, W. *Cat. Today* **2009**, *147*, 1-59.
- (71) Pignatello, J. J.; Oliveros, E.; MacKay, A. *Crit. Rev. Env. Sci. Tec.* **2006**, *36*, 1-84.
- (72) Ayoub, K.; van Hullebusch, E. D.; Cassir, M.; Bermond, A. *J. Hazard. Mater.* **2010**, *178*, 10-28.
- (73) Cheng, M.; Zeng, G.; Huang, D.; Lai, C.; Xu, P.; Zhang, C.; Liu, Y. *Chem. Eng. J.* **2016**, *298*, 582-598.
- (74) Demeestere, K.; Dewulf, J.; Van Langenhove, H. *Crit. Rev. Environ. Scie. Technol.* **2007**, *37*, 489-538.
- (75) Neyens, E.; Baeyens, J. *J. Hazard. Mater.* **2003**, *98*, 33-50.
- (76) Pera-Titus, M.; García-Molina, V.; Baños, M. A.; Giménez, J.; Esplugas, S. *Appl. Catal. B-Environ.* **2004**, *47*, 219-256.

- (77) Anipsitakis, G. P.; Stathatos, E.; Dionysiou, D. D. *J. Phys. Chem. B* **2005**, *109*, 13052-13055.
- (78) Hu, P.; Long, M. *Appl. Catal. B. Environ.* **2016**, *181*, 103-117.
- (79) Mokhbi, Y.; Korichi, M.; Akchiche, Z. *Appl. Water Sci.* **2019**, *9*, 35.
- (80) Ushania, U.; Lu, X.; Wang, J.; Zhang, Z.; Dai, J.; Tan, Y.; Wang, S.; Li, W.; Niu, C.; Cai, T.; Wang, N.; Zhen, G. *Chem. Eng. J.* **2020**, *402*, 126232.
- (81) Navalon, S.; Alvaro, M.; Garcia, H. *Appl. Catal. B. Environ.* **2010**, *99*, 1-26.
- (82) Rastogi, A.; Al-Abed, S. R.; Dionysiou, D. D. *Appl. Catal. B* **2009**, *85*, 171-179.
- (83) Beltrán, F. J.; Rivas, F. J.; Montero-de-Espinosa, R. *Ind. Eng. Chem. Res.* **2003**, *42*, 3210-3217.
- (84) Spanish Royal Decree 140/2003 of 7 february by wich health criteria for the quality of water intended for human consumption are established.
- (85) Dhakshinamoorthy, A.; Navalon, S.; Alvaro, M.; Garcia, H. *ChemSusChem* **2012**, *5*, 46-64.
- (86) Navalon, S.; Dhakshinamoorthy, A.; Alvaro, M.; Garcia, H. *ChemSusChem* **2011**, *4*, 1712-1730.
- (87) Navalon, S.; Dhakshinamoorthy, A.; Alvaro, M.; Garcia, H. *Coord. Chem. Rev.* **2016**, *312*, 99-148.
- (88) Yan, Q.-L.; Gozin, M.; Zhao, F.-Q.; Cohen, A.; Pang, S.-P. *Nanoscale* **2016**, *8*, 4799-4851.
- (89) Dreyer, D. R.; Jia, H.-P.; Bielawski, C. W. *Angew. Chem., Int. Ed.* **2010**, 6813-6816.
- (90) Kasprzyk-Hordern, B.; Ziółek, M.; Nawrocki, J. *Appl. Catal. B: Environ.* **2003**, *46*, 639-669.
- (91) Titirici, M.-M.; Antonietti, M. *Chem. Soc. Rev.* **2010**, *39*, 103-116.
- (92) Albero, J.; Garcia, H. *J. Mol. Catal. A-Chem.* **2015**, *408*, 296-309.
- (93) Dreyer, D. R.; Bielawski, C. W. *Chem. Sci.* **2011**, *2*, 1233-1240.

- (94) Navalon, S.; Dhakshinamoorthy, A.; Alvaro, M.; Garcia, H. *Chem. Rev.* **2014**, *114*, 6179-6212.
- (95) Jain, A.; Balasubramanian, R.; Srinivasan, M. P. *Chem. Eng. J.* **2016**, *283*, 789-805.
- (96) Rideal, E. K.; Wright, W. M. *J. Chem. Soc. Trans.* **1925**, *127*, 1347-1357.
- (97) Wang, Y.; Duan, X.; Xie, Y.; Sun, H.; Wang, S. *ACS Catal.* **2020**, *10*, 13383-13414.
- (98) Espinosa, J.; Navalón, S.; Alvaro, M.; Dhakshinamoorthy, A.; García ómez, H. *ACS Sustain. Chem. Eng* **2018**, *6*, 5607-5614.
- (99) Navalon, S.; Dhakshinamoorthy, A.; Alvaro, M.; Antonietti, M.; García, H. *Chem. Soc. Rev.* **2017**, *46*, 4501-4529.
- (100) Lücking, F.; Köser, H.; Jank, M.; Ritter, A. *Water Res.* **1998**, *32*, 2607-2614.
- (101) Novoselov, K. S.; Geim, A. K.; Morozov, S. V.; Jiang, D.; Zhang, Y.; Dubonos, S. V.; Grigorieva, I. V.; Firsov, A. A. *Science* **2004**, *306*, 666-669.
- (102) Navalón, S.; Ong, W.-J.; Duan, X. *Processes* **2020**, *8*, 672.
- (103) Corma, A.; Garcia, H. *Chem. Soc. Rev.* **2008** *37*, 2096-2126.
- (104) Navalon, S.; Herance, J. R.; Alvaro, M.; García, H. *Mater. Horiz.* **2018**, *5*, 363-378.
- (105) Espinosa, J. C.; Navalón, S.; Álvaro, M.; Garcia, H. *ChemCatChem* **2016**, *8*, 2642 – 2648.
- (106) Wang, Y.; Xie, Y.; Sun, H.; Xiao, J.; Cao, H.; Wan, S. *ACS Appl. Mater. Interfaces* **2016**, *8*, 9710-9720.
- (107) Navalón, S.; Dhakshinamoorthy, A.; Álvaro, M.; García, H. *Chem. Mater.* **2020**, *32*, 4116-4143.

Chapter 1. Introduction

(108) Zeiger, M.; Jäckel, N.; Mochalin, V. N.; Presser, V. J. *Mater. Chem. A* **2016**, *4*, 3172–3196.

(109) Duan, X.; Sun, H.; Wang, S. *Acc. Chem. Res.* **2018**, *51*, 678-687.

Chapter 2

Objectives

The aim of the present Thesis is the use of ozone and peroxymonosulfate as oxidants in water treatments for disinfection by-products control or pollutant degradation.

The specific objectives of each of the chapters of this Thesis are as follows:

To study the impact of the presence of three common cyanobacteria present in surface waters (*Microcystis aeruginosa*, *Anabaena aequalis* and *Oscillatoria tenuis*) on DBP formation when chlorinated with or without pre-ozonation. A relatively low cell concentration of cyanobacteria will be employed (10,000 cells/mL). The specific DBPs will include THMs, HAAs, HAN, HKs, trichloronitromethane and bromates. The influence of the presence or absence of bromides as well as the pH of the aqueous solutions will be evaluated for chlorine demand and DBP formation.

Development of a highly active and stable catalyst based on cobalt nanoparticles supported on functionalized commercial activated carbon (Norit) for PMS activation and aqueous pollutant degradation. Activated carbon function-

alization will be carried out using either thermal or chemical treatments. The influence of several parameters such as solution pH, PMS dosage and the reaction temperature on the resulting catalytic activity will be studied. Catalyst stability will be studied by performing several consecutive reuses. The selective quenching experiment and EPR measurements of spin trap adducts will be employed to characterize the reactive oxygen species involved in the catalytic process.

Development of a highly active and stable metal-free ozonation catalyst based on a high surface area graphite material selectively functionalized at the edges with hydroxyl groups. The catalytic activity of this material will be compared with that of other carbon-based catalysts including the parent high surface area graphite, commercial activated carbon (Norit), commercial multiwall carbon nanotubes, commercial diamond nanoparticles, graphene oxide or reduced graphene oxide as well as benchmark ozonation catalyst such as Co_3O_4 or Fe_2O_3 material. Catalyst stability upon reuse will be evaluated. A catalyst reactivation procedure will be designed and applied if necessary. The catalytic mechanism will be studied by using selective quenching experiments and by EPR measurements of spin-trap adducts.

Development of defective hybrid sp^2/sp^3 core-shell nanodiamonds as metal-free ozonation catalysts. These nanodiamonds will be prepared by thermal annealing of commercial diamond nanoparticles in a tubular oven. As in the previous objective, catalyst stability upon reuse will be studied. A catalyst reactivation procedure will be also designed. The catalytic reaction mechanism will be assessed by using selective quenching experiments and EPR measurements.

Chapter 3

Impact of chlorination and pre-ozonation on disinfection by-products formation from aqueous suspensions of cyanobacteria: *Microcystis aeruginosa*, *Anabaena aequalis* and *Oscillatoria tenuis*

3.1 Introduction

Cyanobacteria, traditionally identified as blue-green algae, occur worldwide in fresh and marine natural aquatic ecosystems exposed to sunlight, allowing the operation of oxygenic photosynthesis necessary for the metabolic synthesis of carbohydrates from CO₂ (Merel et al., 2013). One of the main concerns related with the presence of cyanobacteria in water is the production of toxins for aquatic or terrestrial organisms, animals and humans with unwanted effects by contact or ingestion, including hepatotoxicity and tumor promotion (Carmichael

and Boyer, 2016, Codd et al., 2016 Falconer, 1991; Frazier et al., 1998; Hawkins et al., 1985; Jochimsen et al., 1998; Turner et al., 1990). In the conventional drinking water treatment, the presence of cyanobacteria bloom impedes the settling process and increases the demand of oxidant employed as water disinfectant during the treatment (Chen et al., 2017).

In addition, previous studies have reported that cyanobacteria aqueous suspensions are important precursors of disinfection by products (DBPs) during water chlorination (Goslan et al., 2017). In this context, *Microcystis aeruginosa* has been the preferred cyanobacteria for these studies due to its ubiquity in the surface waters (Daly et al., 2007; Fang et al., 2010; Ho et al., 2006; Zhu et al., 2015), among others. Most of these studies, however, have focused on the total formation of few DBPs, but they do not provide the individual evaluation of each of the various C-DBPs and N-DBPs. For example, some studies have studied the impact of cyanobacteria aqueous suspensions chlorination on the formation of individual families of DBPs such as trihalomethanes (THMs) (Shi et al., 2019), haloacetic acids (HAAs) (Ge et al., 2011) or the concomitant production of few DBPs such as haloacetonitriles (HANs)/THMs (Pu et al., 2013) or THMs/HAA (Hong et al., 2008) among others. It is noteworthy that the formation of unregulated nitrogenous-DBPs (N-DBPs), such as HANs or trichloronitromethane (TCNM) is highly important since some of these DBPs are more genotoxic, cytotoxic or carcinogenic than carbonaceous-DBP (C-DBPs) and the presence of phytoplankton in the raw water increases their formation (Shah and Mitch, 2012) such as THMs or HAAs (Plewa et al., 2004).

Another frequent situation found in the studies of DBP formation from cyanobacteria aqueous suspensions is that some reports have focused on the exclusive formation of chlorinated-DBPs at pH 7. Thus, there is still room to investigate the impact of the presence of bromide ions (Ge et al., 2011; Hong et al., 2008; Plummer and Edzwald, 2001; Shi et al., 2019) at the concentration range naturally occurring and the influence of the pH (Shi et al., 2019) during the chlorination of the water contaminated by cyanobacteria. Nowadays it is well-established that the impact of some brominated DBPs such as THMs, HAAs, HANs on

the human health is higher compared to their corresponding chlorinated analogues (Yang et al., 2014). Brominated DBPs are more cytotoxic and genotoxic than their corresponding chlorinated analogues (Bond et al., 2011). In addition, regardless the higher occurrence and concentration of THMs and HAAs in drinking waters, N-DBPs such as HANs seem to be the responsible DBPs for toxicity (Plewa et al., 2017). Regarding the influence of the pH, most of studies related with cyanobacteria chlorination have been conducted at about pH 7 (Hong et al., 2008; Plummer and Edzwald, 2001; Shi et al., 2019) while most of the surface natural waters have pH values around 8. At pH 8 the main chlorine form is ClO^- , while at pH 7 the main form is HClO (Deborde and von Gunten, 2008). Chlorine speciation influences in large extent DBP formation. Therefore, it is desirable to obtain further information on the influence of the presence of bromide ions and pH on DPB formation during the chlorination of some common cyanobacteria found in fresh waters destined for human consumption.

One of the main strategies employed to minimize the risk of cyanobacteria accumulation in drinking water treatment plants and degrade the toxins released upon cell lysis is the use of ozone as oxidant (Daly et al., 2007; Fan et al., 2014). In addition, ozone has been generally employed as pre-oxidant to minimize DPB formation in the subsequent water chlorination (Richardson et al., 2007). In this context, the number of studies reporting the influence of pre-ozonation of cyanobacteria aqueous suspensions on DPB formation in the chlorination is much lower respect to those limiting only to chlorination (Plummer and Edzwald, 2001). Thus, it would be desirable further gain information on the influence of pre-ozonation also for other common cyanobacteria in water on the formation of DBPs, particularly in the presence of bromide ions that can form brominated THMs performing the experiments at pH values commonly found in natural waters.

Towards this goal, the present study shows the impact of the presence of three common cyanobacteria in surface waters, namely, *Microcystis aeruginosa*, *Anabaena aequalis* and *Oscillatoria tenuis* on DBP formation upon chlorination with or without a pre-ozonation process at relatively low cell concentration (10,000 cells/mL). In particular, THM, HAA, HAN, haloketone (HK) and

chloropicrin or trichloronitromethane (TCNM) formation together with the chlorine demand has been evaluated in the absence and presence of bromide ions as a function of the pH.

Considering the ways in which the presence of cyanobacteria can influence DBP, it has been reported that each class of biomolecule has a different behaviour regarding DBP formation. Thus, some of us have reported that chlorination of carbohydrate aqueous solutions result in a moderate chlorine demand (~ 1.5 mg $\text{Cl}_2/\text{mg C}$ at pH 8 at 20 °C after 3 d) with most of consumed chlorine atoms ending as THMs (100 $\mu\text{g/L}$) (Navalon et al., 2008).

Other studies have reported that the presence of N-containing organic compounds such as amino acids or peptides (Hureiki et al., 1994) results in some cases in chlorine demands higher than humic substances (Hong et al., 2009). For example, some peptides and proteins exhibit chlorine demand between 3 and 4 mg $\text{Cl}_2/\text{mg C}$ (Hureiki et al., 1994). In general, chlorination of N-containing organic compounds results in the formation of C-DBPs including THMs and HAAs, together with lesser amounts of aldehydes and HKs. In this context, it is pertinent to mention that in the case of the cyanobacteria *Oscillatoria tenuis* studied in this work, the main amino acids present in its composition are in average aspartic acid (7.33%), glutamic acid (10.1%), leucine (7.34%), histidine (1.65%) and methionine (0.82%) (Hong et al., 2008). Of note is that aspartic acid have been identified as one of the main non-aromatic HAA precursors (83.2 $\mu\text{g mg}^{-1} \text{C}$) present in the organic matter of natural waters. In addition, N-DBPs (Bond et al., 2011) such as organic haloamines (Hureiki et al., 1994), halonitriles, haloamides, halonitro compounds or cyanogen chloride are also formed upon chlorination of N-containing organic compounds (Trehly et al., 1986). As commented in the introduction, HANs and TCNM are important N-DBP groups due to their high genotoxicity and cytotoxicity compared to regulated C-DBPs such as THMs or HAAs (Plewa et al., 2004).

Regarding to DBP formation upon chlorination of lipids it has been reported that the higher number of double bonds in their structure the higher DBP formation (Deborde and von Gunten, 2008). For example, chlorination of common algal fatty acids showed that the higher amounts of double bonds the

higher amount of TCNM and DCAA (Liang et al., 2012). The reader is referred to some existing reviews and articles for a deeper discussion regarding chlorination mechanisms leading to DBP formation as a function of the structure of the precursor (Deborde and von Gunten, 2008).

Overall, the results obtained indicate that chlorination of fresh water contaminated by three common cyanobacteria at relatively low cell concentration results in significant increase in DBP formation. In addition, a pre-ozonation of waters containing these three cyanobacteria is not useful to decrease the concentration of CDBPs and N-DBPs. Our study indicates the need to remove cyanobacteria from the raw water before ozone pre-oxidation and/or chlorination in order to observe a diminution in the DBP formation.

3.2 Materials and methods

3.2.1 Reagents

All the reagents employed in this work were of analytical or HPLC grade. The list of the reagents includes: a) EPA 501/601 THMs calibration mix (2000 µg/mL each component in methanol; Merck) for the analysis of chloroform (TCM), dichlorobromomethane (BDCM), dibromochloromethane (DBCM) and bromoform (TBM); b) HAA standard mixture (EPA 552.2 Methyl Ester Calibration Mix, Sigma-Aldrich) for the analysis of monochloro-, dichloro-, trichloro-, monobromo-, dibromo-, bromochloro-, bromodichloro-, dibromochloro-, and tribromo-acetic acids (MCAA, DCAA, TCAA, MBAA, DBAA, BCAA, BDCAA, DBCAA, and TBAA, respectively); c) EPA 551B halogenated volatiles mix (2000 µg/mL each component in acetone; Sigma-Aldrich) for the analysis of bromochloroacetonitrile (BCAN), dibromoacetonitrile (DBAN), dichloroacetonitrile (DCAN), 1,1-dichloro-2-propanone (1,1-DCP), 1,1,1-trichloroacetone (1,1,1-TCP), trichloroacetonitrile (TCAN), trichloronitromethane (TCNM). d) Sodium hypochlorite (NaOCl) (5% active chlorine, Acros Organics). The three cyanobacteria under study *Microcystis aeruginosa*, *Anabaena aequalis* and *Oscillatoria tenuis* were supplied Spanish Bank of Algae (BEA-Banco Español de Algas).

3.2.2 Experimental procedures and analysis

Supplementary information describes the detailed description of cyanobacteria aqueous suspensions preparation (Section S1), the pre-ozonation and chlorination experiments (Section S2) and the analytical methods (Section S3) employed in this study. Herein, in contrast to precedents using high Algae concentration of 1,000,000 cells/mL to study DBP formation (Fang et al., 2010), the present work aims to determine the influence of a moderate cyanobacteria concentration on DBP formation upon chlorination, depending on whether or not a pre-ozonation step is performed (Almuhtaram et al., 2018). The range of concentration selected in the present study is more often occurring in water treatment plants, in which the operation conditions makes less probable acute cyanobacteria proliferation.

Optical microscopy confirmed the presence in the aqueous suspension of the three cyanobacteria under study, namely *Microcystis aeruginosa*, *Anabaena aequalis* and *Oscillatoria tenuis*, with their expected morphology (Fig. 1).

In general, the aqueous cyanobacteria solution (10,000 cells/mL; 200 mL) is ozonated at 1.6 mg/L and contacted for 2 h at pH 8. Then, the pre-ozonated solution is chlorinated (100 mL) under headspace free conditions with a chlorine dose of 11 mg/L at either pH 8 or 6.5 at 20 °C for 72 h. More details on the ozonation and chlorination processes can be found in the supplementary information.

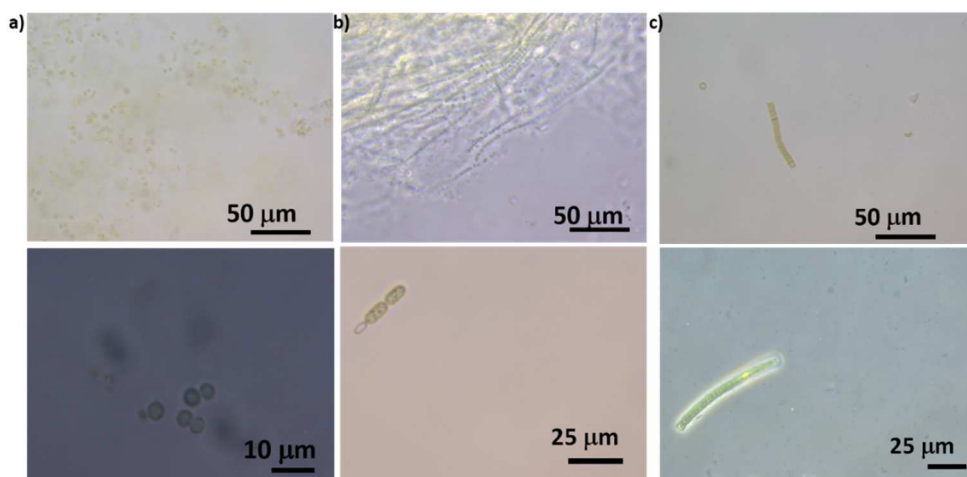


Fig. 1. Optical microscopy images of *Microcystis aeruginosa* (a), *Anabaena aequalis* (b) and *Oscillatoria tenuis* (c).

3.2.3 Cyanobacteria characterization

The three cyanobacteria under study were prepared at 10,000 cells/mL as described earlier. Table 1 collects the TOC of the three cyanobacteria suspensions under study as well as their composition in terms of percentage of lipids, proteins and carbohydrates, determined according to the literature (Cao et al., 1997; Sun et al., 1997). It is important to note that previous studies have reported the formation upon chlorination of several DBPs depending on the type of biomolecule either carbohydrates, proteins or lipids as organic model precursors to understand the behaviour of natural organic matter present in fresh water.

3.3 Results and discussion

Considering the distribution of biomolecules in the three cyanobacteria under study shown in Table 1 and having in mind that each class of biomolecule renders a different distribution of DBP, it was anticipated that chlorination of the three cyanobacteria aqueous suspensions should follow the expected behaviour

respect to C- and N-DBP formation. Thus, in spite of the complexity of the organic components present in the three cyanobacteria under study, the present study attempts to rationalize the observed results on DBP formation upon chlorination based on the cyanobacteria composition in polysaccharide, proteins and lipidlike organic moieties. Note that according to Table 1, the three cyanobacteria exhibit notable differences in the percentages of the three main types of biomolecules.

Table 1. List of cyanobacteria under study, TOC of the employed suspensions and composition in terms of proteins, carbohydrates and lipids.					
	TOC (mg/L) ^a	Carbohydrates (%)	Proteins (%)	Lipids (%)	Ref
<i>Microcystis aeruginosa</i> ^{a,b}	1.04	14.5	82.0	3.57	Cao et al. (1997)
<i>Oscillatoria tenuis</i> ^a	0.7	23.9	64.6	11.6	Sun et al. (1997)
<i>Anabaena aequalis</i> ^a	1.04	39.8	54.6	5.62	Cao et al. (1997)

^a TOC values corresponding to a cell concentration of 10⁴ cells/mL.

^b TOC value of 2.4 mg/L at a cell concentration of 10⁶ cells/mL.

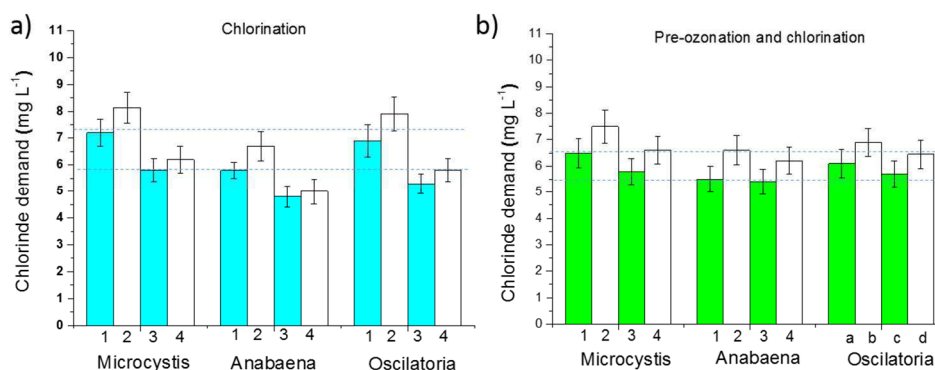


Fig. 2. Chlorine demand of cyanobacteria aqueous suspensions in the presence and in the absence of bromide ions at pH 8 or 6.5. Legend of left figure, a): Chlorination at pH 8 in the absence (1) or the presence (2) bromide ions; Chlorination at pH 6.5 in the absence (3) or the presence (4) bromide ions. Legend of right

part, b): Pre-ozonation followed by chlorination at pH 8 in the absence (1) or the presence (2) bromide ions; Pre-ozonation at pH 8 followed by chlorination at pH 6.5 in the absence (3) or the presence (4) bromide ions. General reaction conditions: Cyanobacteria concentration (10,000 cells/mL), ozone dose (1.6 mg/L), chlorine dose (11 mg/L), pH as indicated, 20 °C, 72 h reaction time.

3.3.1 Influence of the presence of cyanobacteria on chlorine demand during chlorination

One of the negative impacts of the presence of algae in the aquatic resources destined to human consumption is the increase of the chlorine demand that has to lead to higher DBP concentration (Zamyadi et al., 2013). Fig. 2a shows the chlorine demand of the three cyanobacteria aqueous suspensions (10,000 cells/mL) under study namely *Microcystis aeruginosa*, *Anabaena aequalis* and *Oscillatoria tenuis* at pH values 8 or 6.5 in the absence or presence of bromide ions ($300 \mu\text{g L}^{-1}$). On one hand, the chlorine demand for the all three cyanobacteria suspensions at pH 8 in the absence of bromide ions is around 6.6 ± 0.7 mg/L. Considering that TOC values of the three cyanobacteria suspensions at 10,000 cells/mL, chlorine demands are 1.04 ± 0.2 mg/L or ~ 6.3 mg free chlorine/mg TOC. The somewhat higher chlorine demand of *Microcystis aeruginosa* respect to the other two cyanobacteria under study may be partially attributed to its higher protein content (Table 1). These values are in the range of those reported for some N-containing organic compounds, based on amino acids varying from 3.4 to 10 mg/L of C as a function of their chemical structure.

On the other hand, the chlorine demand of the three cyanobacteria under study at pH 6.5 decreases to the average value of 5.3 ± 0.5 mg/L or 5.1 mg/L chlorine per mg of TOC. These results indicate that the higher the pH value during the chlorination of the cyanobacteria suspensions, the higher chlorine demand. The main chlorine species present in water at pH 8 is ClO^- ($E_{\text{RED}}^0 = 0.81$ eV) that is a worst oxidizing and chlorinating agent than HClO ($E_{\text{RED}}^0 = 1.49$ eV)

that is the species present at pH 6.5. Thus, it can be concluded that the experimental higher chlorine demand at basic pH values during cyanobacteria aqueous suspension chlorination should be due to the different organic substances speciation. In this context, it has been reported that saccharide chlorination at basic pH values requires higher chlorine consumption due to the occurrence of oxidation and chlorination compared to the chlorination at acidic pH values (Navalon et al., 2008). Other works have also observed that the chlorine consumption of proteins, peptides and amino acids is also higher at basic pH values due to the N-chlorination pathway that is hampered at acidic pH values in which the amino groups are protonated (Deborde and von Gunten, 2008). The chlorination rates of lipids are mainly controlled by the chlorine speciation at the corresponding pH value of the water (Deborde and von Gunten, 2008). Overall, it is likely to propose that the higher chlorine demand of cyanobacteria at basic pH values is due to both the reaction of chlorine with deprotonated amino groups and the chlorine reaction with carbohydrates through oxidation and chlorination pathways.

The presence of bromide ions at concentrations typically found in ground waters ($300 \mu\text{g L}^{-1}$) either at pH 8 or 6.5 increases the chlorine demand for the three cyanobacteria (10,000 cells/mL) under study. In the presence of bromide, the chlorine demand is also higher at pH 8 than at pH 6.5. This increase of the chlorine demand when Br^- is present can be explained considering that chlorine in the form of HClO or ClO^- oxidizes Br^- to HBrO or BrO^- . The oxidizing character of HBrO ($E^0_{\text{RED}} = 1.33 \text{ eV}$) or BrO^- ($E^0_{\text{RED}} = 0.761 \text{ eV}$) is slightly lower respect to their respective chlorine analogous. In contrast, the reactivity of bromine respect to chlorine is higher towards electrophilic aromatic substitution. This fact is due to the higher carbocation stability substituted by bromide atoms that enjoys higher electron density and smaller bond strength compare with the chlorine ones (Deborde and von Gunten, 2008). The higher chlorine demand in the presence of bromide ions or at pH 8 will be mainly reflected in an increase of THMs and HAAs (see below). In contrast, HANs are formed preferentially at acidic pH values due to their partial instability at basic pH values in which these DBP be-

come hydrolyzed to haloacetamides. Thus, the higher chlorine demand accompanied by higher DBP formation, generally observed during water disinfection, also applies for the case of cyanobacteria chlorination in the presence of bromide ions.

For comparison, the chlorine demand of *Microcystis aurea* in the presence of bromide was also measured at high cyanobacteria concentration (1,000,000 cells/mL) at pH 8. A chlorine demand value of 17.2 mg/L was determined. This chlorine demand when referred to the TOC of the cyanobacteria suspension (2.3 mg/L TOC) is somewhat lower (7.5 mg Cl₂/mg TOC) than that measured for a concentration of 10,000 cells/mL (8.1 mg Cl₂/mg TOC). This deviation may be attributed to the agglomeration of the cyanobacteria at higher concentration in the aqueous suspension and, therefore, decreasing slight chlorine accessibility to biomolecules. As it will be commented latter, the higher cyanobacteria concentration, the higher DBP production in absolute values (µg/L), but the lower chlorine demand referred to the TOC is reflected also in the relatively lower DBP production (µg/mg of TOC).

3.3.2 Influence of cyanobacteria chlorination and pre-ozonation on DBP formation

This section addresses the influence that the presence of the three cyanobacteria (10,000 cells/mL) under study in water on the DBP formation (THMs, HAAs, HANs, TCNM and HKs) upon chlorination with or without pre-ozonation. The study has been carried out at pH values of 8 or 6.5 in the presence or absence of bromide ions. Some of the results are presented in Figs. 3-6 and Tables S1-S3. Figs. 3-5 collects the THM and HAA formation after 1 and 3 days of chlorination. HAN formation is presented after 3 days of chlorination since the values 1 day after chlorination are below the quantification limit (0.5 µg/L). HK formation has not been included in the plots since in all the experiments its value is below the quantification limit (1 µg/L). TCNM was not observed in the chlorination, but it

has been quantified when a pre-ozonation process is performed in the absence of bromide ions (Fig. 6).

In general, the chlorination of the three cyanobacteria under study results in the formation of THMs and HAAs as the main CDBPs. It was observed that DBP formation for *Microcystis aeruginosa* is always somewhat higher than for the other two cyanobacteria under study. This fact follows the higher chlorine demand of *Microcystis aeruginosa* and the higher protein content respect to *Anabaena aequatis* or *Oscillatoria tenuis*. HAN concentrations have been found to be below 5 µg/L.

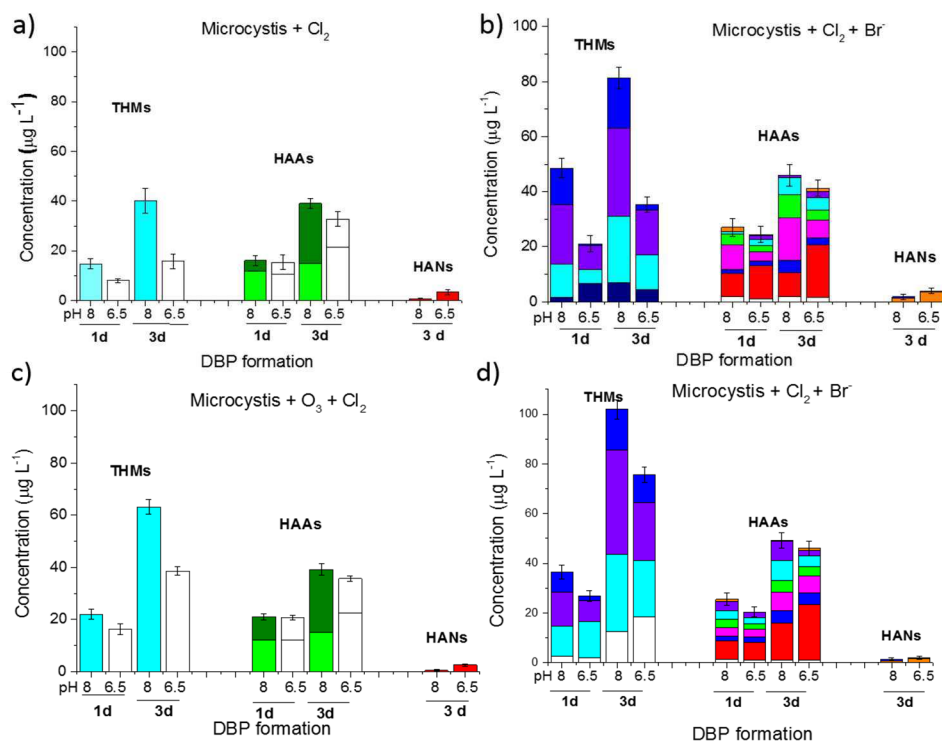


Fig. 3. DBP formation after one (1 d) or three (3 d) days for *Microcystis* aqueous suspensions under chlorination without (a, b) or after pre-ozonation (c, d) as a function of the pH and in the absence (a, c) or presence (b, d) of bromide ions. Legend panels a and c: THMs corresponds to TCM, HAAs correspond to DCAA (bottom part) and TCAA (upper part), HANs correspond to DCAN.

b and d: THMs (TCM-white, BDCM-cyan, CDBM-purple, TBM-blue), HAAs (MCAA-yellow, MBAA-white, DCAA-red, TCAA-blue, BCAA-pink, BDCAA-green, DBAA-cyan, CDBAA-purple, TBAA-orange), HANs (DCAN-orange, TCAN-blue). Reaction conditions: Cyanobacteria concentration (10,000 cells/mL), chlorine dose (11 mg/L), ozone dose (1.6 mg/L), pH as indicated, bromide ions (300 µg/L), temperature (20 °C). (For interpretation of the references to colour in this figure legend, the reader is referred to the Web version of this article)

DBP formation as a function of the pH of the chlorination

Figs. 3-6 show the formation of THMs, HAAs and HANs after chlorination of cyanobacteria aqueous suspensions of *Microcystis aeruginosa*, *Anabaena aequalis* and *Oscillatoria tenuis* upon chlorination at pH 8 or 6.5 during 24 or 72 h. Obviously, exclusive formation of chlorinated DBPs is observed when the chlorination process occurs in the absence of bromide ions. Regardless the slightly higher DBP formation when using *Microcystis aeruginosa* some general comments can be drawn for the three cyanobacteria under study.

The main DBPs formed upon chlorination of cyanobacteria suspensions at pH 8 are THMs and HAAs, reaching concentrations of 35 ± 0.12 and 29 ± 3.6 mg/L, respectively, at 72 h. The only THM observed is chloroform, while the HAAs are mainly constituted by DCAA and TCAA. In addition, THM and HAA concentrations increase over the time, an observation that is in agreement with the stability of these compounds in aqueous solutions under ambient conditions and quasi-neutral pH values. In the case HANs, DCAN is the main DBP observed with concentration values for the three cyanobacteria at pH 8 of about 0.97 ± 0.55 mg/L after 72 h. Previous studies have shown that chlorination of free amino acids leads to the formation of chloroform, DCAN and trichloroacetaldehyde as main DBPs (Trehy et al., 1986). The absence of TCAN was attributed to its high hydrolysis rate (Bond et al., 2011; Glezer et al., 1999).

As commented before, a decrease of the pH of the solution from 8 to 6.5 results in a general decrease about 15% of the chlorine demand. The influence

of the pH during the chlorination is, however, strongly dependent on the DBP nature. When the pH decreases from 8 to 6.5, the THM and HAA concentrations are reduced about 50 and 20%, respectively.

Regarding HAN formation upon cyanobacteria suspension chlorination, its concentration increases as the pH decreases for the three cyanobacteria from 0.97 ± 0.55 mg/L to 3.3 mg/L after 72 h. This observation agrees with previous reports that observed a maximum HAN stability in water at pH 6.5, while an increase of the pH decreases the HAN concentration due to their hydrolysis to their corresponding haloacetamides (Chu et al., 2015; Glezer et al., 1999). Haloacetamides can be further hydrolyzed to their corresponding HAAs (Glezer et al., 1999).

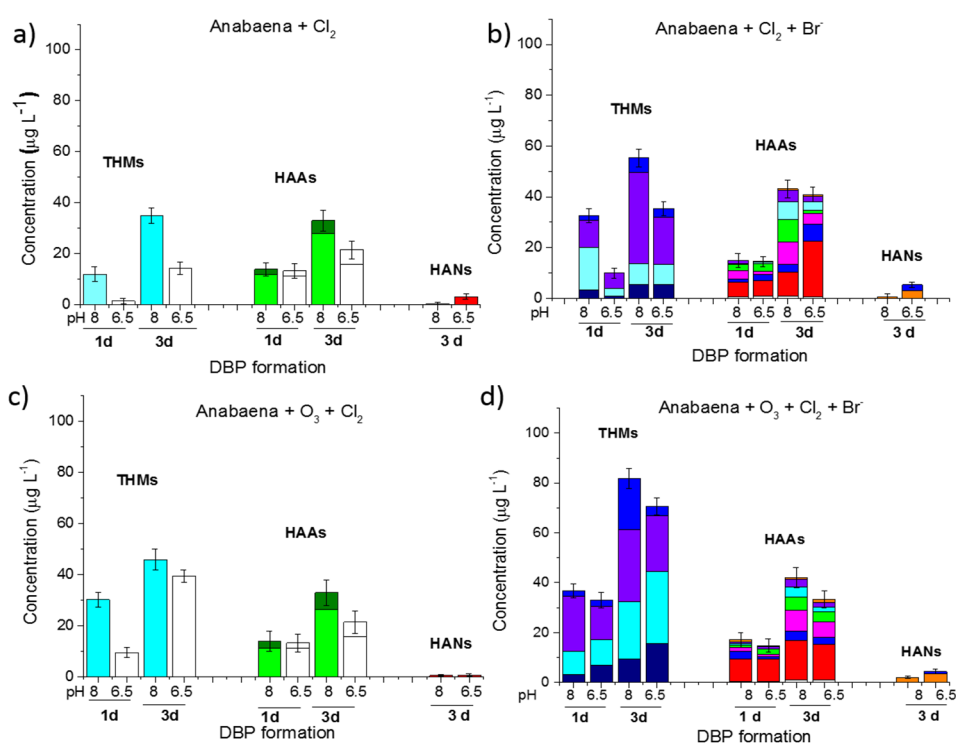


Fig. 4. DPB formation after one (1 d) or three (3 d) days for Anabaena aqueous suspensions under chlorination without (a, b) or after pre-ozonation (c, d) as a function of the pH and in the absence (a, c) or presence (b, d) of bromide ions.

Legend panels a and c: THMs corresponds to TCM, HAAs correspond to DCAA (bottom part) and TCAA (upper part), HANs correspond to DCAN. Legend panels b and d: THMs (TCM-white, BDCM-cyan, CDBM-purple, TBM-blue), HAAs (MCAA-yellow, MBAA-white, DCAA-red, TCAA-blue, BCAA-pink, BDCAA-green, DBAA-cyan, CDBAA-purple, TBAA-orange), HANs (DCAN-orange, TCAN-blue). Reaction conditions: Cyanobacteria concentration (10,000 cells/mL), chlorine dose (11 mg/L), ozone dose (1.6 mg/L), pH as indicated, bromide ions (300 µg/L), temperature (20 °C). (For interpretation of the references to colour in this figure legend, the reader is referred to the Web version of this article)

Effect of the presence of bromide ions on DBP formation during chlorination of the cyanobacteria as a function of the pH

In addition to the influence of the pH on DBP formation, the presence of bromide ions is also an important factor. The general trend observed during water chlorination is that the presence of bromide ions, even at microgram per liter concentrations, increases the total DBP formation and results in the formation of brominated DBPs. Figs. 3-5 summarize the results for the DBP formation from the three cyanobacteria under study (10,000 cells/mL) in the presence of bromide ions at 300 µg L⁻¹ at both pH 8 or 6.5. As it can be seen there, the presence of bromide ions increases the concentration of THMs at both pH 8 and 6.5 reaching average values of 68.7 ± 11.9 and 26.9 ± 14.5 mg/L, respectively. In the case of HAAs, the presence of bromide ions mainly favors the formation of brominated HAAs with slight increase of the total concentration at both pH 8 and 6.5 with average values of 60.7 ± 5.0 and 40.2 ± 1.6 mg/L, respectively. In the case of HANs the presence of bromide ions also increases the total HAN concentration, reaching values of 1.2 ± 0.6 and 4.8 ± 0.7 mg/L at pH 8 and 6.5, respectively, while favoring the formation of brominated HANs.

Fig. 7 shows the bromide incorporated into THMs and HAAs during the chlorination of the three cyanobacteria under study in the presence of bromide ions at pH 8 and 6.5. As it can be seen there, the proportion of brominated THMs

is between 90 and 70% a fact that agrees with the higher stability of brominated methyl anions (CBr_3^-) than chlorinated (CCl_3^-) ones (Navalon S. et al., 2008). In the case of HAAs the proportion of brominated compounds is lower than in the case of THMs especially at pH 6.5. It should be reminded that since HClO pKa is 7.54, it prevails at pH 6.5 in the acid form. Considering that HClO is a stronger oxidant than ClO^- , more oxidized and chlorinated compounds such as DCAA can be expected, as in the present case. This situation, i.e. the lower bromide incorporation at pH 6.5 respect to pH 8, although in less extent, also applies for THMs.

When considering the possible differences in DBP distribution among the three cyanobacteria under study as presented in Fig. 7, it has to be considered that assuming a normal Gaussian distribution, the 95.5% level of confidence for the lower and higher limit for a value corresponds to two times the standard deviation (indicated for each bar). Therefore, there are certain data (as THM values shown in frame c of Fig. 7) that correspond to essentially identical statistical values, while there are others, like formation of CHCl_2Br in *Oscillatoria tenuis* that is certainly below the values formed for the other two cyanobacteria.

In the case of *Microcystis* an additional chlorination was carried out at a cyanobacteria concentration of 1,000,000 cells/mL in the presence of bromide (300 $\mu\text{g/L}$). Formation of THMs, HAAs and HANs of about 143, 87 and 1.9 $\mu\text{g/L}$, respectively (Fig. S1), was measured. Again, the formation of TCNM or HKs was below the quantification limit.

Effect of pre-ozonation on DBP formation

The influence of pre-ozonation on DBP formation was studied at an ozone dose of 1.6 mg/L. This ozone dose is in the average range typically employed in water treatment plants. The use of higher ozone dose can compromise the possibility of using ozone to control DBPs, due to the oxidation of the naturally occurring bromides to bromates. Bromate concentration is limited by most drinking water regulations to the value of 10 $\mu\text{g/L}$ (von Gunten, 2003). In this work, bromate concentrations after ozonation have been always found below 4

$\pm 0.7 \mu\text{g/L}$. Moreover, a pre-ozonation of the cyanobacteria aqueous suspensions under study decreases the chlorine demand respect to the chlorination process (Fig. 2b). However, this chlorine demand decrease does not diminish the concentration of all the DBPs considered in this study (THMs, HAAs, HANs, TCNM or HKs) and in some cases these concentrations even increase significantly. It should be noted that DBP formation occurs in the range of about 0.1 mg/L , while chlorine consumption is one order of magnitude higher in the range of about 6 mg/L .

More specifically, a pre-ozonation followed by chlorination of the three cyanobacteria under study results in an increase of THM formation both at pH 8 or 6.5 either with or without bromide ions up to 50% respect to the chlorination process (Figs. 3-5). In the case of HAA formation from the three cyanobacteria also at pH 8 or 6.5 in the presence of absence of bromide ions, the pre-ozonation process does not significantly diminish and even sometimes slightly increases its concentration. With these precedents, our work further exemplifies that a pre-ozonation at doses commonly employed in the water treatment plants of the three cyanobacteria under study working at relatively low cell concentrations ($10,000 \text{ cells/mL}$) working at either pH 8 or 6.5 with or without bromide ions results in a significant increase of THMs and poor control of HAA concentration that in sometimes increases.

Chapter 3. DBPs from cyanobacteria by chlorination with/without ozonation

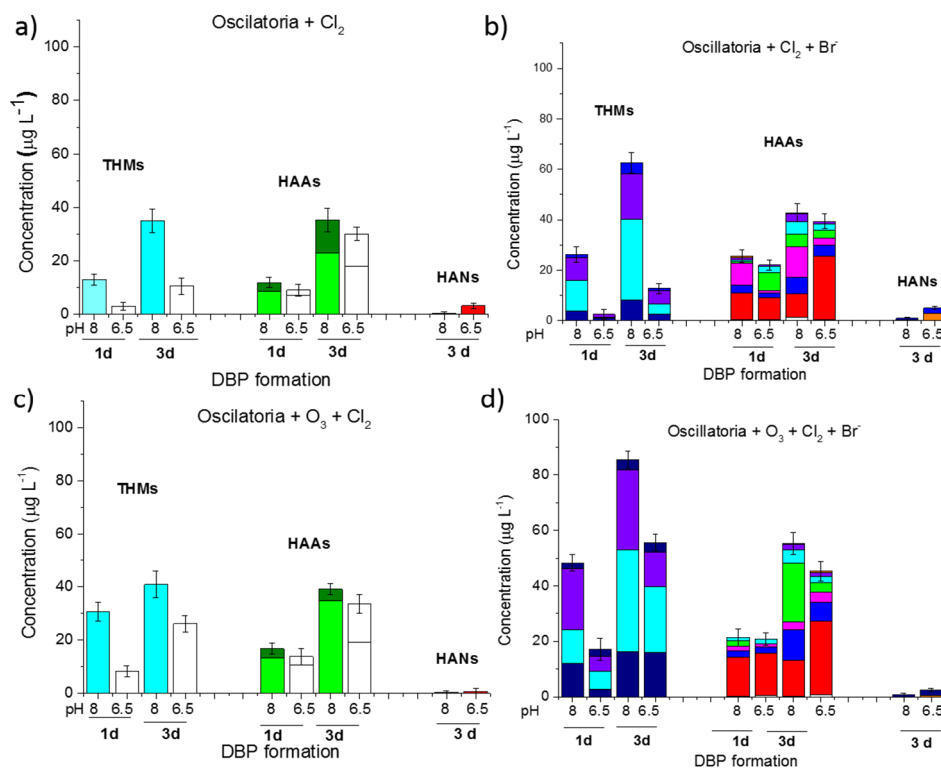


Fig. 5. DBP formation after one (1 d) or three (3 d) days for *Oscillatoria* aqueous suspensions under chlorination without (a, b) or after pre-ozonation (c, d) as a function of the pH and in the absence (a, c) or presence (b, d) of bromide ions. Legend panels a and c: THMs corresponds to TCM, HAAs correspond to DCAA (bottom part) and TCAA (upper part), HANs correspond to DCAN. Legend panels b and d: THMs (TCM-white, BDCM-cyan, CDBM-purple, TBM-blue), HAAs (MCAA-yellow, MBAA-white, DCAA-red, TCAA-blue, BCAA-pink, BDCAA-green, DBAA-cyan, CDBAA-purple, TBAA-orange), HANs (DCAN-orange, TCAN-blue). Reaction conditions: Cyanobacteria concentration (10,000 cells/mL), chlorine dose (11 mg/L), ozone dose (1.6 mg/L), pH as indicated, bromide ions (300 µg/L), temperature (20 °C). (For interpretation of the references to colour in this figure legend, the reader is referred to the Web version of this article)

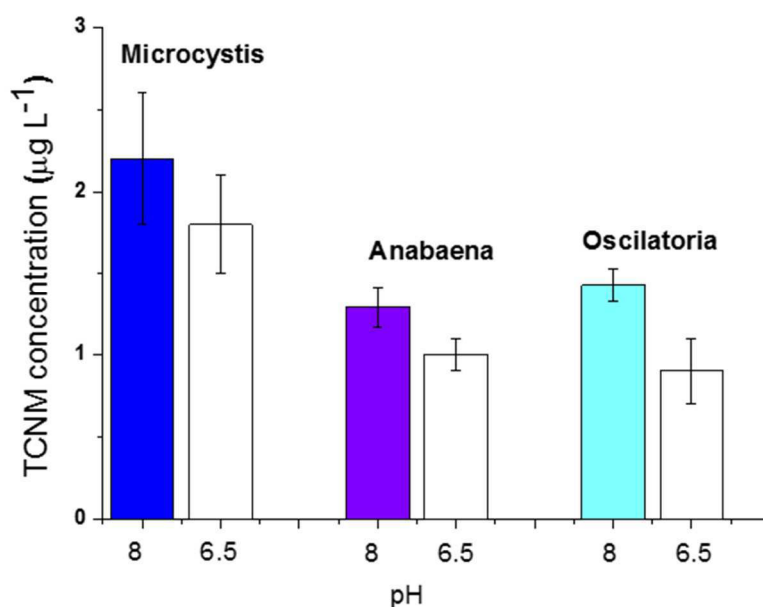


Fig. 6. TCNM formation after 3 days upon pre-ozonation followed by chlorination of the cyanobacteria suspensions as a function of the pH of the aqueous solution. Reaction conditions: Cyanobacteria concentration (10,000 cells/mL), chlorine dose (11 mg/L), ozone dose (1.6 mg/L), pH as indicated, temperature (20 °C).

The reasons for the observed increase of THMs and HAAs due to a pre-ozonation of cyanobacteria aqueous suspensions still remain unknown. On one hand, there is limited knowledge on how ozonolysis transforms complex biomolecules such as those present in cyanobacteria (Sharma and Graham, 2010; von Gunten, 2003). On the second hand, ozonation reaction conditions can determine the contribution of ozonolysis vs. radical mechanism with the generation of hydroxyl radicals (von Gunten, 2003). Besides electrophilic attack of ozone, this molecule can decompose in water, especially at basic pH values, into reactive oxygen species, such as hydroxyl radicals, that can virtually react non-selectively with any organic compound. Thus, further studies about the reactivity of ozone

with natural complex biomolecules are necessary to understand the effect of the pre-ozonation of cyanobacteria on THM and HAA formation.

In this context, some studies have reported the release of free amino acids upon oxidation of peptides and proteins by hydroxyl radicals and this release should influence DBP formation (Liu et al., 2017). For instance, regarding peptide reactivity, it has been reported that free tyrosine (Tyr) forms 74% more chloroform than Tyr-Tyr-Tyr peptide (Chu et al., 2015). The same study also found different chlorine reactivity towards THM formation of NH₂- or COOH-terminated peptide isomers such as tyrosine-alanine or alanine-tyrosine (Chu et al., 2015). Other study has reported that preoxidation of the amino acids leucine and serine by a UV/H₂O₂ treatment followed by chlorination results in an increase of HAA formation (Sakai et al., 2013). In this sense, the increase of HAA formation of pre-ozonized cyanobacteria may be partially attributed to similar reaction pathways. These results exemplify the complexity of chlorine reactivity for peptides.

Similarly to peptides, the reactivity of ozone with polysaccharides and the consequences for DBP formation are difficult to predict (-Sharma and Graham, 2010). Only few studies have reported the production of THMs from mono- and oligosaccharides. It seems that oligosaccharides such as maltopentose or maltotriose produce higher THM amounts than the monosaccharide maltose (Navalon et al., 2008). Other studies have reported that ozonolysis is able to depolymerize polysaccharides containing β -D-aldosidic linkages (Wang et al., 1998). As in the case of proteins, it is not possible to predict the effect of pre-ozonation on THM formation in polysaccharides.

Fig. 7 shows that pre-ozonation increases significantly brominated THMs at pH 8 without changing significantly the percentage of Br-DBP respect to the THM total. Some reports using humic acids as DBP precursors have shown that pre-ozonation results in a shift of DBPs towards brominated ones (Mao et al., 2014), but this is not the case of pre-ozonation of the aqueous suspensions of the three cyanobacteria (Fig. 7c and d).

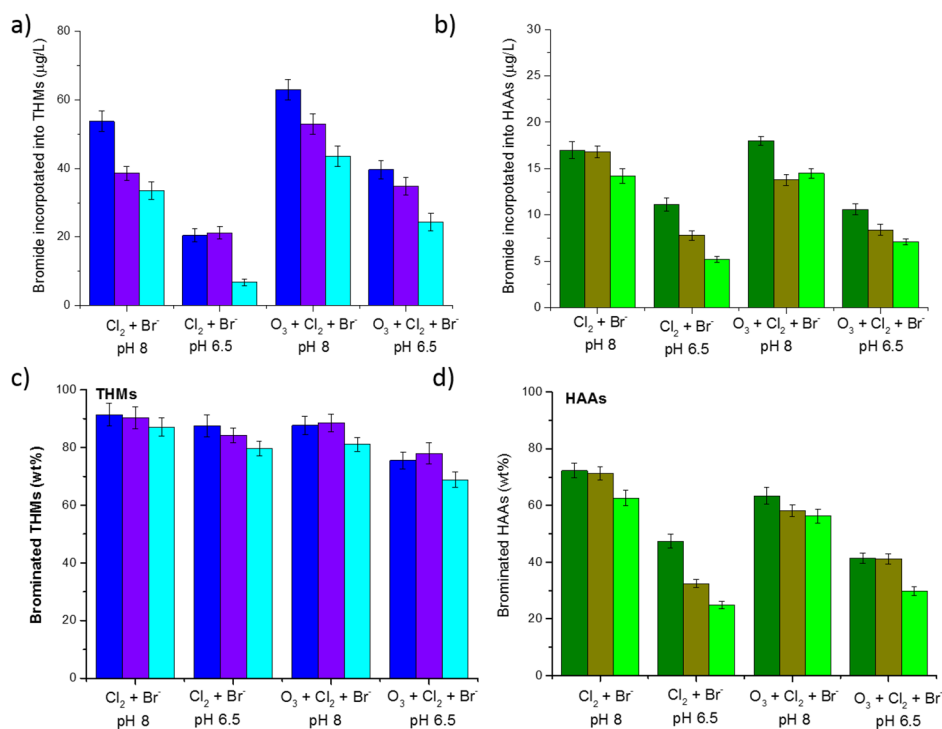


Fig. 7. Bromide incorporation into THMs (a) or HAAs (b) and percentage of brominated THMs (c) or HAAs (d) during the chlorination of *Microcystis aeruginosa* (black bar), *Anabaena aequalis* (red bar) and *Oscillatoria tenuis* (blue bar) cyanobacteria under various reaction conditions as indicated. Cyanobacteria concentration (10,000 cells/mL), chlorine dose (11 mg/L), ozone dose (1.6 mg/L), pH as indicated, bromide ions (300 µg/L), temperature (20 °C). (For interpretation of the references to colour in this figure legend, the reader is referred to the Web version of this article)

Regarding N-DBPs, while TCNM is not observed either at pH 8 or 6.5 when the aqueous suspensions of the three cyanobacteria were submitted to a chlorination, its presence could be quantified after pre-ozonation and chlorination of the samples in the absence of bromide ions (Fig. 6). In agreement with previous works (Hu et al., 2010), TCNM formation is favoured at basic pH values.

The fact that TCNM is again not observed when pre-ozonation is carried out in the presence of bromide ions is due to the formation of other NDBPs related to TCNM, but containing bromide replacing to chlorine atoms (Hu et al., 2010).

A reasonable pathway to understand the formation of TCNM upon pre-ozonation considers the release of free amino acids due to oxidation of peptides and proteins by hydroxyl radicals (Liu et al., 2017), followed by decarboxylation of the amino acid and subsequent halogenation of the resulting amines (Le Lacheur and Glaze, 1996). In this regard, it has been reported that ozone promotes TCNM formation by oxidizing amines to nitro compounds that subsequently undergo chlorination to halo nitro compounds (Fig. 8b) (McCurry et al., 2016). This effect has also been reported when using natural waters (Bond et al., 2011). The higher TCNM formation at basic pH values would be due to the easier oxidation of deprotonated amino groups to nitro groups. In addition, basic pH values favor the partial O₃ decomposition to hydroxyl radicals that are better oxidizing reagents promoting the conversion of amino to nitro groups.

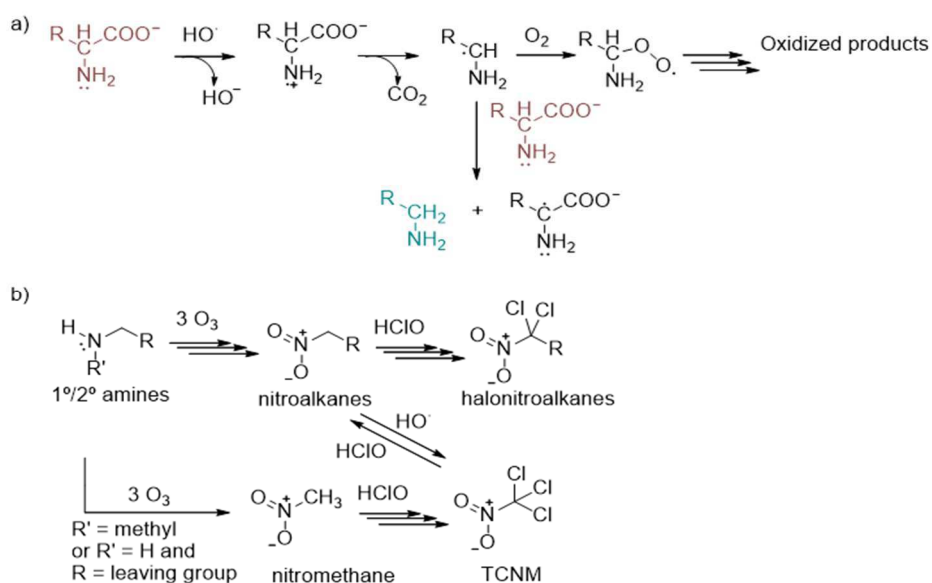


Fig. 8. Proposed reaction pathway for generation of halonitroalkanes upon pre-ozonation and chlorination of amino acids and amines. Adapted from ref. (McCurry et al., 2016).

In accordance to the mechanism leading to TCNM, formation of this DBP after pre-ozonation would occur at the expense of a decrease in the concentration of HANs. Oxidation of the α -carbon to the nitrile by ozone would hamper its chlorination.

3.4 Conclusions

The influence of the presence of three common cyanobacteria commonly encountered in fresh waters, namely *Microcystis aeruginosa*, *Anabaena aequalis* and *Oscillatoria tenuis* at relatively low cell concentration (10,000 cells/mL) on DBP formation depending on the pH and pre-ozonation has been studied. Cyanobacteria chlorination results in the formation THMs and HAAs as main CDBPs, accompanied by minor amounts of N-DBPs such as HANs and absence of HKs and TCNM. Basic pH values increases formation of THM and in less extent HAAs, decreasing HAN concentration. The presence of bromide ions increases THM and HAN concentrations, while the formation of HAAs is promoted in less extent.

Pre-ozonation (1.6 mg/L O₃) of the aqueous suspensions containing the three cyanobacteria under study was carried out under conditions in which bromate formation ($4 \pm 0.7 \mu\text{g/L}$) is below the maximum legal concentration (10 $\mu\text{g/L}$). Pre-ozonation increases THM formation and generates TCNM, while has minor influence on HAA formation. In contrast, this oxidation process decreases HAN formation.

In summary, the present work shows that common cyanobacteria present in freshwaters are important DBP precursors and preozonation is not a general method to decrease the main C- and N-DBPs.

3.5 References

Almuhtaram, H., Cui, Y., Zamyadi, A., Hofmann, R., 2018. Cyanotoxins and cyanobacteria cell accumulations in drinking water treatment plants with a low risk of bloom formation at the source. *Toxins* 10, 430.

Bond, T., Huang, J., Templeton, M.R., Graham, N., 2011. Occurrence and control of nitrogenous disinfection by-products in drinking water - A review. *Water Res.* 45, 4341-4354.

Cao, J., Li, D., Wang, J., 1997. Studies on biochemical composition of 10 species of common freshwater phytoplankton. *Acta Sci. Nat. Univ. Sunyatseni* 36, 22-27.

Carmichael, W.W., Boyer, G.L., 2016. Health impacts from cyanobacteria harmful algae blooms: implications for the North American great lakes. *Harmful Algae* 54, 194-212.

Chen, Y., Xie, P., Wang, Z., Shanga, R., Wang, S., 2017. UV/persulfate pre-oxidation to improve coagulation efficiency of *Microcystis aeruginosa*. *J. Hazard Mater.* 322, 508.

Chu, W., Li, X., Gao, N., Deng, Y., Yin, D., Li, D., Chu, T., 2015. Peptide bonds affect the formation of haloacetamides, an emerging class of N-DBPs in drinking water: free amino acids versus oligopeptides. *Sci. Rep.* 5, 14412.

Codd, G.A., Meriluoto, J., Metcalf, J.S., 2016. Introduction: cyanobacteria, cyanotoxins, Their human impact, and risk management. In: Meriluoto, J., Spoof, L., Codd, G.A. (Eds.), *Handbook of Cyanobacterial Monitoring and Cyanotoxin Analysis*, volume 51. John Wiley & Sons, Ltd, Chichester, UK, pp. 1-8.

Daly, R., Ho, L., Brookes, J.D., 2007. Effect of chlorination on *Microcystis aeruginosa* cell Integrity and subsequent Microcystin release and degradation. *Environ. Sci. Technol.* 41, 4447-4453.

Deborde, M., von Gunten, U., 2008. Reactions of chlorine with inorganic and organic compounds during water treatment kinetics and mechanisms: a critical review. *Water Res.* 42, 13-51.

Falconer, I.R., 1991. Tumor promotion and liver injury caused by oral consumption of cyanobacteria. *Environ. Toxic Water* 6, 177-184.

Fan, J., Ho, L., Hobson, P., Daly, R., 2014. Application of various oxidants for cyanobacteria control and cyanotoxin removal in wastewater treatment. *J. Environ. Eng.* 140, 04014022.

Fang, J., Ma, J., Yang, X., Shang, C., 2010. Formation of carbonaceous and nitrogenous disinfection by-products from the chlorination of *Microcystis aeruginosa*. *Water Res.* 44, 1934-1940.

Frazier, K., Colvin, B., Styer, E., Hullinger, G., Garcia, R., 1998. Microcystin toxicosis in cattle due to overgrowth of blue-green algae. *Vet. Hum. Toxicol.* 40, 23-22.

Ge, F., Wu, X., Wang, N., Zhu, R., Wang, T., Xu, Y., 2011. Effects of iron and manganese on the formation of HAAs upon chlorinating *Chlorella vulgaris*. *J. Hazard Mater.* 189, 540-545.

Glezer, V., Harris, B., Tal, N., Iosefzon, B., Lev, O., 1999. Hydrolysis of haloacetonitriles: linear free energy relationship, kinetics and products. *Water Res.* 33, 1938-1948.

Goslan, E.H., Seigle, C., Purcell, D., Henderson, R., Parsons, S.A., Jefferson, B., Judd, S.J., 2017. Carbonaceous and nitrogenous disinfection by-product formation from algal organic matter. *Chemosphere* 170, 1-9.

Hawkins, P.R., Runnegar, M.T.C., Jackson, A.R.B., Falconer, I.R., 1985. Severe hepatotoxicity caused by the tropical cyanobacterium (blue-green alga) *Cylindrospermopsis raciborskii* (Woloszynska) Seenaya and Subba Raju isolated from a domestic water supply reservoir. *Appl. Environ. Microbiol.* 50, 1292-1295.

Ho, L., Onstad, G., von Gunten, U., Rinck-Pfeiffer, S., Craig, K., Newcombe, G., 2006. Differences in the chlorine reactivity of four microcystin analogues. *Water Res.* 40, 1200-1209

Hong, H.C., Mazumder, A., Wong, M.H., Liang, Y., 2008. Yield of trihalomethanes and haloacetic acids upon chlorinating algal cells, and its prediction via algal cellular biochemical composition. *Water Res.* 42, 4941-4948.

Hong, H.C., Wong, M.H., Liang, Y., 2009. Amino acids as precursors of trihalomethane and haloacetic acid formation during chlorination. *Arch. Environ. Contam. Toxicol.* 56, 638-645.

Hu, J., Song, H., Karanfil, T., 2010. Comparative analysis of halonitromethane and trihalomethane formation and speciation in drinking water: the effects of disinfectants, pH, bromide, and nitrite. *Environ. Sci. Technol.* 44, 794-799.

Hureiki, L., Crou, J.P., Legube, B., 1994. Chlorination studies of free and combined amino acids. *Water Res.* 28, 2521-2531.

Jochimsen, E.W., Carmichael, W., Cardo, D., Cookson, S., Holmes, C., De Antunes, M., De Melo Filho, D., Lyra, T., Barreto, V., Azevedo, S., Jarvis, W., 1998. Liver failure and death after exposure to microcystins at a hemodialysis centre in Brazil. *N. Engl. J. Med.* 26, 873-878.

Le Lacheur, R., Glaze, W., 1996. Reactions of ozone and hydroxyl radicals with serine. *Environ. Sci. Technol.* 30, 1072-1080.

Liang, Y., Lui, Y.S., Hong, H., 2012. Fatty acids and algal lipids as precursors of chlorination by-products. *J. Environ. Sci.* 24, 1942-1946.

Liu, F., Lai, S., Tong, H., Lakey, P.S.J., Shiraiwa, M., Weller, M.G., Pfooschl, U., Kampf, C.J., 2017. Release of free amino acids upon oxidation of peptides and proteins by hydroxyl radicals. *Anal. Bioanal. Chem.* 409, 2411-2420.

Mao, Y., Wang, X., Yang, H., Wang, H., Xie, Y.F., 2014. Effects of ozonation on disinfection byproduct formation and speciation during subsequent chlorination. *Chemosphere* 117, 515-520.

McCurry, D.L., Quay, A.N., Mitch, W.A., 2016. Ozone promotes chloropicrin formation by oxidizing amines to nitro compounds. *Environ. Sci. Technol.* 50, 1209-1217.

Merel, S., Walker, D., Chicana, R., Snyder, S., Baur, E., Thomas, O., 2013. State of knowledge and concerns on cyanobacterial blooms and cyanotoxins. *Environ. Int.* 59, 303-327.

Navalon, S., Alvaro, M., Garcia, H., 2008. Carbohydrates as trihalomethanes precursors. Influence of pH and the presence of Cl⁻ and Br⁻ on trihalomethane formation potential. *Water Res.* 42, 3990-4000.

Plewa, M.J., Wagner, E.D., Jazwierska, P., Richardson, S.D., Chen, P.H., McKague, A.B., 2004. Halonitromethane drinking water disinfection byproducts: chemical characterization and mammalian cell cytotoxicity and genotoxicity. *Environ. Sci. Technol.* 38, 62-68.

Plewa, M.J., Wagner, E.D., Richardson, S.D., 2017. TIC-Tox: a preliminary discussion on identifying the forcing agents of DBP-mediated toxicity of disinfected water. *J. Environ. Sci.* 58, 208-216.

Plummer, J.D., Edzwald, J., 2001. Effect of ozone on Algae as precursors for trihalomethane and haloacetic acid production. *Environ. Sci. Technol.* 35, 3661-3668.

Pu, Y., Kong, L., Huang, X., Ding, G., Gao, N., 2013. Formation of THMs and HANs during bromination of *Microcystis aeruginosa*. *J. Environ. Sci.* 25, 1795-1799.

Richardson, S.D., Plewa, M.J., Wagner, E.D., Schoeny, R., DeMarini, D.M., 2007. Occurrence, genotoxicity, and carcinogenicity of regulated and emerging disinfection by-products in drinking water: a review and roadmap for research. *Mutat. Res. Rev. Mutat. Res.* 636, 178-242.

Sakai, H., Autin, O., Parsons, S., 2013. Change in haloacetic acid formation potential during UV and UV/H₂O₂ treatment of model organic compounds. *Chemosphere* 92, 647-651.

Shah, A.D., Mitch, W.A., 2012. Halonitroalkanes, halonitriles, haloamides, and Nnitrosamines: a critical review of nitrogenous disinfection byproduct formation pathways. *Environ. Sci. Technol.* 46, 119-131.

Sharma, V.K., Graham, N.J.D., 2010. Oxidation of amino acids, peptides and proteins by ozone: a review. *Ozone: Sci. Eng.* 32, 81-90.

Shi, X., Bi, R., Yuana, B., Liao, X., Zhou, Z., Li, F., Sun, W., 2019. A comparison of trichloromethane formation from two algae species during two pre-oxidation-coagulation-chlorination processes. *Sci. Total Environ.* 656, 1063-1070.

Sun, J.H., Tian, C.Y., Zhao, Q., 1997. Studies on nutrient composition of 6 species of high salt microalgae in China. *Sea-lake Salt Chem. Ind.* 26, 20-22 (in Chinese).

Trehy, M.L., Yost, R.A., Miles, C.J., 1986. Chlorination byproducts of amino acids in natural waters. *Environ. Sci. Technol.* 20, 1117-1122.

Turner, P., Gammie, A., Hollinrake, K., Codd, G., 1990. Pneumonia associated with contact with cyanobacteria. *Br. Med. J.* 300, 1165-1175.

von Gunten, U., 2003. Ozonation of drinkingwater: Part II. Disinfection and byproduct formation in presence of bromide, iodide or chlorine. *Water Res.* 37, 1469-1487.

Wang, Y., Hollingsworth, R.I., Kasper, D.L., 1998. Ozonolysis for selectively depolymerizing polysaccharides containing b-d-aldosidic linkages. *Proc. Natl. Acad. Sci. U.S.A.* 95, 6584-6589.

Yang, Y., Komaki, Y., Kimura, S.Y., Hu, H.-Y., Wagner, E.D., Mariñas, B.J., Plewa, M.J., 2014. Toxic impact of bromide and iodide on drinking water disinfected with chlorine or chloramines. *Environ. Sci. Technol.* 48, 12362-12369.

Zamyadi, A., Fan, Y., Daly, R.I., Prevost, M., 2013. Chlorination of *Microcystis aeruginosa*: toxin release and oxidation, cellular chlorine demand and disinfection by-products formation. *Water Res.* 47, 1080-1090.

Zhu, M., Gao, N., Chu, W., Zhou, S., Zhang, Z., Xu, Y., Dai, Q., 2015. Impact of preozonation on disinfection by-product formation and speciation from chlor(am)ination of algal organic matter of *Microcystis aeruginosa*. *Ecotoxicol. Environ. Saf.* 120, 256-262.

3.6 Supplementary material

Section 1. Cyanobacteria aqueous suspension preparation

The preparation of cyanobacteria stock solutions were carried out by simply dilution of the quantified supplied suspensions. The cell concentration was further confirmed following the UNE–EN15204:2007 entitled Guidance standard on the enumeration of phytoplankton using inverted microscopy (Utermöhl technique).

Section 2. Pre-ozonation and chlorination experiments

The pH of the cyanobacteria stock solutions has been adjusted to 6.5 and 8.0 with HNO₃ or NaOH solutions in the presence of a phosphate buffer (10 mM).

For ozonation experiments, 200 mL of the cyanobacteria aqueous solutions at pH 8 were introduced in a glass reactor (300 mL) where the generated ozone was introduced through a gas diffusion glass membrane into the bottom part. Ozone was generated from dried air using a commercially available corona discharge ozone generator with a production of maximum capacity of 140 mg/h. An ozone dose of 1.6 mg/L was supplied to the cyanobacteria aqueous solution and the sample allowed to react for 2 h.

Chlorination experiments of the cyanobacteria solutions, regardless pre-ozonized or not, were carried out in capped amber bottles (100 mL) under head-space-free conditions at 20 °C. In some case, the pH of the ozonated cyanobacteria was adjusted to pH 6.5 using an aqueous HNO₃ solution. The reactions were initiated by adding an aliquot of chlorine stock solution to the buffered cyanobacteria solutions in the presence or absence of bromide ions. After 24 and 72 h one aliquot was withdrawn for the analysis of residual chlorine. Then, the chlorination was stopped by reducing the residual chlorine with thiosulfate (0.1 g).

Each experiment has been carried out at least in triplicate. The data presented in this work corresponds to the average value and standard deviation of the replicate experiments.

Section 3. Analytical methods

Total organic carbon (TOC) was determined with a High-TOC Elementar II analyzer. Free chlorine was analyzed spectrophotometrically by N,N-diethyl-1,4-phenylenediamine (DPD) method monitoring at 515 nm (ISO 7393-2:1985) on a UV-Vis spectrophotometer (Perkin Elmer).

Bromate ions were determined using a Metrohm ion-chromatography equipped with a conductivity detector. The stationary phase was a polyvinyl alcohol with quaternary ammonium groups column. A metrosep A Supp 1 guard column was also employed. The mobile phase employed for the analyses was a basic aqueous solution (3.2 mM Na₂CO₃ / 1.0 mM NaHCO₃ mM).

THM concentration was determined by analysis of the head gas of the vials with GC-ECD (Chromatograph Thermo scientific Trace GC Ultra equipped with an electron capture detector and Thermo Finnigan autosampler HS 2000) following the procedure of the UNE-EN ISO 10301 standard. Briefly, a sample aliquot (10 mL) was transferred into 20 mL vials containing 0.1 g of sodium chloride to facilitate the extraction of THMs and 0.1 g of sodium thiosulfate to stop the effect of chlorine and, then, analyzed by headspace gas chromatography. Then, the vial was heated at 50 °C for 45 min and, then, 0.5 mL of the headspace injected in the gas chromatograph using He as carrier gas (85 kPa), and N₂ as make up gas (110 kPa) in a DB.624 capillary column (30 m, crosslinked 5% phenyl methylsilicone), injecting 0.4 ml of the headspace. The injection and detector temperatures were 220 and 330 °C, respectively. The GC oven temperature program starts at 50 °C, holding this temperature for 1 min and then increasing it at a rate of 3 °C/min up to 180 °C and subsequently at a rate of 10 °C/min up to 210 °C.

HAN and HKs analyses are based on the EPA method 551.1. Briefly, the samples (30 mL) were transferred to 60 mL extraction vials and then potassium phosphate buffer with ammonium chloride (5 mL), MTBE fortified with 1,2,3-trichloropropane as internal standard (3 mL) and anhydrous sodium sulfate (10 g) were added. The vials were shaken using a vortex for 4 min and, then, allowed for phase separation. The organic phase was analyzed on a GC-ECD instrument. A DB624 column was employed as stationary phase. The GC program was: 35 °C for 20 min, 25 °C/min to 145 °C and hold for 10 min, 35 °C/min to 250 °C and hold for 10 min. The injector and detector temperatures were set at 220 and 330 °C, respectively.

HAAs were determined following the EPA method 552.3. For HAA analyses, the samples (40 mL) were transferred to 60 mL extraction vials where $\text{H}_2\text{SO}_{4(c)}$ (2 mL) and sodium sulfate (18 g) were added. Then, MTBE (3 mL) and NaCl (8 g) were added. The vials were shaken using a vortex for 5 min and, then, submitted to phase separation. The organic phase was transferred to a borosilicate glass tube (10 mL) and, then, methylation was performed by addition of a $\text{H}_2\text{SO}_4/\text{MeOH}$ solution (1 mL, 10 %), heating the samples in a water bath for 2 h at 50 °C. Then, the samples were cooled down to room temperature and quenched with a saturated bicarbonate aqueous solution (4 mL). The organic phase was analyzed in a GC-ECD equipped with a DB-1 column. The GC temperature program was: 35 °C for 6 min, 10 °C/min to 220 °C and dwelling time of 0 min. The injector and detector temperatures were set at 200 and 300 °C, respectively.

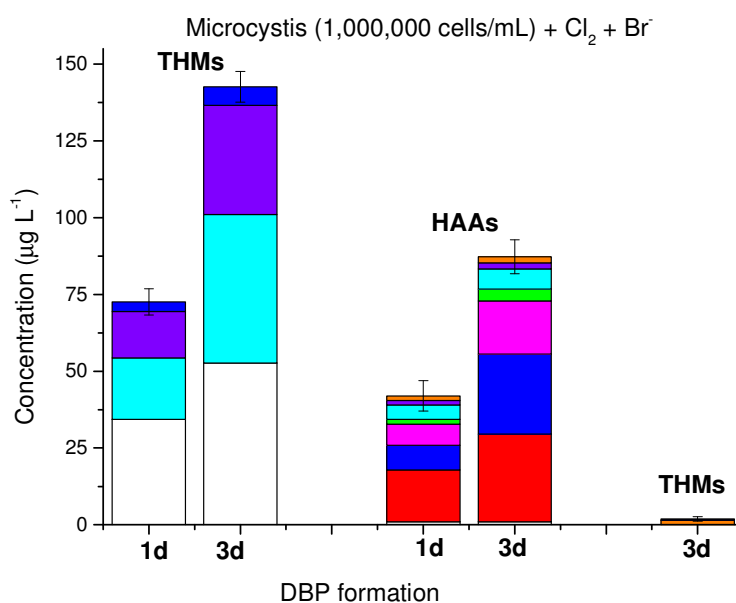


Figure S1. DPB formation from *Microcystis aeruginosa* aqueous suspensions under chlorination at pH 8 in the presence of bromide ions. Legend: THMs (TCM-white, BDCM-cyan, CDBM-purple, TBM-blue), HAAs (MCAA-yellow, MBAA-white, DCAA-red, TCAA-blue, BCAA-pink, BDCAA-green, DBAA-cyan, CDBAA-purple, TBAA-orange), HANs (DCAN-orange, TCAN-blue). Reaction conditions: Cyanobacteria concentration (1,000,000 cells/mL), chlorine dose (18 mg/L), ozone dose (1.6 mg/L), pH 8, bromide ions (300 µg/L), temperature (20 °C).

Table S1. DPB formation after one (1 d) or three (3 d) days for <i>Microcystis</i> aqueous suspensions under chlorination without or after pre-ozonation as a function of the pH and in the absence or presence of bromide ions. ^a									
DBP		Cl ₂		Cl ₂ + Br ⁻		Cl ₂ + O ₃		Cl ₂ + Br ⁻ + O ₃	
		Ave- rage (µg/L)	σ ^b µg/L	Ave- rage (µg/L)	σ µg/L	Ave- rage (µg/L)	σ µg/L	Ave- rage (µg/L)	σ µg/L
THMs (µg/L)	pH 8, 1 d	14.8	1.9	48.5	3.5	22.0	1.8	36.5	2.8
	pH 8, 3 d	40.2	4.9	81.4	3.9	63.1	2.8	102	3.2
	pH 6.5, 1 d	8.0	0.8	5.3	3.1	16.3	2.1	26.9	2.1
	pH 6.5, 3 d	15.8	3.0	35.3	2.8	38.5	1.6	75.7	3.1
HAAs (µg/L)	pH 8, 1 d	16.1	1.9	27.0	3.3	21	1.1	25.6	2.5
	pH 8, 3 d	39.1	2.9	46.0	3.8	39.1	2.2	49.3	3.1
	pH 6.5, 1 d	15.4	2.1	24.5	3.2	20.7	0.8	20.4	2.0
	pH 6.5, 3 d	32.8	2.8	41.3	2.9	17.9	1.0	46.0	3.0
HANs (µg/L)	pH 8, 3 d	0.6	0.5	1.8	0.9	0.4	0.3	1.5	0.5
	pH 6.5, 3 d	3.3	1.1	4.0	1.1	2.5	0.5	2.0	0.5

^a Reaction conditions: Cyanobacteria concentration (10,000 cells/mL), chlorine dose (11 mg/L), ozone dose (1.6 mg/L), pH as indicated, bromide ions (300 µg/L), temperature (20 °C).

^b Standard deviation

Table S2. DPB formation after one (1 d) or three (3 d) days for <i>Anabaena</i> aqueous suspensions under chlorination without or after pre-ozonation as a function of the pH and in the absence or presence of bromide ions. ^a									
DBP		Cl ₂		Cl ₂ + Br ⁻		Cl ₂ + O ₃		Cl ₂ + Br ⁻ + O ₃	
		Average μg/L	σ ^b μg/L	Average (μg/L)	σ μg/L	Average (μg/L)	σ μg/L	Average (μg/L)	σ μg/L
THMs (μg/L)	pH 8, 1 d	12.1	2.9	32.6	2.8	30.2	3.0	36.7	2.8
	pH 8, 3 d	35.0	2.9	55.3	3.5	45.9	4.2	81.8	3.9
	pH6.5, 1 d	1.5	1.1	10.1	2.1	9.5	2.1	33.0	3.0
	pH6.5, 3 d	14.3	2.5	35.3	2.6	39.4	2.5	70.6	3.5
HAAs (μg/L)	pH 8, 1 d	13.9	2.6	15.0	2.7	13.9	4.1	17.1	3.1
	pH 8, 3 d	33.0	3.9	43.2	3.5	33.0	4.9	42.1	3.9
	pH6.5, 1 d	13.3	2.8	14.5	1.9	13.3	3.5	14.8	2.7
	pH6.5, 3 d	21.5	3.5	40.9	3.1	21.4	4.3	33.2	3.4
HANs (μg/L)	pH 8, 3 d	0.04	0.5	0.5	0.9	0.5	0.3	2.0	0.5
	pH6.5, 3 d	3.2	1.0	3.1	0.8	0.7	0.5	4.4	0.9
^a Reaction conditions: Cyanobacteria concentration (10,000 cells/mL), chlorine dose (11 mg/L), ozone dose (1.6 mg/L), pH as indicated, bromide ions (300 μg/L), temperature (20 °C). ^b Standard deviation									

Table S3. DPB formation after one (1 d) or three (3 d) days for <i>Oscillatoria</i> aqueous suspensions under chlorination without or after pre-ozonation as a function of the pH and in the absence or presence of bromide ions. ^a									
DBP		Cl ₂		Cl ₂ + Br ⁻		Cl ₂ + O ₃		Cl ₂ + Br ⁻ + O ₃	
		Ave- rage μg/L	σ ^b μg/L	Ave- rage μg/L	σ μg/L	Ave- rage μg/L	σ μg/L	Ave- rage μg/L	σ μg/L
THMs (μg/L)	pH 8, 1 d	13.1	2.1	26.2	3.2	30.7	3.5	48.3	2.9
	pH 8, 3 d	35.0	4.4	2.5	4.1	41.2	4.9	85.5	3.2
	pH6.5, 1 d	3.1	1.5	62.5	1.9	8.4	1.9	17.1	4.1
	pH6.5, 3 d	10.5	3.0	12.8	2.1	26.2	2.8	55.6	3.0
HAAs (μg/L)	pH 8, 1 d	11.9	2.1	25.6	2.6	16.8	2.0	21.4	3.2
	pH 8, 3 d	35.3	4.4	42.8	3.5	39.2	1.9	55.2	4.1
	pH6.5, 1 d	9.1	2.1	22.1	2.1	13.8	2.9	20.8	2.2
	pH6.5, 3 d	29.9	2.5	39.4	2.9	33.7	3.5	45.3	3.6
HANs (μg/L)	pH 8, 3 d	0.5	0.4	0.9	0.5	0.5	0.5	0.7	0.7
	pH6.5, 3 d	0.7	1.1	5.1	1.9	0.7	0.9	2.4	0.6
^a Reaction conditions: Cyanobacteria concentration (10,000 cells/mL), chlorine dose (11 mg/L), ozone dose (1.6 mg/L), pH as indicated, bromide ions (300 μg/L), temperature (20 °C). ^b Standard deviation									

Chapter 3. DBPs from cyanobacteria by chlorination with/without ozonation

Chapter 4

Engineering of activated carbon surface to enhance the catalytic activity of supported cobalt oxide nanoparticles in peroxymonosulfate activation

4.1 Introduction

Advanced oxidation processes (AOPs) are a class of chemical treatments for pollutant remediation in soil [1,2], water [3–5] and air [6]. The aim of AOPs is the generation of highly aggressive radicals such as $\text{HO}\cdot$, $\text{HOO}\cdot$ or $\text{SO}_4^{\cdot -}$ that able to attack virtually any organic contaminant in aqueous media triggering their aerobic degradation and, eventually, their mineralization [5,7]. In the field of waste water treatments AOPs are frequently employed to degrade recalcitrant, toxic and/or non-biodegradable compounds that cannot be treated using conventional biological water treatments [8]. One of the AOPs with easiest implementation is the (photo)Fenton reaction that employs Fe(II) salts and H_2O_2 at acidic

pH (~3) to generate hydroxyl radicals from H_2O_2 [3,5]. One of the main drawbacks, however, of the (photo)Fenton reaction is the need of acidic pH values in order to avoid iron precipitation. The use of acidic pH values is also beneficial for H_2O_2 stability since at basic pH values it decomposes spuriously to O_2 without generating HO^\cdot radicals. An alternative AOP treatment that is less pH dependent based on the Co(II) ions as homogeneous catalyst to activate peroxydisulfate (PDS) to generate sulfate radicals ($\text{SO}_4^{\cdot-}$) [9–11]. It is worth to mention that in comparison to Fe(II) , Co(II) ions remain soluble in aqueous solutions at pH values below 9.4 [9,10]. Importantly, PDS can operate efficiently at higher pH values including neutral aqueous solutions [9]. At basic pH values PDS decomposition occurs spontaneously at high rates without the need of any catalyst, the challenge being at room temperature developing catalyst for pH values below 7 [11,12]. Sulfate radicals have an oxidation potential fairly independent on the pH value of about 2.5 – 3.1 V vs standard hydrogen electrode, while, in contrast, the redox potential of hydroxyl radicals is strongly dependent of the pH ranging from 1.8 to 2.7 [10]. In addition, sulfate radicals have a longer half-life (30–40 μs) compared to hydroxyl radicals (1 μs) [10].

Regardless the good pollutant degradation efficiencies achieved using the commented homogeneous AOPs under optimal reaction conditions, practical applications are limited due to the need of removal from the treated waters of dissolved transition metals employed in the process to avoid negative environmental impacts and risks for the human health [4,5,10,11]. Cobalt concentration is typically limited in drinking water to values lower than $50 \mu\text{g L}^{-1}$ [11]. The removal of the transition metal ions is generally carried out by precipitation with the disadvantage of needing further addition of chemicals and the subsequent sludge formation. Furthermore, in order to accomplish the water quality regulations, the removal of these transition metal ions should be done at levels below micrograms per liter [13]. These reasons, strongly limit the practical applications of homogenous AOPs using transition metals other than Fe.

In order to solve these problems, heterogeneous catalytic AOPs have been developed [10,11,14–16]. Frequently, metal or metal oxide NPs are supported on a high surface area insoluble material, allowing the easy recovery and

immobilization of the transition metal [10,11,14,15]. In this context, cobalt species are among the most catalyst for PMS activation, leading to the generation of oxyl radicals [17–24]. Recently, nanocarbon materials have also been employed as heterogeneous carbocatalysts for PMS activation [25,26].

However, in spite of the advances done in the field of heterogeneous cobalt-based catalysts for PMS activation, there still remain some challenges to increase further the activity and stability of the catalysts. Among these challenges, those dealing with the preparation of small metal NPs and their stabilization through a strong interaction with the support are crucial to obtain highly efficient and stable materials [10,11,27].

The present work shows the importance of an adequate surface functionalization of activated carbon to support small, active and stable cobalt oxide NPs able to activate PMS at neutral or acidic pH values. In this way, efficient heterogeneous catalyst promoting phenol degradation at neutral and acidic pH values as aqueous model pollutant has been obtained. The highest activity has been determined for the catalyst having the smallest cobalt oxide NPs. Thus, it will be shown that commercial active carbon functionalized by HNO₃ acid treatment under optimal conditions is a suitable support to deposit small cobalt oxide NPs with enhanced catalytic activity. In contrast, activated carbon functionalization with a controlled thermal oxidation results in a catalyst with lower activity due to the bigger cobalt oxide NPs are formed. The influence of the cobalt oxidation state on the resulting catalytic activity has been also evaluated, observing that cobalt oxide NPs are more active than reduced cobalt. Importantly, the activated carbon supported cobalt oxide catalyst can be reused at least eight times at neutral pH and room temperature without observing neither loss of catalytic activity nor metal leaching. Selective quenching experiments and electron paramagnetic resonance (EPR) spectroscopic study prove that PMS activation using the supported cobalt oxide catalyst generates hydroxyl radicals.

4.2 Experimental section

4.2.1 Materials

Oxone® (potassium peroxydisulfate, PMS) ($\text{KHSO}_5 \cdot 1 / 2\text{KHSO}_4 \cdot 1 / 2\text{K}_2\text{SO}_4$, MW 307.38), commercial activated carbon (AC, Norit SX Ultra, ref. 53663), $\text{Co}(\text{NO}_3)_2 \cdot 6\text{H}_2\text{O}$ (> 99.999% purity), Co_3O_4 nanopowder (<50 nm particle size based on transmission electron microscopy measurements) and phenol (>99.5% purity based on gas chromatography analysis) were supplied by Sigma-Aldrich (Madrid, Spain). Other reactants or solvents employed were analytical or high-performance liquid chromatography (HPLC) grade and they were also supplied by Sigma-Aldrich (Madrid, Spain).

4.2.2 Methods

Commercial activated carbon functionalization by nitric acid

Briefly, commercial AC (1 g) was dispersed in concentrated nitric acid (65%, 25 mL) in a round-bottom flask (100 mL) and the system heated at 83 °C for 24 h. Once the system was cooled down to room temperature, the suspension was transferred to two centrifuge tubes (20 mL each) and, then, the suspension centrifuged at 14,000 rpm for 20 min. Then, the supernatant liquid was disposed in an appropriate acid liquid residue container. Subsequently, the centrifuge tubes containing the solid sample were filled with Milli-Q water (20 mL each) and dispersed using a laboratory Vortex mixer. Several consecutive centrifugation-redispersion washings with Milli-Q water were performed until the pH of the supernatant was neutral. Finally, the solid was dried in an oven at 100 °C for 24 h and the sample labelled as ACN.

AC functionalization by thermal treatment

Briefly, commercial AC (200 mg) placed in a ceramic crucible was heated (7 °C min^{-1}) in an oven under static air up to 420 °C and, this temperature was

maintained for 2 h. Then, the sample was cooled down to room temperature and labelled as ACT.

Deposition of cobalt NPs on the AC supports (Co/ACs)

Cobalt NPs were supported on commercial AC, ACN and ACT solids by using the polyol method [28]. Briefly, the corresponding active carbon support (200 mg) placed in a round-bottomed flask (250 mL) was suspended with ethylene glycol (80 mL). Activated carbon was dispersed in ethylene glycol by sonication for 20 min. Subsequently, the flask was placed in a heat-on block and magnetically stirred. Then, the appropriate amount of cobalt salt dissolved in water (1 mL) was added to the suspension to achieve the required metal loading (0.2 or 1 wt%) and the system was heated at 85 °C for 4 h under magnetic stirring. After cooling the system at room temperature, ethanol (80 mL) was added to the flask containing the solid catalyst in ethylene glycol to favor solid sedimentation during centrifugation. Then, the mixture was transferred to eight centrifuge tubes (20 mL each) and centrifuged at 14,000 rpm for 20 min. At this time, the supernatant was removed, additional ethanol (20 mL per centrifuge tube) was added and the sediment redispersed using a Vortex mixer. This process was repeated four times using Milli-Q water as solvent. Finally, the sediment in each centrifuge tube was suspended again using Milli-Q water (20 mL) and the dispersion placed in a round-bottomed flask (250 mL). The flask was frozen using liquid nitrogen and, then, freeze-dried using a lyophilizer (Telstar LyoQuest). The resulting samples were labelled as Co/AC, Co/ACN or Co/ACT. These solid samples (200 mg) were further oxidized in an oven under static air at 180 °C for 2 h and the samples labelled as Co_{ox}/AC, Co_{ox}/ACN or Co_{ox}/ACT. Analogous Fe_{ox} or Cu_{ox} supported on ACN catalysts were also prepared using this methodology employing Fe(NO₃)₃·7H₂O or Cu(NO₃)₂ salts as metal precursors.

Unsupported cobalt oxide NPs were prepared by reduction of an aqueous solution (25 mL) containing cobalt nitrate hexahydrate (10 mg mL⁻¹) using 10-fold excess of NaBH₄ as reducing agent. Although the primary particle size

could be smaller, the solid agglomerate into larger particles that can be recovered by filtration (0.2 μm Nylon filter) and washed with distilled water (500 mL). Finally, the solid was placed in an oven and heated at 180 $^{\circ}\text{C}$ for 2 h.

4.2.3 Catalyst and activated carbon characterization

Powder X-ray diffractograms (PXRD) were collected by using a Philips X-Pert diffractometer equipped with a graphite monochromator operating at 40 kV and 45 mA that employed Ni-filtered CuK α radiation. FTIR spectra were measured by using a Bruker Tensor 27 FT-ATR instrument. Prior to recording the FTIR spectra the samples were dried in an oven for 24 h at 80 $^{\circ}\text{C}$, then, equilibrated at room temperature before the measurements. A Perkin Elmer CHNOS analyzer was employed for combustion elemental analysis. Temperature-programmed desorption (TPD) coupled to a mass-spectrometer (TPD-MS) analyses of the active carbons (100 mg) were carried out in a Micrometer II 2920 connected to a quadrupolar mass-spectrometer measurements were carried out by heating the sample from room temperature to 900 $^{\circ}\text{C}$ at 10 $^{\circ}\text{C min}^{-1}$. X-ray photoelectron spectroscopy (XPS) measurements were performed on a SPECS spectrometer with an MCD-9 detector using a monochromatic Al ($K\alpha=1486.6$ eV) X-ray source. CASA software has been employed for spectra deconvolution setting at 284.4 eV [29] the C1s peak as reference. Isothermal N_2 adsorption measurements were carried out using a ASAP 2010 Micrometrics apparatus. The metal loading (Co, Fe or Cu) on the ACs was determined by inductively coupled plasma combined with optical atomic emission spectroscopy detection (ICP-OES). Cobalt leaching was assessed by ICP-OES in the liquid reaction phase after removal the solid catalyst at the end of the reaction. A JEOL JEM-2100F instrument operating at 200 kW under dark-field scanning transmission electron microscopy (DF-STEM) was employed for metal particle size estimation measuring the dimensions of more than 200 particles. Microanalysis of the particles was performed by using an EDX detector (Oxford instrument) coupled to the DF-STEM measurements.

4.2.4 Catalytic activity and reaction analysis

Catalytic experiments were carried out at least in duplicate. Briefly, the required amount of catalyst was added to a round-bottomed flask (500 mL) containing an aqueous phenol solution (100 mL; 100 mg L^{-1} ; 1.06 mM). In order to achieve a good catalyst dispersion in the aqueous reaction medium and the system was sonicated (450 W) for 20 min analogously to previous reports [30]. The initial pH of the suspension was adjusted to the required value using aqueous solutions of NaOH (0.1 M) except for pH values below 6 where H_2SO_4 (0.1 M) was employed. If necessary, the flask was placed in a heat-on block and heated at the required temperature. The corresponding amount of PMS dissolved in water (1 mL) at the corresponding pH value was added. During the course of the reaction the pH frequently was adjusted at the required value by addition of H_2SO_4 (0.1 M) or NaOH (0.1 M). During the course of the reaction several aliquots (2 mL) were taken and immediately filtered (Nylon filter $0.2 \mu\text{m}$). Then, to each filtered reaction aliquot ten microliters of dimethylsulfoxide (DMSO) were added to quench the oxidation reaction.

In order to study the reusability of the catalyst, the catalytic reaction was carried out as commented above but using a round-bottomed flask of 1 L containing the aqueous phenol solution (600 mL; 100 mg L^{-1} ; 1.06 mM). It should be commented that the use of this reaction volume allows to perform the sampling for both PMS and phenol analysis (about 2 mL each reaction aliquot) as well as recover the catalyst for at least eight consecutive reaction cycles. Thus, after each catalytic cycle the solid was recovered at the end of the reaction by filtration using a nylon membrane ($0.2 \mu\text{m}$), washed with a NaOH aqueous solution (pH 10) and then Milli-Q water to remove possible adsorbed organic or inorganic substances. It should be noted that previous studies on phenol degradation have confirmed that basic washings remove completely all the organic matter from phenol degradation [31]. Then, the catalyst was employed in a new catalytic cycle.

Productivity tests were carried out using large amount of phenol (10 g L^{-1} ; 106.4 mM) and PMS (280 g L^{-1} ; 911 mM) with respect to the catalyst (200 mg

L⁻¹; 0.0067mM of supported cobalt) at pH 7 and 20 °C. The catalyst was reused under these concentrations several times as previously described.

Analysis of phenol, catechol, hydroquinone and p-benzoquinone. Previously filtered reaction aliquots (Nylon filter 0.2 μm) were analyzed by reverse-phase liquid chromatography. The injected volume of the sample was 200 μL. A Kromasil-C18 column was employed as stationary phase. Elution was carried out under isocratic conditions (69:30:1 vol% H₂O/CH₃CN/CH₃COOH). The system used a photodiode array as detector. The samples from the productivity test were diluted 100-fold in Milli-Q water before analysis. The wavelengths for the detection of phenol, hydroquinone, catechol and p-benzoquinone were 209, 221, 230 and 245 nm, respectively.

Total organic carbon (TOC) analysis. A High-TOC Elementar II analyzer was employed for TOC measurements of previously filtered aqueous reaction aliquots. The method is based on the complete combustion of the organic matter present in the aqueous sample at 950 °C catalyzed by Pt and quantification of evolved CO₂ gas by quantitative IR spectroscopy.

PMS measurements. PMS concentration was measured using a spectrophotometric method [32]. Briefly, a previously filtered reaction aliquot (0.5 mL) was diluted with Milli-Q water (100 mL). Then, 5 mL of the diluted reaction aliquot was mixed with a KI solution (0.5 mL, 2 mg/mL) and allowed to react for 10 min before measuring its absorbance at 360 nm.

EPR measurements. EPR spectra were recorded using phenyl tertbutyl nitron (PBN) as spin trapping agent under the following reaction conditions: catalyst (200 mg L⁻¹, 0.0067mM of supported cobalt), PBN (1,000 mg L⁻¹), PMS to PBN molar ratio 1, pH 7, reaction time (5 min). Previously filtered (0.2 μm) and nitrogen-purged aliquots were measured in a Bruker EMX spectrometer using the following typical settings: frequency 9.803 GHz, sweep width 3489.9 G, time constant 40.95 ms, modulation frequency 100 kHz, modulation width 1 G, and microwave power 19.92 mW.

Radical quenching experiments. Selective radical quenching experiments were carried out under the following conditions. Firstly, the catalyst (200 mg L⁻¹;

0.0067 mM) was added to a round-bottomed flask (500 mL) containing an aqueous phenol solution (100 mL, 100 mg L⁻¹). Then, the pH of the reaction system was adjusted to 7 using a NaOH aqueous solution (0.1 M). Then, the quencher agent namely DMSO (0.647 mL), methanol (0.4 mL) or tert-butanol (0.94 mL) was added to the phenol solution (100 mL) achieving a concentration of about 1 M. After that, the system was sonicated for 20 min. Then, the system was placed in a heating plate and magnetically stirred. Finally, PMS (280 mg dissolved in 1 mL and adjusted at pH 7) was added to the flask. The radical quencher to PMS molar ratio is about 10.

4.3 Results and discussion

4.3.1 Support preparation and characterization

The use of carbonaceous materials as metal NP supports is one of the main areas of research in heterogeneous catalysis [15]. In this sense, some examples have shown that the chemical composition, the textural properties and the groups on the surface of the carbonaceous materials determine the resulting metal particle size distribution and, therefore, the catalytic activity [27]. With these precedents in mind, our work starts with the functionalization of commercial activated carbon (Norit), referred as AC, by chemical [33,34] or thermal oxidative treatment [30]. The chemical functionalization of the activated carbon consists in a liquid phase oxidation of AC by nitric acid resulting in a sample labeled as ACN. The thermal functionalization method consists in submitting AC to an aerobic oxidation in static air at 420 °C in an oven. The thermogravimetric analysis of commercial AC solid (Fig. S1a) shows that the sample starts to undergo combustion at about 500 °C. Since the purpose of the thermal treatment is the functionalization of the commercial AC with oxygen functional groups a lower temperature was chosen in accordance to analogous previous reports [30]. The presence of oxygen in the treatment is expected to cause the partial oxida-

tion of the most external layers of AC resulting the generation of hydroxyl, carbonyl and carboxyl functional groups. This partial oxidation will be easily confirmed by chemical analysis (Table 1) and the mineralization degree of the thermal functionalized AC sample was less than 3 wt%. In accordance with this treatment, Raman spectra do not show a decrease in the defect density. This sample is labelled as ACT. The three samples (AC, ACT and ACN) were characterized by combustion elemental analysis, FT-IR and Raman spectroscopy, isothermal N₂ adsorption, XPS, TPD-MS, XRD and SEM.

	C (%)	C/H molar ratio (%)	C/O molar ratio (%)	BET surface area (m ² g ⁻¹)	Pore volumen (cm ³ g ⁻¹)
AC	76.7	14.3	4.5	880	0.32
ACN	58.3	5.4	2.0	710	0.26
ACT	74.3	14.9	4.0	1040	0.35

Elemental analysis data show that the oxidative treatment of AC using HNO₃ is more effective to increase the oxygen content of the carbon than that based on the thermal treatment (Table 1). In particular, the chemical treatment using HNO₃ affords a high decrease of carbon content together with a concomitant increase in oxygen content compared to ACT sample. A small increase of elemental nitrogen in the ACN sample (1.0 wt%) respect to the commercial AC sample (0.3 wt%) was also observed and attributed to the functionalization with nitrogen oxide species [33,34]. Isothermal N₂ adsorption (Figs. S1–S3) of the ACs reveals that, regardless the observed variations respect to AC, the resulting carbonaceous samples exhibits surface areas and pore volumes higher than 700 m² g⁻¹ and 0.26 cm³ g⁻¹, respectively. The lower values observed for the ACN sample can be attributed to space required to accommodate a large density of oxygenated functional groups within the pores of the solid.

Raman spectroscopy of the three AC samples shows the characteristic vibrations modes due to the stretching of sp² carbons at 1597 cm⁻¹ (G band), occurrence of disordered structure at 1317 cm⁻¹ (D band) and the stacking of

the sp^2 network layers at 2567 cm^{-1} (2D band) (Fig. 1a) [35]. Functionalization of AC sample by thermal or chemical methods results in an increase of the defect population as revealed by the increase in the intensity of D respect to G band [35]. FT-IR spectroscopy of the functionalized activated carbons shows an intensity increase of the peaks appearing at 1725 cm^{-1} and 1160 cm^{-1} attributable C=O and C-O stretching bands, respectively, as well as the band appearing at 1560 cm^{-1} corresponding to the presence of conjugated unsaturated C=C bonds (Fig. 1b) [34,36]. All these observations are in agreement with the increase of oxygen content observed by elemental analysis.

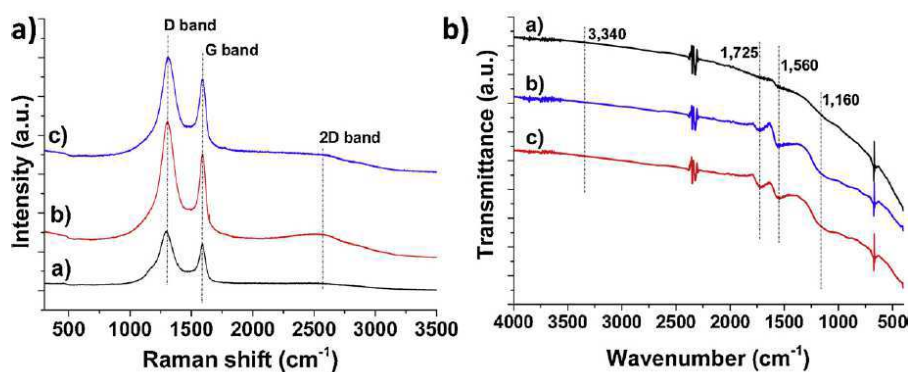


Fig.1. Raman (a) and FT-IR (b) spectra of AC (a), ACT (b) and ACN (c) materials.

The three ACs were further analyzed by TPD (Fig. 2a) and TPD-MS (Fig. 2b and c) measurements under inert atmosphere. In particular, the TPD-MS allows identification by mass spectrometry of H_2O (m/z 18), CO (m/z 28) and CO_2 (m/z 44) [34]. AC functionalization by HNO_3 resulted in the introduction of a large variety of oxygen functional groups including carboxylic acids, lactones, anhydrides, phenolic, carbonyls, ether and quinone among other possible [34,36]. In the case of AC functionalization by an oxidative thermal treatment at $420\text{ }^\circ\text{C}$ the resulting ACT solid results mainly functionalized with phenol, carbonyl and quinone moieties, probably because most of carboxylic acid moieties are unstable at the temperatures of the thermal treatment ($420\text{ }^\circ\text{C}$) or they are not formed [34,36].

The surface of the carbonaceous materials was evaluated by XPS analyses (Figs. 3 and S5) [34]. As expected, AC oxidation by chemical or thermal treatments resulted in a shift of the C1s signals at higher binding energies indicating the oxidation of the carbon surface. In the case of O1s, an increase of the signal intensity for ACN sample or a shift to higher binding energies in the case of ACT agree with a different level of oxidation of AC sample, depending on the treatment. These observations agree with the generation of different oxygen functional groups. The oxidation of the AC by chemical or thermal treatment as well as the increase of acidic oxygen functional groups was verified by measuring the pH of aqueous suspensions of AC, ACT and ACN (10 mg mL⁻¹) corresponding to the values of 6.5, 4.8 and 3.6, respectively.

PXRD of the ACs samples reveals that the structure is maintained after the functionalization of the commercial AC. The diffractograms show the two main characteristic broad bands of activated carbons appearing at around 2 θ 23 and 43° associated with the diffraction from the 002 and 100/101 planes in graphite, respectively (Fig. S4) [37]. SEM images show that the morphological structure is somehow preserved, but as the functionalization degree increases (ACN > ACT) the roughness of the AC surface increases (Fig. S6).

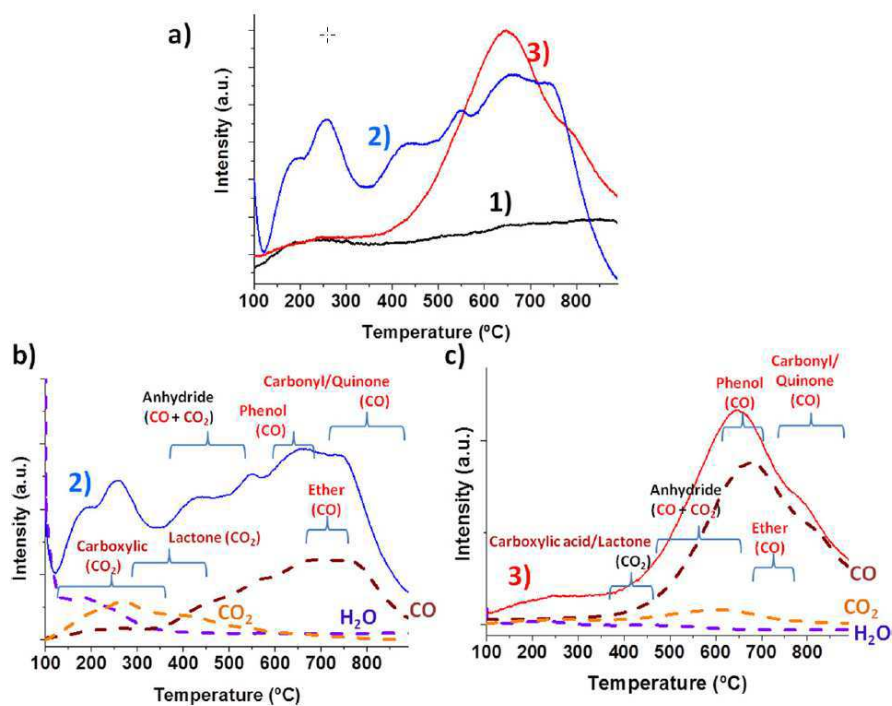


Fig.2. TPD (a) and TPD-MS (b, c) of commercial AC (1, black line), ACN (2, blue line) and ACT (3, red line). Legend: H₂O (violet dash line), CO₂ (orange dash line) and CO (brown dash line). (For interpretation of the references to colour in this figure legend, the reader is referred to the web version of this article)

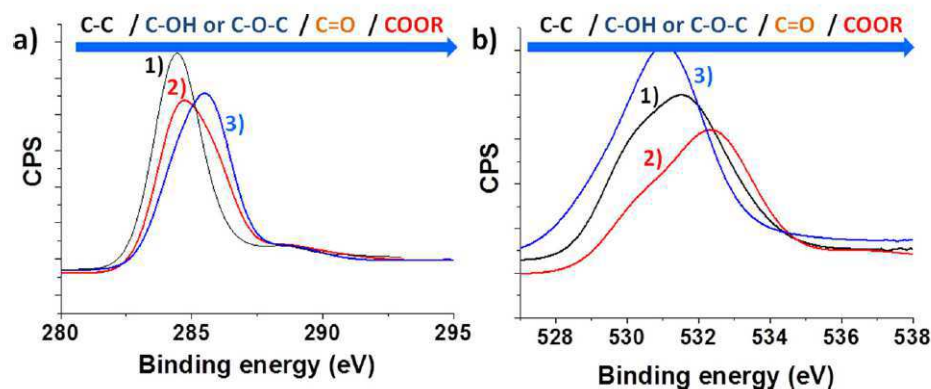


Fig.3. XPS C1s (a) and O1s (b) peaks of AC (1, black line), ACT (2, red line) and ACN (3, blue line). (For interpretation of the references to colour in this figure legend, the reader is referred to the web version of this article)

4.3.2 Metal supported on ACs

Deposition of cobalt NPs on the three activated carbons (AC, ACT and ACN) was carried out using the well-known polyol method [28,38]. In order to study the influence of the cobalt oxidation state on the catalytic activity for PMS activation, the Co NP supported on AC samples were further submitted to an aerobic oxidation under static air at 180 °C for 2 h. Several works have shown the influence of the cobalt oxidation state on PMS activation [10,11]. Table 2 summarizes the list of catalysts employed in the present work, including metal loading, average particle size distribution, standard deviation obtained from TEM measurements (Figs. 4, S7–S9) and the initial reaction rates for PMS activation and phenol degradation.

Table 2. Summary of the analytical and activity data for the catalysts prepared in the present work indicating metal loading, metal average particle size distribution and initial reaction rate for PMS degradation (r_{0_PMS}) and phenol decomposition (r_{0_phenol}).

Entry	Catalyst	Metal loading (wt%)	Average metal particle size and standard deviation (nm)	r_{0_PMS} (mM h ⁻¹)	r_{0_phenol} (mM h ⁻¹)
1	Co/ACN	0.2	2.9 ± 0.14	16.07	2.44
2	Co/ACT	0.2	3.3 ± 0.17	10.55	3.38
3	Co/AC	0.2	4.1 ± 0.23	8.91	3.94
4	Co _{ox} /ACN	0.2	4.7 ± 0.05	23.84	4.52
5	Co _{ox} /ACT	0.2	7.9 ± 0.26	21.22	5.25
6	Co _{ox} /AC	0.2	9.1 ± 0.25	12.51	6.40
7	Co _{ox} /ACN	1.0	5.8 ± 0.24	9.12	1.66
8	Fe _{ox} /ACN	1.0	5.6 ± 0.17	3.91	0.55
9	Cu _{ox} /ACN	1.0	6.3 ± 0.25	2.93	0.47

Selected DF-STEM images and metal particle size distribution histograms are shown in Fig. 4. Regardless the oxidation state of cobalt NPs, the smallest average cobalt particle size and standard deviation at the same metal loading is obtained using ACN as support (Table 2). Thus, it can be speculated that the presence of a high population of oxygen functional groups in ACN support is beneficial to support small metal NPs. As expected, the aerobic oxidation of cobalt NPs supported on ACs (Fig. S7) resulted in an increase of the cobalt oxide average particle size of about 2–3 nm (Table 2 and Fig. S8). Using ACN as support it was observed that an increase of the cobalt oxide content from 0.2 to 1.0 wt % resulted in an increase of both particle size distribution and standard deviation

(entries 4 and 7 in Table 2 and Fig. S9). Analogous catalysts based on iron and copper oxides supported on ACN were also prepared (entries 8 and 9 in Table 2 and Fig. S9) to compare their catalytic activity with that of cobalt-based materials. Formation of cobalt NPs was confirmed by EDX analyses of different points (Fig. S10a), areas (Fig. S10b) and mapping analyses (Fig. 4). In contrast to the small cobalt oxide NPs obtained on the different carbonaceous materials, large particles (> 200 nm) were obtained when the preparation of cobalt oxide was performed without the use of any support (Fig. S11).

XPS analysis was employed to get some insights about the cobalt oxidation state of the prepared catalysts. As it will be shown below $\text{Co}_{\text{ox}}/\text{ACN}$ is the most active catalyst for PMS activation. Initially, XPS of the $\text{Co}(0.2 \text{ wt\%})/\text{ACN}$ exposed to the ambient at room temperature is composed by Co NPs whose external layers are mostly constituted by Co (II) (Fig. 5a1). As expected the thermal aerobic oxidation at 180°C for 2 h of the $\text{Co}(0.2 \text{ wt\%})/\text{ACN}$ (Fig. 5a1) solid favors the further oxidation of the most external layers of Co NPs in the $\text{Co}_{\text{ox}}(0.2 \text{ wt\%})/\text{ACN}$ solid that after the treatment are mostly constituted by Co(II) and Co(III) species (Fig. 5a2). These oxidized Co(II / III) species are similar to those observed in the case of commercial Co_3O_4 solid (Fig. 5a3) and as-made Co_{ox} solid (Fig. 5a4). For the $\text{Co}_{\text{ox}}(0.2 \text{ wt\%})/\text{ACN}$ sample, Fig. 5b shows the deconvoluted peaks at around 779.7 and 781.4 eV attributable to the $\text{Co}^{3+} 2p_{3/2}$ and $\text{Co}^{2+} 2p_{3/2}$, respectively. The accompanying $2p_{1/2}$ spin-orbit component for Co^{3+} and Co^{2+} appear at 794.8 and 796.8 eV, respectively. The energy difference between $\text{Co} 2p_{3/2}$ and $\text{Co} 2p_{1/2}$ peaks is approximately 15 eV. Two Co^{2+} satellite peaks at 786.3 and 804.8 eV are also observed. Similar deconvolution in various cobalt species is obtained for the commercial Co_3O_4 or as-made Co_{ox} solids (Fig. S12). These XPS results agree with the presence of cobalt NPs in the form of Co_3O_4 and/or CoO [39–42]. Similarly, the XPS spectra of $\text{Fe}_{\text{ox}}/\text{ACN}$ and $\text{Cu}_{\text{ox}}/\text{ACN}$ samples reveal the presence of oxidized metal species in the form of $\text{Fe}^{3+}/\text{Fe}^{2+}$ or Cu^{2+} , respectively (Fig. S13) [43,44].

Diffuse reflectance UV–vis spectra of several of the cobalt oxide catalysts under study are presented in Fig. S14. Commercial Co_3O_4 and as-prepared Co_{ox} solids exhibit visible absorption bands in the regions about 400 and 650 nm that

should correspond to the $O^{2-}-Co^{2+}$ and $O^{2-}-Co^{3+}$ ligand to metal charge transfer, respectively. In the cobalt oxide NPs supported on ACN, these absorption bands seem to be masked by the black ACN support [45].

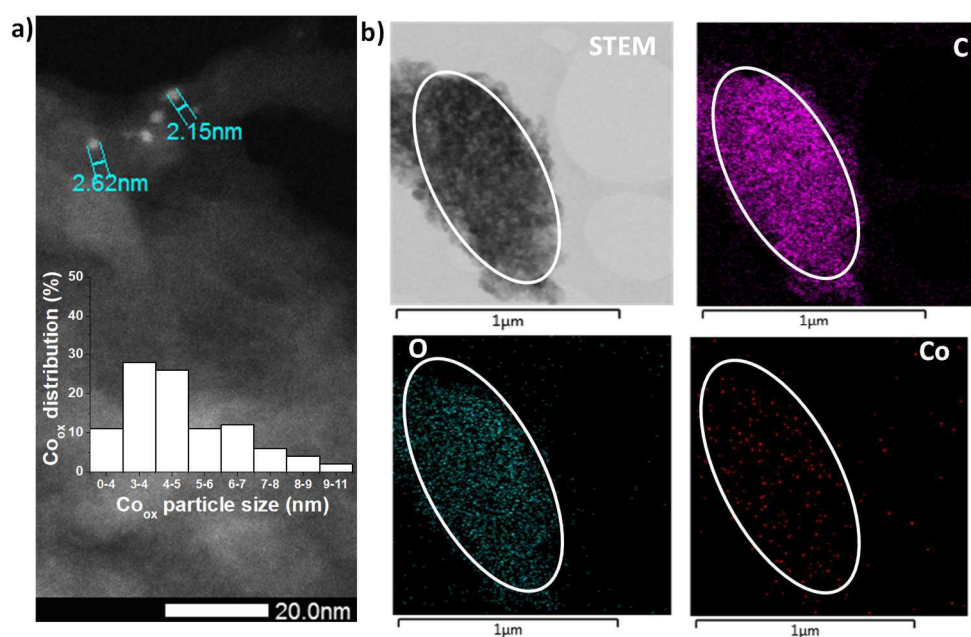


Fig. 4. a) DF-STEM image and cobalt particle distribution of $Co_{ox}(0.2 \text{ wt\%})/ACN$; b) STEM image and element mapping microanalyses of $Co_{ox}(0.2 \text{ wt\%})/ACN$. The inset in panel a shows the particle size distribution of cobalt oxide in $Co_{ox}(0.2 \text{ wt\%})/ACN$.

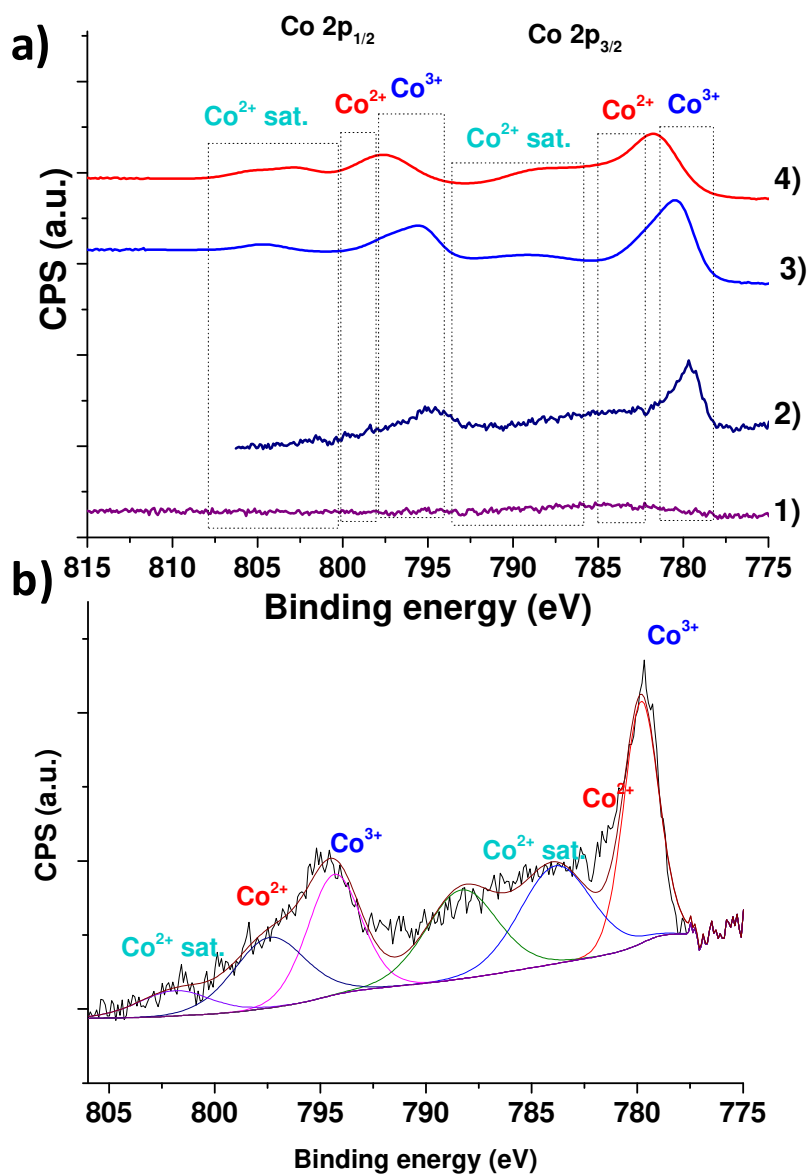


Fig. 5. XP spectra of Co(0.2 wt%)/ACN (a1), Co_{ox}(0.2 wt%)/ACN (a2), commercial Co₃O₄ solid (a3) and as-made Co_{ox} solid (5a4). Deconvoluted XP spectrum of Co_{ox}(0.2 wt%)/ACN (b).

4.3.3 Catalytic Activity

The series of prepared catalysts was tested for phenol degradation using PMS as oxidant. Phenol was selected as organic pollutant because is a non-bio-degradable, recalcitrant and toxic organic compound for the aquatic environment. Preliminary tests indicate that phenol adsorption on the three different ACs is lower than 5% (data not shown). Blank control experiments reveal that activation of PMS in the absence of catalyst is negligible at pH values below 6, but PMS decomposes faster as the pH value increases beyond pH 7 (Fig. S15). As expected, deposition of cobalt NPs supported on the carbonaceous materials increases the catalytic activity for PMS activation and phenol decomposition at pH values below 7 (Fig. 6 and Table 2). Fig. 6b shows that oxidized cobalt NPs supported on ACs (Co_{ox} supported on AC, ACT or ACN) are more active than analogous non-oxidized ones, even though the cobalt particle size distribution of the former indicates the larger average dimensions of Co particles after oxidation. It is a general observation in the field of catalysis by metal NPs that the catalytic activity increases as the size of the metal NP decreases [46]. In the present case, however, it seems that the oxidation state of cobalt NPs is more important than the particle size distribution for the activation of PMS. These results agree with previous reports showing the higher activity of cobalt oxides respect to metallic cobalt [10,11].

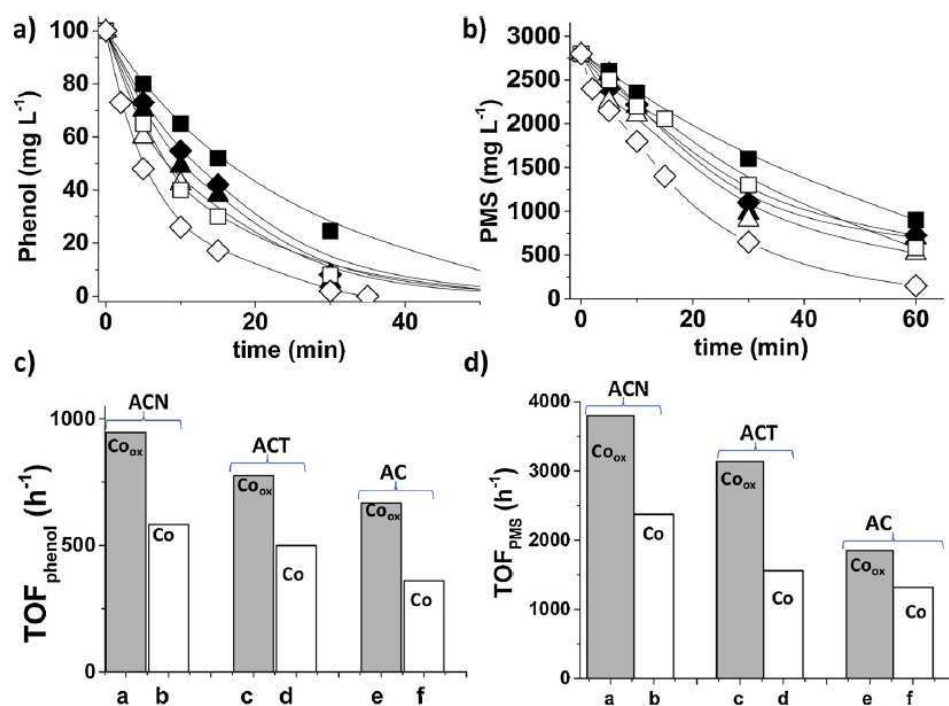


Fig. 6. Phenol degradation (a), PMS decomposition (b) and corresponding turnover frequency (TOF) value (c, d) using Co-NPs supported on AC (■, f), ACT (▲, d) and ACN (◆, b) and Co_3O_4 – NPs supported on AC (□, e), ACT (Δ, c) and ACN (◇, a). Reaction conditions: Catalyst (200 mg L^{-1} ; 0.0067 mM of supported cobalt), phenol (100 mg/L ; 1.06 mM), PMS (2800 mg L^{-1} ; 9.1 mM), $20 \text{ }^\circ\text{C}$, pH 7.

Among the different catalysts based on Co_{ox} NPs supported on ACs (AC, ACN and ACT), the highest catalytic activity has been achieved using the $\text{Co}_{\text{ox}}(0.2 \text{ wt\%})/\text{ACN}$ material that corresponds to that with the smallest cobalt oxidized metal NPs (Fig. 6). Based on the catalytic results and the characterization data of the ACs, it is proposed that the higher amount of oxygen functional groups in the ACN support generated by the chemical treatment allows a good dispersion of small cobalt NPs with enhanced catalytic activity respect to analogous ACT or AC supports. Therefore, considering the minor contribution of CAN (Fig. S15) to

the catalytic activity that is mainly due to cobalt species and the relationship between small particle size and high catalytic activity (Table 2), it is proposed that the main role of the carbon support is just to stabilize cobalt NPs avoiding their growth.

Fig. 7 shows that the catalytic activity of Co_{ox} supported on ACN increases as the cobalt loading decreases from 1.0 to 0.2 wt%. This fact was attributed to the lower cobalt particle size distribution observed with the sample at lower cobalt loading. Fig. 7 also presents the influence of the metal nature on the resulting catalytic activity for phenol degradation and PMS decomposition. The catalyst based on Co_{ox} NPs supported on ACN exhibiting higher activity than analogous catalysts based on Fe_{ox} or Cu_{ox} NPs supported on ACN at the same metal loading (1 wt%).

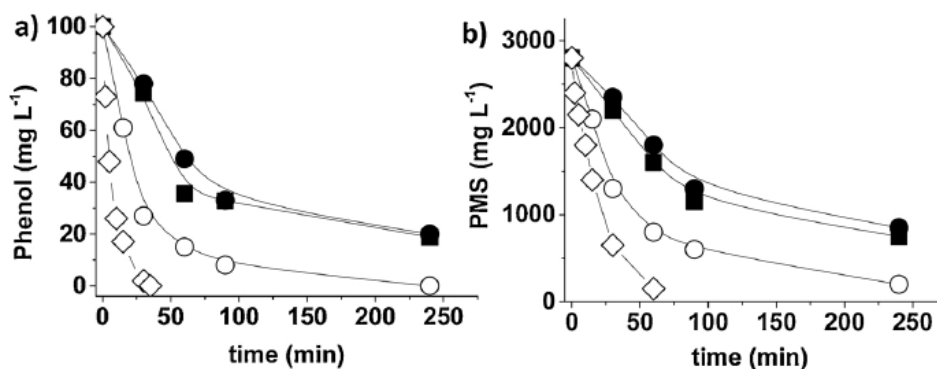


Fig. 7. Phenol degradation (a) and PMS decomposition (b) using Co_{ox} -NPs supported on ACN at 0.2 (◇) and 1 wt% cobalt loading (○). Fe_{ox} -NPs (■) and Cu_{ox} -NPs (●) supported on ACN at 1 wt% metal loading. Reaction conditions: Catalyst (0.0067mM of supported metal), phenol (100 mg/L; 1.06 mM), PMS (2800 mg L⁻¹; 9.1 mM), 20 °C, pH 7.

In order to put into context the catalytic activity of Co_{ox} (0.2 wt %)ACN its catalytic activity was compared to that obtained when using homogeneous Co^{2+}

ions, unsupported as-made Co_{ox} NPs or commercial Co_3O_4 solid as catalysts (Fig. 8). Frequently, phenol oxidation in water by PMS is faster when using Co^{2+} ions as homogeneous catalyst respect to the use of heterogeneous cobalt catalysts, such as cobalt oxide doped carbon aerogel [21]. Surprisingly, in the present work the activity of $\text{Co}_{\text{ox}}(0.2 \text{ wt}\%)\text{ACN}$ is higher ($\text{TOF}_{\text{PMS}} 3800$, $\text{TOF}_{\text{phenol}} 950$) than that obtained using Co^{2+} ions ($\text{TOF}_{\text{PMS}} 1460$, $\text{TOF}_{\text{phenol}} 330$) or as-prepared unsupported Co_{ox} NPs ($\text{TOF}_{\text{PMS}} 740$, $\text{TOF}_{\text{phenol}} 190$). These observations highlight the importance of high surface area, AC surface functionalization with the appropriate nature and population of oxygen functional groups for the dispersion of small metal NPs with specific metal oxidation state.

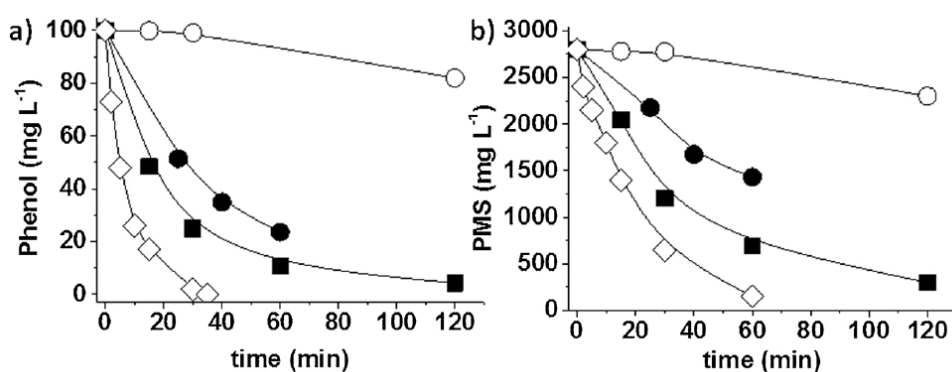


Fig. 8. Phenol degradation (a) and PMS decomposition (b) using Co_{ox} -NPs supported on ACN at 0.2 wt% metal loading (\diamond), using commercial Co_3O_4 NPs (\circ), as-prepared unsupported Co_{ox} NPs (\bullet) and using Co^{2+} as homogeneous catalyst (\blacksquare). Reaction conditions: Catalyst (0.0067mM of cobalt either using homogeneous or heterogeneous catalysts), phenol (100 mg/L; 1.06 mM), PMS (2800 mg L⁻¹; 9.1 mM), 20 °C, pH 7.

One of the main problems associated with AOPs for water treatment is the strong dependence of their efficiency with the pH [14,27]. The use PMS has been reported as one promising alternative to the use of other oxidants such as

H₂O₂ that typically requires strongly acidic pH solutions to achieve good efficiencies [10,11]. Herein it has been shown that Co_{ox}/ACN is an optimal catalyst for PMS activation and phenol degradation even at neutral pH values (Fig. 9). It should be reminded that PMS decomposition occurs spontaneously at an increasing rate as the pH value increases higher than 7 (Fig. S15a,b). This constitutes a significant advantage compared to other heterogeneous Fenton processes that only operate efficiently at strongly acidic pH values [3,5,14]. Previous studies using homogenous Co²⁺ ions or heterogeneous cobalt NPs supported on carbonaceous materials [47] have also found that those catalysts exhibit optimal performance at neutral or quasi-neutral pH values [10,48]. As it can be seen in Fig. 9 the catalytic activity of Co_{ox}(0.2 wt%)/ACN for PMS activation and phenol degradation increases with the pH. On one hand, an increase of the pH favors the formation of the more easily oxidizable phenolate. On the other hand, PMS decomposition should be a function of its speciation in the reaction medium [12]. Acidic pH values would increase the PMS stability and, therefore, it could make more difficult its activation towards radical formation [47,49]. Considering that PMS has a pK₂ in water about 9.4, the prevalent species at quasi-neutral pH values should be HSO₅⁻ (Fig. 9, Eq. (6)) and, therefore, it seems that the selective formation of SO₄^{-•} and/or HO[•] radicals is favored (Eqs. (1), (3) and (4) [12]. Eq. (7) represents a nucleophilic attack on the peroxide hydrogen of HSO₅⁻ by SO₅²⁻ leading to the formation of HSO₆⁻ (Eq. (7)). Finally, according Eq. (8) HSO₆⁻ in the presence of hydroxyl ions decomposes to form O₂ through a non-radical reaction pathway. The influence of pH on the activity of the Co_{ox}(0.2 wt%)/ACN catalyst agrees with the reported prior literature data reflected by Eqs. (1)–(8).



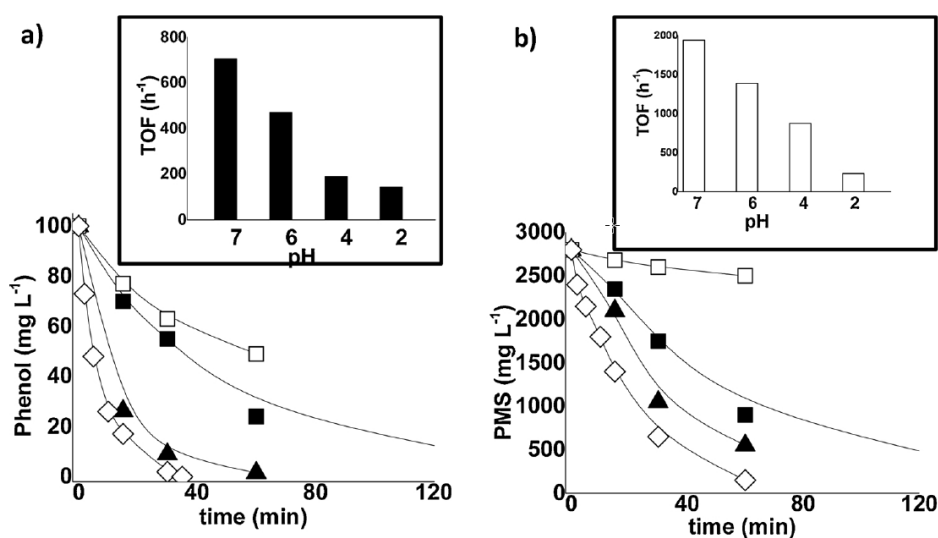


Fig. 9. Phenol degradation (a), PMS decomposition (b) and respective TOF values for phenol (black bar) and PMS (white bar) using $\text{Co}_{\text{ox}}/\text{ACN}$ at pH 2 (□), pH4 (■), pH 6 (▲) and pH 7 (◇). Reaction conditions: Catalyst (200 mg L^{-1} ; 0.0067 mM of supported cobalt), phenol (100 mg/L ; 1.06 mM), PMS (2800 mg L^{-1} ; 9.1 mM), 20°C , pH as indicated.

Other important parameter that should be considered when developing alternative AOPs is the amount of oxidant employed respect to the substrate [14,15,46]. Fig. 10 shows the influence of the initial PMS concentration on the

catalytic activity for phenol degradation. An optimal PMS to phenol molar ratio of 9.3 was found for phenol degradation and, more importantly, degradation of its even more toxic reaction intermediates namely catechol, hydroquinone and p-benzoquinone (Fig. S16). This value is lower than that required in other systems for complete degradation of phenol such as cobalt oxide supported on AC (oxone to phenol molar ratio 25) [20], cobalt oxide doped on carbon aerogel [21] or carbon xerogel [50] with an oxone to phenol molar ratio 12.8 even though still some toxic intermediates such as hydroquinone and p-benzoquinone were detected [21]. Thus, Co_3O_4 NPs supported in reduced graphene oxide employs a phenol to PMS molar ratio of about 60 or $\text{MnO}_2/\text{ZnFe}_2\text{O}_4$ uses a phenol to PMS ratio of 31 [51]. In the present work, under optimized reaction conditions a notable TOC reduction of about 70% was measured. Furthermore, a good relationship was also observed between the TOF for phenol degradation and the amount of PMS (Fig. 10d). The TOF values increase along the PMS concentration with the maximum values of 3300 and 550 h^{-1} achieved for PMS decomposition and phenol degradation, respectively.

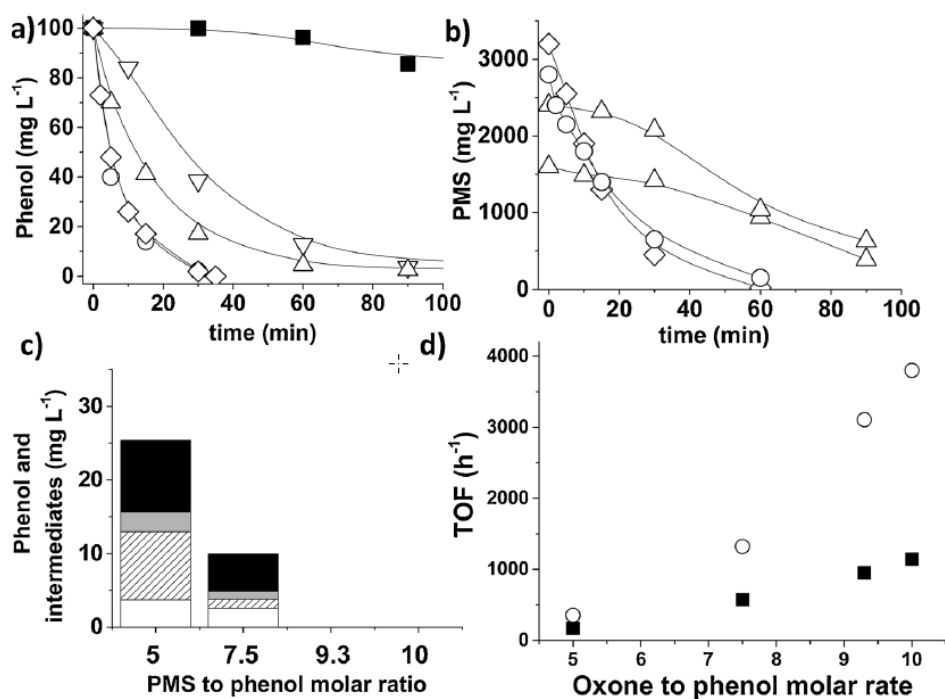


Fig. 10. Phenol degradation (a), PMS decomposition (b), remaining phenol and intermediates (c) and TOF for phenol degradation (○) and PMS decomposition (■) measured at 15 min (d) using Co_{ox}/ACN with different PMS dosages: 1600 mg L⁻¹ (10.5 mM, ■), 2400 mg L⁻¹ (7.9 mM, ○), 2800 mg L⁻¹ (9.1 mM, ▲), 3200 mg L⁻¹ (10.5 mM, □) and 4000 mg L⁻¹ (13.5 mM, ●). Reaction Conditions: Catalyst (200 mg L⁻¹; 0.0067mM of supported cobalt), phenol (100 mg L⁻¹), PMS (as indicated), 20 °C, initial pH 7.

The catalytic activity of the most active catalyst prepared in this work Co_{ox}(0.2 wt%)/ACN using PMS as oxidant was compared with that of H₂O₂ at pH 4 and 7 (Fig. S17). The degradation of phenol by H₂O₂ and Co_{ox}(0.2 wt%)/ACN as catalyst does not take place at neither pH value of 4 or 7. This observation agrees with previous reports showing the higher activity of the homogeneous Co²⁺/PMS systems respect to Co²⁺/H₂O₂ [52,53].

The influence of the temperature on the catalytic activity for PMS activation and phenol degradation using $\text{Co}_{\text{ox}}/\text{ACN}$ as catalyst allowed an estimation of the apparent activation energy for these processes at pH 7 (Fig. 11). The estimated E_a for PMS decomposition and phenol degradation is about 30 and 32 kJ mol^{-1} , respectively. These E_a values indicate that the catalytic ROS generated during the PMS decomposition, such as $\text{SO}_4^{\cdot-}$ and HO^\cdot (see reaction mechanism below), react in an almost barrierless process for phenol degradation. Furthermore, the lower E_a values at pH 7 compared to pH 4 reinforces the idea that is possible to develop AOP based on cobalt-catalyzed PMS activation for aqueous pollutant degradation at neutral pH values. These low E_a values obtained with $\text{Co}_{\text{ox}}(0.2 \text{ wt\%})/\text{ACN}$ compare favorably with similar systems based on cobalt oxide doped carbon aerogel (E_a for phenol 62.9 kJ mol^{-1} , pH not indicated) [21], cobalt oxide loaded on carbon xerogel (E_a for phenol degradation 48.3 kJ mol^{-1} , pH not indicated) [50], cobalt oxide on activated carbon (E_a for phenol degradation 59.7 kJ mol^{-1} , pH not indicated) [20], and other cobalt catalysts on other supports on such as ZSM5, mesoporous silicas such as SBA-15 [54] or SiO_2 ³⁷ with values ranging between 61.7 and 75.5 kJ mol^{-1} . While the previous commented literature E_a values refer to phenol degradation analogous E_a data referring to PMS decomposition are not available. It should be, however, commented the E_a for PMS decomposition is also an important kinetic parameter when comparing two activities of different catalysts, since it refers to the generation of the primary reactive oxygen radicals.

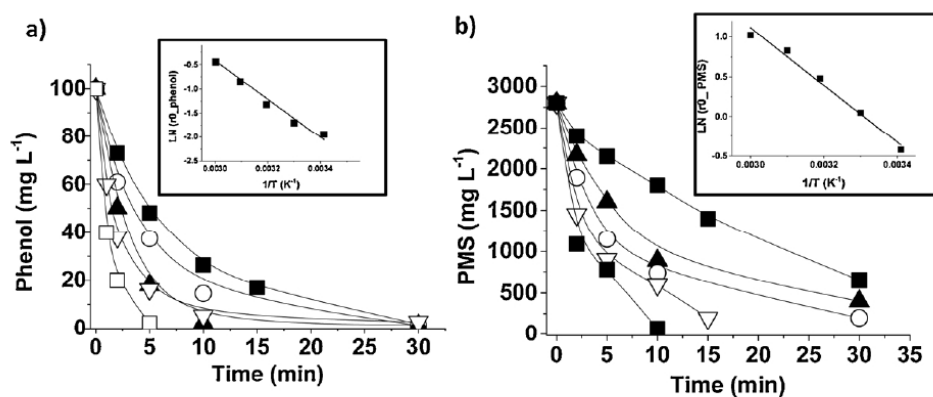


Fig. 11. Phenol degradation (a) and PMS decomposition (b) using Co_{ox}/ACN at 20 °C (■), 30 °C (○), 40 °C (▲) and 50 °C (▽). The inset shows the estimation of the apparent E_a of the process. Reaction conditions: Catalyst (200 mg L⁻¹; 0.0067mM of supported cobalt), phenol (100 mg/L; 1.06 mM), PMS (2800 mg L⁻¹; 9.1 mM), temperature as indicated, initial pH 7.

The stability of the Co_{ox}/ACN catalyst was assessed by performing eight consecutive uses of the same sample at pH 7 without observing decrease of the catalytic activity (Fig. 12a,b). Cobalt leaching from the solid catalyst to the solution after running the reaction at pH 7 was below detection limit (< 1.0 µg/L). The absence of cobalt leaching from Co_{ox}(0.2 wt%)/ACN catalyst compares favorably with the cobalt leaching measured for PMS activation when using SiO₂, TiO₂ or Al₂O₃ as support with values of cobalt leaching of 0.75, 2.83 or 0.94 mg L⁻¹, respectively (pH not indicated) [45]. Other systems based on cobalt oxide on carbon aerogel resulted in cobalt leaching around 1 mg L⁻¹ (pH of reaction not indicated) and concomitant decrease of catalytic activity for phenol degradation upon reuse [21]. In other study, Co NPs embedded on carbon nanofibers resulted in a quite stable catalyst for PMS activation, although still a cobalt leaching of 20 µg L⁻¹ was measured [47]. Another study that employed cobalt supported on TiO₂ as photocatalyst under UV irradiation have resulted in cobalt leaching values of 25 µg L⁻¹ [18]. In our case, blank control experiments using this trace amount

of cobalt to promote phenol degradation by PMS at pH 7 or 4 resulted in negligible catalytic activity indicating the heterogeneity of the reaction process. Importantly, TEM images of eight-times used $\text{Co}_{\text{ox}}(0.2 \text{ wt\%})/\text{ACN}$ shows that metal NP aggregation does not occur (Fig. 12a and b inset).

Furthermore, productivity experiments using a high concentration of phenol (10 g L^{-1} ; 106.4 mM) and PMS (280 g L^{-1} ; 912 mM) respect to the catalyst (200 mg L^{-1} ; 0.0067 mM of supported cobalt) allow determining an accumulated turnover number (TON) after three cycles for phenol and PMS decomposition as high as $\sim 39,000$ and $\sim 400,000$, respectively (Fig. 12c,d). Similarly, TOF values for the first catalytic cycle about $68,000$ and $8 \cdot 10^5 \text{ h}^{-1}$ for phenol degradation and PMS, respectively, were estimated at 5 min of reaction. These TON and TOF values are much higher compared to those reported in the literature using heterogeneous metal catalysts for water pollutant degradation using PMS as oxidant that frequently are lower than 100 [9,20,21,45,47,50,51,55–57]. As commented, different heterogeneous catalysts have been reported for PMS activation but, however, most of these papers do not measure PMS decomposition and, therefore, estimation of TOF and TON values for PMS decomposition is not possible in those cases.

In this study, the good stability of the $\text{Co}_{\text{ox}}/\text{ACN}$ catalyst may be attributed to the presence of oxygen functional groups able to establish strong anchoring interaction with the cobalt NPs. The reusability data of $\text{Co}_{\text{ox}}/\text{ACN}$ compares favorably with analogous catalyst based on oxidized cobalt NPs supported on carbon microspheres [57], on SiO_2 [17,45] or on TiO_2 [45] and Al_2O_3 [45], among others [58], that suffer deactivation upon reuse.

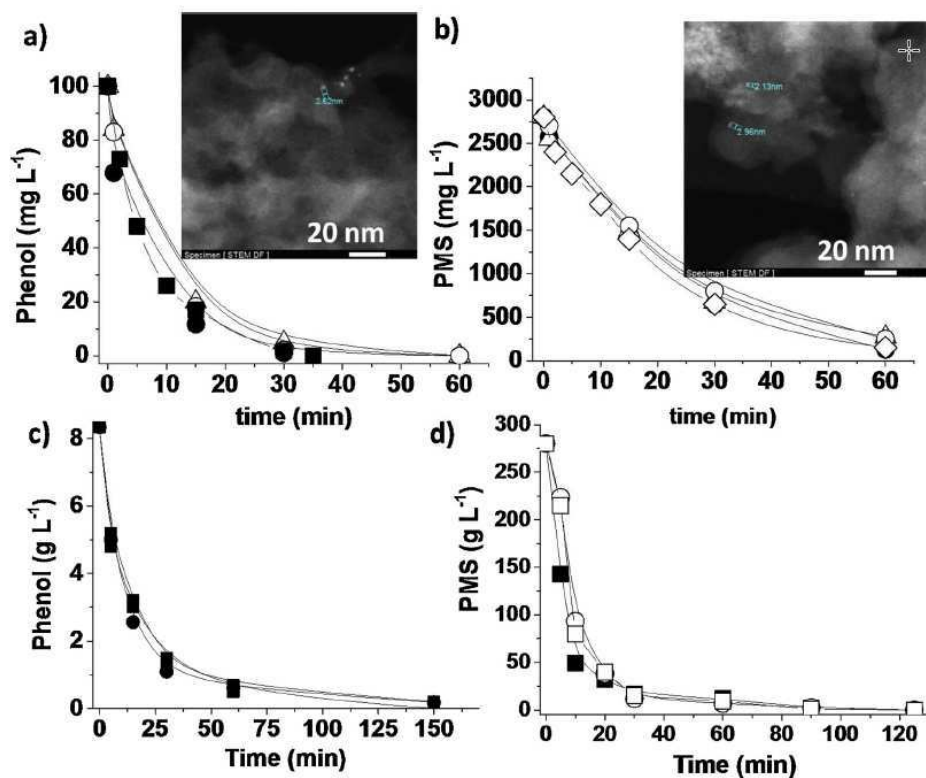


Fig. 12. Reusability of Co_{ox}/ACN at pH 7 and 20 °C under regular (a, b) or under productivity test (c, d) conditions for phenol degradation (a, c) and PMS decomposition (b, c). Legend: first cycle (■), third cycle (●), fifth cycle (Δ) and eighth cycle (○). Regular reaction conditions: Catalyst (200 mg L⁻¹; 0.0067mM of supported cobalt), phenol (100 mg L⁻¹; 1.06 mM), PMS (2800 mg L⁻¹, 9.1 mM), 20 °C, pH 7. Productivity reaction conditions: Catalyst (200 mg L⁻¹; 0.0067mM of supported cobalt), phenol (10 g/L; 106.4 mM), PMS (280 g L⁻¹, 912 mM), 20 °C, initial pH 7.

4.3.4 Reaction mechanism

In order to determine the reactive oxygen species generated in the catalytic system for PMS activation by the action of $\text{Co}_{\text{ox}}/\text{ACN}$ as catalyst, a series of selective radical quenching experiments and EPR measurements were performed. As preliminary experiments the influence of ambient oxygen in the catalytic reaction was evaluated. The presence of oxygen only slightly accelerates in comparison with inert atmosphere (Fig. S18) both phenol degradation and PMS decomposition, therefore, suggesting that oxygen participates in the radical reaction mechanism. The possible formation of radical species was further evaluated using DMSO, methanol and tert-butanol as radical scavengers [19,59,60]. The inhibition of the reaction by presence of DMSO and methanol indicate that hydroxyl and sulfate radicals are involved in phenol degradation [59–61]. tert-Butanol quenching has been considered as a specific agent of hydroxyl radicals [59,60]. Accordingly, the difference in the temporal profile of phenol degradation in the absence or presence of *tert*-butanol can also serve to indirectly evaluate the contribution of sulfate radicals. As it can be seen in Fig. 13, the presence of a large excess of tert-butanol quenches partially phenol degradation indicating that both $\text{SO}_4^{\cdot -}$ and HO^{\cdot} radicals are simultaneously involved. On one hand, tert-butanol decreases the initial reaction rate of phenol degradation by about 60% (attributed to the contribution of hydroxyl radicals to phenol degradation in the absence of tert-butanol), but on the other hand phenol is still degraded in 100% at longer reaction times (degradation caused by contribution due to unquenchable sulfate radicals).

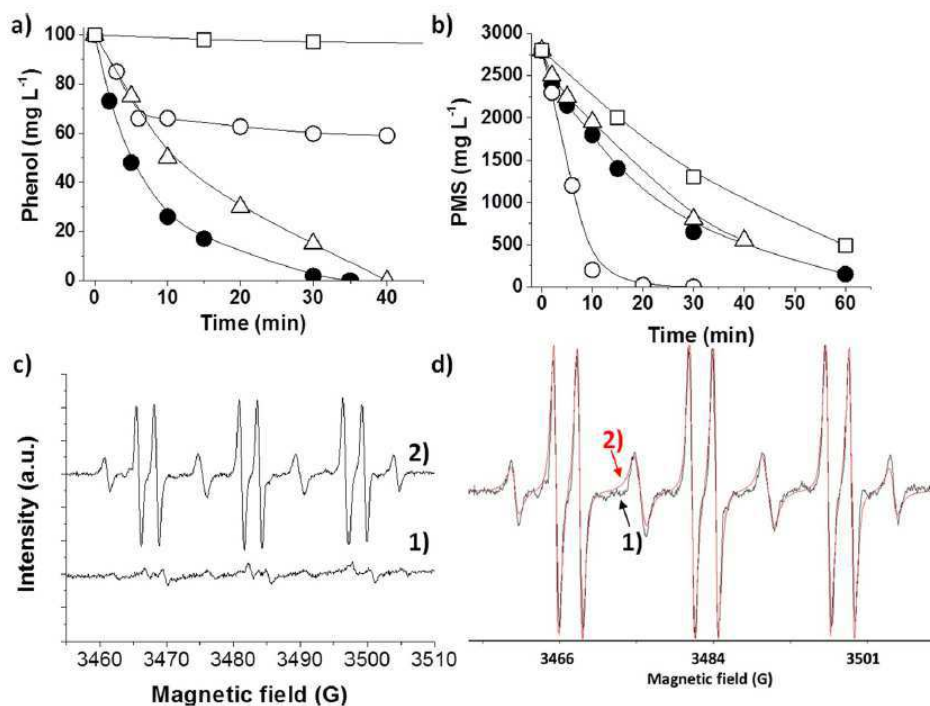
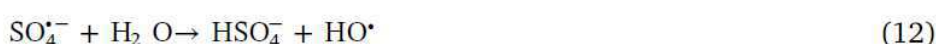
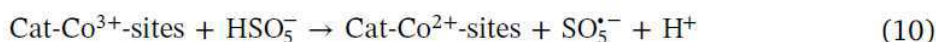
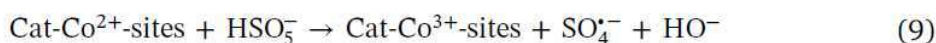


Fig. 13. (a) Phenol degradation and (b) PMS decomposition using Co_{ox}/ACN as catalyst. Legend: air atmosphere (●), air atmosphere with the presence of DMSO (□), methanol (○) or tert-butanol (△) as radical quenchers. Reaction conditions: Catalyst (200 mg L⁻¹; 0.0067mM of supported cobalt), phenol (100 mg L⁻¹; 1.06 mM), PMS (2800 mg L⁻¹, 9.1 mM), 20 °C, initial pH 7, radical quencher to PMS molar ratio 10. (c) Experimental EPR spectra recorded in H₂O at pH 7 in the presence of PMS and the absence (1) or in the presence of Co_{ox}/ACN catalyst (2) after 15 min reaction time. (d) Experimental (1, black line) and simulated (2, red line) EPR spectra under (c) conditions. Hyperfine coupling constants of PBN-OH (~85% area) AG_N=15.4 and AG_H=2.7 and *tert*-butyl aminoxy from degraded PBN AG_N=15.58 and AG_H=13.90. (For interpretation of the references to colour in this figure legend, the reader is referred to the web version of this article)

Additional mechanistic studies were performed by using PBN as trapping agent followed by EPR. PBN has been reported to trap both $\text{SO}_4^{\cdot-}$ and HO^{\cdot} radicals [62]. EPR measurements using PBN as spin trap clearly shows the formation of the PBN–OH adduct under conditions relevant to phenol degradation. Note that the control in the absence of $\text{Co}_{\text{ox}}/\text{ACN}$ only allows to detect very weak EPR signals, indicating that $\cdot\text{OH}$ radicals are formed mainly due to the activity of the $\text{Co}_{\text{ox}}/\text{ACN}$ catalyst (Fig. 13c and d).

Based on these results a one-electron transfer process from Co(II) species to PMS leading to the generation of sulfate radicals is proposed (Eq. (9)). Then, catalytic cycle involves reduction of Co(III) to Co(II) with formation of $\text{SO}_5^{\cdot-}$ radicals (Eq. (10))[10,11]. $\text{SO}_4^{\cdot-}$ radicals can also be generated by reaction of $\text{SO}_5^{\cdot-}$ under acid conditions (Eq. (11))[10,11]. In addition, $\text{SO}_4^{\cdot-}$ radicals can be converted into HO^{\cdot} radicals according Eq. (12) [10].



4.4 Conclusions

The present manuscript has shown the different catalytic behavior of a series of cobalt-containing ACs as a function of the surface pretreatment and metal oxidation state. It has been found that the catalyst activity for AOP using PMS at pH 7 correlates well with the cobalt particle size, the smaller the dimension, the higher the catalyst activity. Furthermore, the oxidized supported cobalt NPs are

catalytically more active than the reduced ones. In this regard, it has been established in the present study that by introducing oxygenated functional groups in AC by a chemical treatment using nitric acid (ACN), it is possible to obtain the cobalt oxide NPs with small average particle size (4.7 ± 0.05 nm) and, therefore, exhibiting an enhanced catalytic activity towards PMS decomposition and phenol degradation. Furthermore, these surface oxygenated groups and the strong anchoring of oxidized cobalt NPs are also responsible for the stability of these NPs, minimizing their growth and allowing their reusability up to eight cycles without decay and the absence of cobalt leaching. It is remarkable that no cobalt leaching is detectable. Productivity tests using a large excess of phenol and PMS respect to the $\text{Co}_{\text{ox}}(0.2 \text{ wt\%})/\text{ACN}$ catalyst allow to determine TON/TOF values as high as $39,000/68,000 \text{ h}^{-1}$ for phenol and $400,000/8 \cdot 10^5 \text{ h}^{-1}$ for PMS at pH 7 and $20 \text{ }^\circ\text{C}$, respectively. In this way the $\text{Co}_{\text{ox}}(0.2 \text{ wt\%})/\text{ACN}$ catalyst compares favorably with those previously reported in the literature is herein described.

4.5 References

- [1] K. Ayoub, E.D. van Hullebusch, M. Cassir, A. Bermond, Application of advanced oxidation processes for TNT removal: a review, *J. Hazard. Mater.* 178 (2010) 10–28.
- [2] M. Cheng, G. Zeng, D. Huang, C. Lai, P. Xu, C. Zhang, Y. Liu, Hydroxyl radicals based advanced oxidation processes (AOPs) for remediation of soils contaminated with organic compounds: a review, *Chem. Eng. J.* 298 (2016) 582–598.
- [3] E. Neyens, J. Baeyens, A review of classic Fenton's peroxidation as an advanced oxidation technique, *J. Hazard. Mater.* 98 (2003) 33–50.
- [4] M. Pera-Titus, V. García-Molina, M.A. Baños, J. Giménez, S. Esplugas, Degradation of chlorophenols by means of advanced oxidation processes: a general review, *Appl. Catal. B: Environ.* 47 (2004) 219–256.

- [5] J.J. Pignatello, E. Oliveros, A. MacKay, Advanced oxidation processes for organic contaminant destruction based on the fenton reaction and related chemistry, *Crit. Rev. Environ. Sci. Technol.* 36 (2006) 1–84.
- [6] K. Demeestere, J. Dewulf, H. Van Langenhove, Heterogeneous photocatalysis as an advanced oxidation process for the abatement of chlorinated, monocyclic aromatic and sulfurous volatile organic compounds in air: state of the art, *Crit. Rev. Environ. Sci. Technol.* 37 (2007) 489–538.
- [7] S. Malato, P. Fernández-Ibáñez, M.I. Maldonado, J. Blanco, W. Gernjak, Decontamination and disinfection of water by solar photocatalysis: recent overview and trends, *Cat. Today* 147 (2009) 1–59.
- [8] I. Oller, S. Malato, J.A. Sánchez-Pérez, Combination of advanced oxidation processes and biological treatments for wastewater decontamination—a review, *Sci. Total Environ.* 409 (2011) 4141–4166.
- [9] G.P. Anipsitakis, E. Stathatos, D.D. Dionysiou, Heterogeneous activation of oxone using Co_3O_4 , *J. Phys. Chem. B* 109 (2005) 13052–13055.
- [10] P. Hu, M. Long, Cobalt-catalyzed sulfate radical-based advanced oxidation: a review on heterogeneous catalysts and applications, *Appl. Catal. B. Environ.* 181 (2016) 103–117.
- [11] F. Ghanbari, M. Moradi, Application of peroxymonosulfate and its activation methods for degradation of environmental organic pollutants: review, *Chem. Eng. J.* 310 (2017) 41–62.
- [12] D.L. Ball, J.O. Edwards, The kinetics and mechanism of the decomposition of Caro's acid, *J. Am. Chem. Soc.* 78 (1956) 1125–1129.
- [13] Council Directive 98/83/EC of 3 November 1998 on the quality of water intended for human consumption.
- [14] S. Navalon, M. Alvaro, H. Garcia, Heterogeneous Fenton catalysts based on clays, silicas and zeolites, *Appl. Catal. B: Environ.* 99 (2010) 1–26.
- [15] S. Navalon, A. Dhakshinamoorthy, M. Alvaro, H. Garcia, Heterogeneous Fenton catalysts based on activated carbon and related materials, *ChemSusChem* 4 (2011) 1712–1730.

- [16] E.G. Garrido-Ramírez, B.K.G. Theng, M.L. Mora, Clays and oxide minerals as catalysts and nanocatalysts in Fenton-like reactions—a review, *Appl. Clay Sci.* 47 (2010) 182–192.
- [17] P. Shukla, H. Sun, S. Wang, H.M. Ang, M.O. Tadé, Nanosized Co₃O₄/SiO₂ for heterogeneous oxidation of phenolic contaminants in waste water, *Separ. Purif. Technol.* 77 (2011) 230–236.
- [18] Q. Yang, H. Choi, Y. Chen, D.D. Dionysiou, Heterogeneous activation of peroxymonosulfate by supported cobalt catalysts for the degradation of 2,4-dichlorophenol in water: the effect of support, cobalt precursor, and UV radiation, *Appl. Catal. B. Environ.* 77 (2008) 300–307.
- [19] Q.J. Yang, H. Choi, D.D. Dionysiou, Nanocrystalline cobalt oxide immobilized on titanium dioxide nanoparticles for the heterogeneous activation of peroxymonosulfate, *Appl. Catal. B: Environ.* 74 (2007) 170–178.
- [20] P.R. Shukla, S. Wang, H. Sun, H.M. Ang, M. Tadé, Activated carbon supported cobalt catalysts for advanced oxidation of organic contaminants in aqueous solution, *Appl. Catal. B: Environ.* 100 (2010) 529–534.
- [21] Y. Hardjono, H. Sun, H. Tian, C.E. Buckley, S. Wang, Synthesis of Co oxide doped carbon aerogel catalyst and catalytic performance in heterogeneous oxidation of phenol in water, *Chem. Eng. J.* 174 (2011) 376–382.
- [22] P.R. Shukla, S.B. Wang, K. Singh, H.M. Ang, M.O. Tade, Cobalt exchanged zeolites for heterogeneous catalytic oxidation of phenol in the presence of peroxymonosulphate, *Appl. Catal. B: Environ.* 99 (2010) 163–169.
- [23] K.-Y. Andrew Lin, H.-A. Chang, Zeolitic imidazole framework-67 (ZIF-67) as a heterogeneous catalyst to activate peroxymonosulfate for degradation of Rhodamine B in water, *J. Taiwan Inst. Chem. Eng.* 53 (2015) 40–45.
- [24] Q. Yang, H. Choi, S.R. Al-Abed, D.D. Dionysiou, Iron-cobalt mixed oxide nanocatalysts: heterogeneous peroxymonosulfate activation, cobalt leaching, and ferromagnetic properties for environmental applications, *Appl. Catal. B: Environ.* 88 (2009) 462–469.

- [25] X. Duan, Z. Ao, H. Zhang, M. Saunders, H. Sun, Z. Shao, S. Wang, Nanodiamonds in sp²/sp³ configuration for radical to nonradical oxidation: core-shell layer dependence, *Appl. Catal. B: Environ.* 222 (2018) 176–181.
- [26] X. Duan, H. Sun, S. Wang, Metal-free carbocatalysis in advanced oxidation reactions, *Acc. Chem. Res.* 51 (2018) 678–687.
- [27] A. Dhakshinamoorthy, S. Navalon, M. Alvaro, H. Garcia, Metal nanoparticles as heterogeneous Fenton catalyst, *ChemSusChem* 5 (2012) 46–64.
- [28] K. Takahashi, S. Yokoyama, T. Matsumoto, J.L.C. Huaman, H. Kaneko, J. - Y. Piquemal, H. Miyamura, J. Balachandran, Towards a designed synthesis of metallic nanoparticles in polyols-elucidation of the redox scheme in a cobalt-ethylene glycol system, *New J. Chem.* 40 (2016) 8632–8642.
- [29] C. López-Santos, F. Yubero, J. Cotrino, A.R. González-Elipe, Lateral and in-depth distribution of functional groups on diamond-like carbon after oxygen plasma treatments, *Diam. Relat. Mater.* 20 (2011) 49–56.
- [30] D. Sempere, S. Navalon, M. Dančíková, M. Alvaro, H. Garcia, Influence of pre-treatments on commercial diamond nanoparticles on the photocatalytic activity of supported gold nanoparticles under natural Sunlight irradiation, *Appl. Catal. B: Environ.* 142–143 (2013) 259–267.
- [31] R. Martín, S. Navalon, M. Alvaro, H. Garcia, Optimized water treatment by combining catalytic Fenton reaction using diamond supported gold and biological degradation, *Appl. Catal. B: Environ.* 103 (2011) 246–252.
- [32] S. Waclawek, K. Gröbel, M. Cerník, Simple spectrophotometric determination of monopersulfate, *Spectrochim. Acta A.* 149 (2015) 928–933.
- [33] L. Fan, C. Moreno-Castilla, M.A. Ferro-Garcia, J.P. Joly, I. Bautista-Toledo, F. Carrasco-Marin, J. Rivera-Utrilla, Surface modifications by nitric acid, hydrogen peroxide, and ammonium peroxydisulfate treatments activated carbon, *Langmuir* 11 (1995) 4386–4392.
- [34] M.S. Shafeeyan, W.M.A.W. Daud, A. Houshmand, Ahmad Shamiri, A review on surface modification of activated carbon for carbon dioxide adsorption, *J. Anal. Appl. Pyrol.* 89 (2010) 143–151.

- [35] N. Shimodaira, A. Masui, Raman spectroscopic investigations of activated carbon materials, *J. Appl. Phys.* 92 (2002) 902–909.
- [36] J.-H. Zhou, Z.-J. Sui, J. Zhu, P. Li, D. Chen, Y.-C. Dai, W.-K. Yuan, Characterization of surface oxygen complexes on carbon nanofibers by TPD, XPS and FT-IR, *Carbon* 45 (2007) 785–796.
- [37] B.S. Girgis, Y.M. Temerk, M.M. Gadelrab, I.D. Abdullah, X-ray diffraction patterns of activated carbons prepared under various conditions, *Carbon Sci.* 2 (2007) 95–100.
- [38] J.C. Espinosa, S. Navalón, M. Álvaro, H. García, Copper nanoparticles supported on diamond nanoparticles as a cost-effective and efficient catalyst for natural sunlight assisted Fenton reaction, *Catal. Sci. Technol.* 6 (2016) 7077–7085.
- [39] R. Shi, G. Chen, W. Ma, D. Zhang, G. Qiu, X. Liu, Shape-controlled synthesis and characterization of cobalt oxides hollow spheres and octahedra, *Dalton Trans.* 41 (2012) 5981–5987.
- [40] J. González-Prior, R. López-Fonseca, J.I. Gutiérrez-Ortiz, B. de Rivas, Oxidation of 1,2-dichloroethane over nanocube-shaped Co_3O_4 catalysts, *Appl. Catal. B: Environ.* 199 (2016) 384–393.
- [41] W. Guo, E. Yifeng, L. Gao, L. Fan, S. Yang, A catalytic nanostructured cobalt oxide electrode enables positive potential operation for the cathodic electrogenerated chemiluminescence of $\text{Ru}(\text{bpy})_3^{2+}$ with dramatically enhanced intensity, *Chem. Commun.* 46 (2010) 1290–1292.
- [42] H.M. Chen, R.-S. Liu, H. Li, H.C. Zeng, Generating isotropic superparamagnetic interconnectivity for the two-dimensional organization of nanostructured building blocks, *Angew. Chem. Int. Ed.* 45 (2006) 2713–2717.
- [43] A. Dhakshinamoorthy, S. Navalon, D. Sempere, M. Alvaro, H. Garcia, Aerobic oxidation of thiols catalyzed by copper nanoparticles supported on diamond nanoparticles, *ChemCatChem* 5 (2013) 241–246.
- [44] I.H. Kim, H.O. Seo, E.J. Park, S.W. Han, Y.D. Kim, Low temperature CO Oxidation over iron oxide nanoparticles decorating internal structures of a mesoporous alumina, *Sci. Rep.* 7 (2017) 40497.

- [45] H. Sun, H. Liang, G. Zhou, S. Wang, Supported cobalt catalysts by one-pot aqueous combustion synthesis for catalytic phenol degradation, *J. Colloid Interface Sci.* 394 (2013) 394–400.
- [46] S. Navalon, A. Dhakshinamoorthy, M. Alvaro, H. Garcia, Metal nanoparticles supported on two-dimensional graphenes as heterogeneous catalysts, *Coord. Chem. Rev.* 312 (2016) 99–148.
- [47] K.A. Lin, W.C. Tong, Y. Du, Cobalt-embedded carbon nanofiber derived from a coordination polymer as a highly efficient heterogeneous catalyst for activating oxone in water, *Chemosphere* 195 (2018) 272–281.
- [48] J. Sun, X. Li, J. Feng, X. Tian, Oxone/Co²⁺ oxidation as an advanced oxidation process: comparison with traditional Fenton oxidation for treatment of landfill leachate, *Water Res.* 43 (2009) 4363–4369.
- [49] W. Guo, S. Su, C. Yi, Z. Ma, Degradation of antibiotics amoxicillin by Co₃O₄-catalyzed peroxymonosulfate system, *Environ. Prog. Sustain. Energy* 32 (2013) 193–197.
- [50] H. Sun, H. Tian, Y. Hardjono, C.E. Buckley, S. Wang, Preparation of cobalt/carbonxerogel for heterogeneous oxidation of phenol, *Catal. Today* 186 (2012) 63–68.
- [51] Y. Wang, H. Sun, H.M. Ang, M.O. Tadé, S. Wang, Facile synthesis of hierarchically structured magnetic MnO₂/ZnFe₂O₄ hybrid materials and their performance in heterogeneous activation of peroxymonosulfate, *ACS Appl. Mater. Interfaces* 6 (2014) 19914–19923.
- [52] G.P. Anipsitakis, D.D. Dionysiou, Radical generation by the interaction of transition metals with common oxidants, *Environ. Sci. Technol.* 38 (2004) 3705–3712.
- [53] S.K. Ling, S. Wang, Y. Peng, Oxidative degradation of dyes in water using Co²⁺/H₂O₂ and Co²⁺/peroxymonosulfate, *J. Hazard. Mater.* 178 (2010) 385–389.
- [54] P. Shukla, H. Sun, S. Wang, H.M. Ang, M.O. Tadé, Co-SBA-15 for heterogeneous oxidation of phenol with sulfate radical for wastewater treatment, *Catal. Today* 175 (2011) 380–385.

- [55] Y. Wang, H. Sun, H.M. Ang, M.O.O. Tadé, S. Wang, 3D-hierarchically structured MnO₂ for catalytic oxidation of phenolsolutions by activation of peroxy-monosulfate: structure dependenceand mechanism, *Appl. Catal. B. Environ.* 164 (2015) 159–167.
- [56] S.B. Hammoudaa, F. Zhaoa, Z. Safaeia, V. Srivastavaa, D.L. Ramasamya, S.I. Iftekhara, S. Kalliola, M. Sillanpää, Degradation and mineralization of phenol in aqueous medium by heterogeneous monopersulfate activation on nanostructured cobalt based-perovskite catalysts ACoO₃ (A=La, Ba, Sr and Ce): characterization, kinetics and mechanism study, *Appl. Catal. B. Environ.* 215 (2017) 60–73.
- [57] G. Zhou, L. Zhou, H. Sun, H.M. Ming Ang, M.O. Tadé, S. Wang, Carbon microspheres supported cobalt catalysts forphenol oxidation with peroxy-monosulfate, *Chem. Eng. Res. Des.* 101 (2015) 15–21.
- [58] S. Muhammad, E. Saputra, H. Sun, H.-M. Ang, M.O.O. Tadé, S. Wang, Heterogeneous catalytic oxidation of aqueous phenol on red mud-supported cobalt catalysts, *Ind. Eng. Chem. Res.* 51 (2012) 15351–15359.
- [59] X. Cheng, H. Guo, Y. Zhang, X. Wu, Y. Liu, Non-photochemical production of singlet oxygen via activation of persulfate by carbon nanotubes, *Water Res.* 113 (2017) 80–88.
- [60] X. Pan, J. Chen, N. Wu, Y. Qi, X. Xu, J. Ge, X. Wang, C. Li, R. Qu, V.K. Sharma, Z. Wang, Degradation of aqueous 2,4,4'-trihydroxybenzophenone by persulfate activated with nitrogen doped carbonaceous materials and the formation of dimer products, *Water Res.* 143 (2018) 176–187.
- [61] A. Rastogi, S.R. Al-Abed, D.D. Dionysiou, Sulfate radical-based ferrouseperoxy-monosulfate oxidative system for PCBs degradation in aqueous and sediment systems, *Appl. Catal. B* 85 (2009) 171–179.
- [62] M.J. Burkitt, R.P. Mason, Direct evidence for in vivo hydroxyl-radical generation in experimental iron overload: an ESR spin-trapping investigation, *Proc. Natl. Acad. Sci. U. S. A.* 88 (1991) 8440–8444.

4.6 Supplementary information

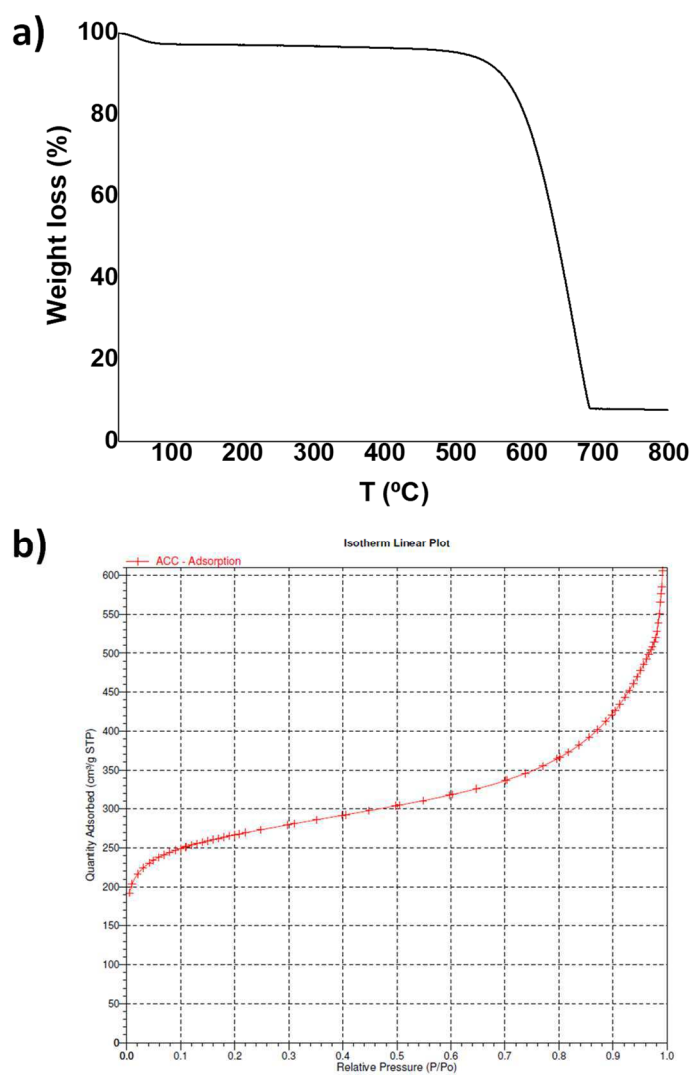


Figure S1. Thermogravimetric analysis (a) and isothermal N₂ adsorption of AC (b).

Chapter 4. Catalytic activity of cobalt oxide nanoparticles in PMS activation

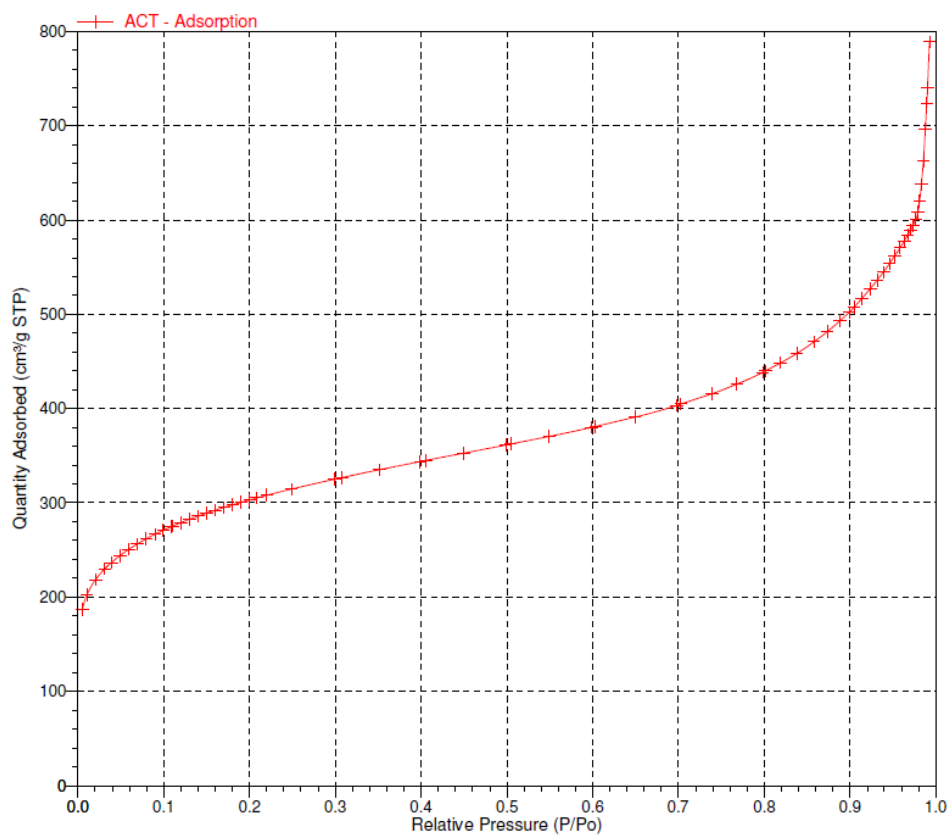


Figure S2. Isothermal N₂ adsorption of ACT.

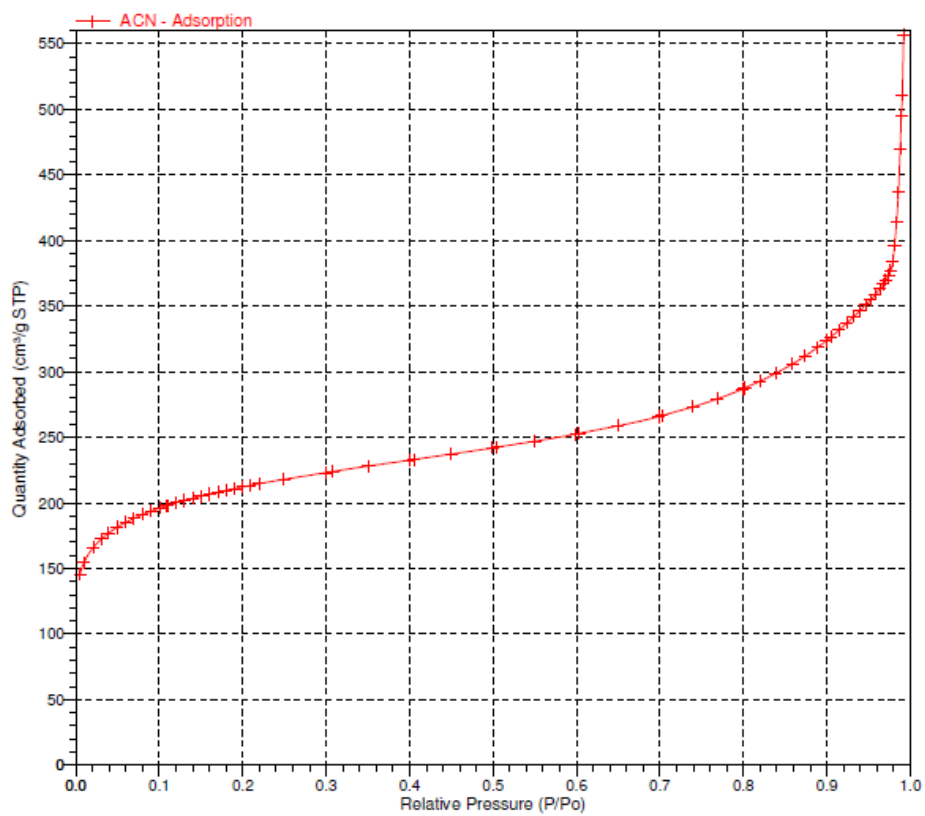


Figure S3. Isothermal N₂ adsorption of CAN.

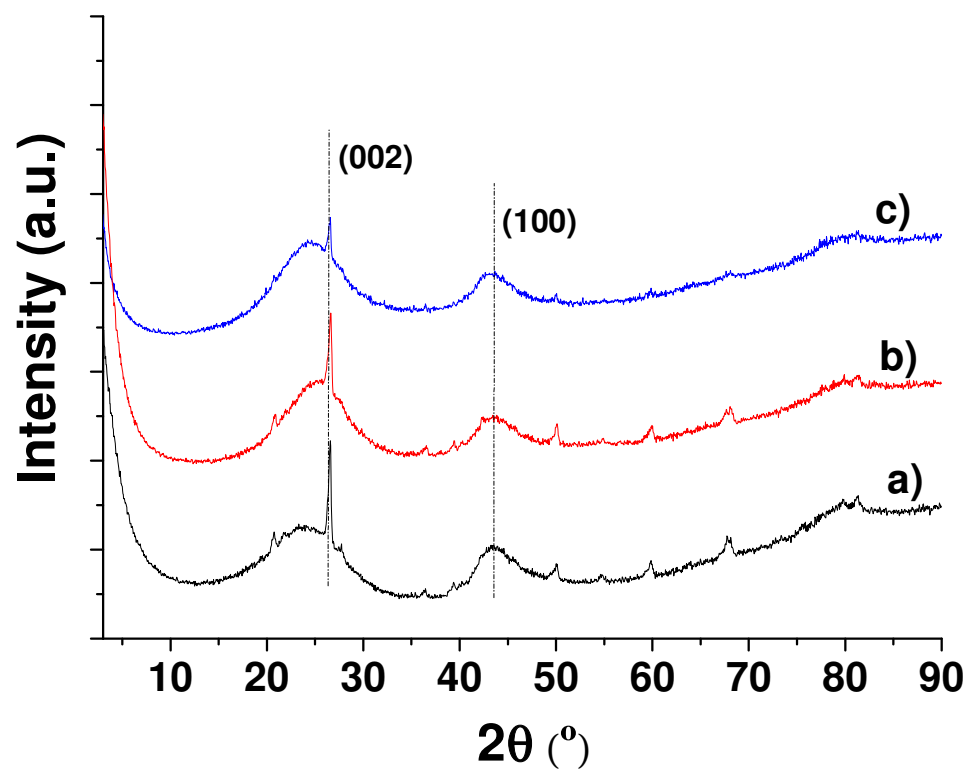


Figure S4. XRD diffractograms of AC (a), ACT (b) and ACN (c).

Chapter 4. Catalytic activity of cobalt oxide nanoparticles in PMS activation

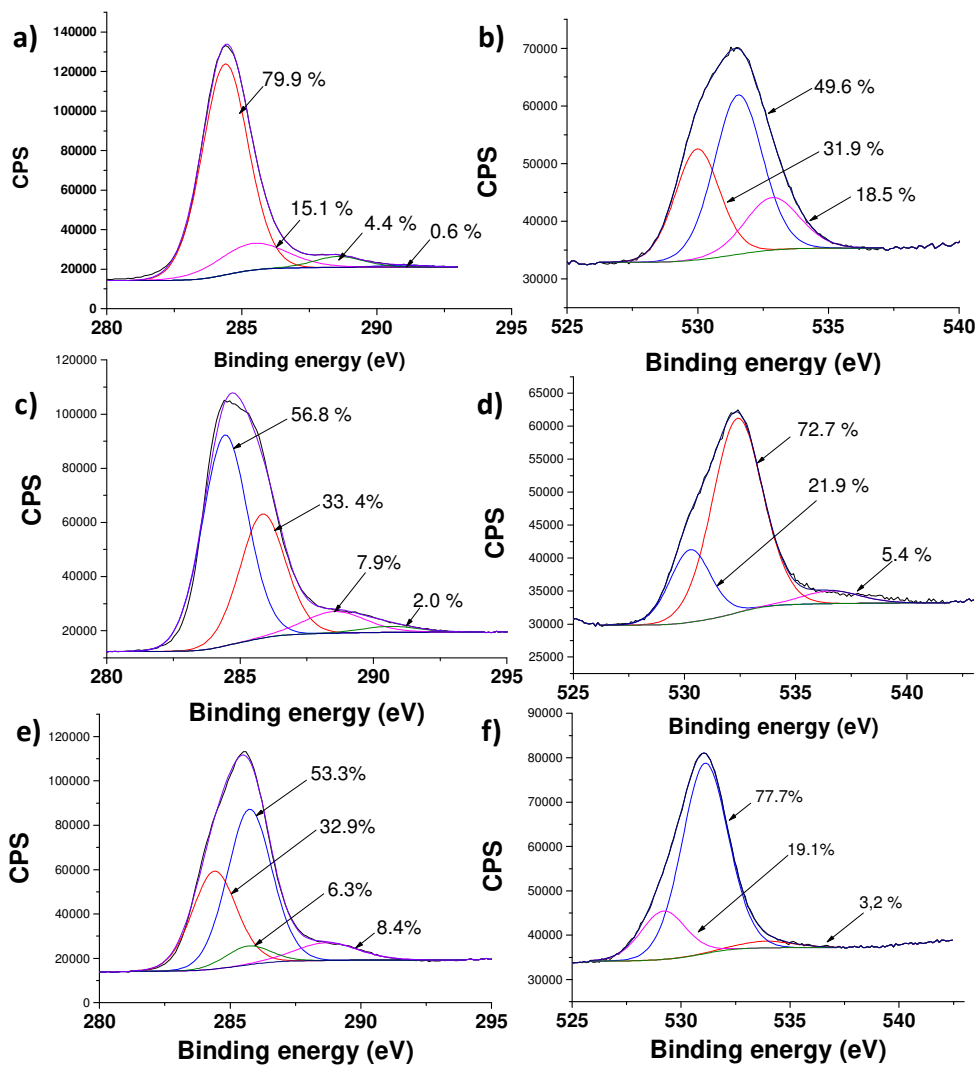


Figure S5. C1s (a, c, e) and O1s (b, d, f) spectra of AC (a, b), ACT (c, d) and ACN (e, f).

Chapter 4. Catalytic activity of cobalt oxide nanoparticles in PMS activation

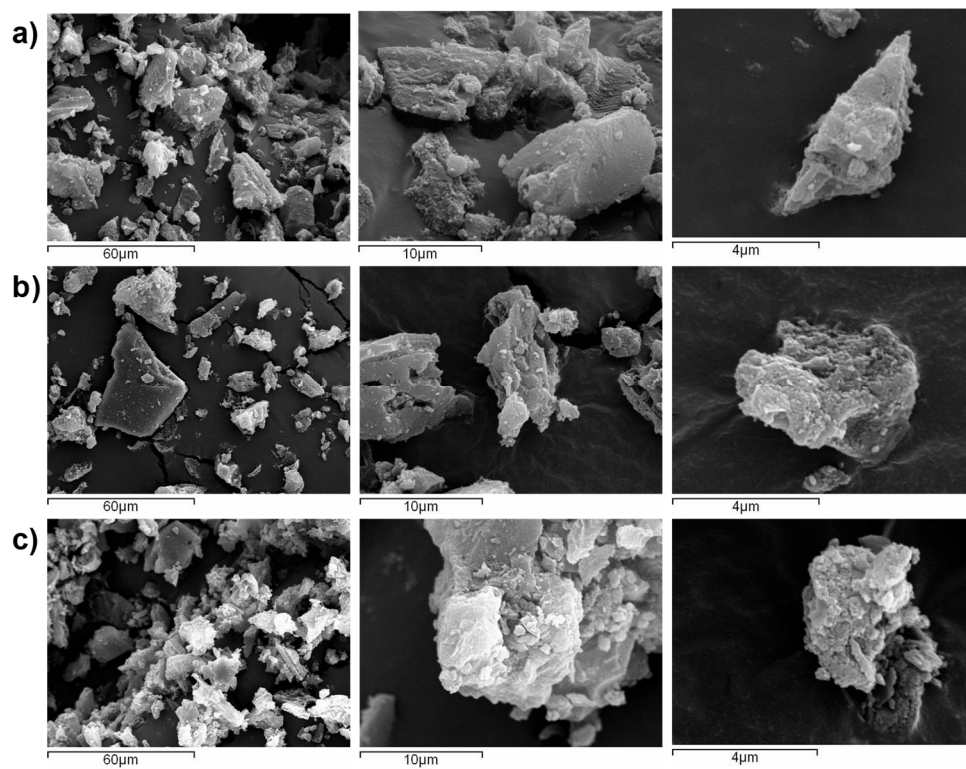


Figure S6. SEM images of AC (a), ACT (b) and ACN (c).

Metal NP characterization

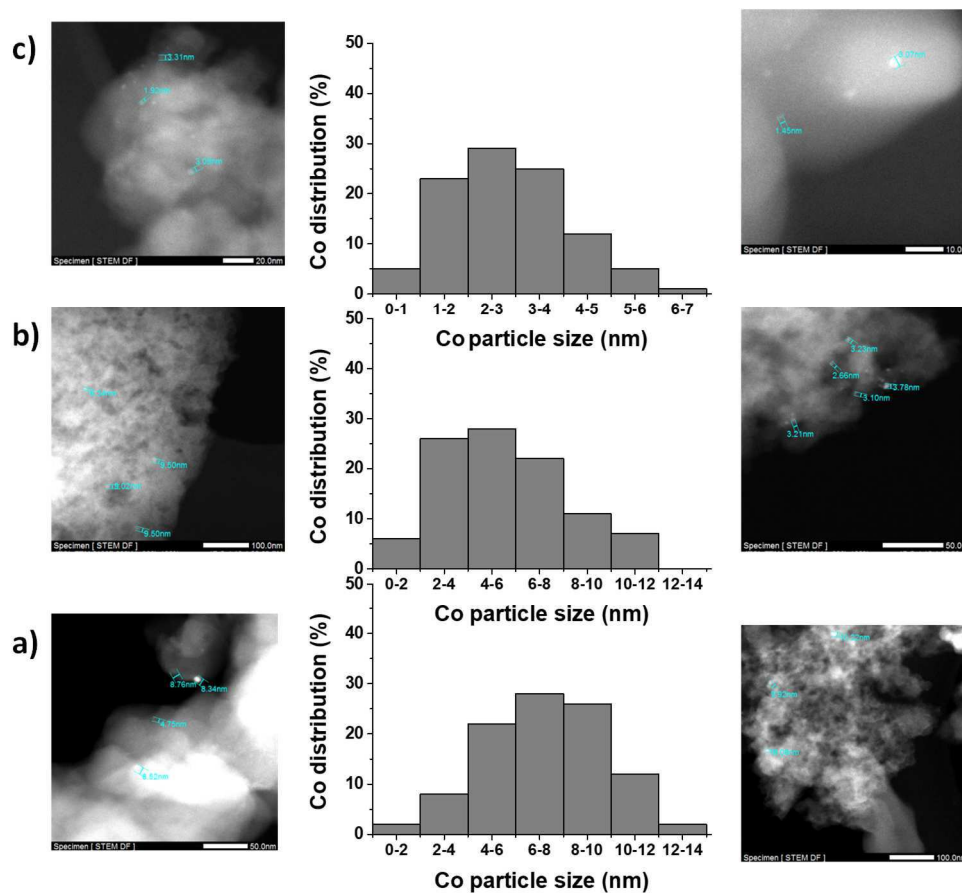


Figure S7. TEM images and particle size distribution of Co NPs supported on AC (a), ACT (b) and ACN (c). Metal loading 0.2 wt%.

Chapter 4. Catalytic activity of cobalt oxide nanoparticles in PMS activation

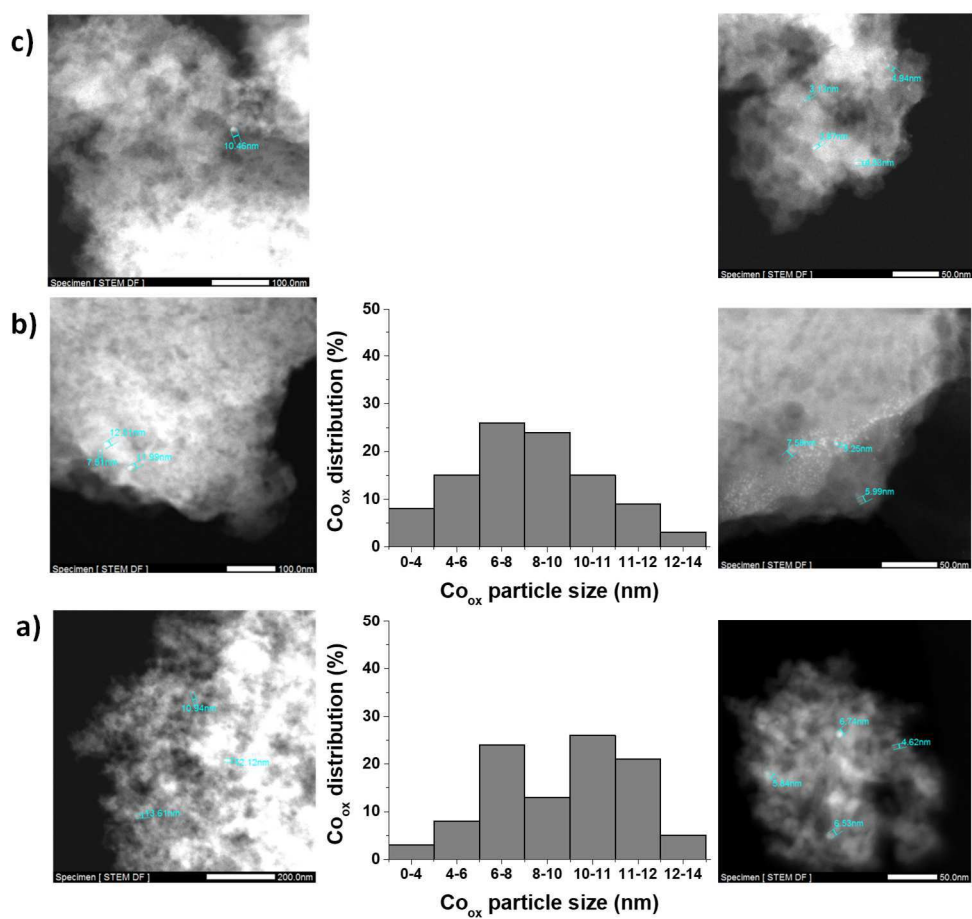


Figure S8. TEM images and/or particle size distribution of Co_{ox} NPs supported on AC (a), ACT (b) and ACN (c). Metal loading 0.2 wt%.

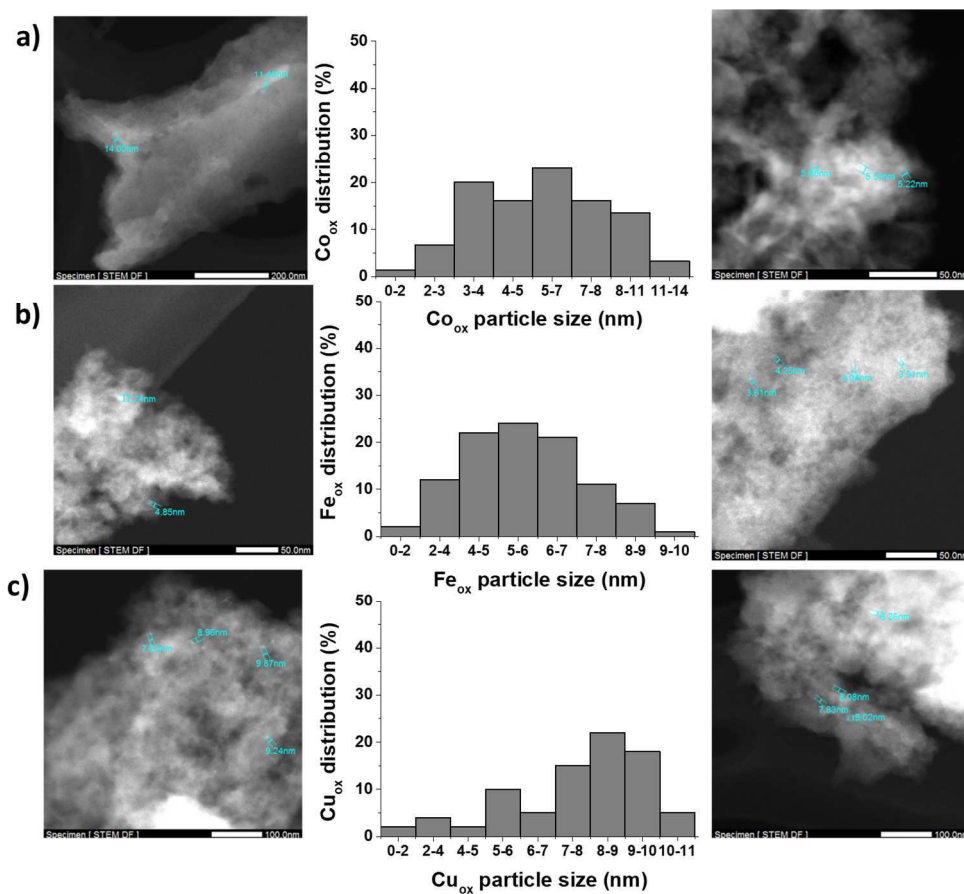


Figure S9. TEM images and particle size distribution of metallic NPs supported on ACN. Legend: a) Co_{ox}/ACN; b) Fe_{ox}/ACN; c) Cu_{ox}/ACN. Metal loading 1 wt%.

Chapter 4. Catalytic activity of cobalt oxide nanoparticles in PMS activation

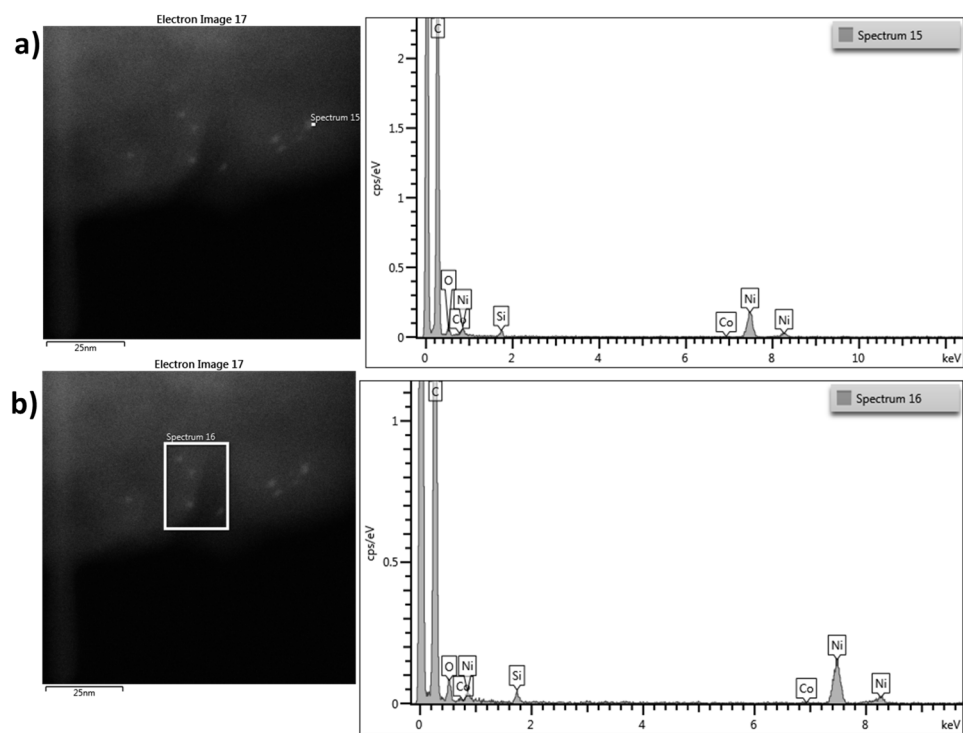


Figure S10. TEM images and EDX spectra of Co_{Ox} (0.2 wt%) supported on ACN.

Chapter 4. Catalytic activity of cobalt oxide nanoparticles in PMS activation

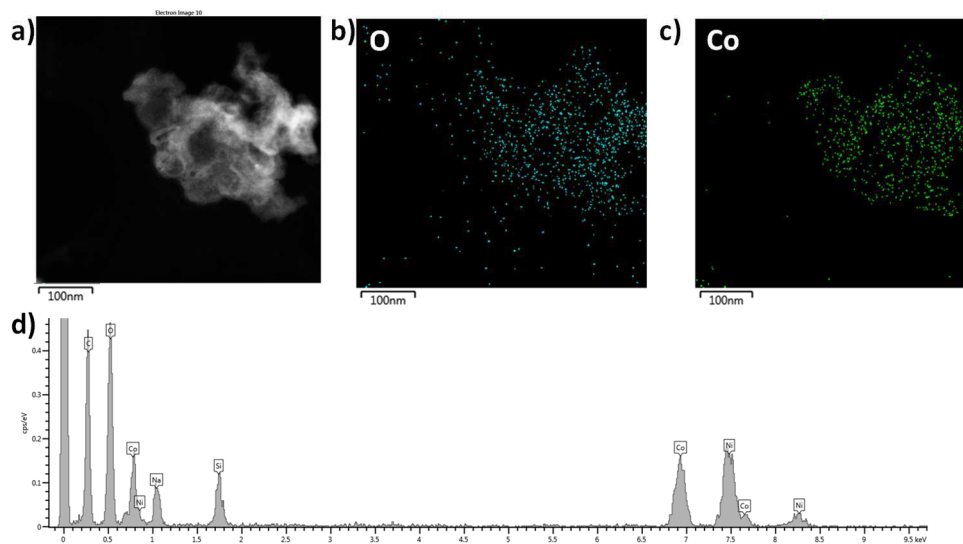


Figure S11. STEM image, mapping of oxygen (b) and (Co) and EDX spectrum of as made unsupported Co_{Ox} solid.

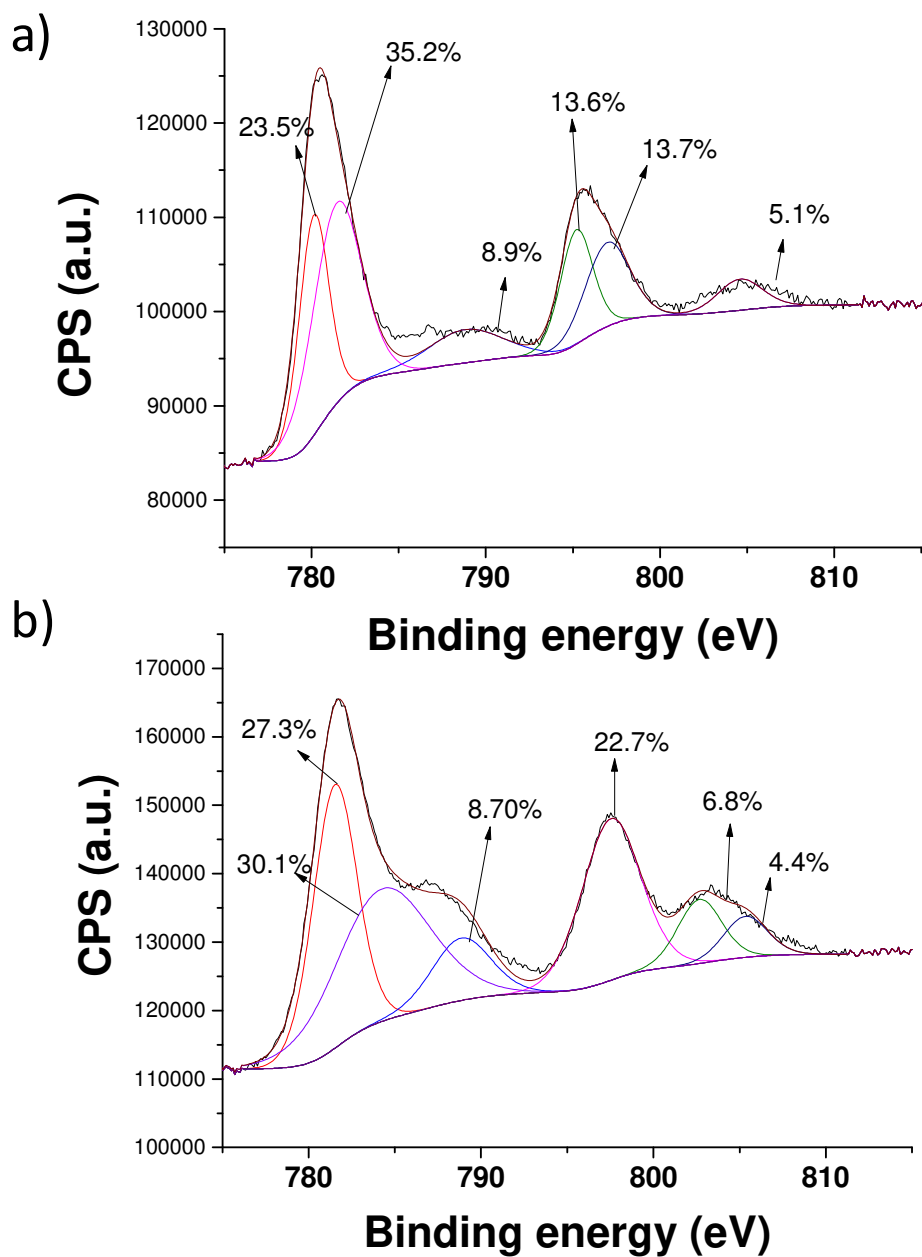


Figure S12. XPS Co 2p peak of commercial Co_3O_4 (a) and synthetic unsupported Co_{ox} NP (b).

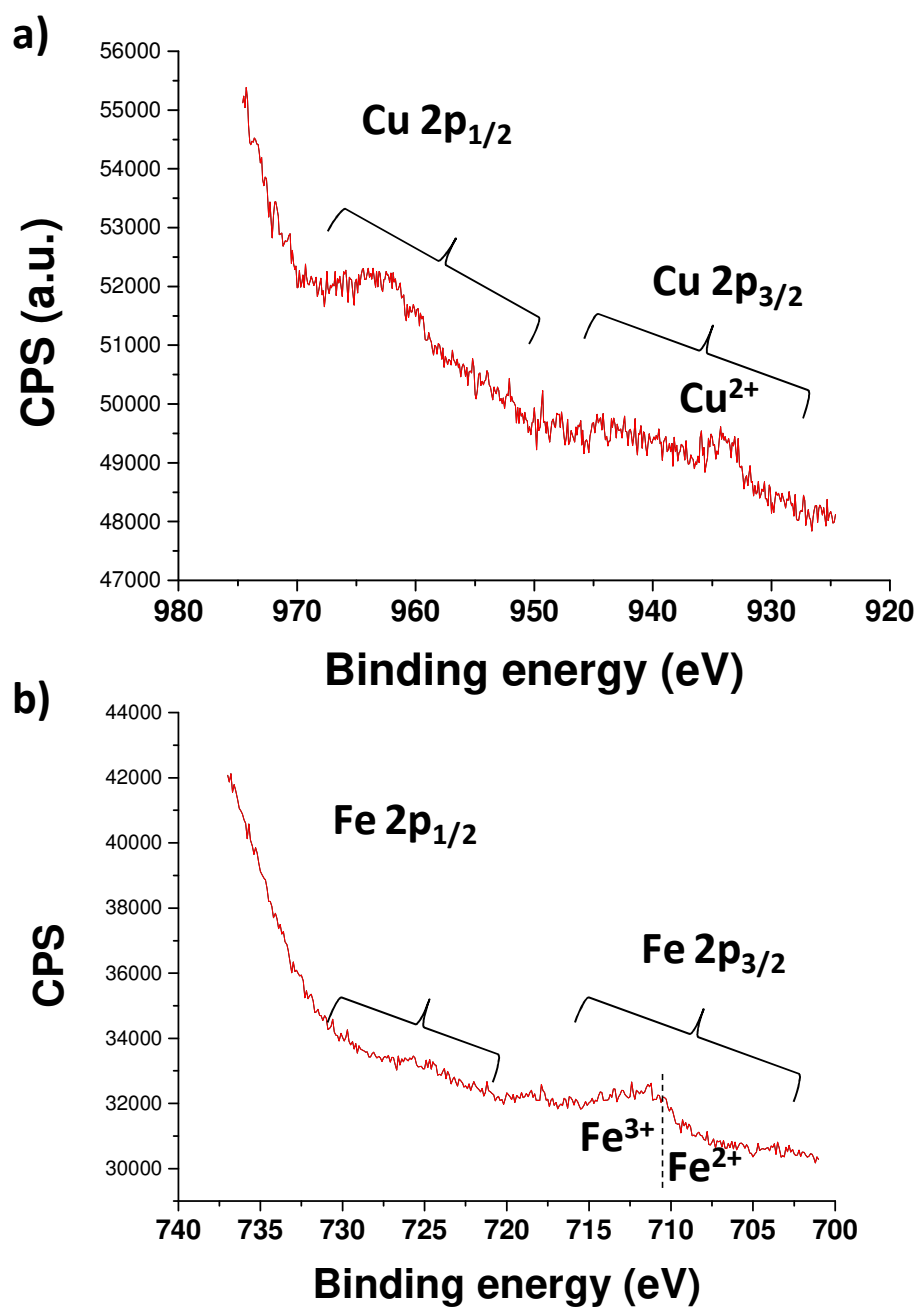


Figure S13. XPS spectra of Cu_{ox}(1.0 wt%)/ACN (a) and Fe_{ox}(1.0 wt%)/ACN (b).

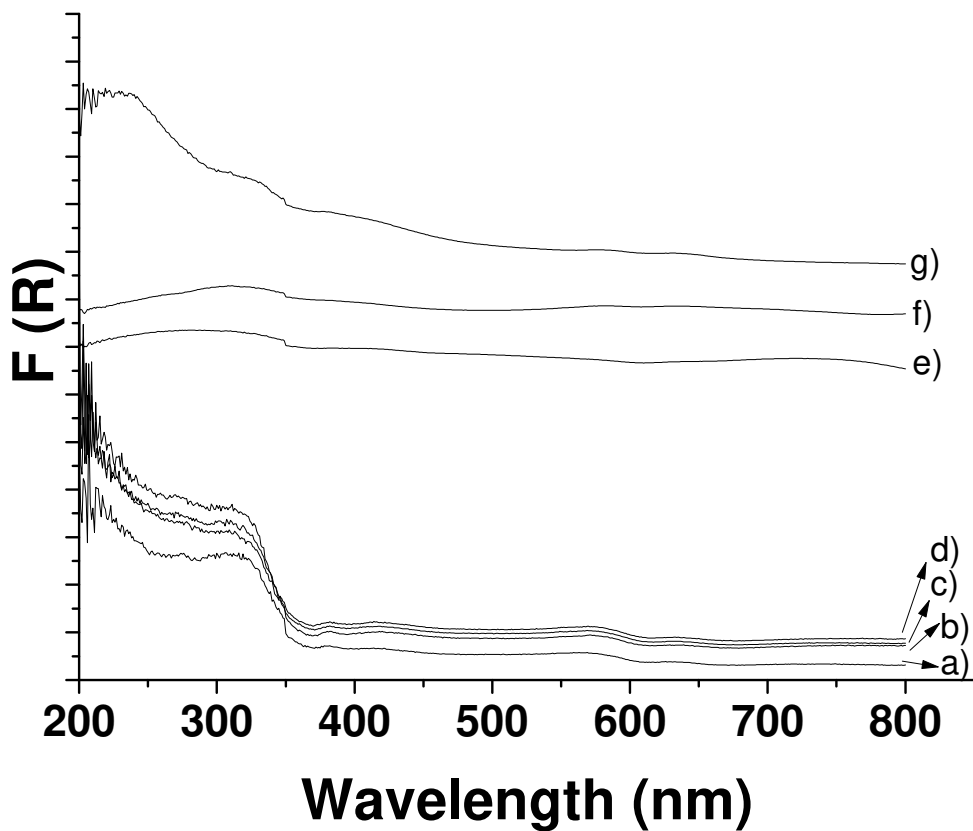


Figure S14. Diffuse reflectance UV-Vis absorption spectra of a) ACN, b) Co(0.2 wt%)/ACN, c) Co_{ox}(0.2 wt%)/ACN, d) Co_{ox}(1.0 wt%)/ACN, e) commercial CoO, f) commercial Co₃O₄, g) unsupported as-made Co_{ox} solid.

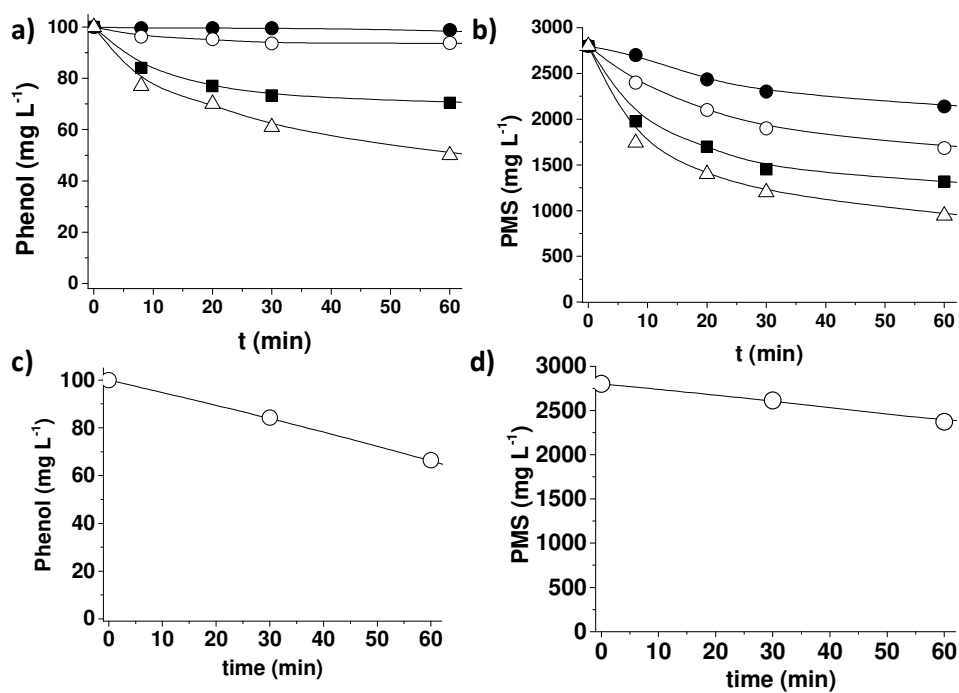


Figure S15. Blank control experiments for phenol degradation (a) and PMS decomposition (b) in the absence of catalyst different at pH 7 (Δ), pH 6 (■), pH 4 (○) and pH 2 (●). Reaction conditions: phenol (100 mg/L; 1.06 mM), PMS (2800 mg L⁻¹; 9.1 mM), 20 °C, pH as indicated. Phenol degradation (c) and PMS decomposition (d) using ACN as catalyst at pH 7. Reaction conditions: Catalyst (200 mg L⁻¹), phenol (100 mg/L; 1.06 mM), PMS (2800 mg L⁻¹; 9.1 mM), 20 °C, pH 7.

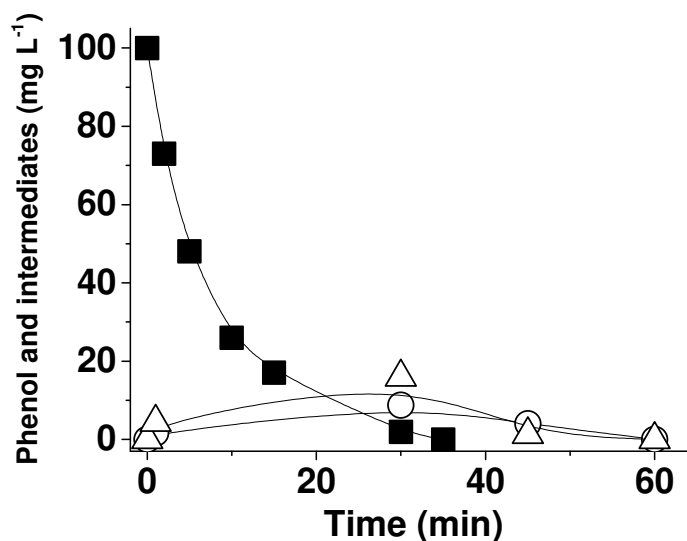


Figure S16. Phenol (■), hydroquinone (○) and p-benzoquinone (Δ) evolution using $\text{Co}_{\text{ox}}(0.2\text{wt}\%)/\text{ACN}$ as catalyst and PMS as oxidant. Catalyst (200 mg L^{-1} ; 0.0067 mM of supported cobalt), phenol (100 mg/L ; 1.06 mM), PMS (2800 mg L^{-1} ; 9.1 mM), $20 \text{ }^\circ\text{C}$, initial pH 7.

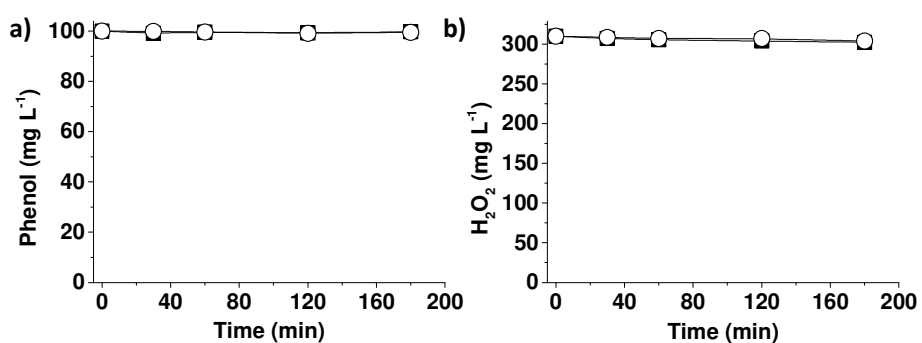


Figure S17. Catalytic activity of $\text{Co}_{\text{ox}}(0.2\text{wt}\%)/\text{ACN}$ for phenol degradation (a) and H_2O_2 decomposition (b) at pH 4 (○) and 7 (□). Reaction conditions: Catalyst (200 mg L^{-1} ; 0.0067 mM of supported cobalt), phenol (100 mg/L ; 1.06 mM), H_2O_2 (310 mg L^{-1} ; 9.1 mM), $20 \text{ }^\circ\text{C}$.

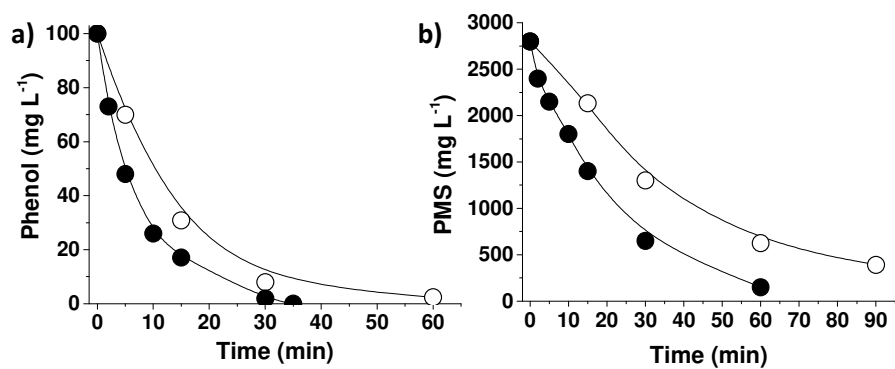


Figure S18. (a) Phenol degradation and (b) PMS decomposition using $\text{Co}_{\text{Ox}}/\text{ACN}$ as catalyst under air (●) or nitrogen atmosphere (○). (○). Reaction conditions: Catalyst (200 mg L^{-1} ; 0.0067 mM of supported cobalt), phenol (100 mg/L ; 1.06 mM), PMS (2800 mg L^{-1} , 9.1 mM), $20 \text{ }^\circ\text{C}$, initial pH 7.

Chapter 4. Catalytic activity of cobalt oxide nanoparticles in PMS activation

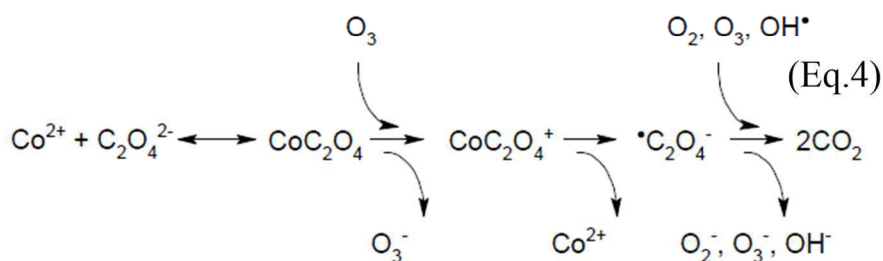
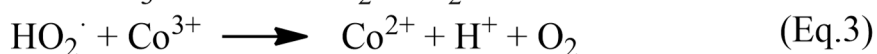
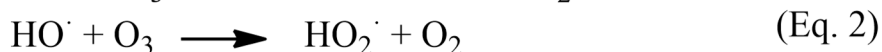
Chapter 5

Catalytic Ozonation Using Edge-Hydroxylated Graphite-Based Materials

5.1 Introduction

Most of industrial chemical processes employ transition metals as catalysts.¹⁻⁵ In the field of environmental applications, advanced oxidations processes (AOPs) employing catalysts are among the preferred technologies for water pollution remediation.⁶⁻¹¹ The most efficient AOPs are based on the use of strong oxidants such as ozone, hydrogen peroxide or peroxymonosulfate/persulfate and transition metal ions as homogeneous catalysts.^{6,9,12-14} Unfortunately, homogeneous catalysis for water remediation has the drawback of the need to remove, in some cases at trace level, the metals employed as catalysts.¹⁵ In this regard, heterogeneous catalysis for AOP may overcome some of the important limitations of homogeneous catalysis.¹⁵⁻²⁰ Heterogeneous catalytic ozonation is an AOP than can be potentially implemented at industrial scale.^{12, 21} Many potable or wastewater treatment plants have already installed in their facilities ozone

generators, being on this way easier to implement a catalytic process. Regardless of its relatively high oxidation potential, E^0 2.07 V, O_3 in the absence of catalysts is not reactive enough to degrade some toxic and recalcitrant pollutants, such as deactivated aromatic compounds and electron-poor aliphatic contaminants.¹² For this reason, the objective of catalytic ozonation is to generate from O_3 other reactive oxygen species (ROS), such as hydroxyl or hydroperoxyl radicals (Equations 1-4) able to unselectively degrade a wide range of recalcitrant pollutants such as oxalic acid.^{12, 21-23} As in the case of homogeneous catalysis, the most efficient heterogeneous catalysts to promote ozonation by generating ROS are, however, transition metals such as cobalt, manganese, iron, cerium, titanium, among others.^{21, 24}



In view of these precedents, it would be convenient to develop additional sustainable and efficient heterogeneous catalysts not based on transition metals for ozonation.²⁵⁻²⁸ In this context, several groups have employed and/or modified activated carbons²⁹⁻³⁷ and, to a lesser extent, other carbonaceous materials such activated carbon fibers³⁸ or multiwalled carbon nanotubes (MWCNTs),^{31, 39} as carbocatalysts for ozone activation. The discovery of graphene (G) in 2004

extended further the interest for carbon-based materials as catalysts.^{40, 41} Recently, reduced graphene oxide (rGO) has been reported as a heterogeneous carbocatalyst to promote the catalytic ozonation.⁴² It was observed, however, that rGO becomes deactivated to a large extent even after one use. In addition, rGO preparation was based on the Hummers method that generates a large amount of wastes.⁴³

Herein, the preparation of a highly active, stable and economically attractive graphite-based catalyst, obtained from commercially available high surface area graphite (HSAG) simply modified at the edges by hydroxyl groups using KOH as reagent (HSAG-OH) is reported. It was observed that the ozonation activity of HSAG-OH is higher than those of several other carbon-based materials, such as graphite (G), commercial HSAG, carbon nanotubes (CNTs), activated carbon, nanometric diamond, graphene oxide, rGO and even higher than that achieved using benchmark metal oxides such as Co_3O_4 , CeO_2 , Al_2O_3 or CuO . HSAG-OH was reused efficiently ten times. Importantly, a reductive thermal treatment of the ten times-used catalyst allows the recovery of its excellent catalytic activity for ozone activation to hydroperoxyl radicals. On the basis of the comparison of the catalytic activity of HSAG-OH with that of several other carbonaceous catalysts it will be concluded that the high activity of the HSAG-OH derives from the integrity of sp^2 graphene layers in a multilayer configuration together with its excellent dispersibility of the HSAG-OH particles in aqueous medium due to the presence of peripheral OH groups.

5.2 Experimental section

5.2.1 Materials

Graphite (CAS 7782-42-5), diamond nanoparticles (ref: 636 444, $\geq 97\%$), activated carbon (AC, Norit SX Ultra, ref 53663), Al_2O_3 , CeO_2 , Co_3O_4 , CuO , dimethylsulfoxide (DMSO, $>99.5\%$), 5,5-dimethyl-1-pyrroline N-oxide (DMPO), 2,2,6,6-tetramethylpiperidine (TEMP) were supplied by Sigma-Aldrich. MWCNTs were supplied by Nanostructured & Amorphous Materials. HSAG was Synthetic

Graphite 8427 supplied by Asbury Graphite Mills Inc. Characterization of HSAG has been reported by some of us in previous studies.⁴⁴⁻⁴⁷ Other reagents employed were analytical or HPLC grade and they were also provided by Sigma-Aldrich.

HSAG oxidation by nitric acid. As previously reported for analogous carbonaceous materials, commercial HSAG (1 g) was dispersed in concentrated HNO₃ (25 mL) in a round-bottom flask, and the mixture heated under stirring at 83 °C for 20 h.⁴⁸ After cooling the reaction system, the suspension was centrifuged at 12,000 rpm for 20 min and washed repeatedly with Milli-Q water until the pH value of the washing liquids was neutral. Finally, the solid sample was recovered by filtration and dried at 100 °C for 12 h. This sample was labelled as HSAG-HNO₃.

HSAG hydroxylation by KOH. As previously reported,^{44,45} HSAG and KOH were reacted in a planetary ball mill (S100 from Retsch), with 0.3 L grinding jar moving on a horizontal plane. The jar was loaded with six ceramic balls having a diameter of 20 mm. HSAG (1 g), KOH powder (20 g) and H₂O (6.5 mL) were put into the jar that was rotated at 300 rpm, at room temperature, for 10 h. After this time, the mixture was placed in a Büchner funnel with a sintered glass disc and repeatedly washed with distilled water (6 × 100 mL) under vacuum. Finally, the obtained solid was put in an oven at 60 °C to remove excess water. This sample was labelled as HSAG-OH. Recently, possibility to perform edge-oxidation of graphites by hydrogen peroxide oxidation has been recently reported.⁴⁹

HSAG-OH functionalization by means of the Reimer-Tiemann/Cannizzaro Domino. As previously reported, in a round bottomed flask equipped with magnetic stirrer and condenser were added KOH powder (3.12 g, 55 mmol), CHCl₃ (1.12 mL, 14 mmol) and H₂O (0.5 mL) in sequence. HSAG-OH (0.500 g) was added to such mixture after few seconds.⁴⁴ The mixture was stirred at room temperature,

for 12 h. After this time, the solvent was removed at reduced pressure. The resulting solid was ground in fine grains in a mortar with a pestle, transferred into a Falcon tube (15 mL) and water (10 mL) was added. The suspension was sonicated for 10 min and centrifuged at 4000 rpm for 10 min (3 times). This sample was labeled as HSAG-OH-COOH.

Reactivation of the HSAG–OH Sample after Six Uses.

Method A: Heating treatment. 0.1 g of 6 times used HSAG-OH sample and CH₂Cl₂ (25 mL) were put in a 50 mL round bottomed flask equipped with magnetic stirrer. The resulting suspension was stirred at room temperature for 12 h. After this time the mixture was filtered and the powder was put in a 5 mL glass vial and heated at 200 °C for 12 h under nitrogen atmosphere.

Method B: Reduction by hydrazine. 0.1 g of 6 times used HSAG-OH sample were put in a 25 mL round bottomed flask equipped with magnetic stirrer. To this suspension, hydrazine monohydrate (1 μ for 1 mg of HSAG-OH) was added. The suspension was stirred at 80 °C for 12 h. After this time the mixture was filtered and the powder was dried.

Pyrolyzed nanometric diamond. Commercial diamond nanoparticles (D NPs) (200 mg) were placed in a tubular oven under Ar atmosphere and heated up to 900 °C at 5 °C/min for 1 h. After cooling the system at room temperature, the samples were washed with ethanol and water and finally dried at 100 °C for 12 h.⁵⁰

5.2.2 Characterization

Combustion elemental analyses were performed using a CHNOS analyzer (Perkin Elmer). Raman spectra were collected at room temperature upon 514 nm laser excitation using a Renishaw In Via Raman spectrophotometer equipped with a CCD detector. Analyses by temperature-programmed desorption (TPD) coupled to a mass spectrometer (TPD–MS) of the carbonaceous samples were performed in a Micrometer II 2920 station connected to a quadrupolar mass

spectrometer. X-ray photoelectron spectroscopy (XPS) measurements were performed with a SPECS spectrometer with an MCD-9 detector using a monochromatic Al ($K\alpha = 1486.6$ eV) X-ray source. The C1s peak at 284.4 eV was employed as reference. Transmission electron microscopy (TEM) images of nanometric diamond samples were acquired using a JEOL JEM-2100F instrument operating at 200 kV

5.2.3 Catalytic reactions

Catalytic Ozonations. Ozone was generated from dried air using a commercially available corona discharge ozone generator. The generated ozone (140 mg/h) was introduced at 570 mL/min through a gas diffuser into the bottom of a 300 mL glass reactor. Typically, the reactor contained 250 mL of Milli-Q water with or without oxalic acid (50 mg L^{-1}) as model organic pollutant together with the dispersed catalyst (100 mg L^{-1}). The course of the reaction was followed by immediately analyzing reaction aliquots previously filtered through a Nylon filter ($0.2 \mu\text{m}$) to remove the catalyst after being taken.

Selective Quenching Experiments and EPR Measurements. These experiments were performed similarly as described for oxalic acid degradation at pH 3, but (i) for selective hydroxyl quenching experiments, dimethyl sulfoxide or *tert*-butyl alcohol (20 mol % with respect to oxalic acid) were also present, and (ii) for EPR experiments, oxalic acid was replaced by DMPO or TEMP as ROS trapping agent at 1 g L^{-1} . EPR measurements were carried out in a Bruker EMX spectrometer (9.803 GHz, sweep width 3489.9 G, time constant 40.95 ms, modulation frequency 100 kHz, modulation width 1 G, microwave power 19.92 mW) at pH 3 and 20 °C and 20 min of reaction.

Ozone Measurements. Ozone calibrations were carried out by iodometry. To determine ozone self-decomposition or decomposition in the presence of carbonaceous solids (50 mg L^{-1}) in water, the pH value of the aqueous solution or suspension was first adjusted using HCl or NaOH aqueous solutions, and then the absorbance of aliquots was measured in a UV-vis spectrometer (JASCO instruments) from 200 to 400 nm. It should be noted that O_3 exhibits a maximum absorption wavelength at 260 nm with an extinction coefficient of $3000 \text{ M}^{-1} \text{ cm}^{-1}$.⁵¹

Oxalic Acid Analysis. Oxalic acid concentration was determined by analyzing reaction aliquots by ion chromatography using a conductivity detector. The stationary phase was a column of poly(vinyl alcohol) with quaternary ammonium groups, while the mobile phase was a basic aqueous solution (3.2 mM Na_2CO_3 /1.0 mM NaHCO_3 mM).

Total Organic Carbon (TOC). The TOC of aqueous oxalic acid solutions was analyzed using a High TOC Elementar II analyzer.

Boehm Titration. Boehm titration was performed to quantitatively determine the content of oxygenated surface groups. In a typical experiment, 0.05 g of the carbon allotrope was dispersed in 50 mL of a 0.05 M NaOH solution and water was removed. After stirring at room temperature for 24 h, the mixture was filtered. Removal of the solid carbon allotrope from the solution is essential to avoid the reaction of the deprotonated groups on the carbon allotrope surface with HCl. A portion of the solution (10 mL) was mixed with a water solution of HCl (0.05 N, 20 mL). CO_2 was removed from solution immediately before the titration. The obtained mixture was titrated using a 0.05 M solution of NaOH.

CO_2 Removal with N_2 . The samples were poured in 40 mL glass vials equipped with glass septum lids. N_2 was bubbled into the vial through a needle submerged

in the solution. The bubbling rate was less than 1 mL/min. The time of degasification was 24 h. After degasification, the samples were transferred to a beaker that had been purged with inert gas and covered with Parafilm, to prevent absorption of atmospheric CO₂.

UV-Vis Titration of O₃. A Hewlett-Packard 8452A diode-array spectrophotometer was used to perform the optical absorption measurements. The dispersions wherein the concentration of O₃ was to be determined (ca. 3 mL) were placed in a 1 cm optical path quartz cuvette with a Pasteur pipet. The UV-visible spectrum reported the absorption as a function of the wavelength of the radiation between 200 and 750 nm.

5.3 Results and discussion

5.3.1 Catalyst characterization

Table 1 lists the carbon materials employed as catalysts in the present work, their precursors, and the preparation methods. The preparation and characterization of some of the materials have been already reported, and references are provided to the papers where these materials were originally disclosed. The synthesis of two other carbon materials, namely, HSAD-HNO₃ and PD in Table 1, has been performed for the first time for this work. Among the most relevant characterization data, XPS provides information on the elements present on the catalyst surface, their relative abundance, and their distribution among the different families. To illustrate the relevant data obtained by XPS, Figure 1 shows C1s and O1s peaks recorded for HSAG-OH, which, as it will be commented below, is the most active ozonation catalyst. As can be seen in this figure, both C and O elements are present on the surface with an atomic proportion of 91.3 and 8.7%, respectively, and their high-resolution experimental peak can be fitted to four and three components for the C and O, respectively. We will come back

later to this point when commenting on the active sites on edge-functionalized graphite and the deactivation mechanism.

Among the samples tested a high-surface area graphite modified with oxygen-functional groups both at edges and on the basal planes was prepared via HNO_3 oxidation treatment (HSAG- HNO_3), similarly to other reported carbonaceous materials.⁴⁸ The oxidation of HSAG material by HNO_3 was confirmed by combustion elemental analysis that provides an estimation that the oxygen content of HSAG- HNO_3 is about 12 wt %. It should be commented that the oxygen content in the commercial HSAG is negligible. XPS C1s and O1s peaks of the HSAG- HNO_3 also confirm the presence on the HSAG surface of oxygen-functional groups having single, double and three C-O bonds such as alcohols, carbonyl and carboxylic derivatives [Figure S1, Supporting Information (SI)]. These oxygen functional groups were also evidenced by FT-IR spectroscopy. Vibration bands at 3300, 1710, and 1200 cm^{-1} are characteristic of O-H, C=O, and C-O bonds, present in alcohols, carbonylic, and carboxylic functional groups, respectively.

Pyrolyzed diamond NPs (PD) were prepared by pyrolysis of commercial nanodiamonds (D) at 900 °C, as previously reported.⁵⁰ Raman spectroscopy of PD clearly shows the formation of a defective sp^2 network characterized by the observation of the D, G, and 2D bands that are absent in the parent D sample (Figure S2a, SI). TPD characterization of PD also confirms the removal of surface functional groups present in the commercial D sample (Figure S2b, SI). In addition, the solid-state ^{13}C NMR spectrum of PD shows the presence of carbon atoms with sp^2 and sp^3 hybridization (Figure S3, SI). Previous studies by our group have reported the absence of sp^2 carbon on commercial D NPs.⁵² The formation of graphene layers on the surface of D upon pyrolysis at 900 °C agrees with a recent report describing also the formation of a few outer graphene layers in a core/shell configuration upon pyrolysis of diamond NPs (Figure S4, SI). In fact, HRTEM of PD further confirms the formation of graphene layers with an interplanar distance of 3.38 Å, while the sp^3 interplanar distance in D NPs is around 2.02 Å. These values measured in the present study are close to the reported 3.56 and 2.06 Å interplanar distances for graphite and D, respectively (Figure S5, SI).⁵³

Table 1. List of catalysts employed in the present work.				
Entry	Name	Abbreviation	Precursor/Preparation method	Ref.
1	Graphite	G	Commercial	
2	High-surface area graphite	HSAG	Commercial	
3	HSAG functionalized with hydroxyl groups in the edges	HSAG-OH	HSAG/KOH	[44, 46]
4	HSAG functionalized with OH and COOH groups in the edges	HSAG-OH-COOH	HSAG/ KOH	[44]
5	HSAG functionalized with oxygen-functional groups in both edges and basal plane	HSAG-HNO ₃	HSAG/HNO ₃	This work
6	Graphene oxide	GO	Graphite/Hummers method	[53]
7	Reduced graphene oxide	rGO	GO/thermal reduction at 200 °C	[53]
8	Multiwall carbon nanotubes	MWCNTs	Commercial	-
9	Diamond nanoparticles	D	Commercial	-
10	Hydroxylated diamond NPs	D-OH	Chemical treatment + hydrogen annealing of D NPs	[54]
11	Pyrolyzed diamond NPs	PD	D NPs/pyrolysis at 900 °C for 2 h	This work
12	Activated carbon	AC	Commercial	-

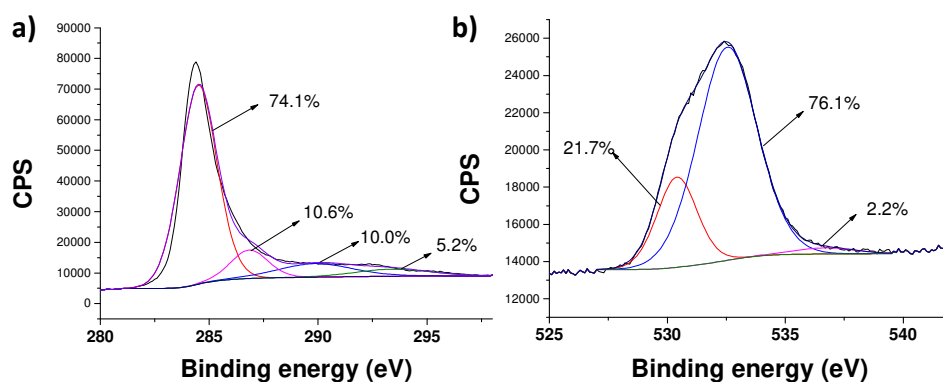


Figure 1. XPS C1s (a) and O1s (b) peaks of fresh HSAG–OH. The figure shows also the best deconvolution of the experimental peaks to individual components and their corresponding percentages.

5.3.2 Catalytic activity

Comparison of Catalytic Efficiency of Various Carbon Materials. In the first stage of the work, the efficiency of different carbonaceous materials as catalysts for the ozonation of organic pollutants in water was compared. Oxalic acid was selected as the probe molecule to determine the efficiency of the catalytic ozonation (Figure 2a).^{14,23} Graphs of Figure 2 show the dependence on time of the concentration of oxalic acid upon reacting with ozone, both in the presence of different carbocatalysts (a) as well as in the presence of transition-metal catalysts (b) and at different pH values with HSAG–OH as the catalyst (c).

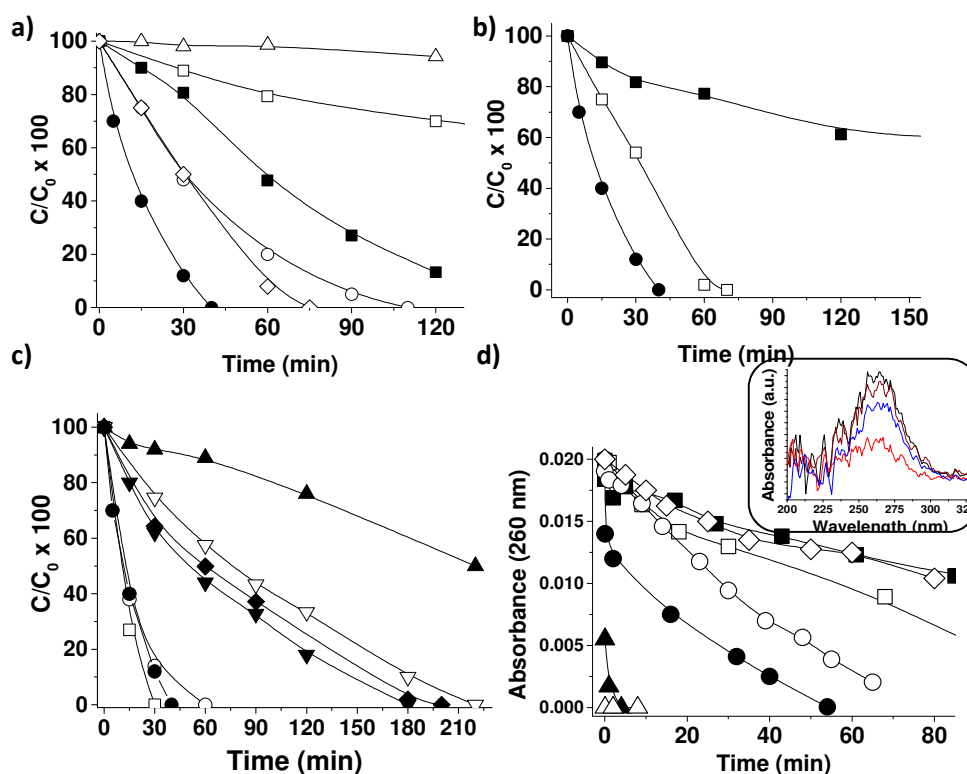


Figure 2. Decomposition of oxalic acid by ozone. (a) Relative oxalic acid concentration vs time at pH 3 without catalyst (Δ) or in the presence of HSAG-OH (\bullet), HSAG (\circ), rGO (\blacksquare), or GO (\square) as catalyst. (b) Relative oxalic acid concentration vs time at pH 3 in the presence of HSAG-OH (\bullet), Co_3O_4 (\square), or Fe_2O_3 (\blacksquare) as catalyst. (c) Relative oxalic acid concentration vs time in the presence of HSAG-OH as catalyst, at pH 2 (\square), pH 3 (\bullet), pH 4 (\circ), pH 5 (\blacktriangledown), pH 7 (∇), pH 9 (\blacklozenge), or pH 12 (\blacktriangle). (d) Ozone stability in water in the absence of catalyst as a function of the pH: pH 2 (\blacksquare), pH 3 (\diamond), pH 5 (\square), pH 7 (\circ), pH 9 (\bullet), pH 10 (\blacktriangle), and pH 12 (Δ). Reaction conditions: catalyst (50 mg L^{-1}), oxalic acid (50 mg L^{-1}), O_3 (140 mg/h), pH as indicated, 20°C , and O_3 to oxalic acid molar ratio 5.3. The inset shows the UV absorption band corresponding to O_3 at 260 nm.

As previously reported,¹⁴ blank control experiments in the absence of catalyst reveal that ozone cannot degrade oxalic acid at pH 3 and 20 °C.²³ In general, oxalic acid adsorption on the different carbonaceous materials at pH 3 and 20 °C is lower than 2 wt %. Importantly, under these experimental conditions, oxalic acid can be degraded by catalytic ozonation using different carbonaceous materials: HSAG–OH (●), HSAG (○), GO (□), or rGO (■) (Figure 2). The most active carbocatalyst is that based on commercial HSAG functionalized with hydroxyl groups on the edges (HSAG–OH), followed by the commercially available parent HSAG. Both HSAG-based catalysts are more active than previously reported rGO obtained from the Hummers method followed by thermal reduction at 200 °C.⁴² In agreement with previous reports, the catalytic activity of GO was lower than that of rGO.⁵⁶ Considering the structure of the various catalysts, these results reinforce the importance of an appropriate content of oxygen functional groups together with sp^2 carbon domains as active sites of ozonation in carbocatalysts. This proposal agrees also with other studies that have reported the higher carbocatalytic activity of rGO with respect to GO as catalysts of oxidations using H_2O_2 or PMS as reagents.²⁷ Importantly, the carbocatalytic activity of HSAG–OH was higher than that of benchmark commercial inorganic catalysts like Co_3O_4 or Fe_2O_3 (Figure 2b).^{12,21}

One of the most important parameters that influences the efficiency of catalytic AOPs is the pH value of the water to be treated.^{9,16,57} Figure 2c shows that HSAG–OH is an efficient ozonation carbocatalyst in a broad pH window, from 2 to 9 units, with optimum values around 4. The broad range of pH for carbocatalytic ozonation, using HSAG–OH, makes the application of this carbocatalyst really feasible for wastewaters for which the pH is either acidic or slightly basic. It should be noted that blank control experiments, performed in the absence of catalysts, do not significantly degrade oxalic acid (<8% conversion) in the range of the adopted pH values, except at pH \geq 12, where slightly higher oxalic acid degradation was observed (~20% at 240 min).

In order to determine the ozone stability in water at different pH values in the absence of catalyst, a series of control experiments were carried out (Figure 2d). In agreement with previous reports, O_3 stability decreases as the pH of the

aqueous medium increases.¹² In fact, at pH values higher than 10, O₃ is almost instantaneously decomposed under the present reaction conditions. It is well-established that O₃ decomposes spontaneously to reactive oxygen species such as hydroperoxyl radicals at basic pH values.¹²

Ozone dose consumption is a decisive factor for the development of AOP with real potential applications.²² In the present work, additional experiments have been conducted for the optimization of the ozone dose. It was observed that, by using HSAG–OH as catalyst, complete oxalic acid degradation at both pH 3 and 5 takes place when using 2.7 equiv of O₃ (Figure S6, SI).²² This value represents a moderate excess with respect to the stoichiometric amount necessary to convert oxalic acid into CO₂.

Stability of Carbocatalysts. One of the basic requirements of any catalyst is its stability under reaction conditions. This aspect was in particular investigated for HSAG–OH and rGO as the catalysts. Results of the reusability test are shown in Figure 3. HSAG–OH was reused up to 10 times with only a slight decrease in catalytic activity, and full oxalic degradation was achieved, at longer reaction times (Figure 3a). These results are definitely better than those collected with rGO prepared by the Hummers method, which rapidly deactivates after one use (Figure 3b). On the basis of a previous work, the thermal treatment of the rGO sample in a muffle at 300 °C allows restoration of its catalytic activity.⁴²

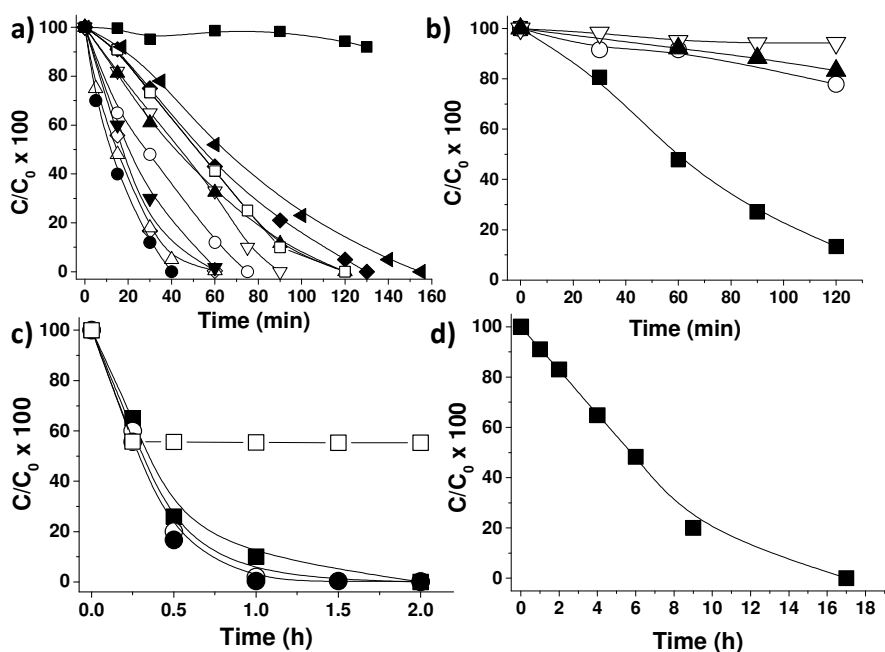


Figure 3. Reaction of oxalic acid with ozone. All the graphs show the relative oxalic acid concentration vs time. (a) HSAG–OH catalyst: (a) 1st use (●), 2nd use (△), 3rd use (◇), 4th use (▼), 5th use (○), 6th use (▽), 7th use (▲), 8th use (□), 9th use (◆), 10th use (◄) and reaction in the absence of catalyst (■). (b) rGO catalyst: 1st use (■), 2nd use (○), 3rd use (▽) and 4th use (▲). (c) HSAG–OH catalyst (●), HSAG–OH removed at 44% oxalic degradation (□), HSAG–OH after six uses and then pyrolyzed under Ar atmosphere (■), HSAG–OH after six uses and then reduced with hydrazine (○). (d) Productivity test using a large excess of oxalic acid with HSAG–OH as catalyst. Reaction conditions: catalyst (50 mg L⁻¹), oxalic acid (50 mg L⁻¹), O₃ (140 mg/h), pH 3, room temperature, and O₃ to oxalic acid molar ratio 5.3. Reaction conditions of productivity test: catalyst (50 mg L⁻¹), oxalic acid (1 g L⁻¹), O₃ (140 mg/h), pH 3, room temperature, and O₃ to oxalic acid molar ratio 5.3.

XPS of the six-times-used HSAG–OH [Figures 4 and S7 (SI)] reveals the partial oxidation of the carbon material during the carbocatalytic reaction. According to the deconvolution of the XPS O1s peak, the deactivated HSAG–OH sample exhibits an increase of the quinone-like oxygens (binding energy 532.5 eV) accompanied by a concomitant decrease of the phenolic-like oxygen (binding energy 530 eV) (Figure 4, part c vs d). Therefore, comparison of the XPS O1s of the fresh and deactivated material suggests the role as active sites of phenolic/quinone-like moieties as a redox pair promoting the O₃ activation. A similar proposal of phenolic/quinone-like redox pairs as active sites was postulated by Su and co-workers for the carbocatalytic oxidative dehydrogenation of ethylbenzene^{58,59} and is in line with the ability of hydroquinones to promote Fenton-like chemistry as organocatalysts.^{54,60} Importantly, the catalytic activity of the 10-times-used HSAG–OH can be restored to the value of the fresh sample by performing a reduction process either with hydrazine as reducing agent or by thermal reduction at 300 °C (Figures 3c and 4e,f). XPS of the 10-times-used HSAG sample treated by thermal treatment or hydrazine confirms the success of the reduction process to restore the used HSAG–OH material by observing the coincidence of the C1s and O1s peaks of the treated samples with those of the fresh HSAG [Figures 4 and S8 (SI)].

The heterogeneity of the reaction was assessed by observing that the reaction stops if the catalyst is removed from the reaction and then ozonation is continued under the same reaction conditions (Figure 3c, □ symbol).

The excellent activity and stability of the HSAG–OH as carbocatalyst was further established by performing a productivity test, which demonstrated that a small amount of carbocatalyst (50 mg L⁻¹) is able to degrade up to 1 g L⁻¹ of oxalic acid (Figure 3d).

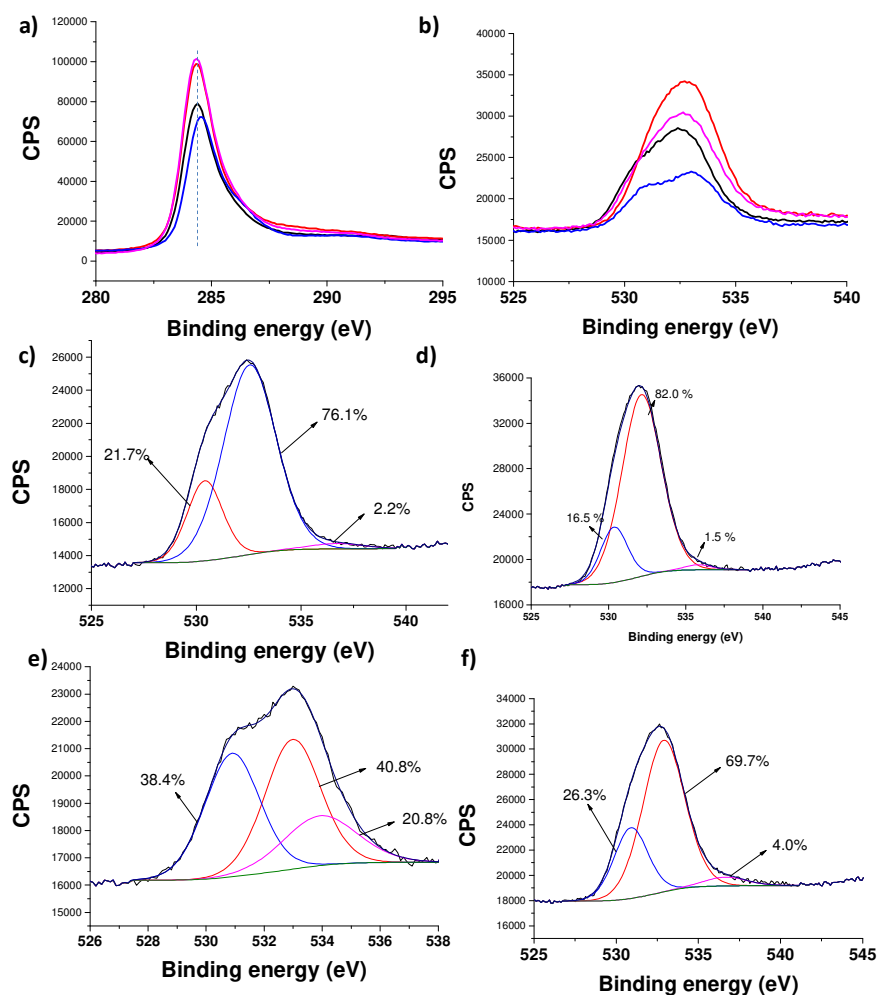


Figure 4. XPS C1s (a) and O1s peaks (b) for the fresh HSAG–OH (black line), HSAG–OH used six times in oxalic acid ozonation (red line), six-times-used HSAG–OH followed by thermal reduction at 300 °C (blue line), and six-times-used HSAG–OH regenerated by chemical reduction with hydrazine (pink line). XPS O1s for fresh HSAG–OH (c), HSAG–OH used six times in oxalic acid ozonation (d), six-times-used HSAG–OH followed by thermal reduction at 300 °C (e), and six-times-used HSAG–OH regenerated by chemical reduction with hydrazine (f). Spectra have been fitted to the best deconvolution of the experimental peaks into individual components.

Insights into the Catalytic Activity of HSAG–OH. In order to get some insights into the origin of the catalytic activity of HSAG–OH, several commercially available carbon materials with or without further modification were also used as catalyst to correlate structure and activity. The temporal profiles of the oxalic acid decomposition by ozone in the presence of the different carbocatalysts are presented in Figure 5.

A first working hypothesis to explain the higher activity of HSAG–OH with respect to HSAG was based on the presence of phenolic functional groups at the graphene edges, which leads to a better water dispersibility, an increase in the work function of the graphene sheets, and the presence of hydroquinone/quinone-like groups as redox centers.

The importance of an adequate HSAG functionalization at the edges by OH or COOH groups, preserving the sp^2 nature of the basal carbon atoms and the high work function, was further evaluated by comparing the activity of non-selective HSAG functionalization with oxygen functional groups, at both edges and the basal planes, using a HNO_3 aqueous medium as oxidant. The carbocatalytic activity of the HSAG– HNO_3 randomly functionalized with oxygen groups was clearly lower than that of HSAG–OH (Figure 5a). This activity order indicates the importance of the presence of sp^2 domains as active sites that should be well-dispersed in water by selective edge functionalization.

To address the role of the sp^2 layer with a high work function due to the presence of electron donor OH groups as active sites for O_3 activation, other commercially available carbon allotropes such as graphite or CNTs were also tested. It was found that these materials also behave as active carbocatalysts in accordance with previous reports (Figure 5b).^{61,62} The lower activity of graphite with respect to HSAG can be attributed to the lower specific surface area of the former and, therefore, the lower density of available sp^2 domains performing as active centers. The use of commercially available activated carbon as carbocatalyst resulted in lower activity with respect to carbon allotropes. A plausible explanation of the lower carbocatalytic activity of activated carbon with respect to the carbon allotropes would be the presence of sp^3 domains on its amorphous

carbon network. In fact, the activity of nanometric diamond constituted by sp^3 carbons as carbocatalyst is negligible, a fact that is in agreement with our proposal of sp^2 domains as centers activating ozonation (Figure 5b). The use of a D solid functionalized with hydroxyl groups (D–OH) does not increase the activity of the D sample (Figure 5b). Notably, if nanometric D samples are submitted to pyrolysis at 900 °C for 2 h, as a result of the surface graphitization of the D NPs, the resulting PD material is as active as HSAG–OH (Figure 4c). Attempts to reuse PD resulted in a decrease of the initial catalytic activity (Figure 4d). Interestingly, HSAG–OH and nanometric PD decompose rapidly O_3 (<2 min) in the absence of oxalic acid at pH 3, while O_3 decomposition at pH 3 in the presence of commercial D NPs follows almost a coincident profile as that measured in the absence of any catalyst. All these findings reinforce the role of high work function sp^2 carbon layers as redox activator in ozonation, although it seems that they become partially oxidized, partially losing activity under reaction conditions.

According to this rationalization, the role of phenolic groups in HSAG–OH would be to increase the electron density of the graphene layers that would act as electron donors versus ozone triggering the generation of reactive oxygen species (see below). Figure 6 illustrates the mechanistic proposal. Related to this rationalization, Wang and co-workers have addressed by DFT the role of oxygens and edges as active sites donating electrons to peroxomonosulfate.⁶³ These –OH groups can be considered as electron-rich hydroquinone moieties.

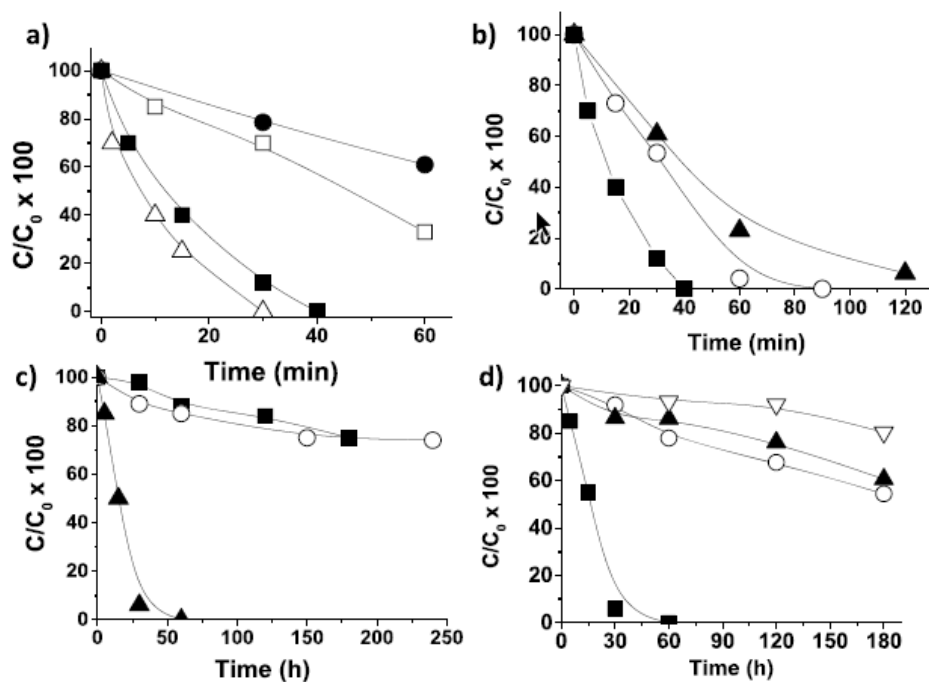


Figure 5. Temporal evolution of oxalic acid concentration upon ozonation in the presence of various catalysts. Catalysts: (a) HSAG-OH-COOH (Δ), HSAG-OH (\blacksquare), HSAG-HNO₃ (\square), graphite (\bullet); (b) HSAG-OH (\blacksquare), MWCNTs (\circ), activated carbon (\blacktriangle); (c) pyrolyzed PD (\blacktriangle), commercial D (\blacksquare), hydroxyl-functionalized D-OH (\circ). (d) Carbocatalytic activity for the first (\blacksquare), second (\blacktriangle), third (\circ), and fourth use (∇) of the PD catalyst. Reaction conditions: catalyst (50 mg L^{-1}), oxalic acid (50 mg L^{-1}), O₃ (140 mg/h), pH 3, 20 °C, and O₃ to oxalic acid molar ratio 5.3.

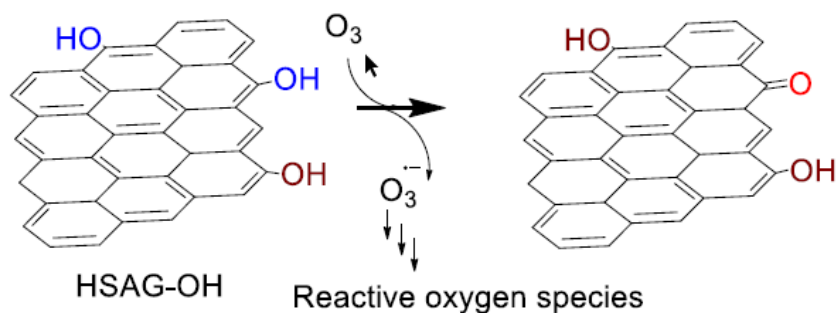


Figure 6. Proposed pathway for the oxidation of phenolic groups present in HSAG–OH to quinone-like moieties and one-electron reduction of ozone and formation of reactive oxygen species.

5.3.3 Role of dispersibility

The previous proposal of sp^2 carbon domains with high work function and phenol/quinone as redox pairs active sites for catalytic ozonation does not consider that the catalyst is constituted by graphite particles (HSAG–OH) that have low hydrophilicity and quickly sediment in a liquid due to the poor dispersibility. To address the role of other possible oxygenated functional groups increasing hydrophilicity and water dispersibility, an analogous HSAG functionalized with carboxylic and hydroxyl groups on the graphene edges was prepared (HSAG–OH–COOH).⁴⁴ To make available the previously commented active sites, an increase in hydrophilicity and dispersibility should be beneficial. In this context, it is interesting to note that the activity of HSAG–OH–COOH is higher than that of HSAG–OH (Figure 4a). This result reinforces the idea that the activity of HSAG-based materials derives mainly from phenolic/quinone-like moieties and the high work function of HSAG–OH layers derived from its unaltered sp^2 network combined with the high dispersibility of the graphite particles in water, due to the polar oxygen-containing functional groups. The content of oxygenated

functional groups was quantitatively evaluated (as described in the Experimental Section) using the Boehm titration method, which allows one to determine groups such as carboxyls, lactones, and phenolics. The total amounts of such functionalities were 0.75, 3.0, and 4.5 mmol/g for HSAG, HSAG-OH, and HSAG-OH-COOH, respectively. Water dispersions of HSAG-OH and HSAG-OHCOOH were prepared, at 1, 0.5, 0.1, 0.05, 0.01, 0.005, and 0.001 mg/mL as the nominal material concentration, and UV-vis absorption analysis was performed (Figures S9 and S10, SI). Details are reported in the Supporting Information and in the Experimental Section. In particular, results from the UV-vis analysis of HSAG-OH and HSAG-OH-COOH suspensions in water, shown in Figures S10 and S11 (SI), reveal the larger stability of HSAG-OH-COOH dispersions.

Reactive Oxygen Species Involved in the Mechanism. In order to get some insight about the nature of the reactive oxygen species formed during the catalytic ozonation in the presence of HSAG-OH catalyst, EPR measurements and selective radical quenching experiments were carried out. The use of DMPO as spin trap of reactive oxygen species (ROS) derived from ozone in aqueous solution in the presence of HSAG-OH has allowed determination of the presence of hydroperoxyl radicals (Figure 7a), while the use of TEMP reveals the formation of $^1\text{O}_2$ (Figure 7b). Selective quenching experiments using DMSO or *tert*-butyl alcohol do not inhibit the carbocatalytic oxalic degradation by ozone and, therefore, rule out the possible presence of hydroxyl radicals.²² These results are in agreement with those obtained by Shaobin and co-workers using rGO prepared by the Hummers method as carbocatalyst for ozone activation, which have firmly ruled out by EPR measurements the possibility of hydroxyl radical generation.⁴² In contrast, those studies have detected hydroperoxyl or $^1\text{O}_2$ species that were considered as responsible for the oxidation reaction.⁴² Those conclusions are coincident with those of the present study. In addition, in this work, TOC measurements of the oxalic acid aqueous solution before and after the catalytic ozonation confirm the complete mineralization of the organic compound to CO_2 and H_2O .

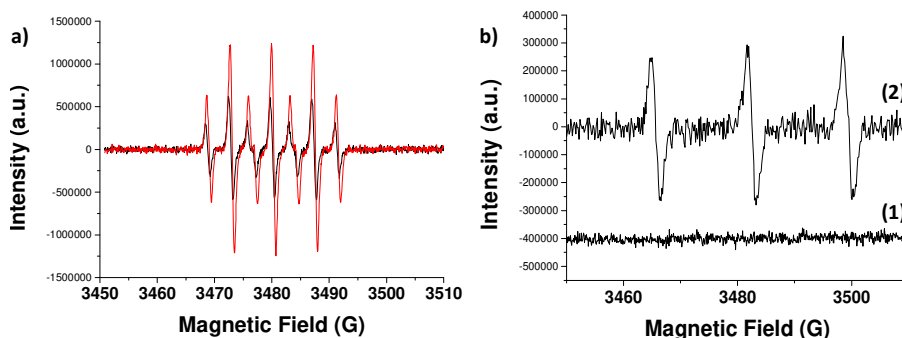


Figure 7. (a) EPR spectra for ozonation in the presence of DMPO as trapping agent recorded in the absence (black line) or presence (red line) of HSAG-OH as catalyst. (b) EPR spectra of O_3 in water in the presence of TEMP as trapping agent recorded in the absence (1) and in the presence (2) of HSAG-OH as catalyst. Reaction conditions: catalyst (50 mg L^{-1}), O_3 (140 mg/h), trapping agent (1 g L^{-1}), pH 3, room temperature, and 30 min reaction.

5.4 Conclusions

Using oxalic acid decomposition as the probe reaction, the present paper has shown the catalytic activity for ozonation of a series of graphite and graphene materials at pH values in the range from 3 to 9. Higher pH values result in the spontaneous, fast, uncatalyzed decomposition of O_3 . It was observed that optimal catalysts are those having sp^2 domains and a suitable work function that can be well-dispersed in water. This requires the presence of hydrophilic OH groups at peripheral positions without disturbing the sp^2 domains. Under the explored reaction conditions, it seems that graphene materials are prone to deactivate, due to auto-oxidation, and that the presence of a dopant element has a detrimental effect on the catalytic activity. EPR measurements using spin trap agents and quenching experiments using selective inhibitors indicate that the

reactive oxygen species generated in the process are mainly hydroperoxyl radicals and singlet oxygen. No evidence for the formation of hydroxyl radicals was obtained

Considering the wide use of ozone for water disinfection, the present results open new opportunities for enhancement of an ozone effect beyond disinfection for pollutant decomposition using transition-metal-free catalysts based on carbon materials that can exhibit even and enhanced catalytic activity.

5.5 References

- (1) Filonenko, G. A.; Van Putten, R.; Hensen, E. J. M.; Pidko, E. A. Catalytic (de)hydrogenation promoted by non-precious metals-Co, Fe and Mn: Recent advances in an emerging field. *Chem. Soc. Rev.* 2018, 47, 1459–1483.
- (2) Johansson Seechurn, C. C. C.; Kitching, M. O.; Colacot, T. J.; Snieckus, V. Palladium-catalyzed cross-coupling: A historical contextual perspective to the 2010 nobel prize. *Angew. Chem., Int. Ed.* 2012, 51, 5062–5085.
- (3) Leenders, S. H. A. M.; Gramage-Doria, R.; De Bruin, B.; Reek, J. N. H. Transition metal catalysis in confined spaces. *Chem. Soc. Rev.* 2015, 44, 433–448.
- (4) Magano, J.; Dunetz, J. R. Large-scale applications of transition metal-catalyzed couplings for the synthesis of pharmaceuticals. *Chem. Rev.* 2011, 111, 2177–2250.
- (5) Xia, Q.-H.; Ge, H.-Q.; Ye, C.-P.; Liu, Z.-M.; Su, K.-X. Advances in homogeneous and heterogeneous catalytic asymmetric epoxidation. *Chem. Rev.* 2005, 105, 1603–1662
- (6) Brienza, M.; Katsoyiannis, I. A. Sulfate radical technologies as tertiary treatment for the removal of emerging contaminants from wastewater. *Sustainability* 2017, 9, 1604.

- (7) Ikehata, K.; Jodeiri Naghashkar, N.; Gamal El-Din, M. Degradation of aqueous pharmaceuticals by ozonation and advanced oxidation processes: A review. *Ozone: Sci. Eng.* 2006, 28, 353–414.
- (8) Neyens, E.; Baeyens, J. A review of classic Fenton's peroxidation as an advanced oxidation technique. *J. Hazard. Mater.* 2003, 98, 33–50.
- (9) Pera-Titus, M.; García-Molina, V.; Baños, M. A.; Giménez, J.; Esplugas, S. Degradation of chlorophenols by means of advanced oxidation processes: A general review. *Appl. Catal., B* 2004, 47, 219–256.
- (10) Pignatello, J. J.; Oliveros, E.; Mackay, A. Advanced oxidation processes for organic contaminant destruction based on the fenton reaction and related chemistry. *Crit. Rev. Environ. Sci. Technol.* 2006, 36, 1–84.
- (11) Klavarioti, M.; Mantzavinos, D.; Kassinos, D. Removal of residual pharmaceuticals from aqueous systems by advanced oxidation processes. *Environ. Int.* 2009, 35, 402–417.
- (12) Kasprzyk-Hordern, B.; Ziółek, M.; Nawrocki, J. Catalytic ozonation and methods of enhancing molecular ozone reactions in water treatment. *Appl. Catal., B* 2003, 46, 639–669.
- (13) Muruganandham, M.; Suri, R. P. S.; Jafari, S.; Sillanpää, M.; Lee, G.-J.; Wu, J. J.; Swaminathan, M. Recent developments in homogeneous advanced oxidation processes for water and wastewater treatment. *Int. J. Photoenergy* 2014, 2014, 821674.
- (14) Beltrán, F. J.; Rivas, F. J.; Montero-de-Espinosa, R. Ozoneenhanced oxidation of oxalic acid in water with cobalt catalysts. 1. Homogeneous catalytic ozonation. *Ind. Eng. Chem. Res.* 2003, 42, 3210–3217.
- (15) Hu, P.; Long, M. Cobalt-catalyzed sulfate radical-based advanced oxidation: A review on heterogeneous catalysts and applications. *Appl. Catal., B* 2016, 181, 103–117.
- (16) Navalon, S.; Alvaro, M.; Garcia, H. Heterogeneous Fenton catalysts based on clays, silicas and zeolites. *Appl. Catal., B* 2010, 99, 1–26.

- (17) Navalon, S.; Dhakshinamoorthy, A.; Alvaro, M.; Garcia, H. Heterogeneous Fenton catalysts based on activated carbon and related materials. *ChemSusChem* 2011, 4, 1712–1730.
- (18) Dhakshinamoorthy, A.; Navalon, S.; Alvaro, M.; Garcia, H. Metal nanoparticles as heterogeneous fenton catalyst. *ChemSusChem* 2012, 5, 46–64.
- (19) Espinosa, J. C.; Catalá, C.; Navalón, S.; Ferrer, B.; Álvaro, M.; García, H. Iron oxide nanoparticles supported on diamond nanoparticles as efficient and stable catalyst for the visible light assisted Fenton reaction. *Appl. Catal., B* 2018, 226, 242–251.
- (20) Espinosa, J. C.; Manickam-Periyaraman, P.; Bernat-Quesada, F.; Sivanesan, S.; Álvaro, M.; García, H.; Navalón, S. Engineering of activated carbon surface to enhance the catalytic activity of supported cobalt oxide nanoparticles in peroxy-monosulfate activation. *Appl. Catal., B* 2019, 249, 42–53.
- (21) Nawrocki, J.; Kasprzyk-Hordern, B. The efficiency and mechanisms of catalytic ozonation. *Appl. Catal., B* 2010, 99, 27–42.
- (22) Ghuge, S. P.; Saroha, A. K. Catalytic ozonation for the treatment of synthetic and industrial effluents - Application of mesoporous materials: A review. *J. Environ. Manage.* 2018, 211, 83– 102.
- (23) Pines, D. S.; Reckhow, D. A. Effect of dissolved cobalt (II) on the ozonation of oxalic acid. *Environ. Sci. Technol.* 2002, 36, 4046– 4051.
- (24) Wang, J.; Bai, Z. Fe-based catalysts for heterogeneous catalytic ozonation of emerging contaminants in water and wastewater. *Chem. Eng. J.* 2017, 312, 79–98.
- (25) Titirici, M.-M.; White, R. J.; Brun, N.; Budarin, V. L.; Su, D. S.; del Monte, F.; Clark, J. H.; MacLachlan, M. J. Sustainable carbon materials. *Chem. Soc. Rev.* 2015, 44, 250–290.
- (26) Duan, X.; Sun, H.; Wang, S. Metal-free carbocatalysis in advanced oxidation reaction. *Acc. Chem. Res.* 2018, 51, 678–687.
- (27) Navalon, S.; Dhakshinamoorthy, A.; Alvaro, M.; Antonietti, M.; García, H. Active sites on graphene-based materials as metal-free catalysts. *Chem. Soc. Rev.* 2017, 46, 4501–4529.

- (28) Navalon, S.; Dhakshinamoorthy, A.; Alvaro, M.; Garcia, H. Carbocatalysis by graphene-based materials. *Chem. Rev.* 2014, 114, 6179–6212.
- (29) Álvarez, P. M.; García-Araya, J. F.; Beltrán, F. J.; Giráldez, I.; Jaramillo, J.; Gómez-Serrano, V. The influence of various factors on aqueous ozone decomposition by granular activated carbons and the development of a mechanistic approach. *Carbon* 2006, 44, 3102–3112.
- (30) Faria, P. C. C.; Órfão, J. J. M.; Pereira, M. F. R. Ozone decomposition in water catalysed by activated carbon: influence of chemical and textural properties. *Ind. Eng. Chem. Res.* 2006, 45, 2715–2721.
- (31) Gonçalves, A. G.; Órfão, J. J. M.; Pereira, M. F. R. Catalytic ozonation of sulphamethoxazole in the presence of carbon materials: Catalytic performance and reaction pathways. *J. Hazard. Mater.* 2012, 239–240, 167–174.
- (32) Sánchez-Polo, M.; von Gunten, U.; Rivera-Utrilla, J. Efficiency of activated carbon to transform ozone into OH radicals: Influence of operational parameters. *Water Res.* 2005, 39, 3189–3198.
- (33) Soares, O. S. G. P.; Faria, P. C. C.; Órfão, J. J. M.; Pereira, M. F. R. Ozonation of textile effluents and dye solutions in the presence of activated carbon under continuous operation. *Sep. Sci. Technol.* 2007, 42, 1477–1492.
- (34) Álvarez, P. M.; Beltrán, F. J.; Masa, F. J.; Pocostales, J. P. A comparison between catalytic ozonation and activated carbon adsorption/ozone-regeneration processes for wastewater treatment. *Appl. Catal., B* 2009, 92, 393–400.
- (35) Cao, H.; Xing, L.; Wu, G.; Xie, Y.; Shi, S.; Zhang, Y.; Minakata, D.; Crittenden, J. C. Promoting effect of nitration modification on activated carbon in the catalytic ozonation of oxalic acid. *Appl. Catal., B* 2014, 146, 169–176.
- (36) Faria, P. C. C.; Orfao, J. J. M.; Pereira, M. F. R. Catalytic ozonation of sulfonated aromatic compounds in the presence of activated carbon. *Appl. Catal., B* 2008, 83, 150–159.
- (37) Sánchez-Polo, M.; Leyva-Ramos, R.; Rivera-Utrilla, J. Kinetics of 1,3,6-naphthalenetrisulphonic acid ozonation in presence of activated carbon. *Carbon* 2005, 43, 962–969.

- (38) Lin, Y.-C.; Chang, C.-L.; Lin, T.-S.; Bai, H.; Yan, M.-G.; Ko, F.-H.; Wu, C.-T.; Huang, C.-H. Application of physical vapor deposition process to modify activated carbon fibers for ozone reduction. *Korean J. Chem. Eng.* 2008, 25, 446–450.
- (39) Gonçalves, A. G.; Figueiredo, J. L.; Orfao, J. J. M.; Pereira, M. F. R. Influence of the surface chemistry of multi-walled carbon nanotubes on their activity as ozonation catalysts. *Carbon* 2010, 48, 4369–4381.
- (40) Geim, A. K.; Novoselov, K. S. The rise of graphene. *Nat. Mater.* 2007, 6, 183–191.
- (41) Navalón, S.; Herance, J. R.; Álvaro, M.; García, H. General aspects in the use of graphenes in catalysis. *Mater. Horiz.* 2018, 5, 363–378.
- (42) Wang, Y.; Xie, Y.; Sun, H.; Xiao, J.; Cao, H.; Wang, S. Efficient catalytic ozonation over reduced graphene oxide for p-hydroxybenzoic acid (PHBA) destruction: Active site and mechanism. *ACS Appl. Mater. Interfaces* 2016, 8, 9710–9720.
- (43) Pei, S.; Wei, Q.; Huang, K.; Cheng, H.-M.; Ren, W. Green synthesis of graphene oxide by seconds timescale water electrolytic oxidation. *Nat. Commun.* 2018, 9, 145.
- (44) Barbera, V.; Brambilla, L.; Porta, A.; Bongiovanni, R.; Vitale, A.; Torrisi, G.; Galimberti, M. Selective edge functionalization of graphene layers with oxygenated groups by means of Reimer–Tiemann and domino Reimer–Tiemann/Cannizzaro reactions. *J. Mater. Chem. A* 2018, 6, 7749–7761.
- (45) Barbera, V.; Guerra, S.; Brambilla, L.; Maggio, M.; Serafini, A.; Conzatti, L.; Vitale, A.; Galimberti, M. Carbon papers and aerogels based on graphene layers and chitosan: Direct preparation from high surface area graphite. *Biomacromolecules* 2017, 18, 3978–3991.
- (46) Barbera, V.; Porta, A.; Brambilla, L.; Guerra, S.; Serafini, A.; Valerio, A. M.; Vitale, A.; Galimberti, M. Polyhydroxylated few layer graphene for the preparation of flexible conductive carbon paper. *RSC Adv.* 2016, 6, 87767–87777.
- (47) Galimberti, M.; Barbera, V.; Guerra, S.; Conzatti, L.; Castiglioni, C.; Brambilla, L.; Serafini, A. Biobased Janus molecule for the facile preparation of water solutions of few layer graphene sheets. *RSC Adv.* 2015, 5, 81142–81152.

- (48) Espinosa, J. C.; Navalon, S.; Alvaro, M.; Dhakshinamoorthy, A.; Garcia, H. Reduction of C=C double bonds by hydrazine using active carbons as metal-free catalysts. *ACS Sustainable Chem. Eng.* 2018, 6, 5607–5614.
- (49) Vittore, A.; Acocella, M. R.; Guerra, G. Edge-oxidation of graphites by hydrogen peroxide. *Langmuir* 2019, 35, 2244–2250.
- (50) Duan, X.; Ao, Z.; Zhang, H.; Saunders, M.; Sun, H.; Shao, Z.; Wang, S. Nanodiamonds in sp²/sp³ configuration for radical to nonradical oxidation: Core-shell layer dependence. *Appl. Catal., B* 2018, 222, 176–181.
- (51) Levanov, A. V.; Isaikina, O. Y.; Tyutyunnik, A. N.; Antipenko, E. E.; Lunin, V. V. Molar Absorption Coefficient of Ozone in Aqueous Solutions. *J. Anal. Chem.* 2016, 71, 549–553.
- (52) Navalon, S.; Sempere, D.; Alvaro, M.; Garcia, H. Influence of hydrogen annealing on the photocatalytic activity of diamond-supported gold catalysts. *ACS Appl. Mater. Interfaces* 2013, 5, 7160–7169.
- (53) Petit, T.; Arnault, J.-C.; Girard, H. A.; Sennour, M.; Kang, T.-Y.; Cheng, C.-L.; Bergonzo, P. Oxygen hole doping of nanodiamond. *Nanoscale* 2012, 4, 6792–6799.
- (54) Espinosa, J. C.; Navalón, S.; Primo, A.; Moral, M.; Sanz, J. F.; Álvaro, M.; García, H. Graphenes as efficient metal-free Fenton catalysts. *Chem. - Eur. J.* 2015, 21, 11966–11971.
- (55) Sempere, D.; Navalon, S.; Dancíková, M.; Alvaro, M.; Garcia, H. Influence of pretreatments on commercial diamond nanoparticles on the photocatalytic activity of supported gold nanoparticles under natural Sunlight irradiation. *Appl. Catal., B* 2013, 142–143, 259–267.
- (56) Liu, J.-N.; Chen, Z.; Wu, Q.-Y.; Li, A.; Hu, H.-Y.; Yang, C. Ozone/graphene oxide catalytic oxidation: a novel method to degrade emerging organic contaminant N, N-diethyl-mtoluamide (DEET). *Sci. Rep.* 2016, 6, 31405.
- (57) Navalon, S.; Dhakshinamoorthy, A.; Alvaro, M.; Garcia, H. Metal nanoparticles supported on two-dimensional graphenes as heterogeneous catalysts. *Coord. Chem. Rev.* 2016, 312, 99–148.

(58) Qi, W.; Liu, W.; Zhang, B.; Gu, X.; Guo, X.; Su, D. Oxidative dehydrogenation on nanocarbon: Identification and quantification of active sites by chemical titration. *Angew. Chem. Int. Ed.* 2013, 52, 14224–14228.

(59) Zhang, J.; Su, D. S.; Blume, R.; Schlögl, R.; Wang, R.; Yang, X.; Gajovic, A. Surface chemistry and catalytic reactivity of a nanodiamond in the steam-free dehydrogenation of ethylbenzene. *Angew. Chem., Int. Ed.* 2010, 49, 8640–8644.

(60) Espinosa, J. C.; Navalón, S.; Álvaro, M.; García, H. Reduced graphene oxide as a metal-free catalyst for the light-assisted Fenton-like reaction. *ChemCatChem* 2016, 8, 2642–2648.

(61) Sun, H.; Liu, S.; Zhou, G.; Ang, H. M.; Tade, M. O.; Wang, S. Reduced Graphene Oxide for Catalytic Oxidation of Aqueous Organic. *ACS Appl. Mater. Interfaces* 2012, 4, 5466–5471.

(62) Zhang, S.; Quan, X.; Zheng, J.-F.; Wang, D. Probing the interphase “HO[rad] zone” originated by carbon nanotube during catalytic ozonation. *Water Res.* 2017, 122, 86–95.

(63) Duan, X.; Sun, H.; Ao, Z.; Zhou, L.; Wang, G.; Wang, S. Unveiling the active sites of graphene-catalyzed peroxymonosulfate activation. *Carbon* 2016, 107, 371–378.

5.6 Supplementary information

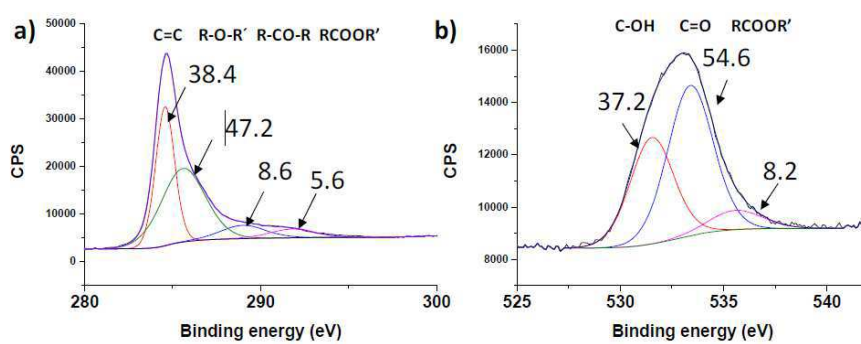


Figure S1. XPS C1s (a) and O1s (b) peaks of the HSAG-HNO₃ sample. The area percentages of the different individual components are also presented.

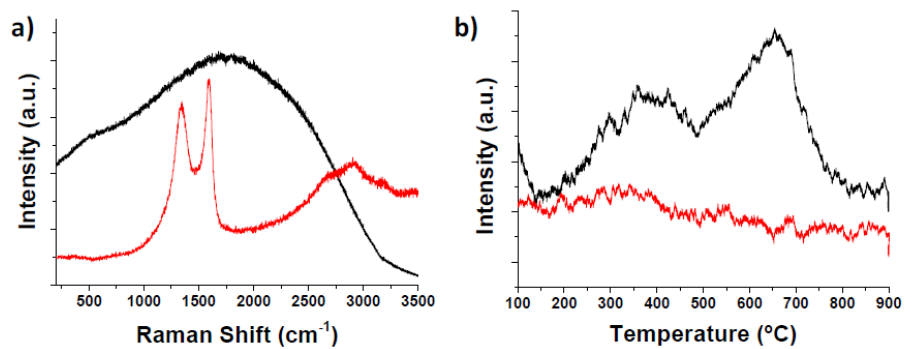


Figure S2. Raman (a) and TPD (b) commercial D (black line) and PD (red line) (a).

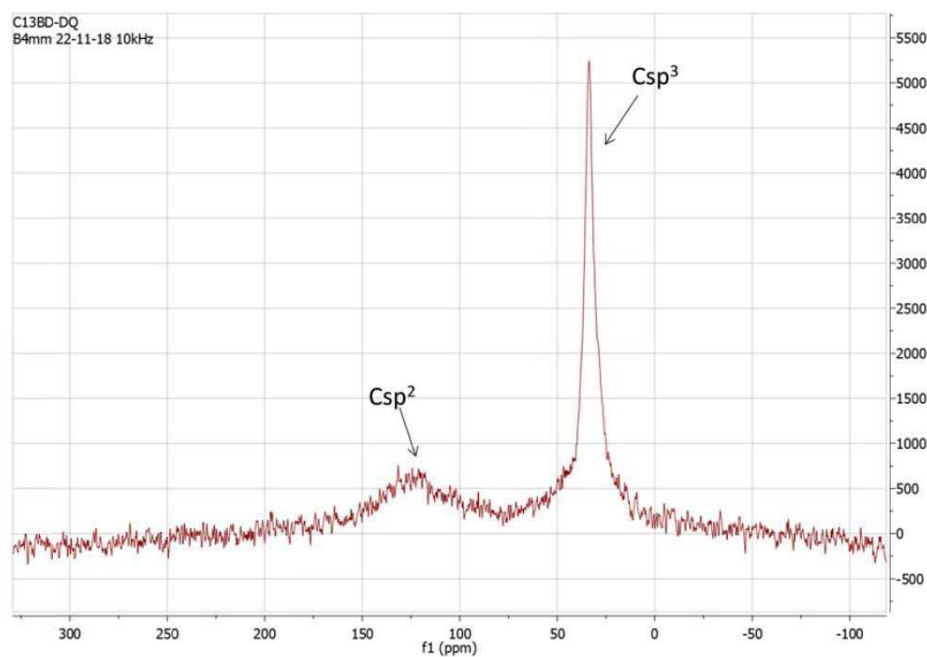


Figure S3. Solid state ¹³C-NMR spectrum of PD sample.

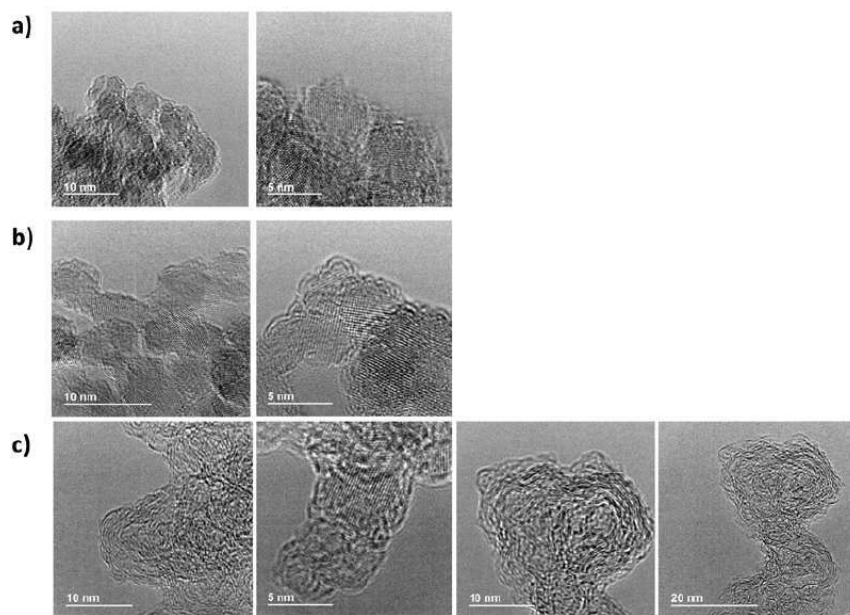


Figure S4. HRTEM of commercial D S4 NPs (a), D-OH (b) and PD (c) samples.

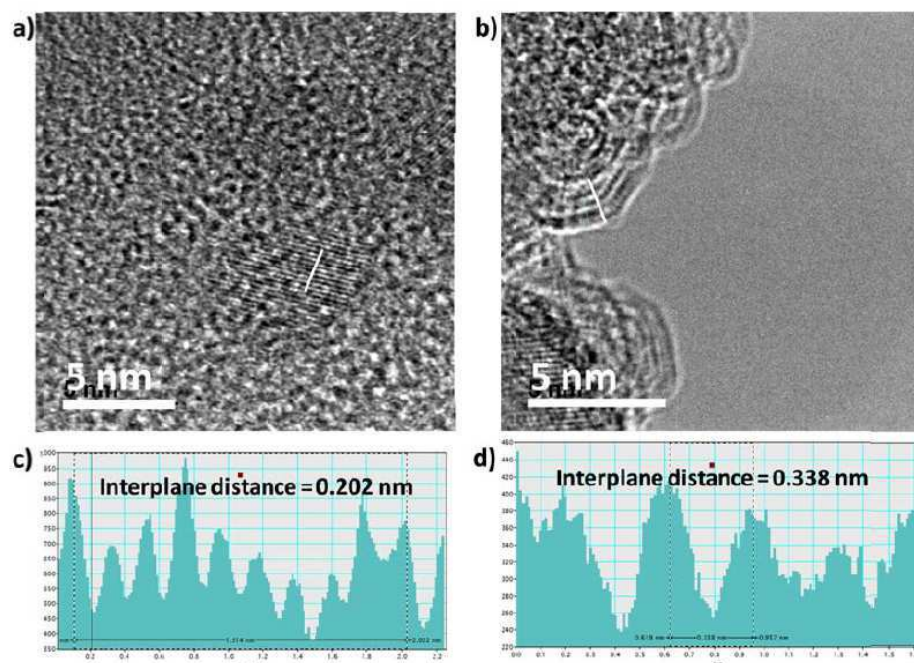


Figure S5. HR-TEM images and interplanar distance of commercial D (a, c) and PD (b, d).

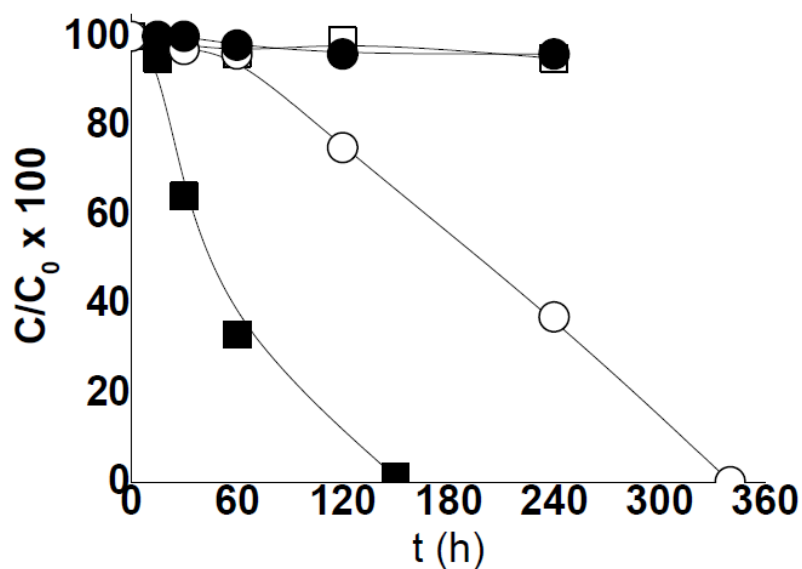


Figure S6. Relative oxalic acid concentration vs time during the reaction with ozone at pH 3 (■) or 5 (○) using HSAG-OH as carbocatalyst and an ozone to oxalic acid molar ratio of 2.7. Blank controls at pH 3 (□) or 5 (●) in the absence of catalyst are also presented. Reaction conditions: Catalyst (50 mg L^{-1}), oxalic acid (50 mg L^{-1}), pH as indicated and $20 \text{ }^\circ\text{C}$.

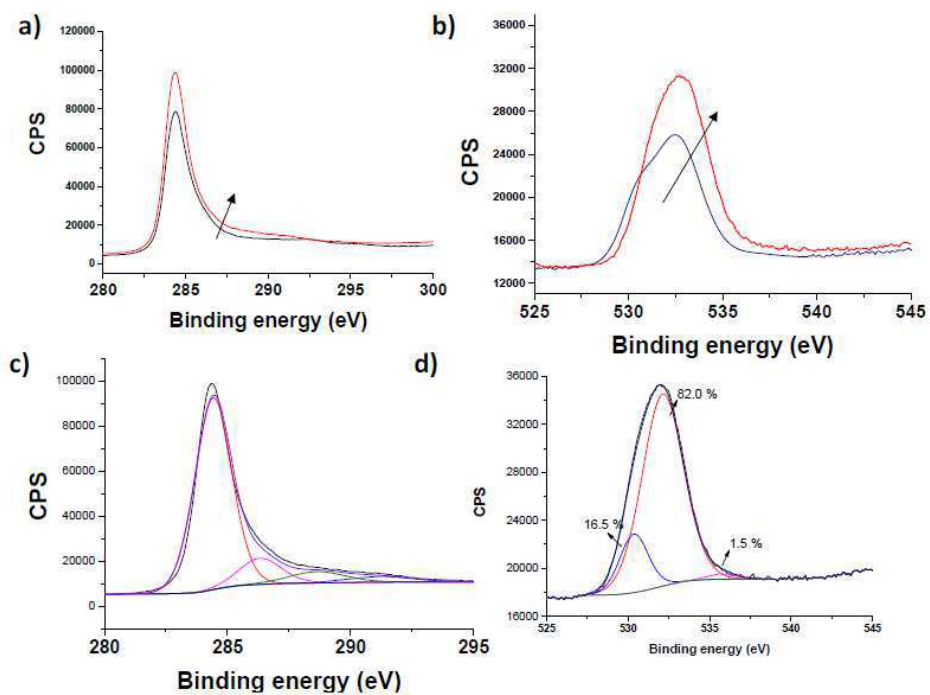


Figure S7. XPS C1s peaks (a, c) and O1s peaks (b, d) of fresh HSAG-OH (a, b black line) and six-times used (c, d) catalyst. The peaks shows also the best deconvolution of the experimental peaks to individual components.

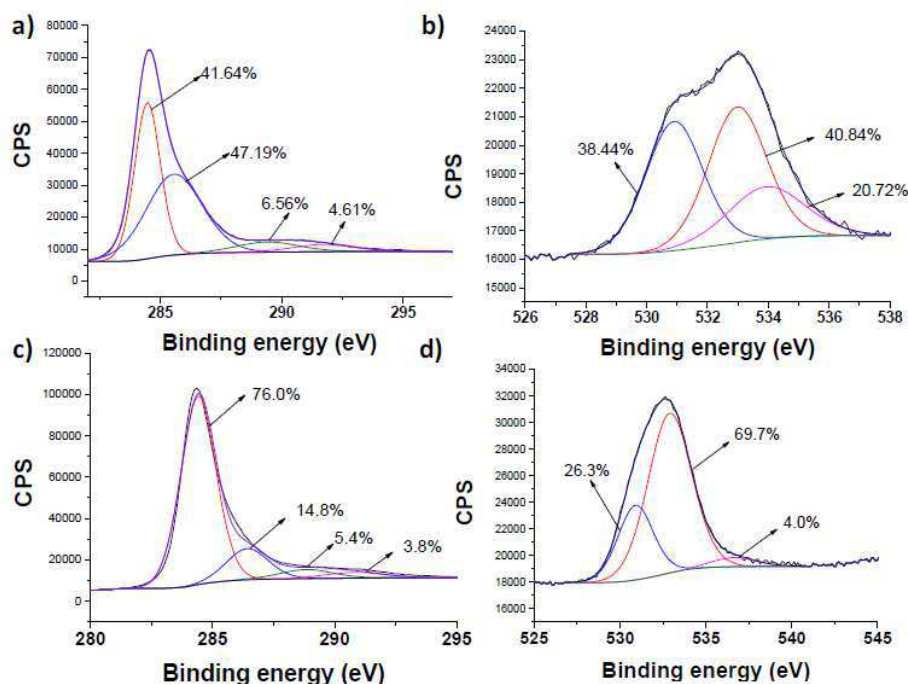


Figure S8. XPS C1s (a and c) and O1s (b and d) for HSAG-OH catalyst used six times in oxalic acid ozonation and then either reduced thermally (a, b) and used six times and then reduced with hydrazine (c, d). The percentages of the individual components are indicated for each.

Water dispersions of HSAG-OH (A) and HSAG-OH-COOH

Dispersions were prepared through a mild sonication and analyzed by UV-Vis absorption analysis as explained in the experimental part.

Figure S9 presents dispersions of HSAG-OH (A) and HSAG-OH-COOH (B) in nominal concentration range from 1 mg/mL to 0.005 mg/mL. Plots of UV-Vis absorbance as a function of the concentration are shown in Figure S10. UV-Vis

absorption spectra of HSAG-OH (A) and HSAG-OH-COOH (B) samples at different concentrations, after sonication and after 3 days are shown in Figure S11. The spectra in Figure S10 and S11 show the larger absorbance and the better stability of HSAG-OHCOOH dispersions. Figure S9 shows that dispersions of HSAG-OH exhibit lighter colour, at low concentrations, and they are even colourless at concentrations of 0.01 and 0.005 mg/mL compared the dispersions based on HSAG-OH-COOH that are darker. These data indicate that HSAG-OH-COOH is more efficiently dispersed in water. The colourless dispersions of HSAG-OH at the lowest concentrations indicates the absence of graphitic material.

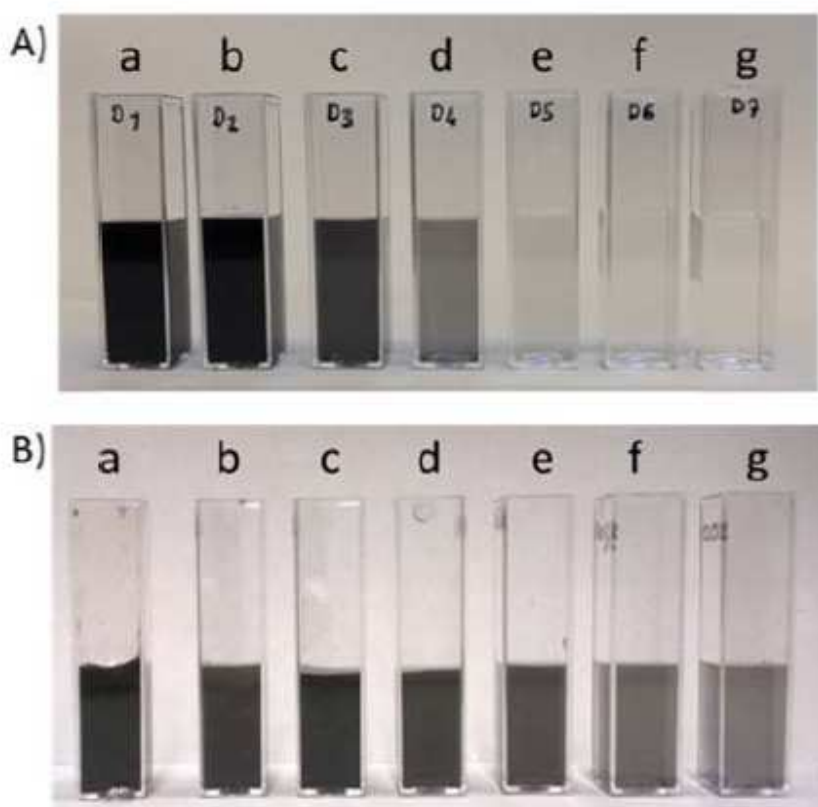


Figure S9. HSAG-OH (A) and HSAG-OH-COOH (B) water dispersions at different concentration: 1 (a), 0.5 (b), 0.1 (c), 0.005 (d), 0.01 (e) and 0.005 (f) mg/ml.

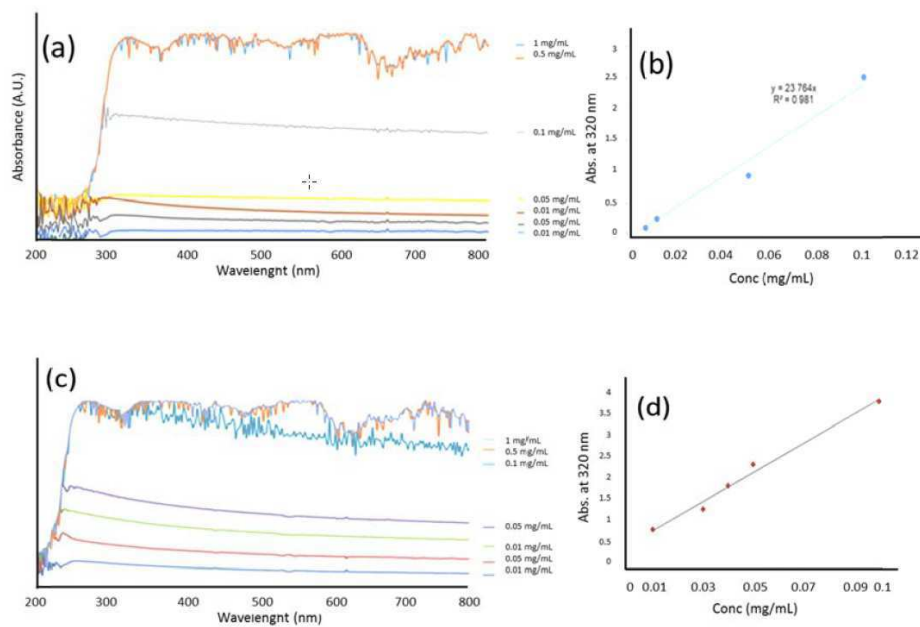


Figure S10. Linear relationship between the absorbance at 320 nm and the concentration of HSAG-OH (a) and HSAG-OH-COOH (c) in water; Plot b and d shows the dependence of UV-Vis absorbance on the concentration of HSAG-OH (b) and HSAG-OH-COOH (d) in water dispersion.

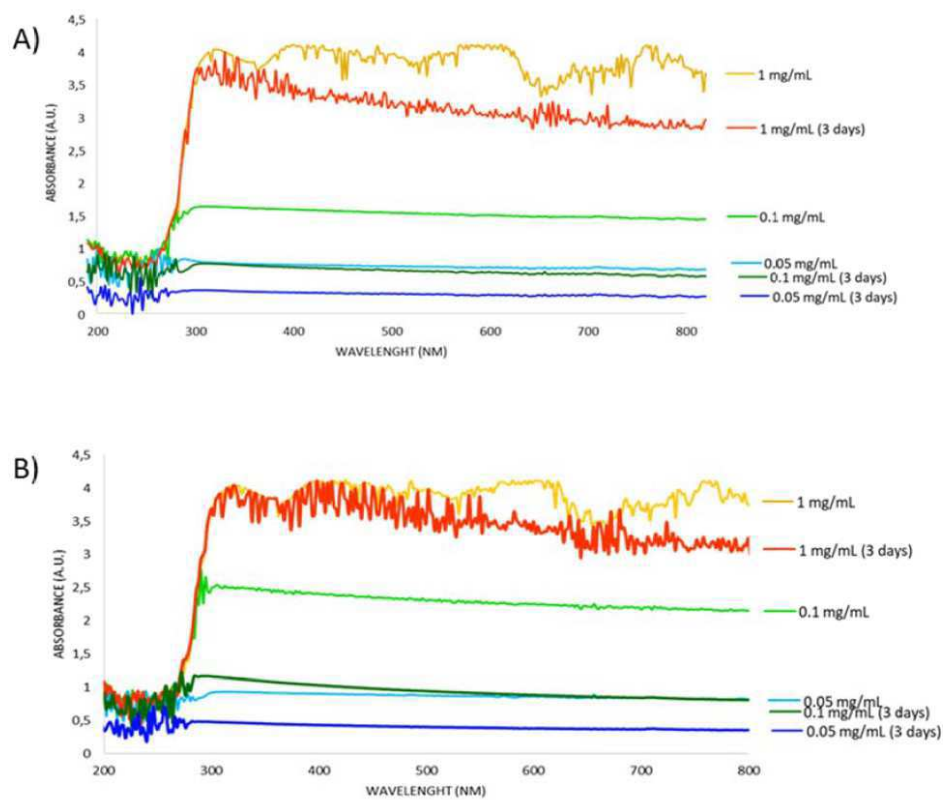


Figure S11. UV-Vis absorption spectra of HSAG-OH (A) and HSAG-OH-COOH (B) samples at different concentrations, after sonication and after 3 days.

Chapter 6

Hybrid sp^2/sp^3 nanodiamonds as heterogeneous metal-free ozonation catalysts in water

6.1. Introduction

The development of metal-free heterogeneous catalysts is an area of great interest for academia and industry [1-9]. The ultimate goal of carbocatalysis is the replacement of transition metal catalysts by sustainable and cost-effective metal-free carbonaceous materials [10-12]. A clear example of sustainability in this area has been the use of activated carbons obtained from biomass as carbocatalysts [13, 14]. The discovery of new carbon allotropes such as nanodiamonds, carbon nanotubes or graphenes, and related carbon materials has expanded the field [15]. Currently, one of the challenges in carbocatalysis is the development of catalytically efficient carbons with atomically precise active sites and specific physico-chemical and electronic properties [16]. The reader is referred to a series of reviews dealing with the development of carbon-based materials such as graphenes,[16-20] carbon nanotubes, nanodiamonds [21-24], carbon dots [25], and other carbonaceous materials such as metal-free catalysts [1, 3, 5, 7].

Since the preparation of nanodiamonds (NDs) at an industrial scale (Tons) by the detonation method there is an increasing interest in their use for several applications including heterogeneous catalysis [21]. In the field of carbocatalysis, partially graphitized nanodiamonds have found applications as metal-free heterogeneous catalysts in some reactions used in petrochemistry, fine chemicals, and environmental remediation [21]. It is generally observed that commercial NDs annealed at temperatures of between ~ 700 and 1300 °C in an inert atmosphere reveal a hybrid structure with a diamond core and graphitic shells that contain some oxygen functional groups or carbon vacancies as defects [21, 26, 27]. Annealing at higher temperatures results in the formation of onion-like carbons exclusively constituted by sp^2 carbons. As one representative example in the area of petrochemistry, Su and co-workers used partially graphitized NDs as carbocatalysts for the dehydrogenation of hydrocarbons such as ethylbenzene[28] and propane[29].

In the area of environmental applications, sp^2/sp^3 hybrid NDs have found applications as metal-free catalysts in advanced oxidation processes (AOP). For example, Shaobin and co-workers have reported the possibility of using these hybrid NDs as active carbocatalysts for peroxydisulfate [30-32] activation and aqueous phase pollutant degradation [1]. In the area of AOPs there is increasing interest in the development of heterogeneous catalytic ozonation processes due to their relatively easy implementation at an industrial scale [33]. The aim of catalytic ozonation is to increase the reactivity of molecular O_3 towards organic or inorganic compounds through the formation of reactive oxygen species (ROS) such as hydroxyl, hydroperoxyl, superoxide radicals, and 1O_2 [33]. Cobalt-based homogeneous or heterogeneous catalysts have proved among the most active for catalytic ozonation. Importantly, several studies have shown the possibility of using carbon-based materials such as activate carbons [34-40], carbon nanofibers [41], carbon nanotubes [38, 42], graphene and related materials [43, 44] as metal-free catalysts for heterogeneous catalytic ozonation [45].

With these precedents we report the development of hybrid and defective sp^2/sp^3 NDs as heterogeneous metal-free catalysts for O_3 activation and oxalic acid degradation as a model pollutant in water. The characterisation data

and catalytic activity reveal the importance of an optimized sp^2/sp^3 structure containing oxygen and nitrogen functional groups on NDs to achieve an excellent level of activity. We are confident that this study will help in the development of nanocarbons with a surface functionalisation that is adequate for acting as active sites for oxidation reactions.

6.2. Experimental section

6.2.1. Materials and methods

Diamond nanopowder (ref: 1321JGY, >98 % purity) was supplied by Nanostructured & amorphous materials, Inc. Dimethyl sulfoxide (DMSO, >99.5%), *tert*-butanol (> 99%), NaN_3 (S2002, >99.5 %), 5,5-dimethyl-1-pyrroline N-oxide (DMPO), and 2,2,6,6-tetramethylpiperidine (TEMP) were supplied by Merck. All other chemicals and solvents employed in this study were analytical or HPLC grade and they were also provided by Merck.

Hybrid sp^2/sp^3 nanodiamond preparation. Commercial diamond nanopowder (Commercial ND; 200 mg) was placed in a tubular oven under argon atmosphere and heated at the corresponding temperatures (700, 900, 1100, 1200 °C) at 5 °C/min for 1 or 4 h. The resulting samples were washed ethanol and water and finally dried at 100 °C for at least 12 h. The samples were labelled as a function of the temperature and annealing time as follows: ND-700, ND-900, ND-1100, ND-1100-4h, ND-1200.

Reactivation of used ND in catalysis. After the reaction, the partially deactivated and most active ND-1100 sample (ND-1100-U, where U means used) was collected from the aqueous solution by filtration through a 0.45 μ m filter and washed with Milli-Q water (500 mL). Then, the ND-1100-U sample was dried in an oven at 100 °C for at least 12 h. Finally, the ND-1100-U was reactivated in a tubular oven under argon atmosphere by heating the sample at 1100 °C at 5 °C/min for 1 h. The resulting sample was labelled as ND-1100-1U-react.

6.2.2 Characterization

Powder X-ray diffractograms (PXRD) were performed in a Philips XPert diffractometer (40 kV and 45 mA) using Ni filtered Cu K α radiation. UV-Raman spectra were collected at room temperature upon 315 nm laser excitation using a Renishaw In Via Raman spectrophotometer equipped with a CCD detector. X-ray photoelectron spectroscopy (XPS) of measurements were recorded with a SPECS spectrometer with an MCD-9 detector using a monochromatic Al (K α = 1486.6 eV) X-ray source. The C1s peak at 284.4 eV was employed as reference. High resolution transmission electron microscopy (TEM) images of nanodiamonds samples were acquired using a JEOL JEM-2100F instrument operating at 200 kV. Isothermal N₂ adsorption measurements were carried out using an ASAP 2010 Micromeritics station.

6.2.3 Catalytic activity

Catalytic Reactions. Catalytic ozonations were carried out as previously reported [43]. Briefly, ozone generation was carried out using a commercially available ozone generator equipped with corona discharge technology. The generated ozone flow (140 mg O₃/h, 570 mL/min) was introduced through a gas diffuser into the bottom of a glass reactor (300 mL). The catalytic experiments were carried out introducing the oxalic acid aqueous pollutant (50 mg L⁻¹; 250 mL) together with the dispersed NDs (100 mg L⁻¹) in the glass reactor. The course of oxalic acid degradation has been followed by analysing reaction aliquots previously filtered (Nylon filter 0.2 μ m) in an ion chromatograph instrument (Metrohm) equipped with a conductivity detector. The stationary phase was a column of poly(vinyl alcohol) with quaternary ammonium groups (Metrosep A Supp 5), while the mobile phase was a basic aqueous solution (Na₂CO₃ 3.2 mM / NaHCO₃ 1.0 mM).

The heterogeneity of the reaction during the catalytic ozonation using ND-1100 as metal-free catalyst was performed as follows. Once the oxalic acid

conversion reached about 50 % an aliquot of the reaction system was sampled and the catalyst removed by filtration (Nylon filter 0.45 μm). Then, the aqueous reaction phase in the absence of catalyst was allowed to react with ozone under the described reaction conditions.

Selective quenching experiments were carried out as described for oxalic acid but with the addition of DMSO or *tert*-butanol as selective hydroxyl radical quenchers (20 mol % respect to oxalic acid) or in the presence of NaN_3 (20 mol % respect to oxalic acid) as selective $^1\text{O}_2$ quencher once the reaction is initiated (~20 % conversion).

EPR measurements. Liquid phase EPR measurements were carried out using DMPO or TEMP as spin trap. Briefly, an aqueous DMPO or TEMP solution (1 g/L; 25 mL) containing the ND-1100 as catalyst (5 mg) a pH 3 was introduced in the ozonator system (140 mg/h) for 30 min. EPR spectra of filtered (0.45 mm Nylon filter) and argon-purged aliquots (5 mL) were measured in a Bruker EMS spectrometer (9.803 GHz, sweep width 3489.9 G, time constant 40.95 ms, modulation frequency 100 kHz, modulation width 1 G, and microwave power 19.92 mW). Similarly, solid phase EPR measurements were carried out using an argon-purged quartz support containing the ND samples and the spectra recorded at 100 K.

Total organic carbon (TOC) measurements of the reaction aliquot at the end of the catalytic ozonation (180 min) using ND-1100 as metal-free catalyst were carried out using a High TOC Elementar II analyzer.

6.3 Results and discussion

6.3.1 Catalyst preparation

In the first step of this study a series of defective hybrid sp^2/sp^3 nanodiamonds were prepared by submitting commercial NDs to several thermal treatments in an argon atmosphere at different temperatures and annealing. Powder XRD of

commercial NDs shows the presence of characteristic diffraction patterns (111) and (220) of polycrystalline NDs (Figure 1). In addition to these diamond diffraction patterns, thermally annealed NDs also show the presence of characteristic graphitic materials (Figure 1). The appearance of a new broad band centred about 26° for the ND samples annealed at temperatures above 1000°C is remarkable. This band is characteristic of the stacking of graphitic carbon atoms with hexagonal crystalline arrangements. These XRD variations agree with previous reports showing the formation of graphene layers from the external surface to the core of the NDs. In fact, the thermally annealed NDs at temperatures above 1000°C exhibited broadened and less intense diamond peaks than pristine ND. This observation agrees with the reduction of the diamond core and concomitant formation of graphitic shells. Therefore, the higher the annealing temperature or time, the greater the degree of graphitisation of the samples.

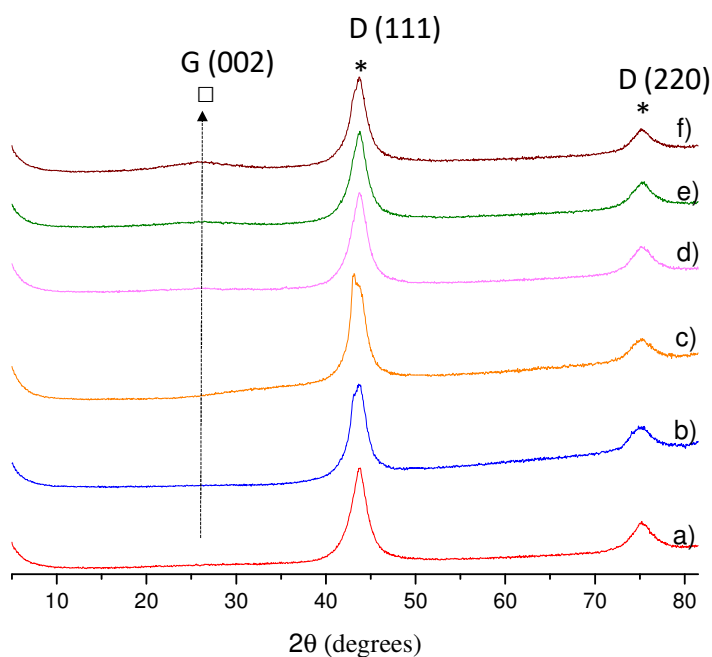


Figure 1. PXRD of commercial (a) and thermally annealed NDs in argon (b-f). Legend: a) commercial ND; b) ND-700, c) ND-900, d) ND-1100; e) ND-1100-4h; f) ND-1200.

High resolution transmission electron microscopy (HR-TEM) measurements of commercial and graphitized NDs in an argon atmosphere (Figure 2 and Figures S1-S7) confirm that high annealing temperatures or long annealing times result in the formation of core-shell structures with a large number of graphene-like layers around a diamond core. Commercial NDs (3 - 10 nm size) are characterised by a crystalline diamond core with (111) planes corresponding to an interplanar distance of about 0.21 nm that are surrounded of unstructured amorphous carbon frequently referred to as soot-matter (Figure 2a). The annealing of commercial NDs at 700 or 900 °C for 1 h still shows the presence of a dominant diamond core with a somewhat disordered graphitic outer shell (Figure 2b,c). When the annealing temperature is above 1100 °C a clear transformation of the commercial ND into a core-shell hybridized sp^2/sp^3 ND with more graphitic layers is observed (Figures 2d, e). The sample annealed at 1200 °C for 2 h exhibits the greatest graphitic appearance with the formation of highly ordered onion-like carbon (OLC) structures (Figure S6) while the core diamond domains can still be observed (Figure S7). The self-compression of the graphitic layers results in a lower plane interdistance between the internal layers (ca 0.42 nm) than the most external layers (ca 0.59 nm) (Figure S6).

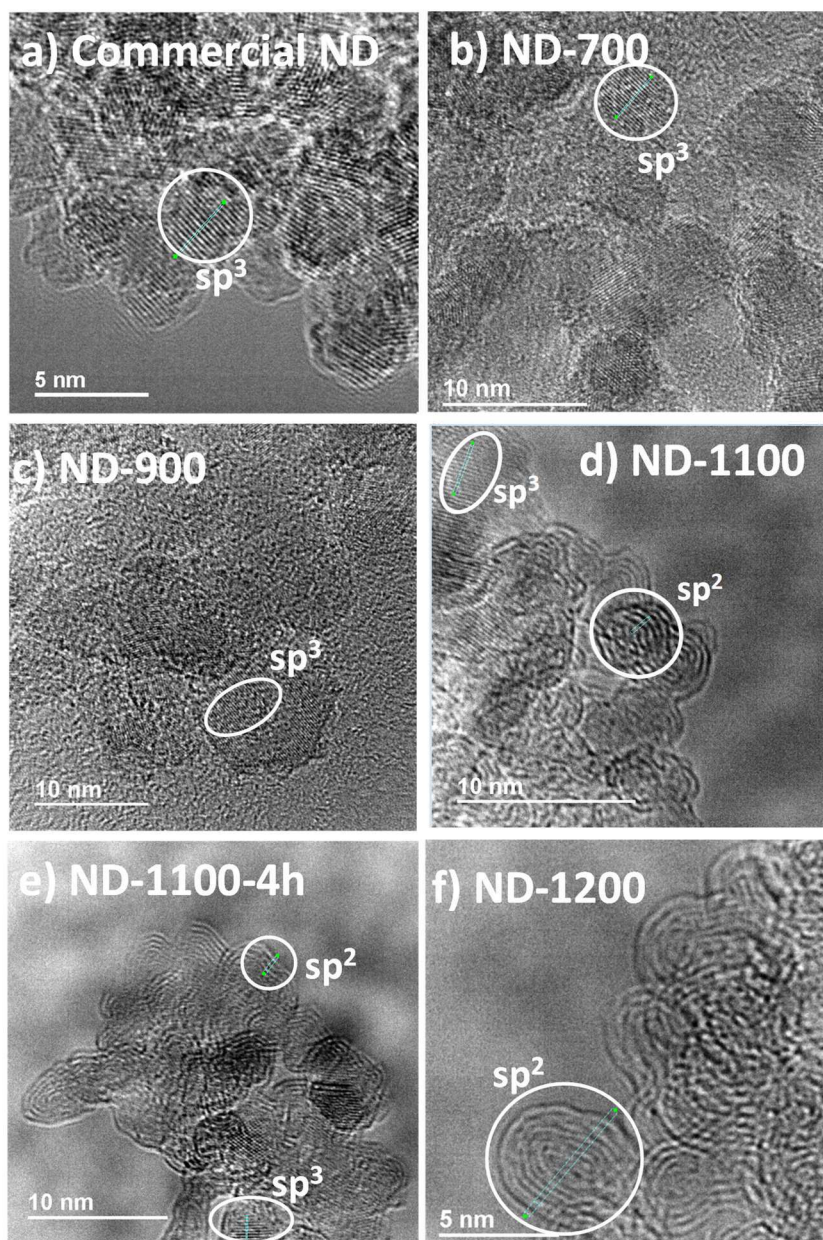


Figure 2. Photographs and HR-TEM images of commercial (a) and thermally annealed NDs in argon (b-f). Legend: a) commercial ND; b) ND-700 c) ND-900, d) ND-1100; e) ND-1100-4h; f) ND-1200.

UV-Raman spectroscopy further confirmed an increase in the degree graphitisation of thermally annealed NDs along with increased annealing temperatures and times (Figures 3a and Figure S8). Figure 3a shows that increasing annealing temperatures or times results in a decrease of the diamond intensity peak at 1326 cm^{-1} together with an increase in graphitic carbon bands (namely, D band at about 1405 cm^{-1} and G-band at 1590 cm^{-1}) [46, 47]. The bands centred at about 1640 and 1720 cm^{-1} are characteristic of hydroxyl and carbonyl groups, respectively [46], and become less important with respect to the graphitic carbon bands (1405 and 1590 cm^{-1}) as the temperature or annealing time increases. A comparison of the I_D/I_G ratios of the different samples reveals that the number of defects in annealed NDs decreases as the annealing temperature or time increases. Overall, the amorphous carbon present in the commercial NDs is transformed/reconstituted during the thermally annealing process into a well-ordered nanocrystalline graphite shell and the diamond core simultaneously decreases [29]. The higher the annealing temperature and time, the fewer are the structural defects and the greater are the presence of OLC structures.

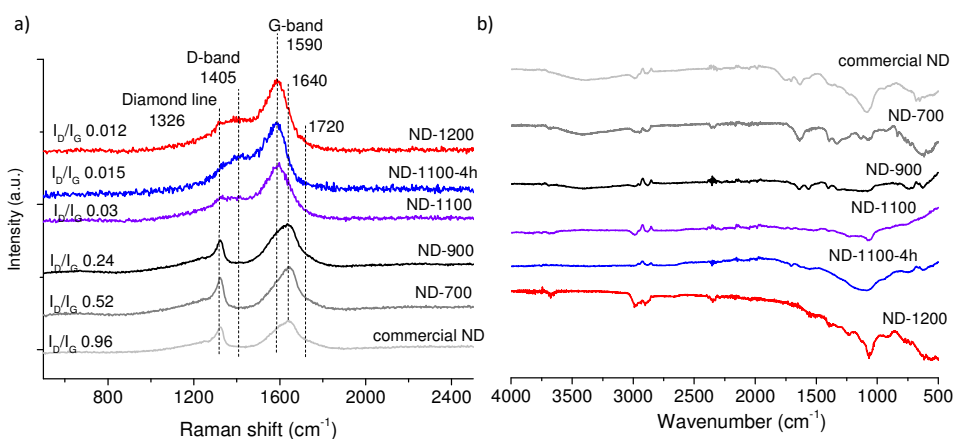


Figure 3. UV-Raman (a) and FT-IR (b) spectra of commercial ND and thermally annealed NDs in argon.

FT-IR spectroscopy has been employed to further study the changes of surface functional groups during the thermal annealing of commercial ND in an Ar atmosphere (Figure 3b). The FT-IR spectrum of commercial NDs shows the presence of several free alcohol groups (3677 and 1094 cm^{-1}) together with a broad band from 1830 till 1704 cm^{-1} that is characteristic of carbonyl groups including anhydrides, esters, lactones, cyclic ketones and carboxylic acids [29, 48]. The bands centred at 1640 and 1384 cm^{-1} can be assigned to a series of alkenes and alkanes functional groups, respectively. The broad band centred at 1080 cm^{-1} is characteristic of C-OH or C-O-C bonds. Annealing of commercial ND at $700\text{ }^{\circ}\text{C}$ causes the removal of the carbonyl groups centred at about 1740 cm^{-1} together with a shift down of the C-O and/or C-O-C band. Annealing at temperatures higher than $900\text{ }^{\circ}\text{C}$ further causes the loss of the band centred at 1640 cm^{-1} that is attributable to alkenes, together with the appearance of a broad band centred at about 1580 cm^{-1} that is characteristic of aromatic C=C bonds. This data confirms that the thermal annealing of commercial ND at increased temperatures or times results in the graphitisation of the samples while some oxygen-functional groups – such as alcohols or ether and phenols – remain even at temperatures as high as $1200\text{ }^{\circ}\text{C}$.

The degree of graphitisation of the thermally annealed commercial NDs was quantified using XPS (Figure 4 and Figures S9-S10). The higher the annealing temperature and the longer the annealing time, the higher the sp^2/sp^3 ratio (Figure 4a) together with a decrease in oxygen content (Figure 4b). The ND-1200 sample exhibits the higher sp^2/sp^3 ratio and reduced oxygen content. Similarly, XPS N1s shows that the nitrogen content of commercial ND ($1.3\text{ at}\%$) decreases as the annealing temperature increases up to $0.9\text{ at}\%$ (Figure S11).

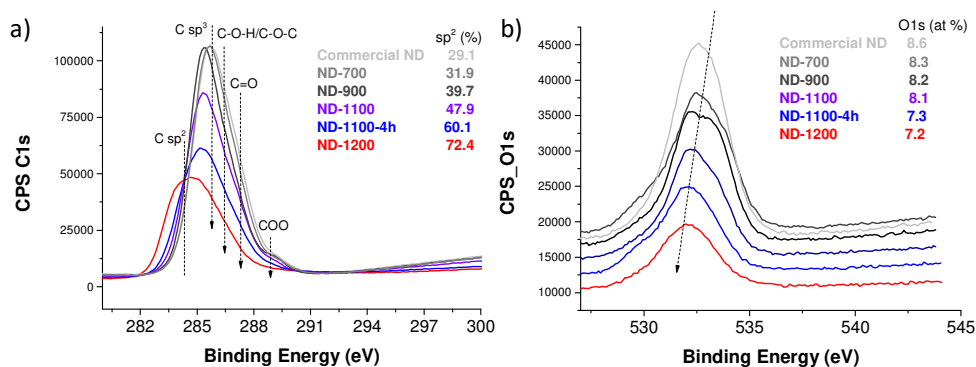


Figure 4. XPS C1s (a) and O1s (b) of commercial ND and thermally annealed NDs in argon.

In agreement with previous reports, isothermal N₂ adsorption measurements (Figure S12) of thermally annealed NDs at temperatures below 1000 °C exhibit similar BET surface areas as the commercial ND sample (286 m²/g) while annealing at higher temperatures shows slightly higher values (311 m²/g) and this is attributed to the thermal expansion of stacked nanodiamonds as the temperature increases [29].

6.3.2 Catalytic activity

The series of graphitized ND were employed as metal-free catalysts for the ozonation of oxalic acid as a model pollutant. Oxalic acid is one of the preferred organic compounds used during catalytic ozonation in water since molecular O₃ can scarcely degrade it under real water treatment conditions [43, 49, 50]. In agreement with previous reports on the absence of catalysts, a negligible oxalic acid degradation was observed when working at pH 3 (Figure 5a). Interestingly, graphitisation of commercial NDs from 600 to 1100 °C for 1 h results in a gradual increase in catalytic activity for oxalic acid degradation at pH 3 (Figure 5a,b). In contrast, graphitisation of ND at 1200 °C for 1 h resulted in a sample with slightly

lower catalytic activity than the ND-1100 sample (Figure 5a,b). Attempts to increase the catalytic activity of the optimised ND-1100 sample by preparing an analogous sample graphitised at 1100 °C for 4 h resulted in a sample with less activity (Figure 5a,b). Thus, the ND-1100 sample exhibits the highest catalytic activity. It should be noted that the catalytic activity of the ND under study does not correlate with the specific BET surface area of the materials and, therefore, other key factors should be responsible for the observed catalytic activity. From XPS it can be concluded that the sp^2/sp^3 ratio increases as the annealing temperature or time increases (Figures 4 and 5c). Interestingly, a volcano-type trend of the catalytic activity with respect to the sp^2 fraction was observed for the carbocatalytic ozonation of oxalic acid at pH 3 (Figure 5d). Figure 5d shows the catalytic activity gradually increasing together with the sp^2 fraction of the ND samples up to the ND-1100 sample. However, further graphitisation of the ND-1100-4 and ND-1200 samples resulted in a decrease in activity. This data reflects the importance of a high proportion of sp^2 carbons, while other factors should be considered to explain the volcano-trend observed.

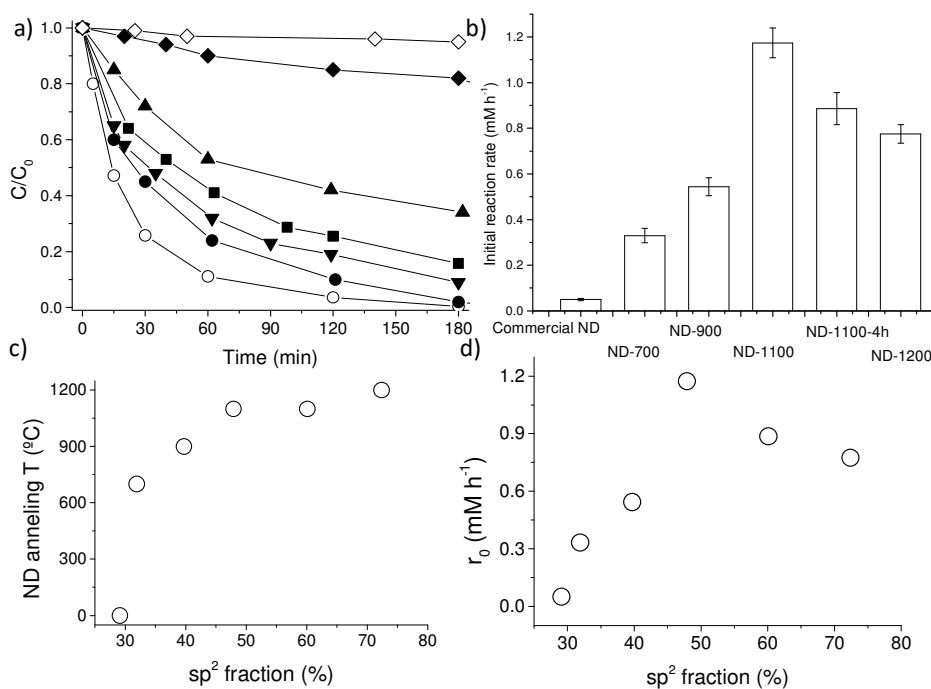


Figure 5. a) Carbocatalytic ozonation of oxalic acid at pH 3 using commercial ND and thermally annealed NDs in argon. Legend: no catalyst (\diamond), commercial ND (\blacklozenge), ND-700 (\blacktriangle), ND-900 (\blacksquare), ND-1200 (\blacktriangledown), ND-1100-4h (\bullet), ND-1100 (\circ). b) Initial reaction rate of oxalic acid degradation during the catalytic ozonation at pH 3 using NDs. c) ND annealing temperature versus sp^2 fraction in NDs. d) Initial reaction rate of the oxalic acid degradation during the catalytic ozonation at pH 3 using NDs with different sp^2 proportions. Reaction conditions: Oxalic acid (50 mg/L), carbocatalyst (100 mg/L), pH 3, temperature 20 $^{\circ}\text{C}$, O_3 to oxalic acid molar ratio 5.3.

In a related precedent we reported that the carbocatalytic activity of a graphite-based material can be increased by introducing hydroxyl functional groups at the edges of the graphene layers [43]. The presence of phenolic groups

on the graphene sheets increases the work function of the graphite-based material and, thus, facilitates one-electron transfer mechanism leading to the simultaneous formation of semiquinone-like units and O_3^- species. Thus, a graphite-like structure with phenolic and semiquinone-like centres is formed. These phenolic/quinone-like subunits in carbon-based materials have been proposed by several authors as redox sites catalysing various reactions including the carbocatalytic dehydrogenation of ethylbenzene [28], aerobic oxidation of cyclohexane [51], Fenton [52] and photo-Fenton [53] reactions, as well as peroxymonosulfate activation [54]. Similarly, Shaobin and co-workers proposed that the presence of sp^3 diamond cores in the sp^2/p^3 diamond nanohybrids enrich the charge density of the graphitic shells, and so favour electron transfer to PMS [30]. It should be, however, commented that as ND samples are obtained from explosive detonation and contain a residual N content, even exposed at the surface (Figure S121), similar role to oxygen can be also played in the present case of NDs by nitrogen in those substructures with aniline/imine functional groups [21].

From XPS measurements (Figure 4 and Figures S9-S10) it can be concluded that the most active samples (namely, ND-1100, ND-1100-4h and ND-1200) exhibit a similar proportion of oxygen-functional groups such as ketonic/quinoid, hydroxyls, and carboxylic derivatives. From XPS it can be also observed that the ND-1100 sample exhibits a somewhat higher oxygen content (8.1 at%) than ND-1100-4h (7.3 at %) or ND-1200 (7.2 at%). Similarly, the ND-1100 sample exhibits slightly higher nitrogen content (1.1 at%) than ND-1100-4h (0.9 at%) or ND-1200 (0.9 at%) (Figure S11). Considering the related commented precedents, the characterisation data of the ND samples under study and the observed catalytic activity, we attribute the higher activity of the ND-1100 sample to a synergistic effect between a unique sp^2/sp^3 configuration and the presence of oxygen and nitrogen functional groups in the graphitic surface that benefits both the charge density and work function of the graphitic layers. The lower carbocatalytic activity of ND-1100-4h or ND-1200 samples is attributed to their higher degree of graphitisation and lower population of oxygen and nitrogen functional groups on the graphene layers that results in a lower work function

than the optimized ND-1100 sample. The samples annealed at temperatures below 1000 °C exhibited poor activity due to their low sp^2 content and despite higher oxygen or nitrogen contents. In fact, the commercial D sample with the lowest sp^2 content and the highest oxygen and nitrogen content shows almost negligible activity.

The influence of the solution pH on the resulting catalytic activity using ND-1100 was observed as catalytic activity increased as the pH values decreased (Figure 6). In a previous study some of us have reported that ozone stability decreases as the pH of the aqueous solution increases, and therefore, the available O_3 in solution decreases along with the pH value [43]. Thus, the lower level of catalytic activity observed when using ND-1100 as the pH increases can be attributed to less ozone interacting with the catalyst for the formation of ROS.

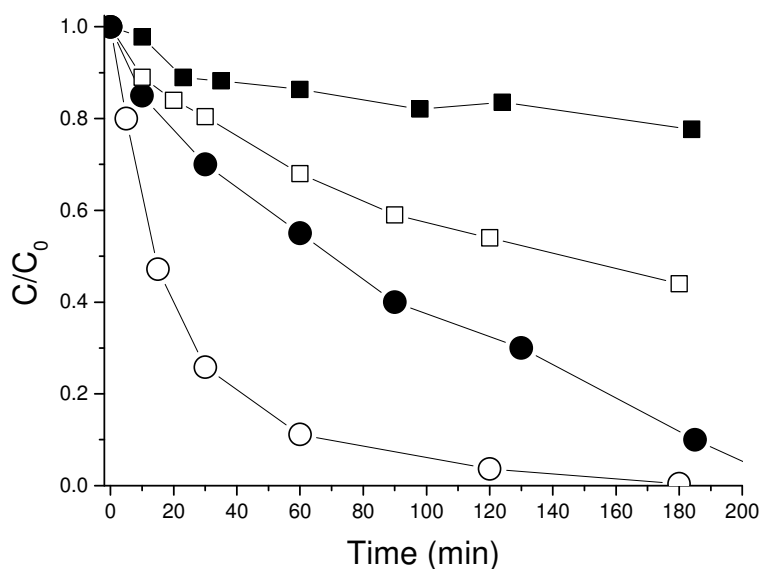


Figure 6. Carbocatalytic ozonation of oxalic acid at different initial pH values using ND-1100. Legend: pH 3 (○), pH 5 (●), pH 7 (□) and pH 9 (■). Reaction conditions: Oxalic acid (50 mg/L), carbocatalyst (100 mg/L), pH 3, temperature 20 °C, O_3 to oxalic acid molar ratio 5.3.

6.3.3. Catalyst heterogeneity and stability

The heterogeneity of the reaction was assessed by performing a filtration test. Figure 7 shows that once the reaction is initiated, if the catalyst is removed and the liquid phase can react under the same conditions, then the oxalic acid degradation stops. Thus, it can be concluded that the carbocatalytic ozonation process using ND-1100 is truly heterogeneous. Furthermore, catalyst stability of the most active ND-1100 sample was assessed by performing several reuses. As can be seen in Figure 7, the catalytic activity decreases on reuse. In a couple of precedents using reduced graphene oxide (rGO) [44] or edge-hydroxylated high surface area graphite [43] as ozonation carbocatalysts, it was reported that catalyst deactivation during the ozonation process is due to the partial oxidation of the catalysts and catalyst reactivation can be obtained by submitting the catalyst to pyrolysis treatment. With these precedents in mind, the used ND-1100 sample was submitted to an annealing treatment at 1100 °C for 1 h. Interestingly, Figure 7 shows that this process enables recovering the catalytic activity of the fresh ND-1100 and the process can be repeated several times.

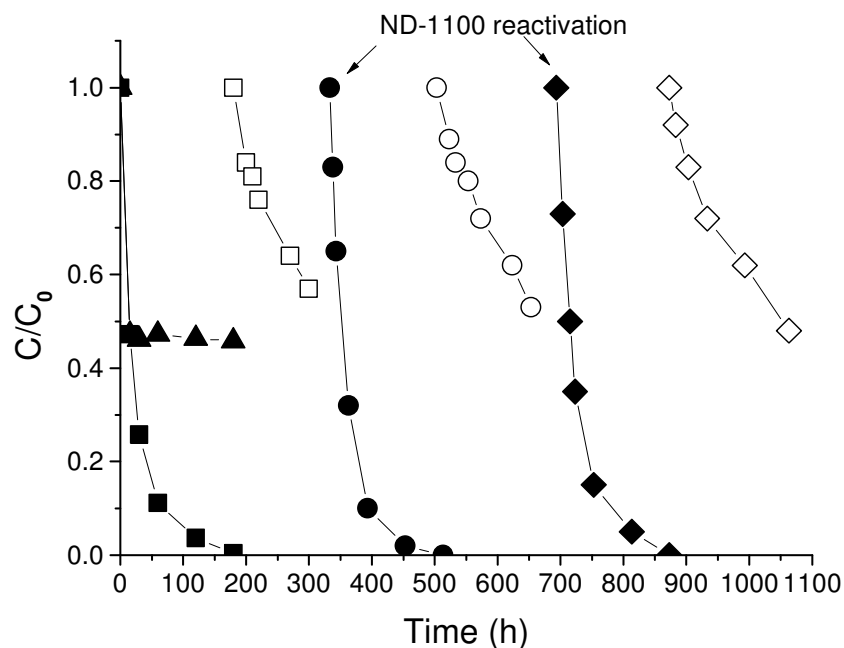


Figure 7. Reusability of the ND-1100 as a metal-free catalyst during the ozonation of oxalic acid at pH 3. Legend: 1st use (■), 2nd use (□), 3rd use after reactivation (●), 4th use (○), 5th use after reactivation (◆), 6th use (◇). Ozonation of oxalic acid after ND-1100 removal at 52 % conversion (▲) during the 1st catalytic cycle (■). Reaction conditions: Oxalic acid (50 mg/L), carbocatalyst (100 mg/L), pH 3, temperature 20 °C, O₃ to oxalic acid molar ratio 5.3.

To obtain insights about the deactivation-activating process, the used ND-1100-1U and reactivated ND-1100-1U-react sample were characterised by PXRD (a series of spectroscopic techniques including UV-Raman, FT-IR, XPS, and EPR together with TEM measurements). PXRD of the used ND-1100-1U sample shows a decrease in the broad band centred about 26 ° – which is a characteristic of the graphitic layers present in the fresh ND-1100 (Figure 8a). Interestingly, the reactivated ND-1100-1U-react sample again shows this graphitic band in the fresh carbocatalyst (Figure 8a). In good agreement with these observations, TEM

measurements reveal that the used ND-1100-1U sample is characterised by fewer graphitic layers and a correspondingly higher number of diamond planes than the fresh ND-1100 sample (Figure 8a, b and Figure S13). Moreover, thermal annealing of the used ND-1100-1U sample again enables the re-graphitisation of this sample (Figure 8c and Figure S14).

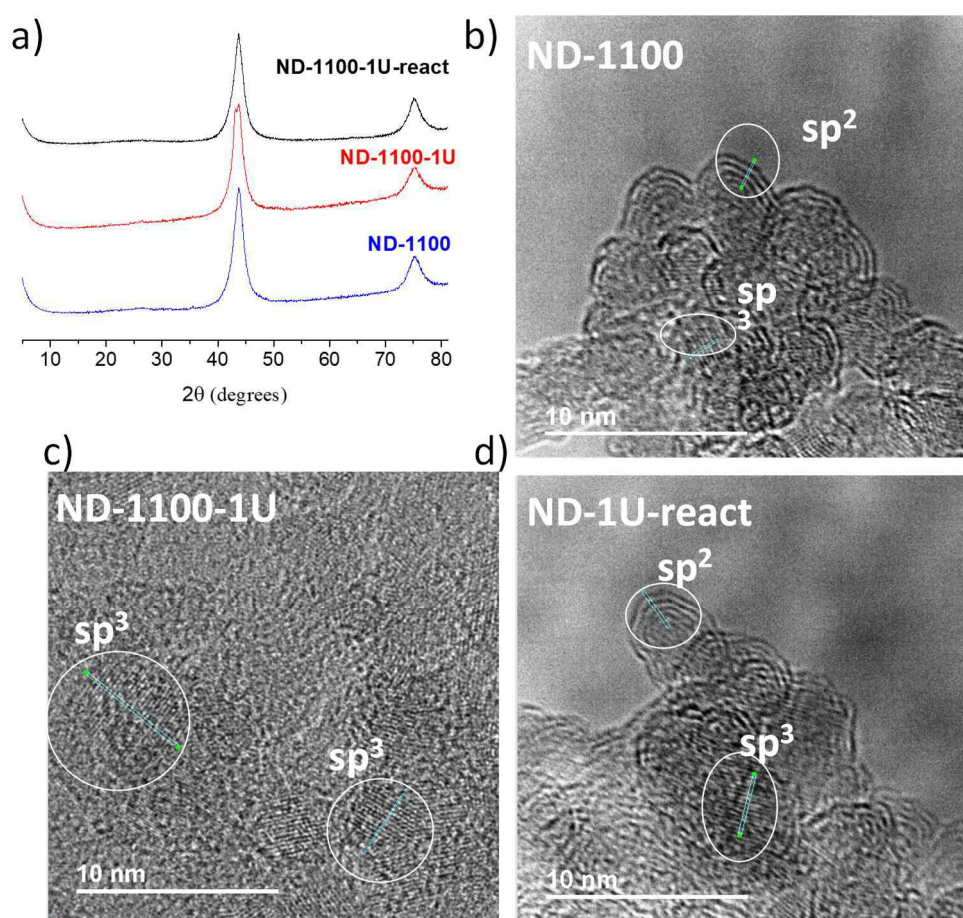


Figure 8. PXR (a) and TEM images of ND-1100 (b), ND-1100-1U (c) and ND-1100-1U-react (d).

UV-Raman, FT-IR, and XPS spectroscopies further confirmed the changes observed by PXRD and TEM measurements. The Raman spectra of the ND-1100-1U sample is characterised by a diamond peak intensity at 1326 cm^{-1} higher than that of fresh ND-1100 – together with a decrease in the graphitic D and G-bands (Figure 9a and Figure S15). Furthermore, the partial oxidation of the ND-1100-1U sample is characterised by an increase of the characteristic bands of hydroxyl and carbonyl groups appearing at 1640 and 1720 cm^{-1} , respectively (Figure 9a and Figure S15). In contrast, the ND-1100-1U-react sample recovers the UV-Raman features of the fresh ND-1100 sample characterised by a graphitised diamond outer part with a small proportion of oxygen-functional groups (Figure 9a and Figure S15). Moreover, the increased I_D/I_G ratio of the ND-1100-1U sample in comparison with the fresh ND-1100, together with the recovery of the I_D/I_G ratio of the ND-1100-1U-react in comparison with the fresh sample, agree with the partial oxidation and reconstitution of the ND samples (Figure 9a). Moreover, the FT-IR spectrum of the ND-1100-1U sample reveals an increase in the hydroxyl, carbonyl, and carboxylic functional groups in comparison with the fresh ND-1100 sample – while the ND-1100-1U-react sample recovers the characteristic FT-IR bands of the fresh ND-1100 sample (Figure 9b). Analogously, comparison of the XPS spectra of the fresh ND-1100 sample with the ND-1100-1U sample shows a shift in the binding energies of both C1s and O1s spectra to higher values attributable to the partial oxidation of the ND-1100 surface (Figure 9c,d and Figure S16). A more intense O1s spectrum for the used ND-1100 sample in comparison with the fresh sample further confirms the oxidation of the ND-1100 surface after use (Figure 9d). Quantitative XPS analyses of the sp^2 carbon fractions as well as oxygen and nitrogen content present in the ND-1100 samples confirm that the used ND-1100 sample becomes oxidised and can be reactivated after pyrolysis at $1100\text{ }^\circ\text{C}$ for 1 h (Figure 9c-e).

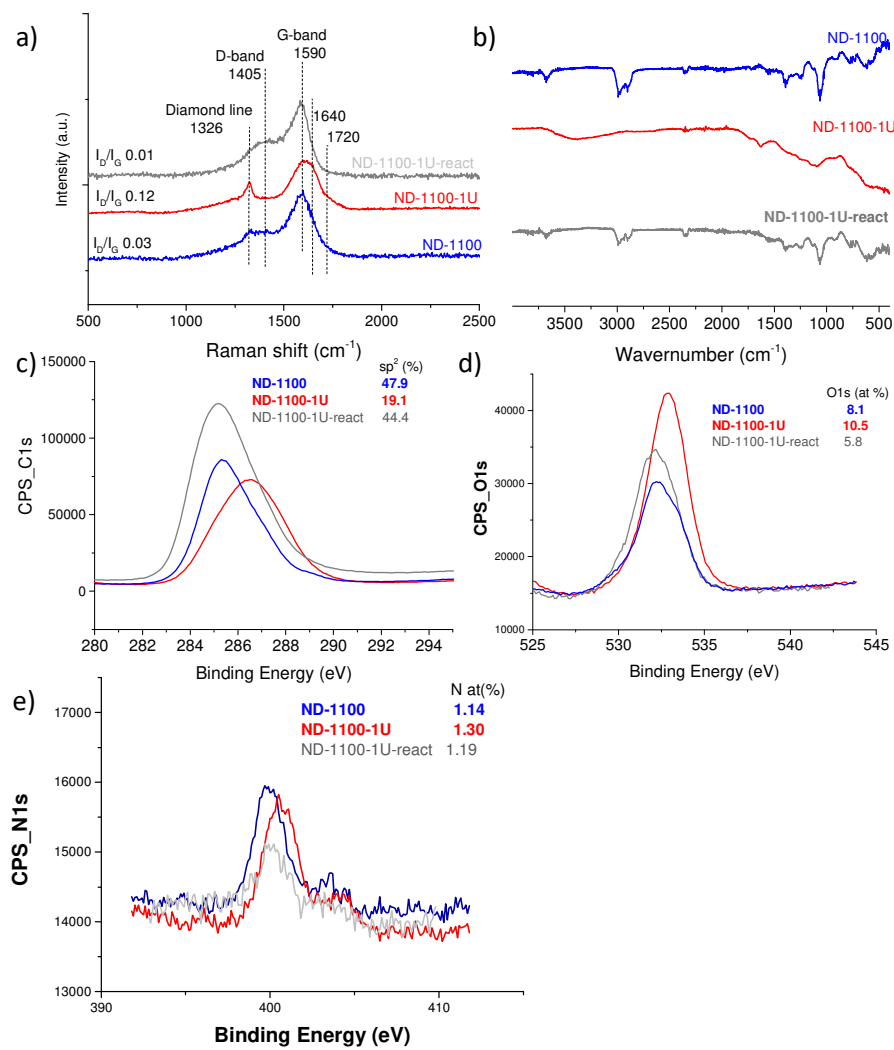


Figure 9. UV-Raman (a), FT-IR (b), XPS C1s (c), XPS O1s (d) and XPS N1s (e) of the fresh (blue line), used (red line), and reactivated (grey line) ND-1100 sample.

EPR spectroscopy has also been employed to investigate the deactivation-activation process of the ND-1100 sample (Figure 10). For the sake of comparison, the commercial ND sample was also measured. Previous studies have shown that the EPR signal of the NDs can be attributed to the presence of carbon dangling bonds with unpaired electrons in the outer part of the ND samples [30, 55]. In our case, the decrease in EPR signal intensity in the ND-1100 samples in comparison with the fresh commercial ND is attributable to the decomposition and reconstruction of the outer part of the NDs leading to the formation of a graphitic shell with a reduced number of dangling bonds. Partial oxidation of the used ND-1100-1U sample after one catalytic cycle exhibits a more intense EPR signal than the fresh ND-1100 sample. Importantly, the reactivated ND-1100-1U-react sample exhibits an EPR spectrum that is remarkably like that of the fresh ND-1100 sample. These observations can be interpreted considering that the surface of the ND-1100 sample is oxidised during the catalytic ozonation with the corresponding formation of dangling bonds – while a subsequent thermal annealing at 1100 °C for 1 h reconstitutes the graphitic shell present in the fresh ND-1100 sample.

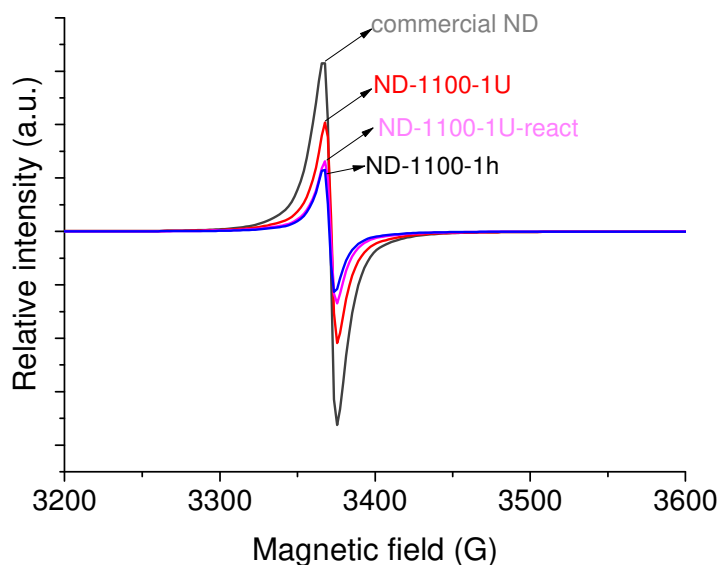


Figure 10. EPR spectra of commercial ND (grey line), ND-1100-1h (blue line), ND-1100 after one catalytic use (ND-1100-1U, red line) and ND-1100 after one catalytic use and reactivated at 1100 °C for 1 h (ND-1100-1U-react, pink line).

6.3.4. ROS during the carbocatalytic ozonation

The nature of the ROS generated during the ozonation process using ND-1100-1h as a metal-free catalyst was addressed using EPR spectroscopy and selective quenching experiments. The use of DMPO and TEMP as spin traps enables the identification of hydroperoxyl and $^1\text{O}_2$ species [43], respectively (Figure 11). The formation of $^1\text{O}_2$ during the catalytic ozonation of oxalic acid in the presence of ND-1100 as a catalyst at pH 3 was further confirmed by observing that the presence of NaN_3 , a selective $^1\text{O}_2$ quenching agent, largely inhibits the oxalic degradation (Figure S17). In contrast, the presence of DMSO or *tert*-butanol during the catalytic ozonation of oxalic acid does not stop the reaction (data not

shown) and this is interpreted as an indirect probe of the absence of hydroxyl radicals during the catalytic process. The generation of hydroperoxyl radicals and $^1\text{O}_2$ and the absence of hydroxyl radicals during the carbocatalytic ozonation using ND-1100 is similar to that found when using analogous carbon-based materials such as edge-hydroxylated graphitic carbon [43] or rGO as ozonation catalysts [44]. Furthermore, TOC measurements of oxalic acid as organic aqueous pollutant before and after the carbocatalytic ozonation using ND-1100 confirm its complete mineralization to CO_2 and H_2O .

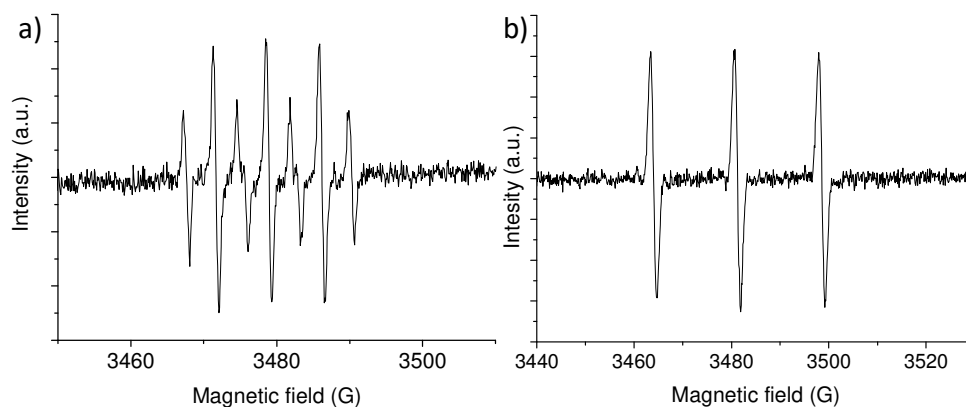


Figure 11. EPR spectra obtained during the ozonation process using ND-1100-1h as a metal-free catalyst in the presence of DMPO (a) or TEMP (b) as trapping agents. Reaction conditions: catalyst (100 mg L^{-1}), O_3 (140 mg/h), trapping agent (1 g L^{-1}), pH 3, room temperature, and 30 min reaction.

6.4. Conclusions

The present study shows that thermally annealing commercial NDs in an inert atmosphere results in the formation of defective hybrid sp^2/p^3 nanodiamonds that perform well as metal-free ozonation catalysts. Characterisation data from

PXRD, spectroscopic techniques (UV-Raman, FT-IR, XPS and EPR) and TEM measurements reveal that the thermal annealing of commercial NDs produces a diamond core and graphitic shell together with oxygen and nitrogen functional groups. The higher the annealing temperature of commercial NDs, the greater the graphitic shell, and the lower the density of structural defects. Importantly, a volcano-type trend relationship between the catalytic activity for oxalic acid degradation and the sp^2/sp^3 ratio of NDs was found. A synergistic effect between the sp^2/sp^3 configuration and the presence of oxygen and nitrogen functional groups for the most active ND-1100 sample was found. It is proposed that the sp^3 core of the ND increases the charge transfer to the graphitic shell while the presence of oxygen functional groups such as hydroxyl, increases the work function of the material and this produces a superior metal-free ozonation catalyst. The activity of the partially spent catalyst can be recovered by a simple thermal annealing process in an inert atmosphere at 1100 °C. EPR spectroscopy and selective quenching experiments have revealed that hydroperoxyl radicals and 1O_2 are the main ROS generated during the catalytic process.

This study has shown the possibility of tailoring the physico-chemical properties of commercial NDs to develop highly active metal-free ozonation catalysts. We are confident that this work will further contribute to expanding the field of metal-free heterogeneous catalysis.

6.5. References

- [1] X. Duan, H. Sun, S. Wang, Metal-free carbocatalysis in advanced oxidation reactions, *Acc. Chem. Res.*, 51 (2018) 678-687.
- [2] X.-K. Kong, C.-L. Chen, Q.-W. Chen, Doped graphene for metal-free catalysis, *Chem. Soc. Rev.*, 43 (2014) 2841-2857.
- [3] X. Liu, L. Dai, Carbon-based metal-free catalysts, *Nat. Rev. Mater.*, 1 (2016) 16064.
- [4] D.W. Stephan, Catalysis, FLPs, and Beyond, *Chem. Mater.*, 6 (2020) 1520-1526.
- [5] D.S. Su, S. Perathoner, G. Centi, Nanocarbons for the development of advanced catalysts, *Chem. Rev.*, 113 (2013) 5782–5816.
- [6] Y. Wang, X. Wang, M. Antonietti, Polymeric graphitic carbon nitride as a heterogeneous organocatalyst: From photochemistry to multipurpose catalysis to sustainable chemistry, *Angew. Chem. Int. Ed.*, 51 (2012) 68-89.
- [7] B. Daelemans, N. Bilbao, W. Dehaen, S. De Feyter, Carbocatalysis with pristine graphite: on-surface nanochemistry assists solution-based catalysis, *Chem. Soc. Rev.*, 50 (2021) 2280-2296.
- [8] L. Liu, Y.-P. Zhu, M. Su, Z.-Y. Yuan, Metal-free carbonaceous materials as promising heterogeneous catalysts, *ChemCatChem*, (2015) 2765-2787.
- [9] D.S. Su, G. Wen, S. Wu, F. Peng, R. Schlögl, Carbocatalysis in liquid-phase reactions, *Angew. Chem. Int. Ed.*, 56 (2017) 936-964.
- [10] D.R. Dreyer, C.W. Bielawski, Carbocatalysis: Heterogeneous carbons finding utility in synthetic chemistry, *Chem. Sci.*, 2 (2011) 1233-1240.
- [11] S. Navalón, W.-J. Ong, X. Duan, Sustainable catalytic processes driven by graphene-based materials, *Processes*, 8 (2020) 672.
- [12] M.-M. Titirici, R.J. White, N. Brun, V.L. Vitaliy L. Budarin, D.S. Dang Sheng Su, F. del Monte, J.H. Clark, M.J. MacLachlan, Sustainable carbon materials *Chem. Soc. Rev.*, 44 (2015) 250-290.

[13] J.C. Espinosa, S. Navalon, M. Alvaro, A. Dhakshinamoorthy, H. Garcia, Reduction of C=C double bonds by hydrazine using active carbons as metal-free catalysts *ACS Sustain. Chem. Eng.*, 6 (2018) 5607-5614.

[14] A. Schraut, G. Zmiga, H.-G. Sockel, Composition and structure of active coke in the oxydehydrogenation of ethylbenzene, *Appl. Catal.*, 29 (1987) 311-326.

[15] E.H.L. Falcao, F. Wudl, Carbon allotropes: Beyond graphite and diamond, *J. Chem. Technol. Biotech.*, 82 (2007) 524-531.

[16] S. Navalon, A. Dhakshinamoorthy, M. Alvaro, M. Antonietti, H. García, Active sites on graphene-based materials as metal-free catalysts, *Chem. Soc. Rev.*, 46 (2017) 4501-4529.

[17] S. Navalon, A. Dhakshinamoorthy, M. Alvaro, H. Garcia, Carbocatalysis by graphene-based materials, *Chem. Rev.*, 12 (2014) 6179-6212.

[18] S. Navalón, J.R. Herance, M. Álvaro, H. García, General aspects in the use of graphenes in catalysis, *Mater. Horizons*, 5 (2018) 363-378.

[19] D.R. Dreyer, A.D. Todd, C.W. Bielawski, Harnessing the chemistry of graphene oxide, *Chem. Soc. Rev.*, 43 (2014) 5288-5301.

[20] H. Hu, J.H. Xin, H. Hu, X. Wang, Y. Kong, Metal-free graphene-based catalyst-insight into the catalytic activity: A short review, *Appl. Catal. A-Gen*, 492 (2015) 1-9.

[21] S. Navalón, A. Dhakshinamoorthy, M. Alvaro, H. García, Diamond nanoparticles in heterogeneous catalysis, *Chem. Mater.*, 32 (2020) 4116-4143.

[22] X. Duan, W. Tian, H. Zhang, H. Sun, Z. Aoc, Z. Shao, S. Wang, sp²/sp³ framework from diamond nanocrystals: A key bridge of carbonaceous structure to carbocatalysis, *ACS Catal.*, 8 (2019) 7494-7519.

[23] A. Krueger, Beyond the shine: recent progress in applications of nanodiamond, *J. Mater. Chem.*, 21 (2011) 12571-12578.

[24] A. Krueger, D. Lang, Functionality is key: recent progress in the surface modification of nanodiamond, *Adv. Func. Mater.*, 22 (2012) 890-906.

[25] G. Filippini, M. Prato, C. Rosso, Carbon dots as nano-organocatalysts for synthetic applications, *ACS Catal.*, 10 (2020) 8090-8105.

[26] Y. Lin, X. Sun, D.S. Su, G. Centi, S. Perathoner, Catalysis by hybrid sp²/sp³ nanodiamonds and their role in the design of advanced nanocarbon materials, *Chem. Soc. Rev.*, 47 (2018) 8438-8473.

[27] M. Zeiger, N. Jäckel, V.N. Mochalin, V. Presser, Review: carbon onions for electrochemical energy storage, *J. Mater. Chem. A*, 4 (2016) 3172-3196.

[28] J. Zhang, D.S. Sheng Su, R. Blume, R. Schlögl, R. Wang, X. Yang, A. Gajovic, Surface chemistry and catalytic reactivity of a nanodiamond in the steam-free dehydrogenation of ethylbenzene, *Angew. Chem. Int. Ed.*, 49 (2010) 8640 -8644.

[29] R. Wang, X. Sun, B. Zhang, X. Sun, D. Su, Hybrid nanocarbon as a catalyst for direct dehydrogenation of propane: formation of an active and selective core-shell sp²/sp³ nanocomposite structure, *Chem. Eur. J.*, 20 (2014) 6324 - 6331.

[30] X. Duan, Z. Ao, H. Zhang, M. Saunders, H. Sun, Z. Shao, S. Wang, Nanodiamonds in sp²/sp³ configuration for radical to nonradical oxidation: Core-shell layer dependence, *Appl. Catal. B. Environ.*, 222 (2018) 176-181.

[31] X.G. Duan, C. Su, L. Zhou, H.Q. Sun, A. Suvorova, T. Odedairo, Z.H. Zhu, Z.P. Shao, S.B. Wang, Surface controlled generation of reactive radicals from persulfate by carbocatalysis on nanodiamonds, *Appl. Catal. B. Environ.*, (2016) 7–15.

[32] X.G. Duan, Z.M. Ao, L. Zhou, H.Q. Sun, G.X. Wang, S.B. Wang, Occurrence of radical and nonradical pathways from carbocatalysts for aqueous and nonaqueous catalytic oxidation, *Appl. Catal. B. Environ.*, 188 (2016) 98–105.

[33] B. Kasprzyk-Hordern, M. Ziółek, J. Nawrocki, Catalytic ozonation and methods of enhancing molecular ozone reactions in water treatment, *Appl. Catal. B Environ.*, (2003) 639-669.

[34] P.M. Álvarez, F.J. Beltrán, F.J. Masa, J.P. Pocostales, A comparison between catalytic ozonation and activated carbon adsorption/ozone-regeneration processes for wastewater treatment., *Appl. Catal., B*, 92 (2009) 393–400.

[35] P.M. Alvarez, J.F. García-Araya, F.J. Beltrán, I. Giráldez, J. Jaramillo, V. Gomez-Serrano, The influence of various factors on aqueous ozone decomposition by granular activated carbons and the development of a mechanistic approach. , *Carbon* 44 (2006) 3102–3112.

[36] P.C.C. Faria, J.J.M. Orfao, M.F.R. Pereira, Catalytic ozonation of sulfonated aromatic compounds in the presence of activated carbon. , *Appl. Catal., B* 83 (2008) 150–159.

[37] P.C.C. Faria, J.J.M. Órfão, M.F.R. Pereira, Ozone decomposition in water catalysed by activated carbon: influence of chemical and textural properties, *Ind. Eng. Chem. Res.*, 45 (2006) 2715–2721.

[38] A.G. Gonçalves, J.J.M. Órfão, M.F.R. Pereira, Catalytic ozonation of sulphamethoxazole in the presence of carbon materials, *J. Hazard. Mater.*, 239–240 (2012) 167–174.

[39] M. Sánchez-Polo, U. von Gunten, J. Rivera-Utrilla, Efficiency of activated carbon to transform ozone into OH radicals: Influence of operational parameters., *Water Res.* , 39 (2005) 3189–3198.

[40] O.S.G.P. Soares, P.C.C. Faria, J.J.M. Órfão, M.F.R. Pereira, Ozonation of textile effluents and dye solutions in the presence of activated carbon under continuous operation., *Sep. Sci. Technol.* 2007, 42 (2007) 1477–1492.

[41] Y.-C. Lin, C.-L. Chang, T.-S. Lin, H. Bai, M.-G. Yan, F.-. Ko, C.-T. H.; Wu, C.-H. Huang, Application of physical vapor deposition process to modify activated carbon fibers for ozone reduction, *Korean J. Chem. Eng.* , 25 (2008) 446–450.

[42] A.G. Gonçalves, J.L. Figueiredo, J.J.M. Orfao, M.F.R. Pereira, Influence of the surface chemistry of multi-walled carbon nanotubes on their activity as ozonation catalysts, *Carbon* 48 (2010) 4369–4381.

[43] F. Bernat-Quesada, J.C. Espinosa, V. Barbera, M. Álvaro, M. Galimberti, S. Navalon, H. García, Catalytic Ozonation Using Edge-Hydroxylated Graphite-Based Materials, *ACS Sustainable Chem. Eng.*, 7 (2019) 17443–17452.

[44] Y. Wang, Y. Xie, H. Sun, J. Xiao, H. Cao, S. Wang, Efficient catalytic ozonation over reduced graphene oxide for p-hydroxybenzoic acid (PHBA) destruction: Active site and mechanism., *ACS Appl. Mater. Interfaces*, 8 (2016) 9710–9720.

[45] Y. Wang, X. Duan, Y. Xie, H. Sun, S. Wang, Nanocarbon-based catalytic ozonation for aqueous oxidation: Engineering defects for active sites and tunable reaction pathways, *ACS Catal.*, 10 (2020) 13383–13414.

[46] J. Ackermann, A. Krueger, Efficient surface functionalization of detonation nanodiamond using ozone under ambient conditions, *Nanoscale*, 11 (2019) 8012–8019.

[47] V. Mochalin, S. Osswald, Y. Gogotsi, Contribution of functional groups to the Raman spectrum of nanodiamond powders, *Chem. Mater.*, 21 (2009) 273–279.

[48] T. Ando, K. Yamamoto, M. Ishii, M. Kamo, Y. Sato, Vapour-phase oxidation of diamond surfaces in O₂ studied by diffuse reflectance Fourier-transform infrared and temperature-programmed desorption spectroscopy, *J. Chem. Soc. Trans. Faraday*, 89 (1993) 3635–3640.

[49] F.J. Beltran, F.J. Rivas, R. Montero-de-Espinosa, Ozone-enhanced oxidation of oxalic acid in water with cobalt catalysts. 1. Homogeneous catalytic ozonation., *Ind. Eng. Chem. Res.*, 42 (2003) 3210–3217.

[50] D.S. Pines, D.A. Reckhow, Effect of dissolved cobalt(II) on the ozonation of oxalic acid., *Environ. Sci. Technol.*, 36 (2002) 4046–4051.

[51] Y. Cao, X. Luo, H. Yu, F. Peng, H. Wang, G. Ning, sp²- and sp³-hybridized carbon materials as catalysts for aerobic oxidation of cyclohexane, *Catal. Sci. Technol.*, 3 (2013) 2654–2660.

[52] J.C. Espinosa, S. Navalón, A. Primo, M. Moral, J. Fernández Sanz, M. Álvaro, H. García, Graphenes as efficient metal-free Fenton catalysts, *Chem. Eur. J.*, 21 (2015) 11966–11971.

[53] J.C. Espinosa, S. Navalón, M. Álvaro, H. García, Reduced graphene oxide as a metal-free catalyst for the light-assisted Fenton-like reaction, *ChemCatChem*, 8 (2016) 2642–2648.

Chapter 6. Nanodiamonds as metal-free ozonation catalyst

[54] X. Duan, H. Sun, Z. Ao, L. Zhou, G. Wang, S. Wang, Unveiling the active sites of graphene-catalyzed peroxymonosulfate activation, *Carbon*, 107 (2016) 371-378.

[55] A.A. Soltamova, I.V. Ilyin, P.G. Baranov, A.Y. Vul', S.V. Kidalov, F.M. Shakhov, G.V. Mamin, S.B. Orlinskii, N.I. Silkin, M.K. Salakhov, Detection and identification of nitrogen defects in nanodiamond as studied by EPR, *Physica. B*, 404 (2009) 4518-4521.

6.6. Supplementary Material

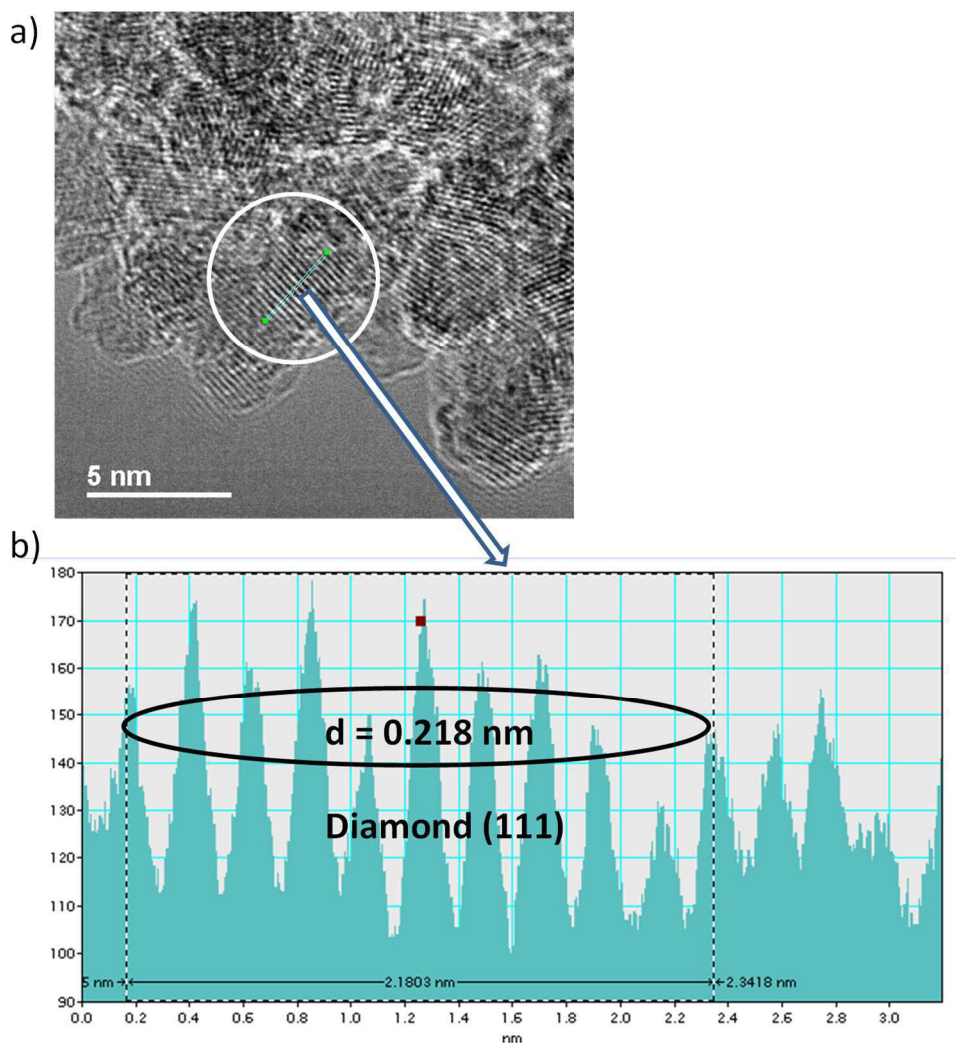


Figure S1. Representative TEM image of commercial ND (a) and interplane distance measurement of selected region from panel a) (b).

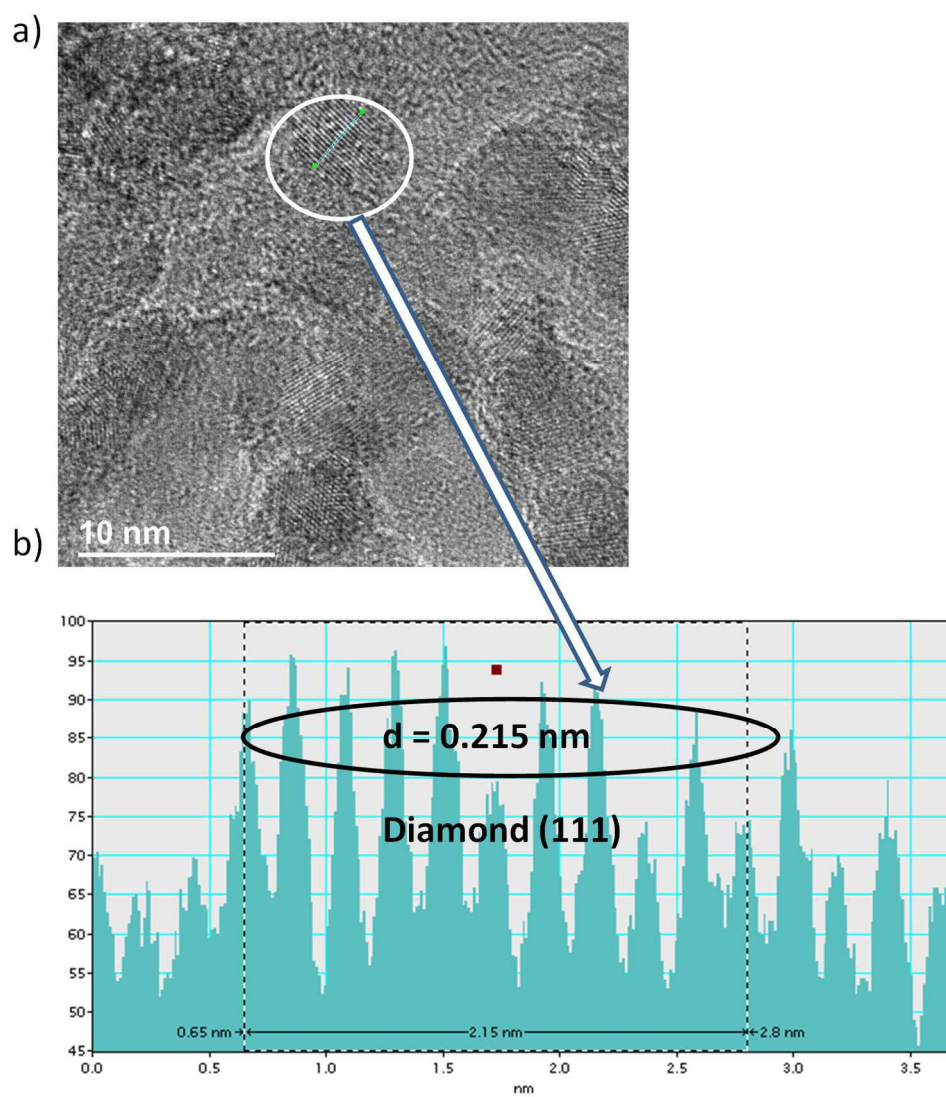


Figure S2. Representative TEM image of commercial ND-700 (a) and interplane distance measurement of selected region from panel a) (b).

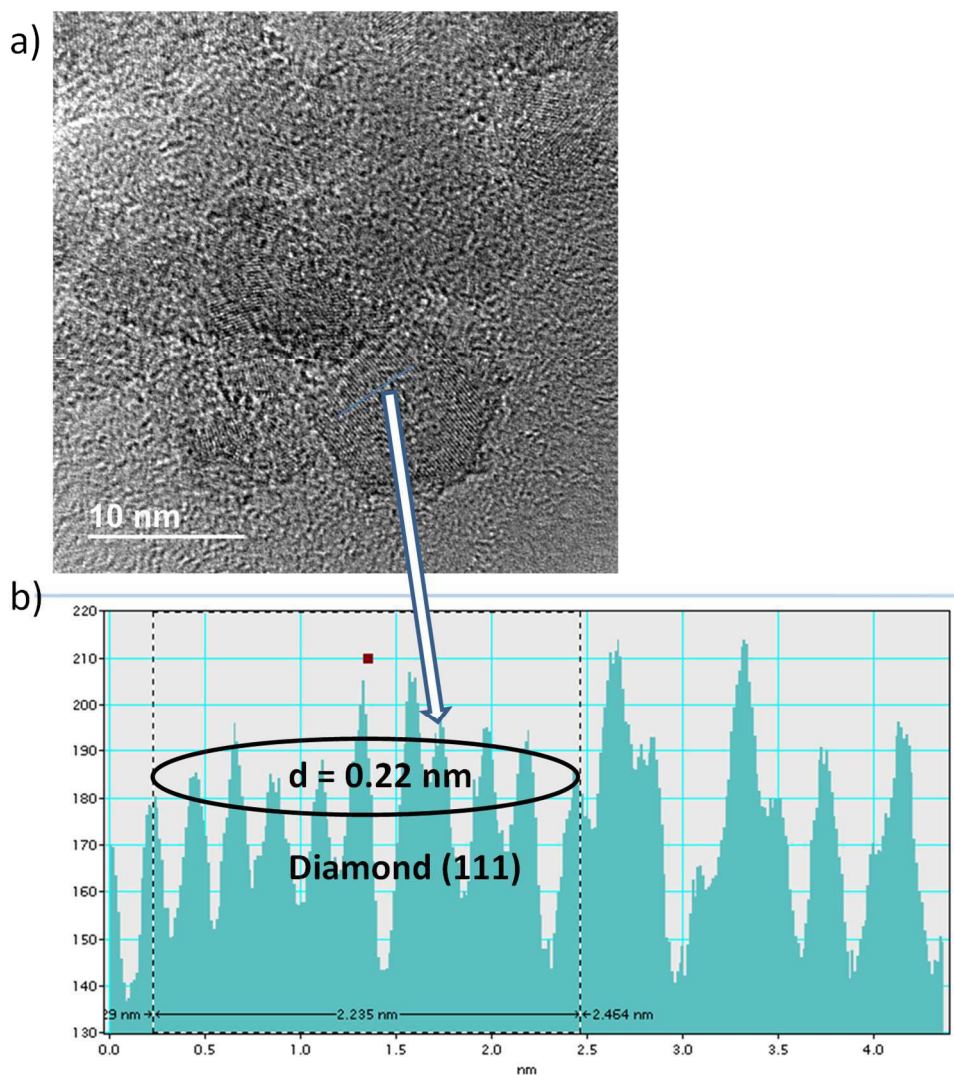


Figure S3. Representative TEM image of commercial ND-900 (a) and interplane distance measurement of selected region from panel a) (b).

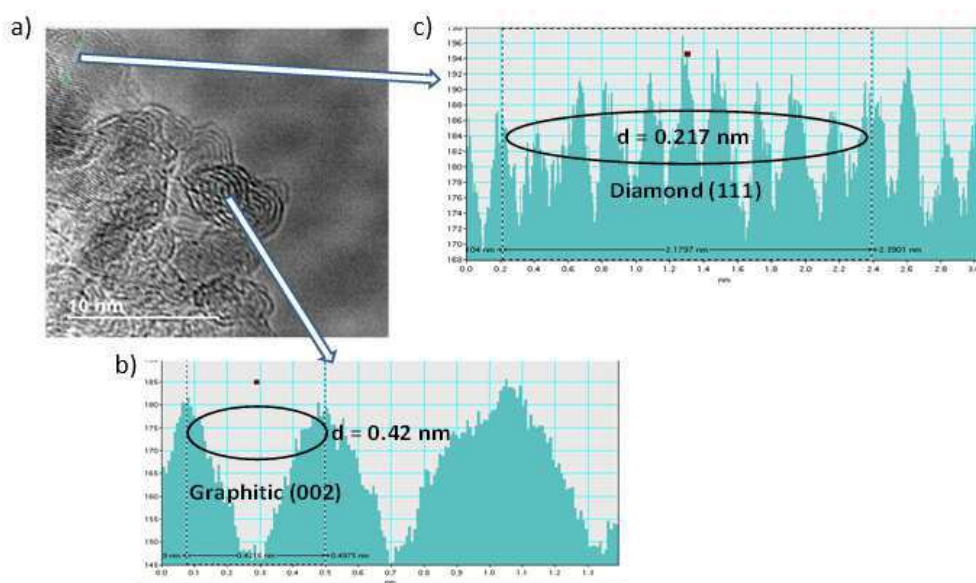


Figure S4. Representative TEM image of commercial ND-1100 (a) and interplane distance measurement of selected region from panel a) (b, c).

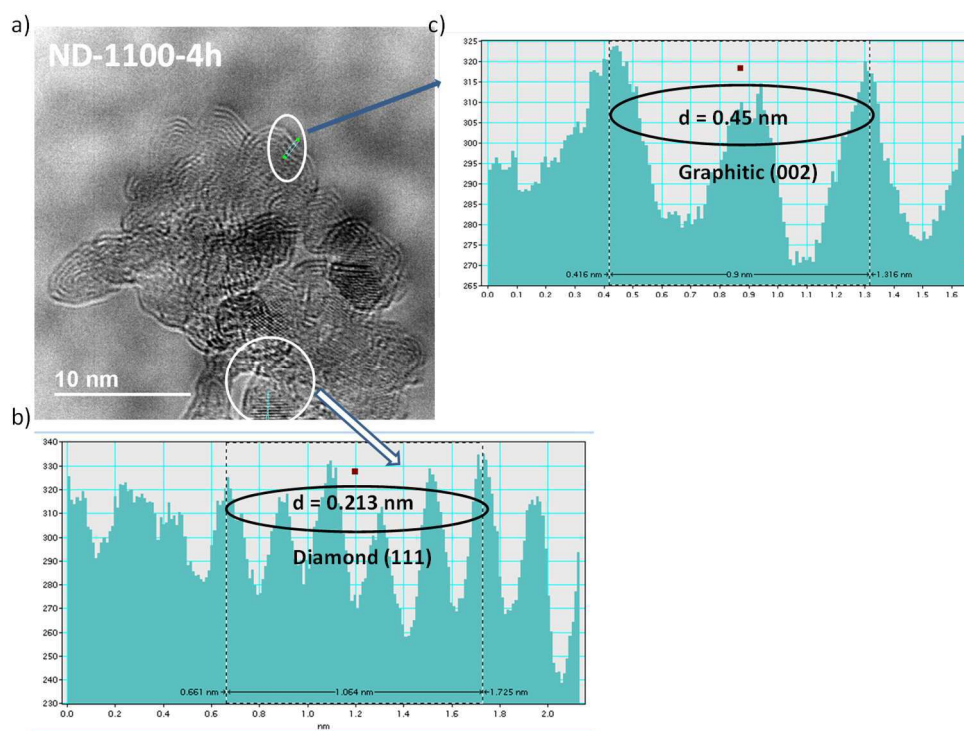


Figure S5. Representative TEM image of commercial ND-1100-4h (a) and inter-plane distance measurement of selected region from panel a) (b, c).

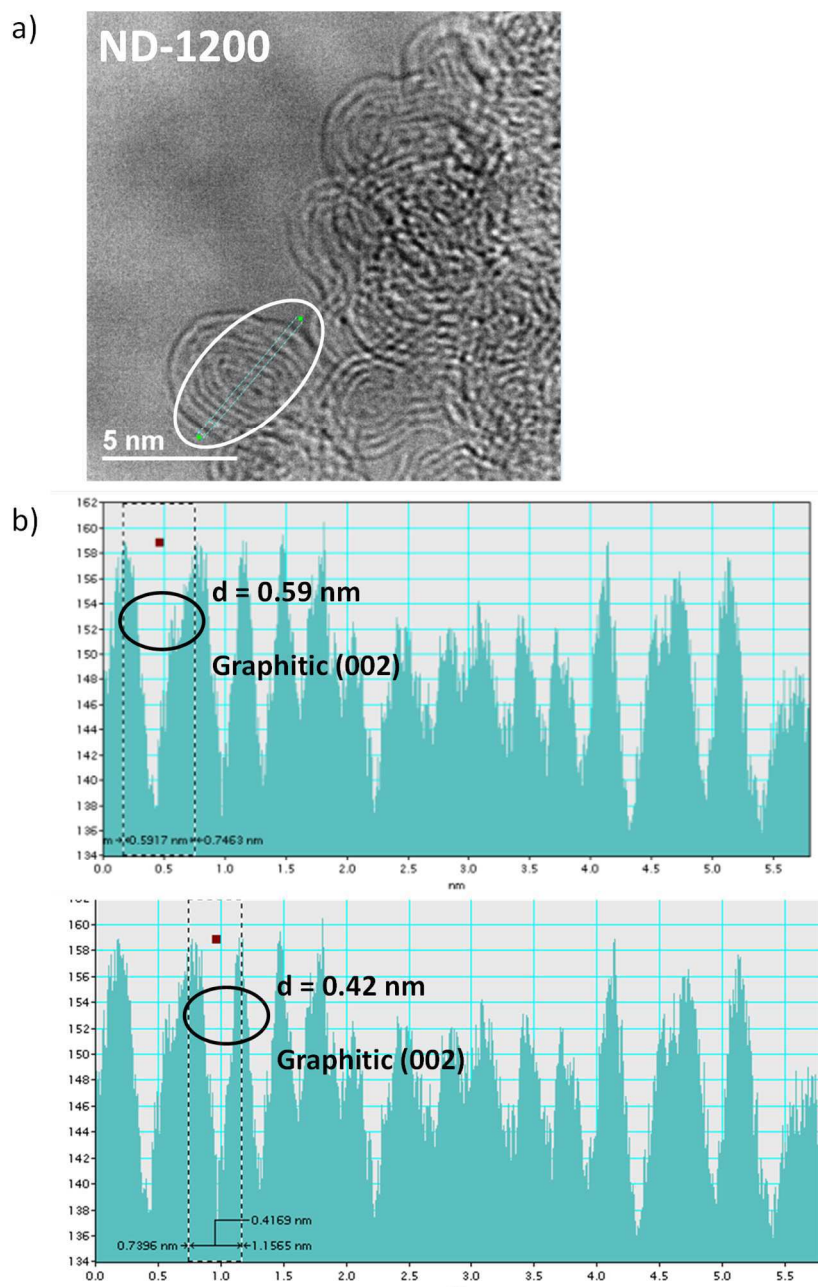


Figure S6. Representative TEM image of commercial ND-1200 (a) and interplane distance measurements of selected region from panel a) (b).

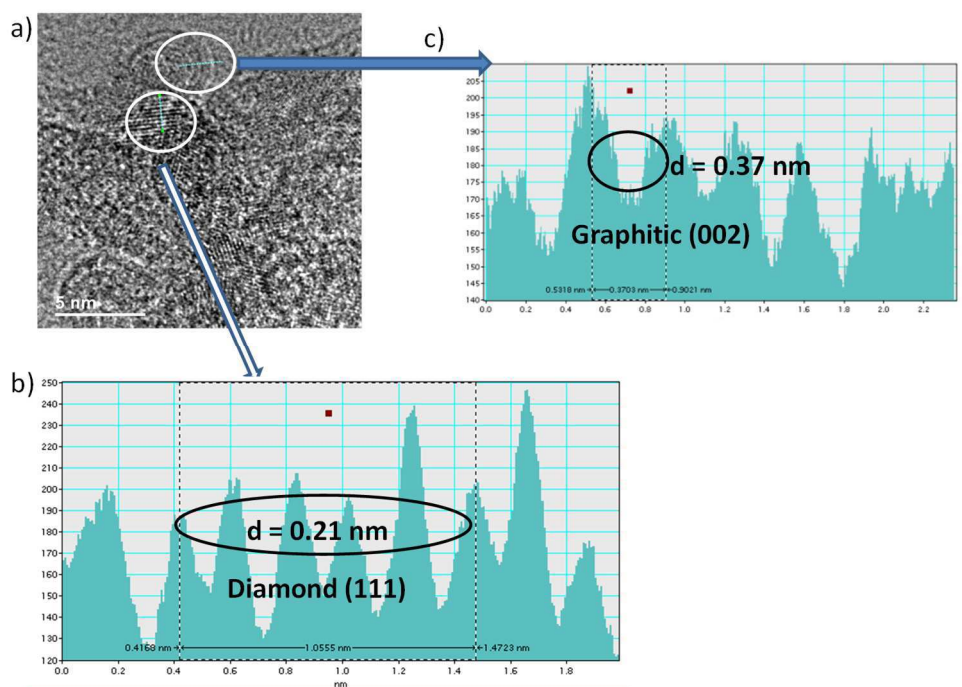


Figure S7. Representative TEM image of commercial ND-1200 (a) and interplane distance measurements of selected region from panel a) (b, c)

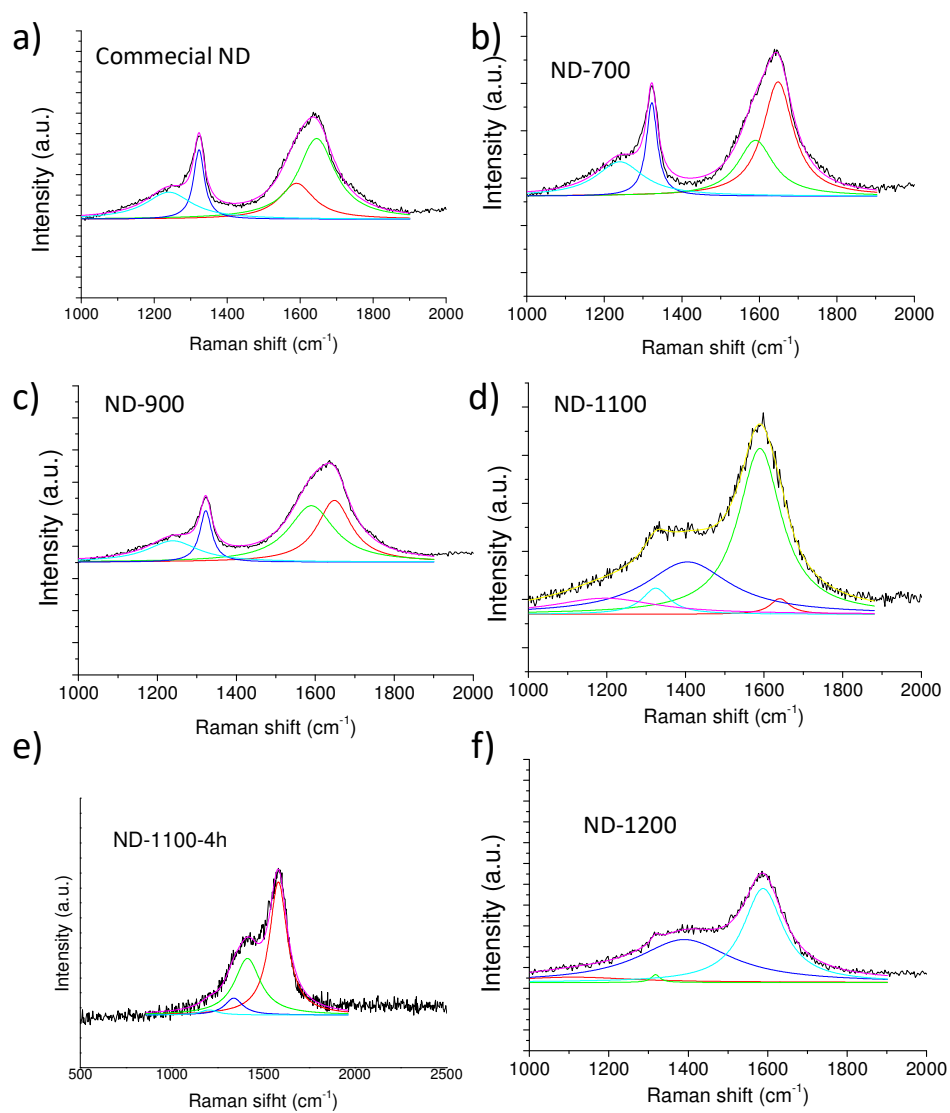


Figure S8. UV-Raman spectra of ND samples. Legend: a) Commercial ND; b) ND-700; c) ND-900; d) ND-1100; e) ND-1100-4h; f) ND-1200.

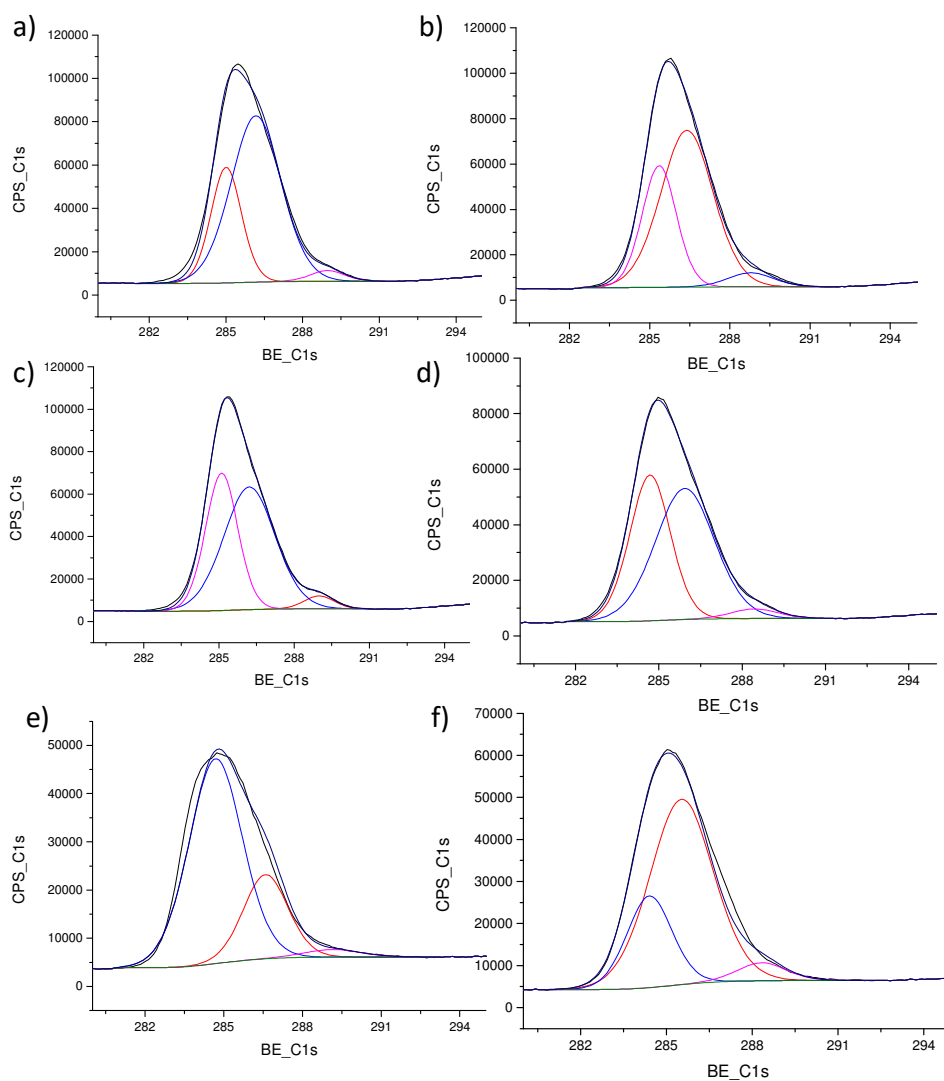


Figure S9. XPS C1s spectra of ND samples. Legend: a) Commercial ND; b) ND-700; c) ND-900; d) ND-1100; e) ND-1100-4h; f) ND-1200.

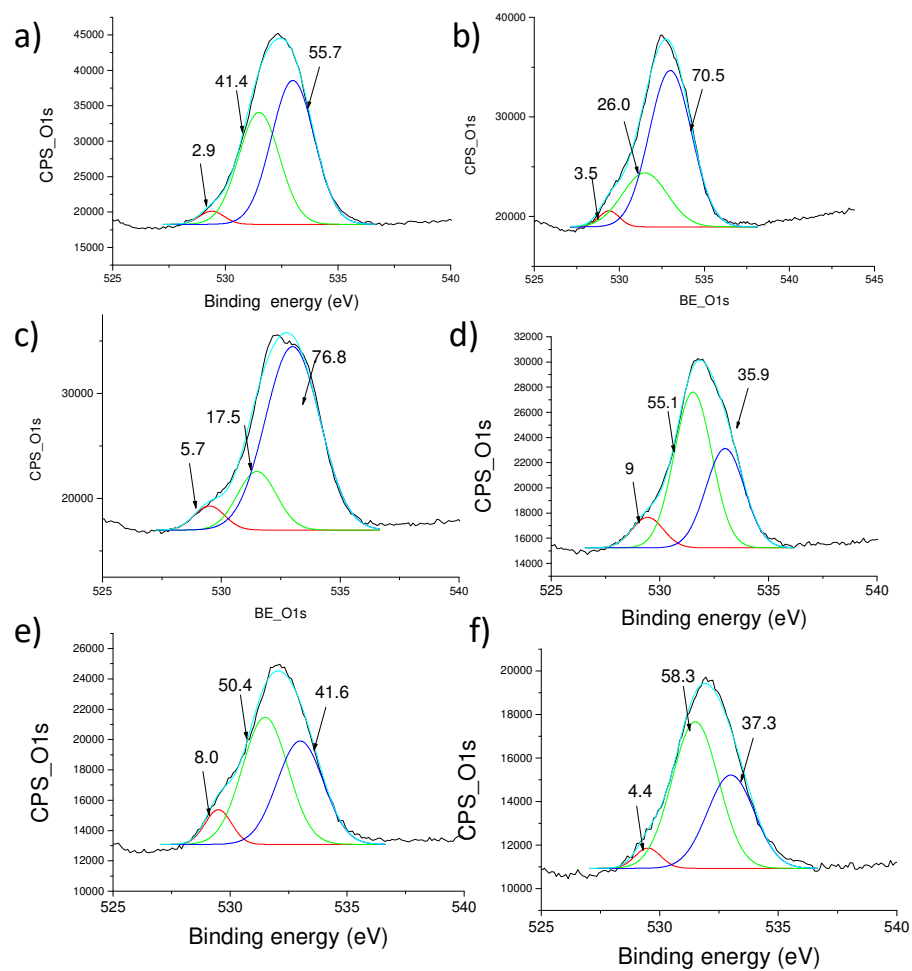


Figure S10. XPS O1s spectra of ND samples. Legend: a) Commercial ND; b) ND-700; c) ND-900; d) ND-1100; e) ND-1100-4h; f) ND-1200.

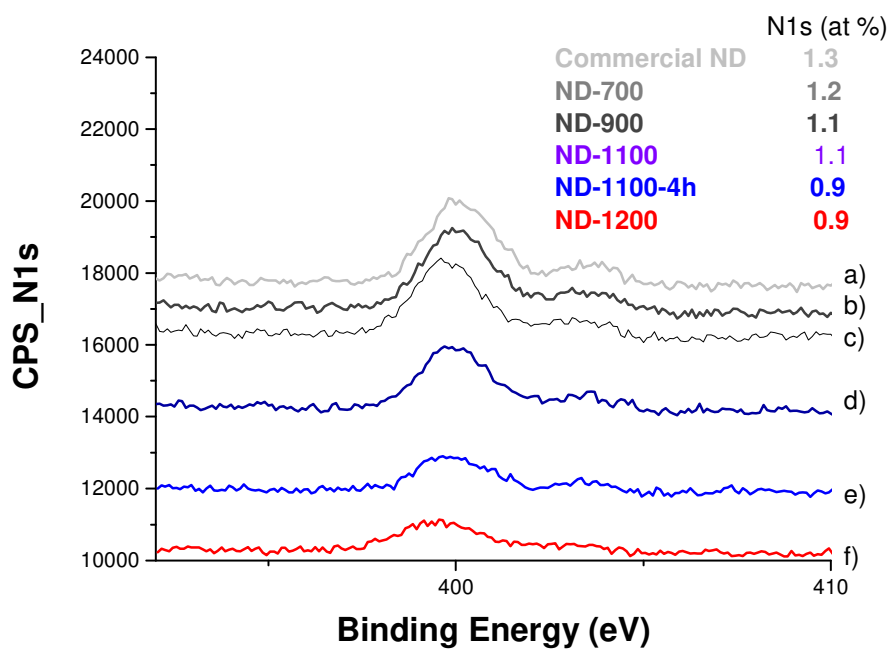


Figure S11. XPS N1s spectra of ND samples. Legend: a) Commercial ND; b) ND-700; c) ND-900; d) ND-1100; e) ND-1100-4h; f) ND-1200.

Chapter 6. Nanodiamonds as metal-free ozonation catalyst

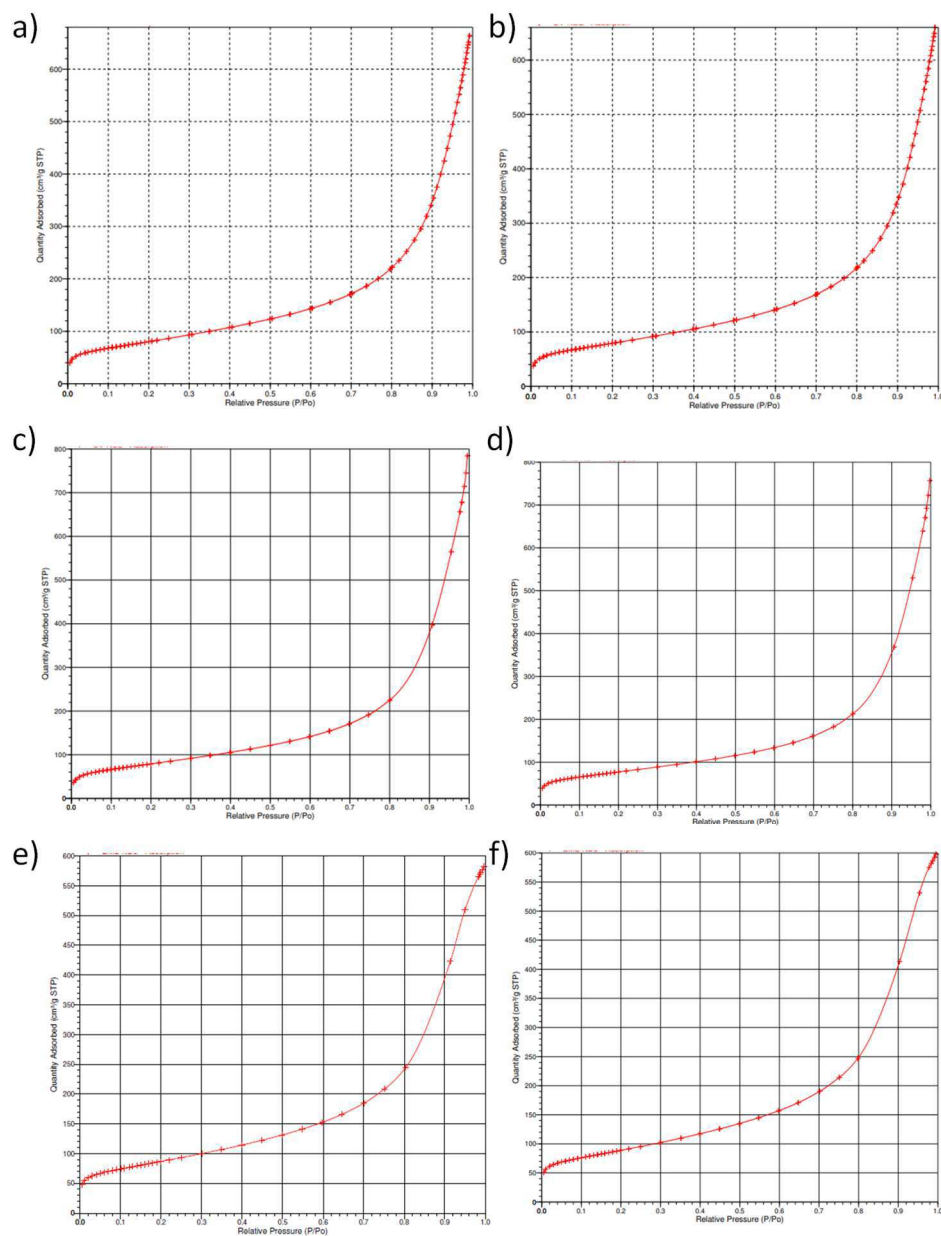


Figure S12. Isothermal N₂ adsorption curves of commercial ND (a; 282 m²/g), ND-700 (b, 279 m²/g), ND-900 (c, 279 m²/g), ND-1100 (d, 287 m²/g), ND-1100-4h (e, 311 m²/g) and ND-1200 (f, 317 m²/g).

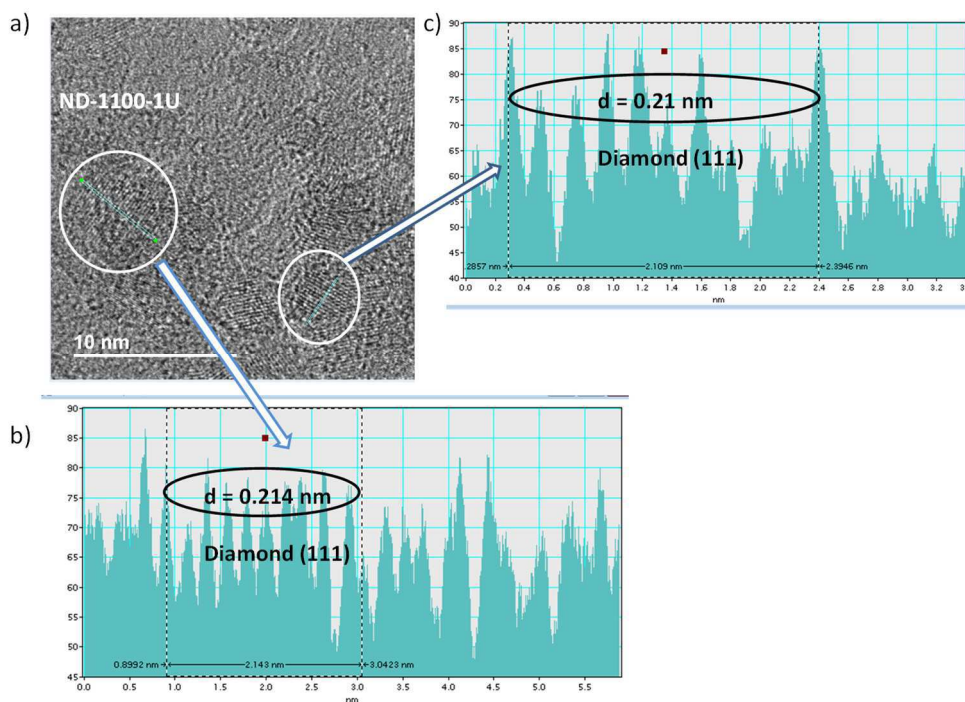


Figure S13. Representative TEM image of commercial ND-1100-1U (a) and inter-plane distance measurement of selected region from panel a) (b, c).

Chapter 6. Nanodiamonds as metal-free ozonation catalyst

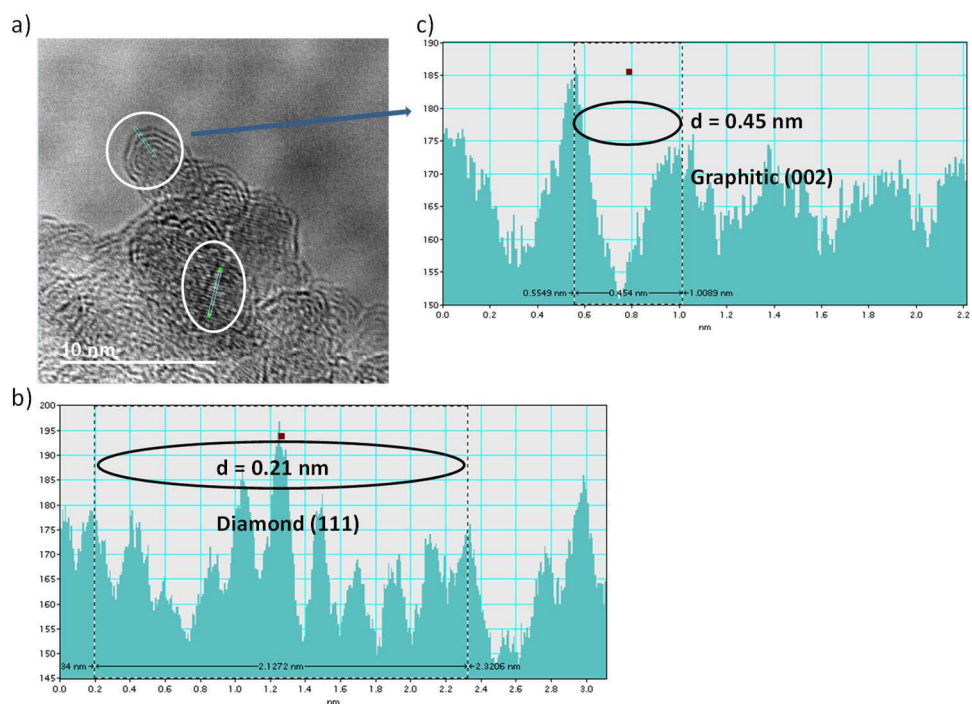


Figure S14. Representative TEM image of commercial ND-1100-1U-react (a) and interplane distance measurement of selected region from panel a) (b, c).

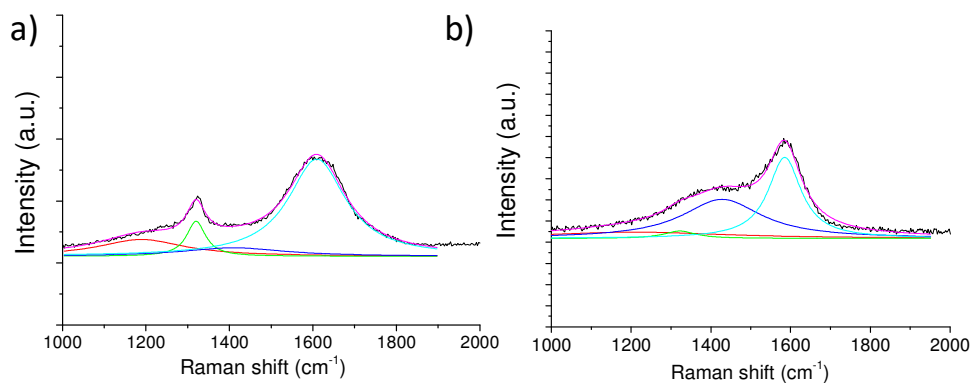


Figure S15. Raman spectra of ND-1100-1U (a) and ND-1100-1U-react (b).

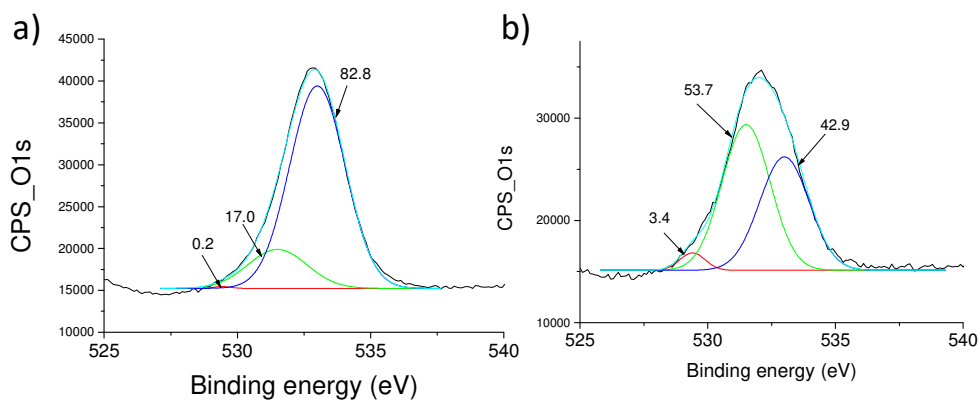


Figure S16. C1s XPS spectra of ND-1100-1U (a) and ND-1100-1U-React (b).

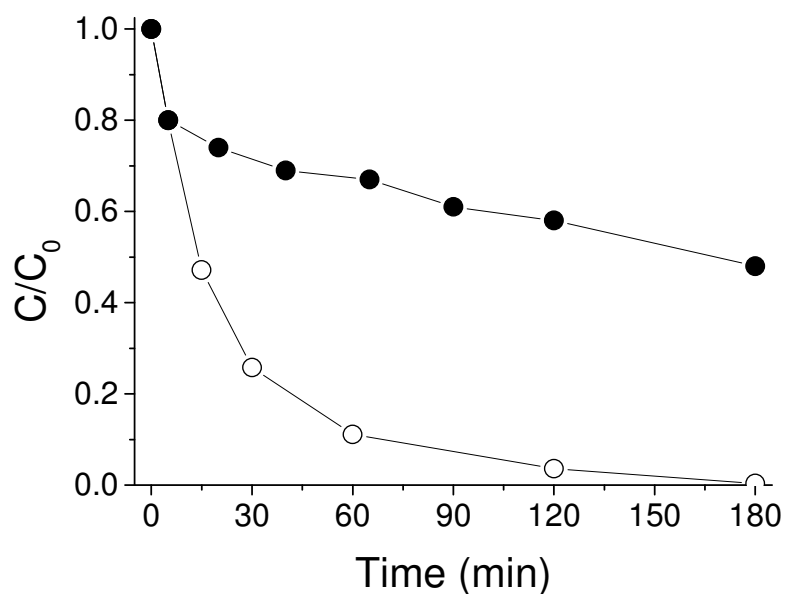


Figure S17. Carbocatalytic ozonation of oxalic acid at pH 3 using ND-1100 as carbocatalyst in the absence (○) or in the presence (●) of NaN₃ as selective ¹O₂ quencher. Reaction conditions: Oxalic acid (50 mg/L), carbocatalyst (100 mg/L), pH 3, temperature 20 °C, O₃ to oxalic acid molar ratio 5.3.

Chapter 7

Conclusions

In view of the results of the present Thesis, it can be concluded that the pre-ozonation of water containing cyanobacteria, even at relatively low concentrations (10,000 cell/mL), is not an appropriate method of controlling the formation of DBPs, including THMs, HAAs, HANs and HKs. The use of an appropriate activated carbon surface functionalization by chemical methods is important for the deposition of small cobalt nanoparticles with superior activity for PMS activation and aqueous pollutant degradation. The thesis has also shown the possibility of developing highly active metal-free carbon-based materials as ozonation catalysts. The conclusions of each chapter are as follows.

The chlorination of water containing relatively low concentrations of common cyanobacteria present in surface waters such as *Microcyst* results in the formation of considerable amounts of THMs and HAAs accompanied by minor amounts of HANs and the absence of HKs and trichloronitromethane. Basic pH values during the chlorination process increase THM formation, have a minor

influence on HAAs formation, while HAN concentration is reduced. The presence of bromide ions during chlorination increases the formation of THMs and HANs with a minor influence on HAA formation. A pre-ozonation process (1.6 mg/L) reduces the chlorine demand while bromate formation is observed in the presence of bromide ions (300 µg/L). This pre-ozonation increases THM formation, generates trichloronitromethane, has a minor influence on HAA formation and reduces HAN formation.

The functionalization of commercial activated carbon by a chemical treatment using nitric acid is an appropriate method to obtain a large population of oxygen-functional groups to anchor small cobalt nanoparticles. The most active catalyst is based on oxidized cobalt nanoparticles (0.2 wt%) supported on a nitric acid functionalized activated carbon support. The catalytic activity of this material for PMS activation and phenol degradation is higher than the benchmark commercial Co_3O_4 solid and even than that of homogeneous Co^{2+} ions. The catalyst is active even at pH 7 and 20 °C reaching a TON and TOF value for PMS activation as high as $4 \cdot 10^5$ and $8 \cdot 10^5 \text{ h}^{-1}$, respectively. An optimized PMS to phenol molar ratio of 9.3 allows phenol degradation together with its reaction intermediates (hydroquinone, catechol and *p*-benzoquinone) and a TOC abatement of 70 %. Catalytic activity increases along with temperature, following the Arrhenius model. The catalyst is stable during at least eight consecutive cycles without cobalt leaching or cobalt nanoparticle aggregation. Based on selective quenching experiments and EPR measurements, it was confirmed that the catalyst decomposes PMS in water, leading to the formation of sulfate and hydroxyl radicals.

An edge-hydroxylated high surface area graphite material was found to be a highly active metal-free ozonation catalyst for oxalic acid degradation. This carbocatalyst shows higher activity than the parent graphite, commercial activated carbon (Norit), commercial multiwall carbon nanotubes, commercial diamond nanoparticles, graphene oxide, and reduced graphene oxide as well as the benchmark ozonation catalysts Co_3O_3 or Fe_2O_3 . The edge-hydroxylated graphite-based material can be reused 10 times with a gradual decrease of activity while achieving full oxalic acid degradation at longer reaction times. The catalytic

activity of the partially-spent carbocatalyst can be easily recovered by thermal or chemical reduction procedures. EPR measurements and selective quenching experiments revealed the formation of hydroperoxyl and $^1\text{O}_2$ as ROS. The excellent activity of this carbocatalyst can be attributed to the presence of the sp^2 domain with an appropriate work function due to the presence of edge-hydroxylated functional groups that also favor the dispersion of the carbon material in water.

A series of defective hybrid sp^2/sp^3 core-shell nanodiamonds were developed and used as metal-free ozonation catalysts. A volcano-trend relationship between the catalytic activity for oxalic acid degradation and the annealing temperature was observed. From the characterization data it can be concluded that the most active sample annealed at 1100 °C for 1 h has a unique sp^2/sp^3 core-shell configuration with appropriate oxygen and nitrogen functional groups that favours the electron enrichment of the outer sp^2 shell and also exhibits an appropriate work function due to the presence of hydroxyl/ether functional groups that enhance its catalytic activity. The catalytic activity of the partially deactivated carbocatalyst can be recovered by annealing at 1100 °C for 1 h. EPR measurements and selective quenching experiments revealed that the main ROS generated during the catalytic ozonation are hydroperoxyl radicals and $^1\text{O}_2$ species.

Chapter 7. Conclusions

Chapter 8

Abstract of the thesis

Abstract

Water is essential for life. The present Thesis studied the use of ozone and peroxymonosulfate as oxidants in water treatments for disinfection by-products control or pollutant degradation. Pre-ozonation of natural water was considered as a general drinking water treatment able to minimize the formation of DBPs. In this Thesis, however, it has been demonstrated that pre-ozonation of surface water containing common cyanobacteria is not a suitable treatment for controlling chlorination-based DBPs (trihalomethanes, haloacetic acids, haloacetoneitriles, haloketones and trichloronitromethane).

AOPs based on ozone and peroxymonosulfate are considered to be some of the preferable technologies for water pollutant degradation. This Thesis has shown that appropriate activated carbon functionalization by chemical treatment results in a surface functionalization with a large population of oxygen functional groups able to deposit small cobalt nanoparticles. The resulting material exhibits a catalytic activity for PMS activation and phenol degradation superior to most of the previous studies in the field. It has also shown the possibility of developing highly active metal-free ozonation catalysts based on edged-hydroxylated high surface area graphite or defective sp^2/sp^3 nanodiamonds.

Resumen

El agua es esencial para la vida. La presente Tesis ha estudiado el uso de ozono y peroximonosulfato como oxidantes en tratamientos de agua para el control de subproductos de desinfección o degradación de contaminantes. La preozonación del agua natural, se consideró como un tratamiento general del agua potable capaz de minimizar la formación de subproductos de la desinfección (DBP). En esta tesis, sin embargo, se ha demostrado que la preozonación de aguas superficiales que contienen cianobacterias comunes, no es un tratamiento adecuado para controlar los DBP basados en cloración (trihalometanos, ácidos haloacéticos, halonitrilos, halocetonas y tricloronitrometano).

Los procesos de oxidación avanzada (POAs) basados en ozono y peroximonosulfato se consideran algunas de las tecnologías preferibles para la degradación de contaminantes del agua. Esta tesis ha demostrado que la funcionalización adecuada del carbón activo mediante tratamiento químico da como resultado una funcionalización superficial del carbón con una gran población de grupos funcionales de oxígeno capaces de depositar pequeñas nanopartículas de cobalto. El material resultante exhibe una actividad catalítica para la activación del PMS y la degradación del fenol superior a la mayoría de los estudios previos en este campo. También ha mostrado la posibilidad de desarrollar catalizadores de ozonización libres de metales altamente activos basados en grafito de alta área superficial hidroxilado en los bordes o en nanodiamantes sp^2 / sp^3 defectuosos.

Resum

L'aigua és essencial per a la vida. La present Tesi ha estudiat l'ús d'ozó i peroxi-monosulfat com oxidants en tractaments d'aigua per al control de subproductes de desinfecció o degradació de contaminants. La preozonació de l'aigua natural, es va considerar com un tractament general de l'aigua potable capaç de minimitzar la formació de subproductes de la desinfecció (DBP). En aquesta tesi, però, s'ha demostrat que la preozonació d'aigües superficials que contenen cianobacteries comuns, no és un tractament adequat per controlar els DBP basats en cloració (trihalometans, àcids haloacètics, halonitrils, halocetones i tricloronitrometà).

Els processos d'oxidació avançada (POAs) basats en ozó i peroxi-monosulfat es consideren algunes de les tecnologies preferibles per a la degradació de contaminants de l'aigua. Aquesta tesi ha demostrat que la funcionalització adequada del carbó actiu mitjançant tractament químic dóna com a resultat una funcionalització superficial de l'carbó amb una gran població de grups funcionals d'oxigen capaços de dipositar petites nanopartícules de cobalt. El material resultant exhibeix una activitat catalítica per a l'activació del PMS i la degradació del fenol superior a la majoria dels estudis previs en aquest camp. També ha mostrat la possibilitat de desenvolupar catalitzadors d'ozonització lliures de metalls altament actius basats en grafit d'alta àrea superficial hidroxilat en les vores o en nanodiamants sp^2 / sp^3 defectuosos.

Chapter 8. Abstract

Chapter 9

Publications & Conferences

List of publications

1. Francisco Bernat-Quesada; Mercedes Álvaro; Hermenegildo García; Sergio Navalón. Impact of chlorination and pre-ozonation on disinfection by-products formation from aqueous suspensions of cyanobacteria: *Microcystis aeruginosa*, *Anabaena aequalis* and *Oscillatoria tenuis*. *Water Research*. 183, pp. 116070. 2020
2. F. Bernat-Quesada; J.C. Espinosa; V. Barbera; M. Álvaro; Maurizio Galimberti; S. Navalón; H. García. Catalytic ozonation using Edge-hydroxylated graphite-based materials. *Clave A, ACS Sustain. Chem. Eng.* 7, 17443-17452, 2019.
3. Espinosa J.; Manickam-Periyaraman P.; Bernat-Quesada F.; Sivanesan S.; Álvaro M.; García H.; Navalón S. Engineering of activated carbon surface to enhance the catalytic activity of supported cobalt oxide nanoparticles in peroxymonosulfate activation. *Clave A, Applied Catalysis B: Environmental*. 15, pp. 42 - 53. 2019.

4. Francisco Bernat-Quesada, Cristina Vallés-García, Eva Montero-Lanzuela, Antón Lopez-Francés, Belén Ferrer, Herme G. Baldoví, Sergio Navalón. Hybrid sp^2/sp^3 nanodiamonds as heterogeneous metal-free ozonation catalysts (submitted manuscript)

List of conferences

1. Bernat-Quesada, Francisco; Navalón Oltra, Sergio, Alvaro Rodríguez, Maria Mercedes, García Gómez, Hermenegildo "Low-Cost Carbon Materials as Sustainable Metal-Free Catalysts in Advanced Oxidation Processes using Ozone", World Congress on Chemistry (WCC), October 2019. Oral communication